Universidad Zaragoza

1474

Tesis Doctoral

Electrocardiographic Markers for Cardiac Risk Stratification and Ventricular Dyssynchrony Assessment

Autor

Saúl D. Palacios Rosales

Director/es

Juan Pablo Martínez Cortés
Esther Pueyo Paules

Escuela de Ingeniería y Arquitectura

2025

Saúl Palacios, 2025
Electrocardiographic Markers for Cardiac Risk Stratification and Ventricular Dyssynchrony Assessment

Date of current version: July 18, 2025

This Ph.D. thesis has been developed within the Department of Electronic Engineering and Communications and the Aragón Institute for Engineering Research (I3A) at the University of Zaragoza (Zaragoza, Spain).

The research presented in this thesis was supported by the FPI grant BES-2017-080587 from the Ministerio de Economía y Competitividad (Spain), the projects PID2019-105674RB-I00, PID2019-104881RB-I00, PID2022-140556OB-I00, TED2021-130459B-I00 from the Ministerio de Ciencia e Innovación (Spain) and projects ERC-StG 638284 (European Research Council). It was also funded by Gobierno de Aragón (Spain) through Reference Group BSICoS T39_23R and projects LMP124_18, LMP94_21 cofunded by FEDER 2014-2020 "Building Europe from Aragon", and by CIBER in Bioengineering, Biomaterials & Nanomedicine (CIBER-BBN) through Instituto de Salud Carlos III.

The computation of some parts of this thesis was performed at the High Performance Computing platform of the NANBIOSIS ICTS, CIBER-BBN and Aragón Institute of Engineering Research (I3A), Zaragoza, Spain.

This thesis was printed thanks to the financial support of BSICoS Group at University of Zaragoza.

I would like to dedicate this thesis to anyone who admits that they know nothing . . .

Acknowledgements

Cuando estoy a punto de finalizar este periplo de formación pre-doctoral, quiero acordarme de todas aquellas personas que de alguna manera han sido parte de esta maravillosa travesía y darles las gracias.

A mis directores de tesis, los profesores Juan Pablo Martínez y Esther Pueyo, por haberme guiado y aconsejado durante estos años. Es un gran honor haber trabajo bajo la supervisión de dos personas de gran calidad humana y científica.

Al grupo de investigación Biomedical Signal Interpretation and Computational Simulation (BSICoS) por la ayuda prestada, empezando por aquella época en la que realizaba mi trabajo final de máster. Las circunstancias han hecho que haya podido estar ubicado en distintos lugares, laboratorios, y esto me ha servido para poder conocer de manera más personal a algunos de los miembros. De todos, tanto si hemos compartido espacios de trabajo como si no ha sido así, tanto si siguen vinculados directamente al grupo como si no es así, hay una pequeña gran impronta en mí de cada uno.

Al personal del Departamento de Ingeniería Electrónica y Comunicaciones, tanto docentes e investigadores como personal de administración y servicios. Gracias por vuestra colaboración. Lo mismo se podría decir de aquellas personas que conocí, y aún conozco, en el Instituto de Investigación en Ingeniería de Aragón (I3A), y en general a todos con los que he coincidido en algún momento en el conjunto de edificios que conforman el Campus Río Ebro.

A la Universidad de Zaragoza, por la investigación de calidad que he podido realizar en sus instalaciones durante todo este periodo de formación. Así mismo a todas aquellas personas que en mayor o menor medida me han ayudado sin ser yo totalmente consciente de ello.

Al conjunto de estudiantes que me han tenido en el aula y en el laboratorio mientras ejercía mi rol de profesor durante estos años. No solo se aprende recibiendo clases sino que también en los momentos en los que se está delante de la pizarra. Una experiencia docente que la han hecho inolvidable y que espero repetir en otras ocasiones.

Al personal de la Unidad de Arritmias, Servicio de Cardiología del Hospital Clínico Universitario Lozano Blesa. En especial a los Dres. Javier Ramos, Mercedes Ramos, Daniel Meseguer, Davinia Chofre, las enfermeras Inés Julián, Laura Sorinas y Rebeca Tabernero por todas las explicaciones pormenorizadas y el tiempo dedicado en la colaboración que se ha llevado a cabo y que sigue en marcha.

Special thanks to Dr. Pavel Jurák for the abroad experience at the Institute of Scientific Instruments of the Czech Academy of Sciences in Brno, which allowed me to broaden my knowledge about different type of pacing and discover a new high-frequency technique. I also wish to thank the research team, Dr. Josef Halamek, Dr. Filip Plesinger, Radovan Smisek, my labmates Jan and Petr. I felt as part of MediSig team. An additional special thanks to Dr. Karol Curila for helping me to understand several physiological issues related to different cardiac stimuli.

To my beloved friends. We have lived through so many adventures and shared countless hours of conversations in the pursuit of the truth and the meaning of the life, among whom I wish to thank in particular for their help, input and enriching personal discussion: Miguel 'Mike' G., Sofía 'Sofi' S., José Manuel 'jtmeros' F., Anabel 'Lady' M. and Valentín G. Some of you had been my first focus group on several topics with different points of view. I appreciate your fully, even sometimes painful, honesty and your willingness to approach issues in an intelligent way. Thanks for encouraging me. You are so important to me that I could not even describe it totally. Never forget that neither distances nor time could prevent me from getting in touch with each one of you. I would also like to remember those friends who are no longer so close: Daniel B. & Gregorio L.

A mi a*preciado*, *bienquisto*, re*conocido*, mirífico, eximio,... (mini) **grupo** 'Red de Vida' (or 'Living network'), tanto a los actuales miembros que lo conforman como a los que alguna vez compartieron mesa y productivas

reuniones conmigo. Habéis sido, y aún sois, un gran apoyo para mí. Solo de pensar que únicamente iba a ser algo temporal, de transición y de acogida se me escapa una sonrisa. Mencionaré, sabiendo que me olvido de mucha gente, a: Eli V., Ana I., Virginia I., Laura I., Juan José M., Kristina L., Cintia R. and David A., Elisabet G., María R. and Jesús B., Denisse D., Mélody I., Verónica de P. and Xavier P.,... Algunos incluso habéis actuado como cariñosos críticos y revisores.

To Sergio 'pescador' M. and Yolanda T., pastors of the Baptist Church in Zaragoza (IEBZ). Your vision, which I completely agree, and attitude are accomplishing that the congregation grows and strengthens. Thanks for your help, your wise words and for counting on me. Agradezco a los Word Seekers' leaders, Tim W. y Stuart D., así como al resto de los *seekers*, por las enseñanzas y conversaciones en inglés.

To my parents and my brother. Thanks for being so patient and loving with me and for the great support you always give me. I am a better human being because you three help me.

Last but never the least, my endless thanks are to Almighty God for letting me to expand a bit more my knowledge about the Universe through the human heart. He created all things, even me.

GRACIAS - THANKS - MERCI - GRAZIE - DANKE - DĚKUJI - ΕΥΧΑΡΙΣΤΩ - YUSULPAYKI - شكرا

Engañoso es el corazón	*The heart is deceitful*
más que todas las cosas,	*above all things,*
y perverso;	*and desperately wicked:*
¿quién lo conocerá?	*who can know it?*
(Jeremías 17:9)	*(Jeremiah 17:9)*

Abstract

Cardiovascular disease (CVD), a term used to describe conditions that affect the heart and blood vessels, is the leading cause of disease burden worldwide. Chronic heart failure (CHF) stands out as one of the most important and commonly studied diseases and may be due to structural and/or functional abnormalities. Certain cardiovascular diseases are associated with dyssynchrony in the transmission of electrical impulses throughout the heart. These diseases lead to a diminished quality of life.

The study and application of various markers derived from electrocardiographic signals (ECG), as well as other available medical recordings, are highly valuable tools for the early detection of CVD and for assessing the risk of mortality associated with CVD. The analysis of these markers is crucial to advance our understanding of the complex interactions between cardiac function and autonomic regulation, offering possibilities for future research and use in medical applications.

The main objective of this thesis is to better understand the influence of the sympathetic nervous system on changes in cardiac repolarization by calculating ECG markers. One of the investigated markers is called Periodic Repolarization Dynamics (PRD). PRD quantifies the low-frequency oscillations (below 0.1 Hz) of the angle between consecutive T waves, the magnitude of which is influenced by sympathetic activity. Other investigated markers are related to activation (AT) and repolarization times (RT). By calculating these times, it is possible to assess ventricular dyssynchrony in ECG leads.

The methods used to calculate PRD are fully described in Chapter 2. The steps taken to measure the angle dT° between consecutive T waves are detailed together with the modifications made to a previously proposed method of computation to improve its robustness. Once the time series of the angles

dT° is obtained, two techniques to measure PRD are presented. The Continuous Wavelet Transform (CWT) technique calculates the pseudo-frequencies associated with each scale of the wavelet transform. The other technique, which is associated with a lower computational cost, is called Phase-Rectified Signal Averaging (PRSA). This technique involves the identification of windows around anchor points identified according to the changes seen in the dT° series.

The methods used to calculate AT and RT are fully described in Chapter 4. The center of mass of the QRS complex, in the case of AT, and of the T wave, in the case of RT, is measured for each of the precordial ECG leads V1-V6. Furthermore, the spatial dispersion of AT (RT) is calculated as the difference between the last activated (repolarized) lead and the first activated (repolarized) lead for each recording. Assessment of heart rate variability and the semiautomated algorithm to remove cardiac pacing stimuli in stimulated recordings are also described.

Chapter 2 examines the response of the cardiovascular system when exposed to artificial microgravity for 60 days, using a ground-based analogue known as Head-Down Bed Rest (HDBR). The experiments were conducted at European Space Agency (ESA) facilities. The effectiveness of two types of countermeasures to mitigate the harmful effects of artificial microgravity was tested. One of the countermeasures was based on the physical activities performed by the volunteers when lying on the bed. The other countermeasure was based on diet modifications. Chapter 3 analyzes the MUSIC (MUerte Súbita en Insuficiencia Cardiaca) database, focusing specifically on heart failure patients who experienced sudden cardiac death (SCD) or pump failure death (PFD) during follow-up. In both Chapter 2 and Chapter 3, PRD was measured and used to assess the response of the cardiovascular system to microgravity exposure and predict mortality due to SCD or PFD. The findings of Chapter 2 indicate that there is significant sympathetic activation during the tilt test performed after prolonged exposure to artificial microgravity. Furthermore, our results show that the activity-based countermeasure is able to mitigate the adverse effects of microgravity, while the diet-based countermeasure only partially reduces these effects. The findings of Chapter 3 confirm that PRD is a strong predictor of SCD in patients with a history of

heart failure. The predictive accuracy of PRD is improved when combined with ECG markers such as the Index of Average Alternans (IAA), which quantifies the magnitude of T wave alternans, and the Turbulence Slope (TS), which reflects the rate of increase of the RR interval following the initial heart rate acceleration.

Chapters 4 and 5 focus on comparing different cardiac stimulation techniques, including right ventricular pacing at the apex (RVAP) or septum (RVSP), left ventricular septal pacing (LVSP), left bundle branch pacing (LBBP) and His bundle pacing (HBP), with LBBP and HBP being selective or non-selective. The analyzed ECG recordings include high-frequency (1,000 Hz) and ultra-high-frequency (5,000 Hz) recordings obtained at some of the following times: before intervention, immediately after, the day after intervention and one year after intervention. The aim is to determine to what extent the different pacing techniques resemble the characteristics of spontaneous rhythm in patients with no conduction disorders that require pacing as an antibradycardia treatment. For that, several variables representative of ventricular activation dyssynchrony and of irregularities in ventricular repolarization are measured. Indices quantifying AT and RT and their spatial interventricular and intraventricular dispersions are proposed. The PRD index and other QT-based and T-wave-based indices are also measured. Our results show that physiological stimulation techniques, such as LBBP and HBP, produce ventricular electrical responses that are close to electrical activity under spontaneous rhythm, whereas techniques based on pacing the ventricular myocardium, such as RVAP or RVSP, do not achieve comparable spontaneous responses. Furthermore, our findings confirm that LBBP offers an effective alternative to HBP when activation and repolarization of the left ventricle are evaluated.

Chapter 6 presents the conclusions. The main contributions of the thesis are highlighted, indicating that the thesis develops robust and efficient methodologies to measure the characteristics of ventricular depolarization and repolarization from ECG recordings. The PRD marker is shown to reflect a microgravity-induced increase in sympathetic modulation of ventricular repolarization by quantifying the magnitude of the oscillations in the angle between consecutive T waves. Furthermore, the predictive capacity of PRD to

stratify CHF patients for the risk of SCD and PFD, alone and in combination with other ECG markers, is corroborated. In addition, this thesis compares different cardiac pacing techniques and shows that physiological pacing techniques targeting the cardiac conduction system are capable of mimicking ventricular activity under spontaneous rhythm, as indicated by similarities in ECG depolarization and repolarization, particularly when focusing the analysis on the left ventricle.

Keywords: Periodic Repolarization Dynamics, PRD, activation time, repolarization time, microgravity, heart failure, HF, sudden cardiac death, SCD, pump failure death, PFD, ultra-high-frequency recordings, UHF-ECG, cardiac pacing, right ventricular pacing, RVP, left bundle branch pacing, LBBP.

Resumen y conclusiones

Las enfermedades cardiovasculares (ECVs), término utilizado para denominar las enfermedades que afectan al corazón y los vasos sanguíneos, son la principal causa de fallecimiento en todo el mundo. La insuficiencia crónica cardiaca es una de las principales, además de ser una de las más estudiadas, y puede estar debida a anormalidades estructurales o funcionales. Algunas ECVs están asociadas a la disincronía en la transmisión del impulso eléctrico a lo largo del corazón. Estas enfermedades conllevan una peor calidad de vida.

El estudio y uso de diferentes biomarcadores procedentes de la señal electrocardiográfica (ECG), como de otros registros médicos disponibles, es de gran utilidad para una detección temprana de ECVs, y para determinar el riesgo de fallecer por alguna condición cardiovascular. El análisis de estos marcadores permiten tener una mayor comprensión de las interacciones complejas que existen entre las funciones cardiacas y la regulación autonómica, ofreciendo posibilidades para una mayor investigación futura y para uso en aplicaciones clínicas.

El principal objetivo de esta tesis es entender mejor la influencia del sistema nervioso simpático sobre los cambios que se producen en la repolarización cardiaca, mediante el cálculo de diferentes marcadores. Uno de ellos es la dinámica de repolarización periódica (PRD, *Periodic Repolarization Dynamics*). El marcador PRD mide las oscilaciones de baja frecuencia (menor a 0.1 Hz) de los cambios en el ángulo entre ondas T consecutivas, que se produce por la actividad simpática. Otros marcadores investigados están relacionados con los tiempos de activación (AT, *activation time*) y repolarización (RT, *repolarization time*). Mediante el cálculo de estos tiempos se consigue evaluar la disincronía ventricular en las derivaciones de los registros ECG.

Los métodos usados para calcular el marcador PRD están descrito en el Capítulo 2. Los pasos realizados para medir la serie de ángulos consecutivos de las ondas T, dT°, están detallados junto con las modificaciones hechas respecto de un método propuesto anteriormente para mejorar la robustez. Posteriormente, una vez obtenida la serie de dT°, se presentan dos técnicas de cálculo para hallar el valor de PRD. La técnica CWT (*Continuous Wavelet Transform*) calcula las pseudofrecuencias asociadas a cada escala de la transformada wavelet. La otra técnica, asociada con un menor coste computacional, es PRSA (*Phase-Rectified Signal Averaging*). En esta técnica se identifica las ventanas alrededor de los puntos ancla que se obtienen según los cambios observables en la serie de dT°.

Los métodos de cálculo para AT y RT están descritos en el Capítulo 4. El centro de masas del complejo QRS, en el caso del AT, y de la onda T, para el RT, son calculados en cada derivacion precordial, V1-V6, del ECG. Adicionalmente, la dispersión de AT (o RT) se calcula como la diferencia entre la derivación que se activa (o repolariza) más tarde y la primera derivación que se activa (o repolariza) para cada registro. La evaluación de la variabilidad del ritmo cardiaco y el algoritmo semiautomático para eliminar los estimulos cardiacos en los registros estimulados también son descritos.

En el Capítulo 2 se examina la respuesta del sistema cardiaco ante la exposición durante 60 días a microgravedad artificial, por medio de un modelo de simulación denominado *Head-down bed-rest* (HDBR). Los experimentos fueron llevados a cabo en las instalaciones de la Agencia Espacial Europea (ESA). Se midió la capacidad de mitigar los efectos nocivos de la microgravidad artificial en dos tipos de contramedidas. Una de las contramedidas estaba basada en actividades físicas que realizaban los voluntarios, y la otra estaba basada en el tipo de dieta diaria que ellos recibían. En el Capítulo 3 se analiza la base de datos MUSIC (MUerte Súbita en Insuficiencia Cardiaca) con pacientes de insuficiencia cardiaca que fallecieron por muerte súbita cardiaca o por fallo de bomba cardiaca. En ambos capítulos (2 y 3), el PRD fue medido y usado para evaluar la respuesta del sistema cardiovascular ante la exposición a la microgravedad y para medir su capacidad predictora de fallecer por algunas de las dos causas mencionadas. Los hallazgos del Capítulo 2 indican que existe una activación simpática significativa cuando se realiza la prueba de

inclinación después de la exposición prolongada a la microgravedad artificial. Además, nuestros resultados muestran que las contramedidas relacionadas con actividades físcias son efectivas para contrarrestrar los efectos adversos de la microgravedad, mientras que las contramedidas alimenticias solo consiguen reducir parcialmente estos efectos. Los hallazgos del Capítulo 3 confirman que el marcador PRD es un buen predictor de riesgo de muerte súbita cardiaca en pacientes con antecedentes de fallo cardiaco. Y su capacidad de predicción mejora cuando se combina con los biomarcadores índice de alternancia promedio (*index of average alternans*, IAA), que cuantifica la magnitud de las alternancias de la onda T; y turbulence slope (TS), el cual refleja la ratio de incremento del intervalo RR después de la aceleración de la frecuencia cardiaca inicial.

Los Capítulos 4 y 5 se centran en comparar varios tipos de estimulación cardiaca, incluyendo estimulación de ventrículo derecho, en el apex o en el septo, estimulación del septo del ventrículo izquierdo, estimulación de rama izquierda y del haz de His, tanto selectivo como no selectivo. Los registros analizados incluyen señales de alta (1,000 Hz) y muy alta frecuencia (5,000 Hz) obtenidos en alguno de los siguientes momentos: antes, justo después, al día siguiente o después de un año de la intervención. El objetivo es determinar en qué medida las distintas técnicas de estimulación se asemejan a las características del ritmo espontáneo en pacientes que no tienen trastornos de conducción y que requieren estimulación como tratamiento antibradicardia. Para ello, varias variables representativas de disincronía de activación ventricular y de irregularidades en la repolarización ventrciular se midieron. Se propusieron varios índices que cuantifican AT, RT y las dispersiones inter e intraventriculares y también se midieron el marcador PRD e índices basados en QT y en la onda T. A partir de los resultados que se obtienen, se concluye que las técnicas fisiológicas de estimulación cardiaca producen una mejor respuesta ventricular, mientras que las técnicas relacionadas con la estimulación del miocardio ventricular no consiguen una respuesta similar a la que se observa en registros espontáneos. Además, nuestros hallazgos confirman que la técnica de estimulación de rama izquierda es una alternativa efectiva a la estimulación del haz de His, cuando se evalúa la activación y repolarización del ventrículo izquierdo.

En el Capítulo 6 se presenta las conclusiones. Las principales contibuciones de esta tesis se destacan, indicando el desarrollo de metodologías para medir las características de la depolarización y repolarización ventricular de manera eficiente y robusta a partir de registros ECG. El marcador PRD es capaz de detectar los cambios inducidos por la microgravedad en la modulación simpática de la repolarización ventricular, mediante la cuantificación de la magnitud en las oscilaciones de los ángulos de ondas T consecutivas. También se ha evaluado la capacidad predectiva del marcador PRD para estratificar el riesgo de fallecer por muerte súbica cardiaca o fallo de bomba en sujetos con insuficiencia cardiaca crónica, tanto individual como en combinación con otros marcadores del ECG. Además, en esta tesis se ha comparado diferentes técnicas de estimulación cardiaca y se ha visto que las técnicas fisiológicas consiguen devolver el comportamiento ventricular espontáneo, como se muestra por la similitudes en la depolarización y repolarización del ECG, especialmente cuando nos enfocamos en el análisis del ventrículo izquierdo.

Palabras clave: Dinámica de repolarización periódica, PRD, tiempo de activación, tiempo de repolarización, microgravedad, insuficiencia cardiaca, muerte súbita cardiaca, muerte por fallo de bomba, registro de ultra alta frecuencia, UHF-ECG, estimulación cardiaca, estimulación convencional, estimulación de rama izquierda

Contents

List of Figures

List of Tables

List of Acronyms

AHF	Acute Heart Failure
ANS	Autonomic Nervous System
AP	Action potential
APD	Action potential duration
ARI	Activation-recovery interval
AT	Activation time
AV	Atrioventricular
BNP	B-type natriuretic peptides
CD	Cardiac death
CHD	Coronary heart disease
CHF	Chronic heart failure
CRT	Cardiac resynchronization therapy
CSP	Conduction system pacing
CTRL	Control groups in HDBR studies
CV	Cardiovascular
CVD	Cardiovascular disease
CWT	Continuous Wavelet Transform
$\mathbf{dAT}_{4-6}$	Dispersion of activation times between V4-V6
dAT	Dispersion of activation time
$\mathbf{dATs}_{4-6}$	Dispersion of activation times between V4-V6 including the sign
dATs	Dispersion of activation times including the sign

DLR Deutsche Zentrum für Luft- und Raumfahrt e. V., also known as German Aerospace Center

dRT$_{4-6}$ Dispersion of repolarization times between V4-V6

dRT Dispersion of repolarization time

dRTs$_{4-6}$ Dispersion of repolarization times between V4-V6 including the sign

dRTs Dispersion of repolarization times including the sign

ECG Electrocardiogram

ECM Extracellular matrix

EKG Elektrokardiogramm, see also **ECG**

ESA European Space Agency

HBP His-bundle pacing

HCLB Hospital Clínico Lozano Blesa

HDBR Head-Down Bed Rest

HF Heart failure

HF High-frequency band

HFn Normalized high-frequency band

HR Heart rate

HRV Heart rate variability

IHD Implantable cardioverter defibrillators

IHD Ischemic heart disease

IQR Interquartile range

JUMP Physical countermeasure in HDBR studies

LA Left atrium

LBB Left bundle branch

LBBAP Left bundle branch area pacing, see also **LBBP**

LBBB Left bundle branch block

LBBP Left bundle branch pacing

LBNP Lower body negative pressure

LF Low-frequency band

LFn Normalized low-frequency band

LV Left ventricle

LVEF Left ventricular ejection fraction

LVSP Left ventricular septal pacing

MEDES Institut de médecine et physiologie spatiale

μg Microgravity

MUSIC MUerte Súbita en Insuficiencia Cardiaca, study

NUTR Nutritional countermeasure in HDBR studies

NYHA New York Heart Association

PFD Pump failure death

PRD Periodic repolarization dynamics

PRSA Phase-Rectified Signal Averaging

PSD Power spectral density

RA Right atrium

RBBB Right bundle branch block

RT Repolarization time

RV Right ventricle

RVAP Right ventricular apical pacing

RVP Right ventricular pacing

RVSP Right ventricular septal pacing

SA Sinoatrial

SCD Sudden Cardiac Death

TMP Transmembrane potential

TTT Tilt-table test

UHF-ECG Ultra-high-frequency ECG

VCG Vectorcardiogram

VDI Ventricular Dyssynchrony Imaging

Haec consideratio in admirationem altissimae Dei virtutis ducit: et per consequens in cordibus hominum reverentiam Dei parit.
This consideration [of God's works] leads to admiration of God's sublime power, and consequently inspires in men's hearts reverence for God.

Summa Contra Gentiles. Thomas Aquinas

1 Introduction

1.1 Motivation

Doctors and philosophers have long wondered how the heart works and how it manages to maintain its ability to beat even when it is not in the body. The study of cardiac anatomy dates back several millennia. This study is said to have started in Egypt, was elaborated by ancient Greeks and was better defined in Alexandria. Significant contributions to our present understanding were made by anatomists, philosophers, and even artists. Following the decline of the Roman Empire, this knowledge was conserved within the Islamic world and European monasteries and later reached universities with the resurgence of anatomical dissection [40, 344]. According to many historians, the story of our understanding of cardiovascular (CV) diseases (CVDs) begins with the work of William Harvey[1] [113].

CVDs are chronic, noncommunicable diseases that affect the heart and blood vessels and account for approximately a third of all deaths globally

[1] *De Motu Cordis et Sanguinis* (1628)

[181] and a similar value (32.7%) in the European Union [117]. World Health Organization (WHO) estimates that by 2030, 22.2 million people will die from CVDs per year [441]. CVD has a notable influence on the European workforce. Frequently, this condition culminates in disability, premature retirement, and increased absenteeism, leading to a decrease in productivity and economic results. All of these issues affect society and individuals through a greater economic burden. Based on ESC Atlas data, the total cost of CVD in the European Union was estimated to be € 282 billion in 2021 [222]. Furthermore, CVDs had a direct and indirect cost estimated at $ 407.3 billion annually in the United States during 2018-2019, according to the Medical Expenditure Panel Survey [401]. Globally, CVD remains a growing challenge in developing regions, with almost 80% of CVD cases occurring in low- and middle-income countries [213].

Heart failure (HF) is an increasing problem in our current society. Routine procedures for HF treatment are coronary bypass surgery, angioplasty, stenting, implantation of pacemakers and / or defibrillators, and valve replacement [173]. Two of the leading causes of mortality among patients with HF are sudden cardiac death (SCD) and pump failure death (PFD) [445]. SCD often results from malignant arrhythmias, while PFD is due to loss of contractile mass and myocardial function [348, 448]. Given the high mortality rates associated with both endpoints, there is a critical need for effective risk stratification strategies in the HF population. The use of reliable ECG-based markers plays a fundamental role in identifying patients with increased risk.

Cardiac pacing is the primary therapeutic approach for the prevention and suppression of bradyarrhythmias [299]. The purpose of cardiac pacemakers is to restore an adequate heart rate and ensure sufficient cardiac output [407]. The most widely used pacing technique is right ventricular pacing (RVP), but has been associated with several long-term limitations, including cardiac electromechanical asynchrony [219]. These limitations have led to the exploration of new cardiac stimulation sites [339], including physiological pacing targeting the cardiac electrical conduction system (CSP). His bundle pacing (HBP), the most physiological pacing strategy, has been reported to be able to deliver electrical ventricular resynchronization that is superior to conventional pacing [422, 168, 406]. However, several limitations remain

when HBP is performed, including the difficulty in identifying the His bundle in certain patients, a high and unstable pacing threshold, and potential limitations in long-term performance [452]. Recently, left bundle branch pacing (LBBP) has been proposed as an alternative method to HBP. LBBP paces the heart in a more distal and deeper area than HBP. Although the feasibility and safety of this technique have been demonstrated in various case reports and series[165, 425, 177], there is a lack of data on the long-term outcomes of physiological pacing strategies.

The processing of biomedical signals, such as surface electrocardiograms (ECGs), plays an important role in modern medicine by enabling the extraction of noninvasive clinical markers to improve diagnosis, risk stratification, and treatment decision-making. Through advanced signal processing techniques, it is possible to identify subtle patterns and abnormalities that might be overlooked in traditional analyses. In this thesis, various advanced signal processing and techniques will be employed to characterize the temporal and spectral properties of ECG signals that lead to precise and robust clinical markers.

1.2 The Heart

1.2.1 Anatomy and function

The heart is an electromechanical pump, about the size of a fist, that contributes to the transport of oxygen-rich blood, nutrients, and other elements throughout the human body. It is located two thirds to the left of the midline of the thoracic cavity within the middle mediastinum between the lungs [261].

In mammalian hearts, the right atrium (RA) and the right ventricle (RV) are responsible for pumping blood from the systemic veins into the pulmonary circulation, while the left atrium (LA) and the left ventricle (LV) pump oxygenated blood back into the systemic circulation [185], as can be seen in Figure 1.1. There is a one-way flow of blood through the heart, which is maintained by four valves. The atrioventricular (AV) valves, namely the tricuspid and mitral (or bicuspid) valves, allow blood to flow only from the atria to the ventricles. The semilunar valves, namely the pulmonary and aortic valves, allow blood to flow only from the ventricles out of the heart and

through the great arteries [173]. These valves open and close in response to the heart's rhythmic pressure changes, facilitating the flow of blood between different chambers while preventing any backflow (regurgitation). Figure 1.2 illustrates the different cardiac chambers and the course of blood through them.

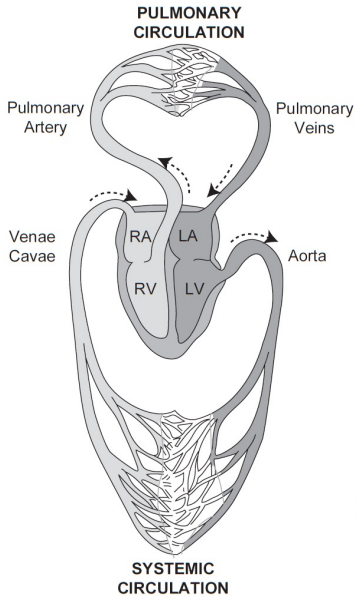

Figure 1.1 Relationship between each side of the heart and type of circulation. Extracted from [185].

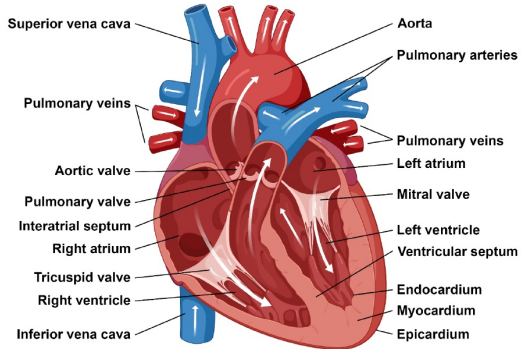

Figure 1.2 Cardiac chambers and valves. Arrows indicate the course of blood through them.

The atria and ventricles are separated by a dense connective tissue, which can be viewed as an insulator that prevents electrical impulses from being conducted between the atria and the ventricles. The AV bundle is a specialized cardiac muscle strand that penetrates this insulator and normally provides the only conducting pathway between the atria and the ventricles [185].

The wall of the heart comprises three distinct layers: the innermost layer, called the endocardium; the middle layer, known as the myocardium; and the outer layer, the epicardium. The heart is surrounded by the pericardium, which is a membranous sac that protects the heart. The endocardium, which lines the chambers and valves of the heart, is made up of endothelial cells, smooth muscle cells, fibrous collagen cells, and cardiac cells [60]. These cells play a dual role, contributing to the structural integrity of the heart and to its function.

The myocardium, which makes up the majority of the heart wall, consists mainly of cardiomyocytes, which represent approximately 70% of the volume of myocardial tissue [271, 426]. In addition, fibroblasts are present and contribute to its structural composition [150]. Cardiomyocytes, also known as cardiac myocytes or cardiac muscle cells, are striated muscle cells, similar to skeletal muscle fibers, but with unique properties that allow them to contract rhythmically and continuously throughout a person's lifetime. They are highly organized and interconnected to facilitate coordinated contractions of the heart [43]. Fibroblasts play a critical role in maintaining the structural integrity of cardiac tissue by producing and breaking down extracellular matrix (ECM) proteins and various signaling factors [66].

1.2.2 Cardiac Electrophysiology

Blood flow within the heart is governed by pressure gradients, which arise from various stages of the cardiac cycle [130]. Each cardiac cycle is classically divided into two principal phases: (a) systole, characterized by ventricular contraction and ejection of blood from the heart; and (b) diastole, marked by ventricular relaxation and the filling of blood. At the beginning of the cardiac cycle, the heart is in diastole, with both the atria and ventricles in a relaxed state [173].

Synchronized contraction of cardiomyocytes is possible by the propagation of electrical impulses, known as action potentials (APs), through the cardiac conduction system [337]. This system can be categorized into two functional elements: (a) impulse-generating nodes, featuring specialized cardiomyocytes known as pacemaker cells; and (b) the impulse-propagating His-Purkinje system, primarily composed of Purkinje-type cells distributed in fibers [286, 78]. In particular, pacemaker cells within the sinoatrial (SA) node, located at the junction of the right common cardinal vein and the wall of the RA [55], initiate cardiac conduction by spontaneously generating APs [337].

The generated electrical impulse rapidly conducts through the atrial tissue, leading to contraction of the atria. This propagation continues until it reaches the AV node, which is located in the interatrial septum. The AV node serves as a direct electrical connection between the atria and ventricles and plays a crucial role by causing a brief delay before ventricular excitation. This delay allows for the completion of the atrial contraction [253]. From the AV node, the impulse then travels through the bundle of His (right and left bundle branches) and the Purkinje fibers, which are specialized fibers that allow rapid propagation of the impulse throughout the ventricles simultaneously to the right and left ventricle sides [420]. It is important to note that the beat rate and rhythm of the heart are regulated by cells that exhibit the highest intrinsic pacemaker activity, known as automaticity. Under normal circumstances, this role is fulfilled by the pacemaker cells of the SA node, which dictate the sinus rhythm [183]. Cells within the AV node, the His-Purkinje system and ventricular cardiomyocytes possess lower automaticity and are therefore classified as subsidiary or latent pacemakers. In cases of SA node dysfunction, the AV node can assume the role of the primary pacemaker and serve as the origin of the AP initiation, a condition known as a junctional rhythm [215]. The electrical pathway and the parts of the heart involved in it are represented in Figure 1.3.

Cardiac action potential

Cardiac APs are driven by the movement of ion charges, such as sodium (Na^+), calcium (Ca^{2+}) and potassium (K^+). These ion flows are governed

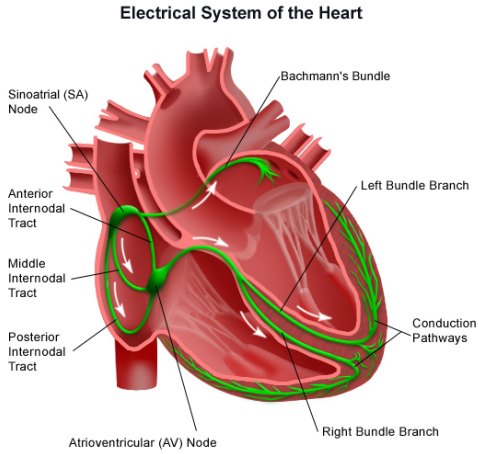

Figure 1.3 Electrical conduction system of the heart. Extracted from [80].

by specific ion channels along the cardiomyocyte membrane that create and maintain chemical and electrical gradients [142, 11, 320]. The transmembrane potential (TMP) represents the voltage difference between the inside and outside of a cardiac cell, defined as TMP = V_{in}-V_{out}. When there is a net influx of positive ions into the cell, the TMP becomes more positive, a process known as depolarization. In contrast, when there is a net movement of positive ions out of the cell, the TMP becomes more negative, leading to repolarization. Specific ion flux-induced changes in TMP are observed in all five AP phases [223, 274, 320]. For a typical ventricular myocyte, these phases are shown in Figure 1.4:

- **Phase 4** - Resting phase. The cell is at rest during diastole. Inward rectifier channels on the membrane cause a persistent outward leak of K^+ resulting in a resting TMP between -95 and -85 mV, in normal working myocardial cells. In this phase, the Na^+ and Ca^{2+} channels are closed.

- **Phase 0** - Depolarization phase. An AP is initiated by a neighboring cardiomyocyte or pacemaker cell. The TMP increases until the threshold potential of -70 mV is reached. Fast Na^+ channels open for a short

period of time, causing rapid cell depolarization. The Na^+ channels begin to close when the TMP has become high enough.

- **Phase 1** – Early repolarization phase. With fast Na^+ channels closing, TMP is triggered above 0 mV before some K^+ channels open briefly and allow for an outward flow of K^+, which returns TMP back to 0 mV. Na^+ and K^+ channels are responsible for the small downward deflection present in the AP (spike-and-dome morphology).

- **Phase 2** – Plateau phase. The delayed rectifier K^+ channels cause a constant outflow of K^+, while an influx of Ca^{2+} is sustained through the L-type Ca^{2+} channels. Local elevations of intracellular Ca^{2+} promote its own release from intracellular calcium stores. This phenomenon, known as calcium-induced calcium release (CICR), initiates cardiomyocyte contraction. The two countercurrents, K^+ and Ca^{2+}, are electrically balanced during phase 2 of the AP, causing the TMP to plateau just below 0 mV.

- **Phase 3** – Repolarization phase. In this phase, Ca^{2+} channels are gradually inactivated while the continued outflow of K^+ through rectifier channels gradually restores the resting potential of the AP (between -95 and -85 mV). This potential is maintained throughout phase 4 by the activity of an inward rectifier potassium current and the currents associated with pumps and transporters.

1.3 Electrocardiogram

The electrocardiographic signal or electrocardiogram (abbreviated ECG in English or EKG in Dutch) is the biosignal most used by cardiologists for diagnostic purposes. The ECG is measured noninvasively and provides key information on the electrical activity of the heart. For decades, cardiovascular specialists have been analyzing ECG waveforms to diagnose different cardiac diseases and abnormalities, including arrhythmias and myocardial infarction, among others [132, 245].

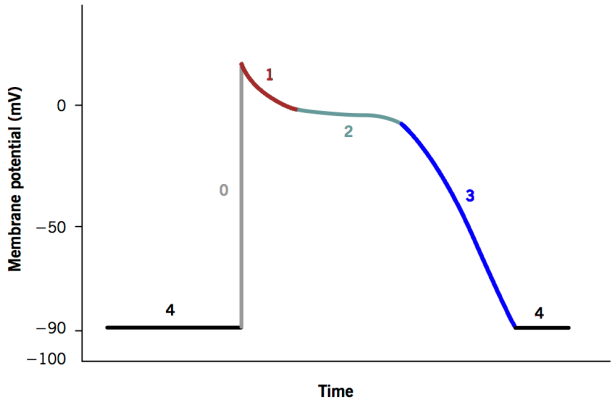

Figure 1.4 AP phases for a ventricular myocyte. Extracted and modified from [174].

The conventional ECG is made up of 12 leads that are subdivided into two groups: limb leads and precordial leads. Limb leads are classified into standard bipolar leads (I, II, and III) and augmented unipolar leads (aVL, aVF, and aVR).Precordial leads include leads V1 to V6. The limb leads provide a vertical-plane perspective of the heart, while the precordial leads view the heart's electrical activity in the horizontal plane. The position of the leads establishes distinct anatomical relationships: leads II, III and aVF capture the inferior surface of the heart; leads V1 to V4 capture the anterior surface; leads I, aVL, V5 and V6 capture the lateral surface; and leads V1 and aVR provide a direct view from the right atrium into the cavity of the left ventricle. The ECG represents a graphic record of the electrical activity of the heart during one cardiac cycle. The underlying principle that governs ECG recording involves an electromagnetic force, current, or vector characterized by both magnitude and direction. Depolarization currents moving toward the electrode are recorded as positive deflections, while those moving away are defined as negative deflections.

Positive and negative deflections, also called waves, are labeled with the letters P, Q, R, S, T, and U, as shown in Fig. 1.5. The timing and morphology of these waves are studied to identify cardiac pathologies that alter the electrical activity of the heart. The ECG waves, corresponding to the different phases of cardiac depolarization and repolarization, appear

as deviations from the isoelectric line, or baseline level, of the ECG. This line represents the resting state of all cardiac cells. The P wave represents the sequential activation of the right and left atria, and the QRS complex represents the activation of the right and left ventricles, with the left ventricle having a greater contribution due to its larger mass. The T wave represents the ventricular repolarization, whereas the U wave, which is not commonly observed, has been associated with the delayed repolarization of papillary muscles, Purkinje fibers, or ventricular regions. There is a period during which all the ventricular myocardium is depolarized, manifested as a nearly horizontal line between the end of the S wave and the onset of ventricular repolarization, known as the ST segment.

Other segments and intervals in the ECG signal include the PR (or PQ) segment and the PR interval, which represents the conduction of the impulse from the upper part of the atrium to the ventricle. The QT interval comprises from the beginning of ventricular depolarization through the plateau phase to ventricular repolarization.

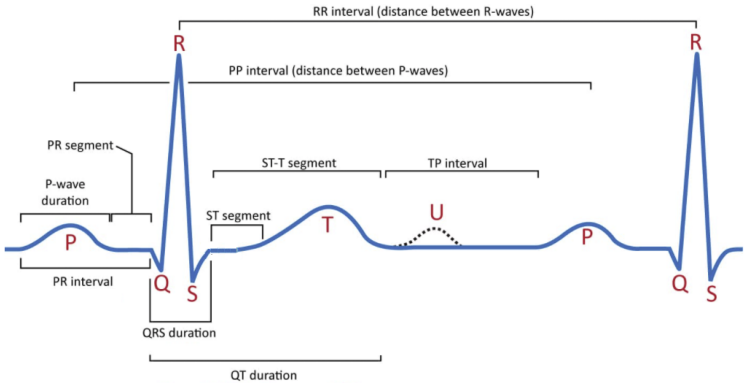

Figure 1.5 Waveforms, segments and intervals of a conventional ECG. Adapted from [378].

1.4 Autonomic Nervous System

Sustained ventricular arrhythmias are one of the most important causes of SCD, with an estimated 75% to 80% of cases [345, 188]. Bradyarrhythmias, which are characterized by abnormally slow resting heart rates of less than

60 beats per minute and irregular heart beats, as well as various conduction disorders, can cause syncope, fatigue due to chronotropic incompetence, and sudden death caused by asystole or ventricular tachycardia.

The three main factors involved in the development of arrhythmias are arrhythmogenic substrates, triggers, and modulators, which form Coumel's triangle of arrhythmogenesis [120]. Alterations in the Autonomic Nervous System (ANS) are considered relevant modulating elements [458], making the ANS a potential therapeutic target in the treatment of cardiac arrhythmias [126].

The ANS plays a critical role in regulating cardiac function through its two primary branches, namely the sympathetic and parasympathetic systems. Together, they regulate the dynamics of heart rate, rhythm, contractility, and electrical activity. Sympathetic innervation, often associated with the fight-or-flight response, originates mainly from the right and left stellate ganglia. The action of the sympathetic branch improves cardiac performance by increasing heart rate (positive chronotropy), strengthening myocardial contractions (positive inotropy), and accelerating atrioventricular conduction (positive dromotropy) [397]. The action of the parasympathetic branch (vagal activity) promotes self-maintenance rest and digest processes and is mediated through the vagus nerve, which originates in the medulla. The vagal system exerts its effects primarily by inducing bradycardia (negative chronotropy) and reducing myocardial contractile strength, resulting in a decrease in cardiac output [33, 291].

1.5 Abnormal cardiac conditions and diseases studied in this thesis

1.5.1 Microgravity

The effect of gravity on an object can be completely canceled out when it experiences a free fall. This state is called weightlessness. The term microgravity refers to a state in which weightlessness is not fully achieved, due to the existence of small residual forces, such as air drag or solar pressure.

Microgravity is expressed as a fraction of g, where g is the gravitational acceleration at the Earth's surface, on average 9.81 m/s^2 [116].

The relationship between microgravity and human health is a crucial field of research in space exploration. Under microgravity conditions, such as those experienced by astronauts in space, the effects of gravity on the human body are significantly altered. The absence of gravity force for a prolonged time has an impact on various physiological systems, including the cardiovascular, immune, and musculoskeletal systems [107]. One of the most notable phenomena is the hydrodynamic changes due to the redistribution of blood volume towards the upper body, which can affect the workload of the heart and the regulation of blood pressure. Furthermore, microgravity can cause a decrease in cardiac muscle mass and changes in the electrical function of the heart. Some known risks associated with microgravity and spaceflight missions in the cardiovascular system are orthostatic intolerance, decreased aerobic capacity, cardiac atrophy, and arrhythmias during orbital activities [391, 201, 139].

Space agencies have long been concerned about the potential impact of weightlessness in space on the increased risk of arrhythmia during spaceflight. Various instances of arrhythmias have been documented throughout human spaceflight and appear to be frequent but transient [413]. Premature atrial and ventricular contractions, short-duration atrial fibrillation, and nonsustained ventricular tachycardia are commonly reported occurrences. During the Gemini and Apollo missions, occasional premature ventricular contractions and premature atrial contractions were observed [31]. In particular, during the Apollo 15 mission, instances of premature ventricular beats and coupled ventricular contractions were observed in an astronaut [158]. Data from other studies [187] do not support the idea that there is a higher risk of arrhythmia in space, at least not with respect to atrial fibrillation.

Electrocardiogram analysis of astronauts or people subjected to microgravity usually shows electrophysiological alterations induced by molecular and cellular changes that cause channelopathies and later cardiomyopathies [157], as well as the presence of isolated ventricular extrasystoles, malignant arrhythmias, risk of repolarization instability, premature atrial contraction, increased QRS complex, QT and PR intervals, and even SCD [98, 70, 377, 391].

There are limited data from space missions. Thus, it is necessary to use ground-based models to simulate microgravity conditions [281]. The most accurate ground-based model to simulate the physiological changes associated with weightlessness is Head-Down Bed Rest (HDBR) [310]. During HDBR, participants remain in the head-down-tilt position all the time with their heads tilted 6° below the horizontal position for several days. This model is used mainly because of its ability to replicate headward fluid redistribution, achieved by maintaining a -6° angle of the bed [432]. This angle (-6°) produces an effect in the body comparable to a gravitational force of approximately -0.1 Gz. This setup creates a microgravity analogue characterized by immobilization, inactivity, confinement, elimination of gravitational stimuli, and induction of effects such as upward fluid shift, unloading of the body's upright weight, absence of work against gravity, reduced energy requirements, and overall reduction in sensory stimulation [89, 31].

Studies in simulated microgravity conditions provide valuable information on how the heart adapts to a gravity-free environment. This knowledge is essential for developing effective countermeasures that preserve the cardiovascular health of astronauts during long-duration space missions. Understanding the interaction between microgravity and the cardiac system not only benefits space exploration but also sheds light on cardiovascular physiology on Earth. Countermeasures designed to preserve cardiovascular health in astronauts when they are in space, such as specific exercise regimens, have been shown to be useful in preventing heart disease in athletes [63] and the general population [88]. These innovations contribute to the promotion of healthy lifestyles and prevention of common cardiac conditions [408].

1.5.2 Heart failure

In the last decade, between 1 and 2% of the Western adult population has been diagnosed with HF [315, 360]. HF represents the endpoint of many heart diseases [136]. The universal consensus on the definition of HF is a clinical syndrome with symptoms and/or signs caused by a structural and / or functional cardiac abnormality and corroborated by elevated levels of natriuretic peptides and / or objective evidence of pulmonary or systemic congestion [56]. Based on left ventricular ejection fraction (LVEF), there

are three subtypes of HF, namely HF with reduced ejection fraction, HF with midrange ejection fraction, and HF with preserved ejection fraction, according to the LVEF ranges $\leq$ 40%, 41-49% and $\geq$ 50%, respectively [360]. In Europe, based on 2019 Heart Failure Association ATLAS data, the median prevalence of HF is estimated to be 17 cases per 1000 people, ranging from less than 13 in Greece and Spain to more than 30 in Lithuania and Germany. The average annual incidence of HF in 12 member countries of the European Society of Cardiology was 3.2 per 1000 person-years [372]. The prevalence of HF in the United States was 24 per 1000 people in 2012 and will rise to 30 per 1000 people in 2030, according to the American Heart Association [162].

A significant risk factor for HF is ischemic heart disease (IHD). The population-attributable risk associated with HF and IHD is estimated to be 65% for men and 48% for women [412]. Globally, IHD contributed to 26.5% of the age-standardized prevalence rate of HF in 2017, with a higher incidence observed in areas of higher income [57]. Nevertheless, even in developing regions, IHD is emerging as a growing problem, reflecting the epidemiological changes accompanying economic and social development, characterized by an increasing burden of comorbidities and factors associated with lifestyle [137].

Hypertension is recognized as a contributing factor to HF. Various studies [125, 193, 227] have shown its role as the underlying cause in patients with HF and reduced LVEF. The evidence supporting hypertension as a trigger for HF is reinforced by the reduction in HF cases when hypertension is treated [359]. Analysis of HF cases from low-income countries reveals rheumatic heart disease as the primary etiology. Its prevalence ranges from 2.7 to 21.1 cases per 1000 inhabitants for manifest clinical and subclinical cases, respectively [96, 347].

Hospitalizations for HF constitute 1–2% of all hospital admissions in the western world [279]. HF is the most common cause of hospitalization among individuals over 65 years of age [44]. Approximately 30 to 40% of patients with HF have a history of hospitalization for HF [87, 143] and 50% are readmitted 1 year after their initial diagnosis of HF [277, 207]. The different causes of death might reflect the heterogeneity of the HF population in terms

of age, comorbidity burden, and, consequently, HF phenotypes. Although CV death predominates in HF, emerging evidence suggests a gradual shift towards non-CV death over the past two decades [358]. Most deaths in patients with HF are SCD and PFD [445]. Among patients who die from non-CV events, cancer diagnosis stands out as the most common cause of death, followed by infections and respiratory disease. Importantly, the proportion of CV deaths has decreased over time, mainly due to a decrease in the risk of sudden death [376, 262, 82].

A recognizable clinical categorization is that of acute versus chronic HF. Acute HF (AHF) is characterized by the onset of severe symptoms, typically manifesting as shortness of breath, that require urgent or emerging intervention, and therapy is directed to prompt the amelioration of these symptoms. Chronic HF (CHF), on the other hand, is often characterized by persistent but usually stable symptoms. Therapeutic interventions in CHF have also been shown to improve mortality and morbidity outcomes. Although there are instances of de novo AHF, the majority of cases of AHF represent decompensations of pre-existing CHF [287]. The New York Heart Association (NYHA) classification system is the simplest and most widely used method to describe the severity of HF (Table 1.1) [243]. The NYHA classification is based on symptoms and there are many other better prognostic indicators in HF [69].

There is no unique element in the clinical history or symptoms that could be a diagnostic of CHF, although many signs and symptoms in combination are helpful to assess the probability of HF [190]. Some tests for the evaluation of patients with suspected CHF, used to determine possible causes and identify comorbidities, are [170, 247]:

- **Physical tests**. Almost all patients with HF have dyspnea during exertion, but only 30% of the causes of dyspnea are associated with HF [267]. Some common physical examinations are related to hepatojugular reflux, cool, dependent edemas in the extremities, and cyanosis or pallor.

- **Blood and laboratory tests**. These tests can help identify alternative and potentially reversible causes of HF. B-type natriuretic peptides

	Description
Class I	No limitations of physical activity. Ordinary physical activity does not cause undue fatigue, palpitation or shortness of breath.
Class II	Slight limitation of physical activity. Comfortable at rest, but ordinary physical activity results in undue breathlessness, fatigue, or palpitations.
Class III	Marked limitation of physical activity. Comfortable at rest, but less than ordinary activity results undue breathlessness, fatigue, or palpitations.
Class IV	Unable to carry on any physical activity without discomfort. Symptoms at rest can be present. If any physical activity is undertaken, discomfort is increased.

Table 1.1 New York Heart Association functional classification based on severity of symptoms and physical activity. Adapted from [247]

(BNP) and N-terminal pro-BNP levels are used to assess dyspnea in patients. BNP is released by the atria and ventricles as a result of the stretching of the myocardial wall [270]. These changes could be associated with age, gender, anemia, body mass index, ethnicity, or other causes [119, 189]. Systematic reviews have concluded that BNP and N-terminal pro-BNP levels can effectively rule out a diagnosis of HF, but more screening is needed to establish the diagnosis [176, 28, 230, 315, 169, 270].

- **Chest X-ray**. This test allows to check changes in the size and shape of the heart, whether there is fluid in or around the lungs or air surrounding a lung, or whether a lung condition could be causing HF symptoms. It is almost considered an obsolete tool in some indications, but recent studies have shown its prognostic value for the quantification of congestion [254, 192].

- **Cardiac ultrasound, echocardiography**. The transthoracic echocardiograph is a method to assess cardiac function. It provides information on several parameters such as LVEF, chamber size, wall thickness, and

valve function and can confirm systolic or diastolic HF [206, 247, 302]. Its use is associated with a significant reduction in mortality [84].

- **Electrocardiography**. All patients with suspected HF should have an ECG [405, 247]. An abnormal ECG has a relatively high sensitivity for diagnosing HF, 89% (95% CI 77–95%), but moderate specificity 56% (95% CI 46–66%). This suggests that HF is quite unlikely in the presence of a normal ECG [236, 394]. The ECG may reveal cardiac abnormalities that increase the likelihood of a diagnosis of HF and may also guide therapy [247].

Pharmacotherapy is the main approach to the treatment of HF. It should be started before considering device therapy in combination with nonpharmacological interventions. Treatment for patients with HF is focused on three main goals: (i) reduce mortality; (ii) prevent recurrent hospitalizations due to HF worsening; and (iii) improve clinical status, functional capacity, and quality of life [10, 14, 315].

Modulation of the renin-angiotensin-aldosterone system and the sympathetic nervous system through the use of angiotensin-converting enzyme inhibitors (ACE-I) or an angiotensin receptor-neprilysin inhibitor (ARNI), beta-blockers, and mineralocorticoid receptor antagonists (MRA) has shown efficacy in improving survival, decreasing the risk of hospitalizations related to HF and reducing symptoms in patients with HF. These drugs are the core of the pharmacotherapy for these patients [249, 134, 194]. In addition, sodium-glucose cotransporter 2 (SGLT2) inhibitors dapagliflozin and empagliflozin, when added to ACE-I/ARNI/beta-blocker/MRA therapy, have shown a reduction in the risk of CV death and worsening of HF in patients with reduced LVEF [248, 293].

A high proportion of deaths in patients with HF, especially those with less severe symptoms, occur suddenly and unexpectedly. Many of them are due to electrical disturbances and acute vascular events [247, 447]. Implantable cardioverter defibrillators (ICDs) have been tested and found to be effective in rectifying potentially lethal ventricular arrhythmias and preventing bradycardia. Certain antiarrhythmic drugs can reduce the incidence of tachyarrhythmias and SCD, but they do not reduce overall mortality [32].

The decrease in the number of deaths due to SCD in patients with moderate or severe HF may be due to a worsening of their HF condition [32]. Consequently, ICD therapy is not recommended for patients with NYHA class IV, characterized by severe symptoms refractory to pharmacological therapy. Patients in this category have a markedly reduced life expectancy and are likely to suffer from PFD [357, 247].

Cardiac resynchronization therapy, CRT, is recommended for patients with reduced LVEF, sinus rhythm, and QRS duration $\geq$130 ms and for patients with NYHA Class III–IV with reduced LVEF, atrial fibrillation, and long QRS duration. This therapy shows a spectrum of stabilization or improvement in disease progression to even recovery of the disease [81, 440, 141]. Despite its known clinical and cost effectiveness, it remains underutilized as a treatment. In Europe, only one out of three eligible patients actually receives a CRT device due to a lack of awareness of CRT therapy [328, 133].

1.5.3 Cardiac pacing

Cardiac bradyarrhythmias, including sinus bradycardia, sinus node dysfunction, and high-grade AV block, can significantly alter ventricular filling and ejection efficiency [39], leading to electrical dyssynchrony by altering the normal sequence of myocardial activation [381]. When intrinsic pacemaker activity fails or conduction delays occur, the resulting bradycardia alters the coordinated spread of electrical impulses across the atria and ventricles. This leads to heterogeneous depolarization patterns, particularly in patients with pre-existing conduction system disease, exacerbating electrical dyssynchrony.

Electrical dyssynchrony is defined by an asynchronous electrical activation of the LV leading to a prolonged QRS duration (longer than 120 ms) on ECG, and may be due to conduction anomalies such as left bundle branch (LBB) block (LBBB) [129]. Numerous studies [399, 184, 379, 450] have shown the prevalence of ventricular dysfunction in patients with HF. In some mild cases, this dysfunction can predispose to bradyarrhythmias and worsen electrical dyssynchrony by creating zones of delayed conduction. In severe cases, this results in electromechanical dissociation, where delayed electrical activation fails to trigger synchronous mechanical contraction.

Much information on ventricular conduction abnormalities has been obtained using the 12-lead ECG. The duration and morphology of the QRS are ECG measurements to make a recommendation for the implantation of conventional pacing techniques in patients [141]. Although the use of QRS duration has generally been regarded a good marker to quantify asynchrony, this measurement cannot distinguish between conduction abnormalities on the right or left sides and between interventricular and intraventricular dyssynchrony [24, 45]. Regarding QRS morphology, it has been reported to be prone to subjective interpretation, and there are multiple definitions for specific conduction disturbances [276].

Pacing therapy remains an essential component in the treatment of bradyarrhythmias, but the choice of pacing site critically influences the outcomes. In recent years, various novel pacing techniques have been explored to determine if they offer benefits when clinical improvement does not occur using RVP or when conventional transvenous implantation is not successful. The placement of a lead in the cardiac conduction system has been shown to improve outcomes when the classical techniques are not effective [423]. CSP field is growing in interest due to the theoretical possibility of achieving physiological ventricular activation. The initial studies focused on HBP. Although HBP achieves excellent cardiac synchrony, its implantation can be challenging, with success rates ranging from 56% to 95% [41, 374, 424]. Long-term studies have raised concerns about ventricular undersensing and increasing thresholds [285, 305]. LBB Area Pacing (LBBAP) is a relatively recent form of CSP. This technique has shown promising results in observational studies for patients with HF. The reported success ranged from 80% to 94% and significant improvements in left ventricular systolic function were shown [294, 295, 453]. However, additional multicenter studies with longer follow-up periods will be necessary to validate the results obtained. Figure 1.6 shows different lead positions for CSP techniques.

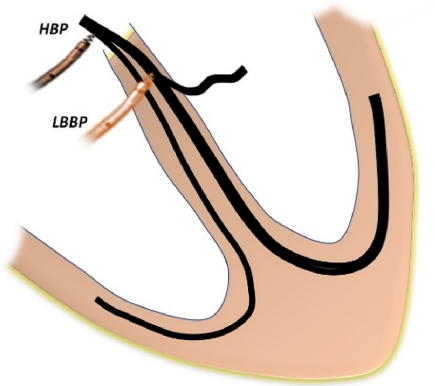

Figure 1.6 Lead position for common cardiac pacing techniques (CSP): His bundle pacing (HBP) and left bundle branch pacing (LBBP). Extracted and modified from [317].

1.6 Ventricular depolarization and repolarization markers

The use of the ECG allows for the characterization of electrical changes in the heart. Different ECG-based markers have been proposed to assess the risk of mortality for different cardiac conditions [205]. It is well known that electrical changes associated with the fast depolarization phase of the AP in ventricular myocytes produce the QRS complex of the ECG [19]. During repolarization, small gradients of membrane potential are observed between neighboring cells, which contribute to the generation of the cardiac electric field [23] and produce the T wave of the ECG. Repolarization heterogeneities across the ventricles are key in determining the characteristics of the T wave. Heterogeneity comes from the different activation times and the different durations of AP (APD) of the ventricular cells, attributed to the heterogeneous distribution of repolarizing currents across the ventricles [16, 274].

Several markers have been proposed to characterize abnormalities in the morphology of the T wave, the duration, area, and amplitude of the T wave, the symmetry, flatness, and notching properties of the T wave, and additional measures based on a vectorcardiographic representation (vectocardiogram, VCG) of the ECG. Some ECG repolarization markers evaluated in large population studies are:

- **QT interval:** It is the time interval measured between the onset of the Q wave and the end of the T wave, as shown in Figure 1.5. It represents the total duration of the depolarization and subsequent repolarization of the ventricles. A prolonged QT interval is widely acknowledged as an indicator of increased risk of Torsades de Pointes, a ventricular arrhythmia that can lead to syncope or SCD [386, 403], incident stroke [383], and severity of ischaemic heart disease [259].

- **Corrected QT interval:** Correcting the QT interval for heart rate is common to obtain measurements that are independent of heart rate, leading to a corrected QT (QTc). Various population-based QT heart rate correction formulas have been proposed in the literature, but not all adequately correct for the effect of heart rate in all populations. This has led to the proposal of so-called individualized formulas that take into account the specific characteristics of a population or an individual [257, 324]. The prolongation of the QTc interval has been identified as a marker of arrhythmic risk in the general population [205, 437].

- **QT dispersion:** The QT interval is known to vary between leads, which some studies hypothesized to reflect regional differences in ventricular repolarization. To quantify this variation, some studies proposed measuring a marker known as QT dispersion (QTd). QTd is calculated as the difference between the maximum and minimum QT intervals measured on all 12 leads of the ECG. Initially, it was suggested as an indicator of ventricular arrhythmia [99]. However, it was later determined that this dispersion of QT intervals may be caused by different projections of cardiac repolarization activity in the lead system [197], and may not necessarily be related to pro-arrhythmic activity [232].

- **QT variability:** Temporal variations in the QT interval of the ECG represent the beat-to-beat fluctuations in ventricular repolarization [354, 355]. Numerous studies have shown that temporal repolarization lability, as indicated by elevated QT interval variability (QTV), is associated with cardiac mortality [37, 364]. Although innovative techniques for assessing QTV have improved sensitivity and robust-

ness [38, 365, 289], current methods still fail to provide a complete description of QTV [37].

- **QT dynamicity:** Dynamic changes in cardiac repolarization can lead to increased vulnerability to ventricular arrhythmias [404]. Evaluating dynamic changes in ventricular repolarization can be performed by examining the relationship between the QT interval and heart rate [264]. Some studies have focused on the hysteresis of the QT interval after abrupt changes in heart rate and have quantified the time required by the QT interval to reach a steady state after a sharp increase or decrease in heart rate [324, 322, 327]. Mechanisms underlying prolonged adaptation of the QT interval in response to a sudden change in heart rate have been proposed [353, 326]. Other studies have evaluated the so-called QT dynamicity [300, 172, 37, 444] in 24-hour ECG recordings and have measured the slope of the steady-state QT-RR relationship. The capacity of all these markers as predictors of arrhythmic events has been tested [392, 147].

- **Tpeak-Tend (Tpe) and Tpe/QT ratio:** Tpeak-Tend (Tpe) is calculated by measuring the interval from the peak of the T wave to its end [319, 403]. Initially proposed as an indicator of transmural dispersion in ventricular repolarization [18], several experiments showed a correlation between an increase in Tpe and life-threatening arrhythmic events [421, 85, 71]. Other studies have suggested that Tpe may be a marker of global, rather than transmural, dispersion of repolarization [403]. Repolarization heterogeneity, measured by Tpe, may be associated with adverse outcomes, including mortality, in the general population [319]. To account for the dependence of Tpe on QT, some studies have proposed to divide Tpe by the QT interval, resulting in the Tpe/QT ratio. Despite dynamic changes in Tpe and QT, the Tpe/QT ratio remains relatively stable, falling within a range of values of 0.17 to 0.23. An increase in the ratio has been considered to possibly be indicative of a higher dispersion of repolarization, which could be proarrhythmic. However, its predictive value for arrhythmic events remains a matter of debate [149, 402].

- **Amplitude-based T-wave markers:** ECG markers have been proposed to characterize flatness, symmetry, and presence of notches in the T wave [13]. Markers describing flatness are determined on the basis of the kurtosis of the area-normalized JT segment. The symmetry markers are calculated from the ratio of the area under the ascending portion of the T wave to the area under the descending portion of the T wave, or, alternatively, from the respective durations. The notch score is derived from the radius of curvature of the JT segment, describing the degree of curvature or fluctuations present in this segment. It is important to note that symmetry markers based on gradients of the T wave are highly sensitive to high-frequency noise, which can easily distort the values of the ascending and descending slopes [59]. Nevertheless, this set of markers can be used to distinguish between patients with long QT syndrome and healthy controls [387].

- **T-wave alternans:** In addition to changes in the morphology of the T wve, beat-to-beat T-wave changes have been shown to consistently correlate with ventricular arrhythmia [298]. T-wave alternans (TWA) were one of the first candidates to characterize this spatio-temporal repolarization instability [309]. TWA involves a repeating ABAB pattern in the amplitude or shape of the ST-T complex. It has been proposed as an independent indicator of susceptibility to ventricular arrhythmias and has been applied in clinical evaluations [430, 416, 429]. The value of TWA for predicting the risk of cardiovascular mortality and SCD is based on the assessment of the degree of heterogeneity of ventricular repolarization and abnormalities in intracellular calcium cycling and voltage [404].

- **Periodic Repolarization Dynamics:** Periodic repolarization dynamics (PRD) is a novel ECG phenomenon that refers to previously overlooked oscillations of cardiac repolarization. These oscillations occur in the low frequency range (≤ 0.1 Hz) and are independent of the underlying heart rate variability [343]. PRD has been proposed to reflect the impact of phasic sympathetic activation on ventricular myocytes. PRD has been shown to be a significant predictor of mortality in cohorts of

patients with post-myocardial infarction, regardless of whether they have preserved or reduced LVEF [342, 340]. In this thesis, PRD has been used to assess sympathetic modulation of ventricular activity and to assess cardiac risk in different populations. High resolution ($\geq$ 1,000 Hz) ECG recordings were analyzed and techniques to robustly measure PRD were developed, with a comparison of their performance.

- **Activation and repolarization timing:** Although methods have been established to characterize ventricular activation time (AT) from electrograms [384, 325], there is still no consensus on how to determine repolarization times (RT). RT can be evaluated from electrograms using various markers associated with the slow repolarization phase of the AP [361]. In most of the works, the AT was defined as the interval from the onset of the QRS complex to local activation, while the RT was defined as the interval from the onset of the QRS complex to the local end of repolarization [361, 54, 200]. AT and RT have been used to assess changes over time during ventricular pacing in canine and rabbit models [435]. In this thesis, we propose to calculate AT and RT for each individual precordial ECG lead as the center of mass of the absolute QRS complex and the T wave, respectively. AT and RT, as well as the dispersion of AT (dAT) and RT (dRT) on the six precordial leads, are used to assess ventricular changes in patients who undergo different cardiac pacing techniques. Comparisons are made between the values obtained from the ECG recordings acquired in a basal state (before any stimulation) and those recorded during and after each type of cardiac stimulation.

1.7 Objectives of the thesis

The objectives of this thesis are to provide a better understanding of the influence of the sympathetic system on the electrical activity of the human ventricular observed in the ECG and to use it to, first, characterize the effects of microgravity and, second, assess the risk of SCD and PFD in patients with HF. In addition, this thesis aims to investigate how cardiac pacing has different effects on ventricular depolarization and repolarization depending

on whether the stimulation is applied to the ventricular myocardium or the electrical conduction system of the heart. ECG signals are processed and a set of markers is quantified both for arrhythmic risk stratification and for the characterization of pacing effects.

More specifically, the objectives of the different parts of this thesis are:

1. Propose strategies to quantify sympathetic modulation of ventricular electrical activity using ECG signals from healthy volunteers subjected to simulated microgravity. Since elevated sympathetic activity is often observed in microgravity due to environmental stress and this commonly manifests as orthostatic intolerance, tilt tests recordings during HDBR are analyzed. ECG markers quantifying PRD and HRV are evaluated and used for characterization of sympathetic effects on the ventricles before and after simulation of microgravity conditions.

2. Compare two methods, one based on Continous Wavelet Transform (CWT) and the other one based on Phase-Rectified Signal Averaging (PRSA), to calculate PRD. A correlation analysis is conducted to assess the similarity between the two methods. Upon confirmation that they are equivalent, a method is chosen for each application of interest.

3. Propose PRD thresholds to stratify patients with HF according to their risk of suffering from SCD and PFD. PRD is used as a risk marker individually and in combination with other clinical and ECG markers.

4. Characterize ventricular dyssynchrony generated by different cardiac pacing techniques. ECG markers are measured before and after applying a set of cardiac pacing techniques. High-frequency (1,000 Hz) and ultra-high-frequency (5,000 Hz) ECG recordings acquired at two different hospitals are analyzed and novel markers are proposed to assess the effects of pacing on the activation and repolarization sequences.

1.8 Outline of the thesis

The thesis is organized as follows.

- **Chapter 2: Periodic Repolarization Dynamics in simulated microgravity.** In this chapter, the techniques to calculate the PRD marker are described. This marker quantifies the magnitude of the low-frequency oscillations in the angle between consecutive T waves, which is related to sympathetic modulation of ventricular repolarization. ECG signals acquired from volunteers who underwent simulated microgravity using the HDBR model are analyzed. The capacity of two countermeasures, one physical and one dietary, to reduce or eliminate the adverse effects of microgravity is tested. Additionally, a study is carried out to compare the performance of two methods used for PRD calculation, one based on the wavelet transform and the other based on PRSA. The research described in this chapter has been published in a journal paper:

  – **S. Palacios**, E. Caiani, F. Landreani, J.P. Martínez and E. Pueyo. Long-term microgravity exposure increases ECG repolarization instability manifested by low-frequency oscillations of T-wave vector. *Frontiers in Physiology*, 10:1510, 2019.

  and was presented in the following conferences:

  – **S. Palacios**, J.P. Martínez, E. Pueyo. Changes in Sympathetic Modulation of ECG Repolarization Associated with long-term microgravity exposure. *XXXV Congreso Anual de la Sociedad Española de Ingeniería Biomédica*, Bilbao, Spain.

  – **S. Palacios**, E. Caiani, J.P. Martínez and E. Pueyo (2018). Microgravity Exposure Alters Sympathetic Modulation of Ventricular Repolarization Quantified from the ECG via Periodic Repolarization Dynamics. *XLV International Conference on Computing in Cardiology*, Maastricht, Netherlands.

  – **S. Palacios**, E. Caiani, E. Pueyo and J.P. Martínez (2019). Response of Ventricular Repolarization to Simulated Microgravity Measured by Periodic Repolarization Dynamics using Phase-Rectified Signal Averaging. *XLVI International Conference on Computing in Cardiology*, Singapore, Singapore.

  - **S. Palacios**, E. G. Caiani, J.P. Martínez and E. Pueyo (2019). Cardiac Response to Sympathetic Activation is altered by long-term microgravity exposure. *26th European Low Gravity Research Association Biennial Symposium and General Assembly. 14th International Conference on Two-Phase Systems for Space and Ground Applications*, Granada, Spain.

In addition, this work was awarded the following prizes:

  - Semifinalist of the *Rosanna Degani Young Investigator Award*, 2018. Microgravity Exposure Alters Sympathetic Modulation of Ventricular Repolarization Quantified from the ECG via Periodic Repolarization Dynamics. *XLV International Conference on Computing in Cardiology*.
  - *Mortara mobility fellowship*, 2019. Response of Ventricular Repolarization to Simulated Microgravity Measured by Periodic Repolarization Dynamics using Phase-Rectified Signal Averaging. *XLVI International Conference on Computing in Cardiology*.
  - Finalist of the *Rosanna Degani Young Investigator Award*, 2019. Response of Ventricular Repolarization to Simulated Microgravity Measured by Periodic Repolarization Dynamics using Phase-Rectified Signal Averaging. *XLVI International Conference on Computing in Cardiology*.

■ **Chapter 3: Sudden cardiac death prediction by Periodic Repolarization Dynamics.** In this chapter, high-resolution ECG recordings (1,000 Hz) from CHF patients are analyzed. PRD is calculated from ECG and is used as a risk marker to stratify patients for two endpoints, SCD and PFD. After comparing the prediction power of PRD and other clinical and ECG markers, new combined markers are derived and used for the prediction of SCD and PFD. The research described in this chapter was published in a journal paper:

  - **S. Palacios**, I. Cygankiewicz, A. Bayés-de-Luna, E. Pueyo and J.P. Martínez. Periodic Repolarization Dynamics as Predictor of

Risk for Sudden Cardiac Death in Chronic Heart Failure Patients. *Scientific Reports*, 11:20546, 2021.

and was presented in several conferences:

- **S. Palacios**, I. Cygankiewicz, A. Bayés-de-Luna, J.P. Martínez and E. Pueyo (2020). Sudden Cardiac Death Prediction in Chronic Heart Failure Patients by Periodic Repolarization Dynamics. *Proceedings of the XLVII International Conference on Computing in Cardiology*, Rimini, Italy.
- **S. Palacios**, I. Cygankiewicz, A. Bayés-de-Luna, E. Pueyo and J.P. Martínez (2020). Dinámica periódica de la repolarización como predictor de muerte súbita en pacientes con insuficiencia cardíaca crónica. *IX Jornada de Jóvenes Investigadores del I3A*, Zaragoza, Spain.
- **S. Palacios**, I. Cygankiewicz, A. Bayés-de-Luna, J.P. Martínez and E. Pueyo (2020). Predicción de muerte súbita en pacientes con insuficiencia cardíaca crónica mediante el estudio de la dinámica periódica de la repolarización. *XXXVIII Congreso Anual de la Sociedad Española de Ingeniería Biomédica*, Valladolid, Spain.
- **S. Palacios**, I. Cygankiewicz, A. Bayés-de-Luna, J.P. Martínez and E. Pueyo (2021). Estudio de la dinámica periódica de la repolarización para la predicción de muerte súbita en pacientes con insuficiencia cardíaca crónica. *I Congreso Anual de Estudiantes de Doctorado*, Elche, Spain.

■ **Chapter 4: Short-term evaluation of ECG ventricular depolarization and repolarization response to conventional and physiological pacing.** In this chapter, ultra-high-frequency ECGs (5,000 Hz) recorded before and after pacemaker implantation were analyzed. ECGs are acquired from patients who require cardiac pacing as antibradycardia treatment. The response to physiological pacing techniques is compared with the response to pacing techniques targeting the ventricular myocardium. ECG markers are proposed to assess spatial dyssynchrony in ventricular activation and repolarization. This chapter contains the

work carried out during a research visit to the MediSig Department of the Institute of Scientific Instruments (ISI) of the Czech Academy of Sciences in Brno under the supervision of Dr. Pavel Jurák. The results have been included in a manuscript that has been submitted for publication as a journal article.

- **S. Palacios**, R. Smisek, K. Curila, U. Nguyen, F.W. Prinzen, J. Halamek, F. Plesinger, P. Jurak, J.P. Martínez and E. Pueyo. Ventricular activation and repolarization in response to physiological and conventional pacing using ultra-high-frequency electrocardiography. 2025. Under review.

and was presented in several conferences:

- **S. Palacios**, K. Curila, U. Nguyen, F.W. Prinzen, J. Halamek, F. Plesinger, P. Jurak, E. Pueyo and J.P. Martínez (2023). Spatial Dispersion of Activation and Repolarization Times Associated with Different Cardiac Pacing Modes. *Proceedings of the L International Conference on Computing in Cardiology*, Atlanta, USA.
- **S. Palacios**, R. Smisek, K. Curila, U. Nguyen, F.W. Prinzen, J. Halamek, F. Plesinger, P. Jurak, J.P. Martínez and E. Pueyo (2023). Dispersión espacial de los tiempos de activación y repolarización asociada a diferentes modos de estimulación cardiaca. *XLI Congreso Anual de la Sociedad Española de Ingeniería Biomédica*, Cartagena, Spain.

■ **Chapter 5: Long-term evaluation of ECG ventricular depolarization and repolarization response to conventional and physiological pacing.** In this chapter, high-resolution ECG recordings (1,000 Hz) are processed to assess the effects of conventional and physiological techniques in patients with pacemaker implantation to treat bradycardia. The short- and long-term changes induced by both types of pacing techniques are analyzed. This chapter presents the results obtained from a scientific collaboration with Hospital Clínico Universitario Lozano

Blesa in Zaragoza, Spain. The research described in this chapter has been presented in several conferences and a journal paper is currently in preparation:

- C. Sales, **S. Palacios**, J. Melero, I. Julián, J. Ramos, J.P. Martínez, A. Mincholé, E. Pueyo (2022). Right Ventricular vs Left Bundle Branch Pacing-Induced Changes in ECG Depolarization and Repolarization. *Proceedings of the XLIX International Conference on Computing in Cardiology*, Tampere, Finland.
- **S. Palacios**, C. Sales, J. Melero, M. Cabrera, J. Ramos, A. Mincholé, E. Pueyo and J.P. Martínez (2024). Changes in Ventricular Repolarization After Right Ventricular and Left Bundle Branch Pacing. *13^{th} European Study Group on Cardiovascular Oscillations Meeting*, Zaragoza, Spain.
- **S. Palacios**, C. Sales, J. Melero, M. Cabrera, J. Ramos, A. Mincholé, E. Pueyo and J.P. Martínez. Electrical Dyssynchrony Comparison Between Right Ventricular Pacing and Left Bundle Branch Pacing. 2025. In preparation.

■ **Chapter 6: Conclusions and future work.** This chapter presents the most relevant conclusions of the thesis and discusses future extensions of the work.

Le cœur a ses raisons, que la raison ne connaît point; on le sait en mille choses.
The heart has its reasons which reason does not know. We feel it in a thousand things.

Pensées. Blaise Pascal

2

Periodic Repolarization Dynamics in simulated microgravity

2.1 Motivation

Over millions of years, humans, and all living organisms on Earth have adapted to live influenced by the gravity. This implies that a constant gravitational force has modeled the human anatomy and physiology. During spaceflight, astronauts experience an extended period of microgravity (μg), leading to various physiological responses. One of the initial responses is the inability of the vestibular system to adjust to the absence of gravity. A disease called space motion sickness, which has symptoms similar to other forms of motion sickness, includes pallor, increased body warmth, cold sweating, malaise, loss of appetite, nausea, fatigue, vomiting, and anorexia; occurs in astronauts during the first 72 hours of a space mission [349].

Other physiological adaptations due to microgravity are bone loss, muscle atrophy, fluid shifts, decreased plasma volume, and cardiovascular decondi-

tioning, leading to orthostatic intolerance and decreasing exercise aerobic capacity. Orthostatic intolerance emerges as a significant post-flight issue for astronauts, with an incidence of approximately 80% after long-duration spaceflight missions [251] and between 20% and 30% after short-duration missions [311].

Changes in convection, buoyancy, and sedimentation due to microgravity affect the human body, leading to cardiovascular problems (Table 2.1). In the absence of convection, there is no dissipation of body heat, impeding sweat evaporation, which leads to a potential disturbance in the perception of temperature, particularly in the lower extremities. Furthermore, in the absence of buoyancy, fluids characterized by varying densities, for instance, water and air, do not exhibit a tendency to segregate in a stratified manner; instead, air bubbles tend to persist in a suspended state within the water, requiring the application of an external force of acceleration to induce a separation between the fluids. In addition, in the absence of sedimentation, particles within the fluid environment tend to maintain an even distribution in suspension. This phenomenon could have implications on the functionality of the otoliths located in the inner ear, which are responsible for providing crucial information on the position of the body [278, 31]. Some important cardiovascular diseases induced by μg are found in Figure 2.1.

Variables	Initial Reaction	ST Response	LT Response	Ref
Blood volume	$\uparrow$	$\downarrow 10-15\%$	$\downarrow 10-15\%$	[413]
Haematocrit	$\uparrow$	$\downarrow 10-15\%$	Unchanged or $\downarrow$	[413, 202]
Cardiac output	$\uparrow$	$\uparrow 18-24\%$	$\uparrow 41\%$	[321, 380, 284, 283]
Stroke volume	$\uparrow$	$\uparrow 46\%$	$\uparrow 35\%$	[321, 283]
Ventricular size	$\uparrow 20\%$	$\downarrow 10\%$	$\downarrow 10\%$	[268, 46, 303]
Central venous pressure	$\downarrow$	$\downarrow$	$\downarrow$	[61, 128, 419]
Mean arterial pressure	Unchanged	Unchanged	$\downarrow 10$ mmHg	[283, 434, 156, 282]
Systolic blood pressure	Unchanged	Unchanged	$\downarrow 8$ mmHg	[283, 434, 156, 282]
Diastolic blood pressure	Unchanged	$\downarrow 5$ mmHg	$\downarrow 9$ mmHg	[283, 434, 156, 282]
Systemic vascular resistance	Unchanged	Unchanged	$\downarrow 39\%$	[283, 282]
Heart rate	Unchanged	Unchanged or $\downarrow$	Unchanged or $\downarrow$	[128, 255]

Table 2.1 Microgravity-induced cardiovascular adaptions. Abbreviations: References (Ref); short-term (ST); long-term (LT); increase ($\uparrow$); decrease ($\downarrow$). Adapted from [31]

Given the detrimental impact of the microgravity environment on human organ systems (such as the cardiovascular and musculoskeletal systems),

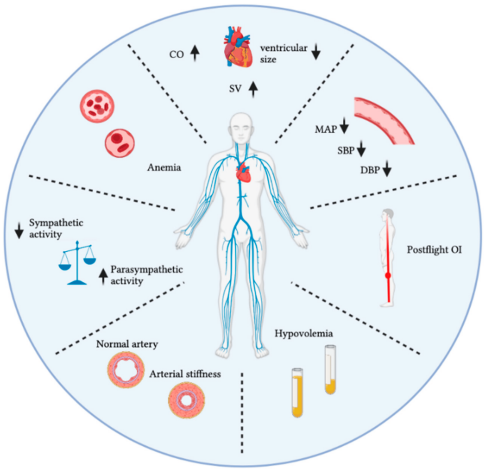

Figure 2.1 Spaceflight-induced cardiovascular diseases. Abbreviations: cardiac output (CO); stroke volume (SV); mean arterial pressure (MAP); systolic blood pressure (SBP); diastolic blood pressure (DBP); orthostatic intolerance (OI); increase (↑); decrease (↓). Source: [31]

it is necessary to develop appropriate tools and countermeasures to ensure successful space missions. Not all experiments can be performed in space due to constraints in time, costs, equipment, and manpower. Hence, ground-based models that mimic the effect of microgravity play a crucial role in complementing our understanding of the space environment and evaluating countermeasures for near-term spaceflight research [106].

Among the models developed are human analogs, including bed rest, physical stress, academic stress, and confinement, which simulate certain aspects of spaceflight stressors [395, 101]. Mechanical unloading and physical deconditioning, which are believed to be key components in the effects of microgravity on the human body, have also broader clinical applications on Earth, such as in the cases of prolonged bed rest or in inactive geriatric patients [349].

The most common *in vivo* ground-based analogue to simulate μg in bed rest is called HDBR. It is chosen because the observations of headward fluid redistribution (owing to a -6° angle of the bed, figure 2.2) exceed those observed in horizontal bedrest (without an angle) [432]. The HDBR model provides physiological changes similar to μg with respect to reduction of

bone mineral density, changes in bone architecture, increase in calcium levels in urine, increased susceptibility to renal stone formation, total peripheral resistance, systolic blood pressure, and fluid changes [301, 12, 31].

Figure 2.2 A subject is lying down and tilted at 6 degrees. Credit: German Aerospace Center (DLR)

To assess the functional response of the sympathetic nervous system within the cardiovascular system, it is common practice to activate the sympathetic reflex, as it facilitates the detection and localization of disorders related to the nervous system [456]. To test such a reflex arc, the afferent pathway of the autonomic reflex arc must initially be stimulated from the resting state of the human organism, typically through a suitable stimulus like an orthostatic test when assessing the baroreceptor reflex. It is essential for the test subject to remain in a relaxed state during the procedure, to be able to attribute any changes observed to the applied disturbance stimulus [436]. Therefore, each test should be performed after an adequate rest period, particularly when subjects have been in a prolonged position of bedrest.

The most straightforward and frequently used approach to evaluate cardiovascular feedback involves monitoring cardiovascular parameters (such as heart rate, blood pressure, and noradrenaline concentration) during a transition from lying horizontally to standing vertically [175]. This maneuver results in a temporary decrease in venous return to the heart, which consequently reduces stroke volume and arterial blood pressure [457]. The orthostatic test can be conducted actively, with the test subject standing independently (Schellong test), or passively, using a tilt table (ideally set at a 60° angle) for the tilt-table test (TTT) [26].

Exercise and nutrition (or medical drugs) have long been suggested as countermeasures to mitigate the effects of microgravity and to combat the sedentary nature of space living. A lower body negative pressure (LBNP) device is used to create ambient pressure lower than normal atmospheric pressure to the lower portion of the body, prompting a change in fluids towards the feet. The device consists of a sealed chamber attached to the iliac crest of the subject, with pressures ranging from -40 to -60 mmHg, simulating the force experienced on Earth [62, 393]. When combined with saline ingestion, typically 6–9 g of NaCl in 900–1200 ml of water, LBNP is typically used in spatial missions in the days leading up to landing to enhance orthostatic tolerance [135, 74]. Combined with treadmill running, LBNP serves as both a musculoskeletal countermeasure and cardiovascular countermeasure [269, 433, 460, 226, 366].

On the other hand, a high-protein diet resulted in mild metabolic acidosis, affecting bone metabolism after bed rest [459]. To counteract the acidifying effects of whey protein, some researchers combined it with a potassium bicarbonate supplement in bed rest studies. Although this combination partially mitigated skeletal muscle atrophy, it also diminished the reductions in muscle fiber oxidative capacity due to disuse [47, 53]. The main types of pharmacological drugs are related to caloric restriction, polyphenols, natural extracts, and medications to directly counteract adverse effects [273]. These countermeasures are mainly designed to improve skeletal muscle mass and strength [462, 52, 220], but more research is necessary to determine if they also produce improvements in cardiovascular health.

PRD is an electrocardiographic index that measures low-frequency oscillations (below 0.1 Hz) in cardiac repolarization instability related to sympathetic activity. It was first described in 2014 by Rizas et al. [343]. Considering the substantial evidence suggesting the pivotal role of sympathetic mechanisms in the development of malignant tachyarrhythmias [234, 221, 348], PRD is one of the markers for assessing the influence of sympathetic activity on ventricular changes through surface ECG recordings.

In this chapter, the PRD biomarker was measured from ECG recordings to assess sympathetic activation in a group of volunteers subjected to long-term HDBR (60 days). To provoke sympathetic activation, the tilt test was applied

to all subjects before starting and at the end of the HDBR period. In addition, two types of countermeasures, physical exercise and a specific diet, were tested to determine whether they were capable of mitigating the negative effects of microgravity simulation on the cardiovascular system.

2.2 Materials

2.2.1 Head-Down Bed Rest experiments

ECG recordings were acquired from two long-term (60 days) -6° HDBR campaigns organized by the European Space Agency (ESA) as part of their bed rest studies. These studies were carried out between 2015 and 2017 in the :envihab facility of the Institute of Aerospace Medicine at the German Aerospace Center-DLR (Cologne, Germany) and at the Institute of Space Medicine and Physiology-MEDES (Toulouse, France).

For both studies, the inclusion criteria were as follows: male, between 20 and 45 years old, body mass index between 20-26 kg/m^2, non-smoking, no medication, no competitive athlete and no history of bone fractures. The characteristics at baseline are shown in Table 2.2. In Cologne, 22 volunteers (29 ± 6 years, 181 ± 5 cm, 77 ± 7 kg) were enrolled and randomly distributed into the countermeasure group (JUMP), who performed physical activities during the HDBR time period, or the control group (CTRL), who did not exercise.

For the Toulouse experiment, 20 volunteers were enrolled (34 ± 7 years, 176 ± 4 cm, 73 ± 7 kg). They were randomly assigned in a double-blind manner to the countermeasure group (NUTR), receiving a nutritional countermeasure daily consisting of a cocktail of antioxidants and vitamins, or to the control group (or placebo) (CTRL), who did not receive this nutritional integration.

All subjects underwent a comprehensive medical examination prior to the selection process and provided their written informed consent to participate in the study, which was approved in advance by the respective Ethics Committees for Human Research at the host institutions.

	DLR		MEDES	
	CTRL	JUMP	CTRL	NUTR
N	12	12	10	10
Age (years)	28 ± 6	30 ± 7	34 ± 8	35 ± 7
Heigh (cm)	180 ± 7	182 ± 5	176 ± 5	176 ± 5
Body mass (kg)	78 ± 8	72 ± 5	75 ± 9	73 ± 6
BMI (kg/m2)	24 ± 2	23 ± 2	24 ± 2	24 ± 2

Table 2.2 Volunteers' anthropometric characteristics at baseline for DLR and MEDES campaigns. Data are means and standard deviations; N, sample size; BMI, Body Mass Index.

2.2.2 Experimental Protocol

Both campaigns were divided into three phases: 15 days of PRE-HDBR baseline (BDC-15 to BDC-1), when subjects became physiologically and psychologically accustomed to the facilities; 60 days of bed rest (HDT1 to HDT60), when subjects were in strict –6° HDBR (24 h/day); and 15 days of recovery from POST-HDBR (R+0 to R+14). The subjects were continuously monitored by the medical and paramedical staff to ensure compliance with the protocol. Figure 2.3 illustrates these three phases.

Each subject was accommodated in a single-person room, in the DLR campaign, or in double bedrooms, in MEDES campaign. These rooms were equipped with television, telephone, and laptop computer with Internet access. During the pre-bed rest and recovery phases, the subjects were allowed to walk freely and slept at 0° (supine position). From HDT1 to HDT60, subjects carried out all activities in -6° HDBR: eating, hygienic procedures (teeth brushing, bowel movement, showering) and free time activities (reading, watching, or using the computer). At any given moment, at least one shoulder was kept on the bed. Also, all subjects had the same scheduled wake-up (at 6:30 a.m. and 7:00 a.m. in the DLR and MEDES campaigns, respectively) and light-off (at 11:00 p.m.).

Two orthostatic TTTs were performed, one 2 days before the start of the HDBR period (BCD-2) and the other just after completion (R+0). In each TTT, the subject was tilted head-up to an angle of 80° for up to 15 min. If the subject did not experience any presyncopal episode during that time,

Figure 2.3 Scheme of HDBR experiments and date of each tilt-table test. BCD-2, two days prior 60-day HDBR; R+0, after finishing HDBR experiment

he was exposed to LBNP following a protocol of 3-min –10 mmHg steps for a maximum duration of 15 min. Thirty of the 84 recordings analyzed did not have presyncopal episodes when TTT was performed, of which 18 corresponded to PRE-HDBR and 12 to POST-HDBR.

The JUMP group training protocol during the 60 days of HDBR comprised a total of 48 training sessions. Each training session consisted of performing squats, heel raises, hops, and countermovement jumps against a resistive force, while lying in a horizontal position on a sledge jump system.

During their bed rest phase, subjects in the NUTR group received a daily antioxidant supplement in terms of six pills (two pills per meal). They consisted of a polyphenol supplement equivalent to a daily dose of 530 mg of polyphenol, 168 mg of vitamin E, 80 μg of Selenium-Solgar®, and 2.1 g of Omega-3 – Omacor®.

2.3 Methods

High-resolution (1,000 Hz) 24-hour Holter 12-lead ECG signals (Mortara Instrument) recorded on days BCD-2 and R+0 (both including a TTT) were available for this study. For each TTT, a 5-minute interval prior to the start of the tilt phase, the first 5 minutes immediately following its start, and the last 5 minutes of the tilt phase (possibly including LBNP) were analyzed (Figure 2.4). If the tilt phase lasted for less than 5 minutes, its entire duration was analyzed.

2.3.1 Preprocessing

Raw ECG signals were preprocessed with a 50 Hz notch filter to remove powerline interference. Taking these preprocessed ECG signals as input, QRS

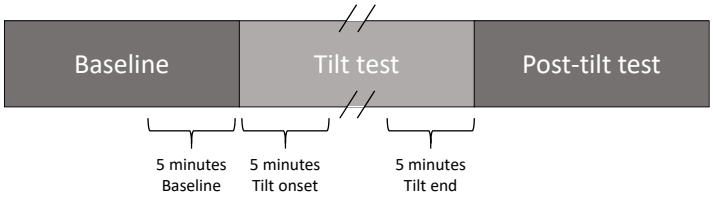

Figure 2.4 Timing for 5-minute ECG recording before, during and at the end of each tilt-table test

detection and ECG wave delineation were performed using a wavelet-based single-lead automatic system [242]. The output of the detection and delineation system was combined using rules to obtain multi-lead ECG delineation marks [242]. Since subsequent analysis focused on the T wave, a 40 Hz low-pass filter was applied to remove noise without altering the shape of the T wave. Finally, cubic spline interpolation was applied to estimate and remove baseline wander. An example of an ECG recording as originally acquired and after applying different pre-processing steps is shown in Figure 2.5.

2.3.2 Angles between consecutive T waves

To obtain the PRD marker, the change in angles between consecutive T waves, dT° is calculated from preprocessed ECG signals. An updated method based on the original method proposed in [343] was applied to the preprocessed ECG signals to compute the angles between consecutive T waves. This method introduced a refinement on the temporal window for the T-wave definition so as to guarantee that the two consecutive T waves involved in each angle computation had comparable T-wave onset and end windows, as follows:

1. Orthogonal leads X, Y, and Z were obtained from the 12-lead ECG using the inverse Dower matrix [112].

2. The onset and end of each T wave, denoted by T_{on} and T_{off}, were identified by the delineation system described above. When the delineation failed to identify a T-wave onset (T-wave end, respectively) for a given beat, its location was established based on the locations of T_{on} (T_{off}, respectively) for adjacent beats with respect to their corresponding

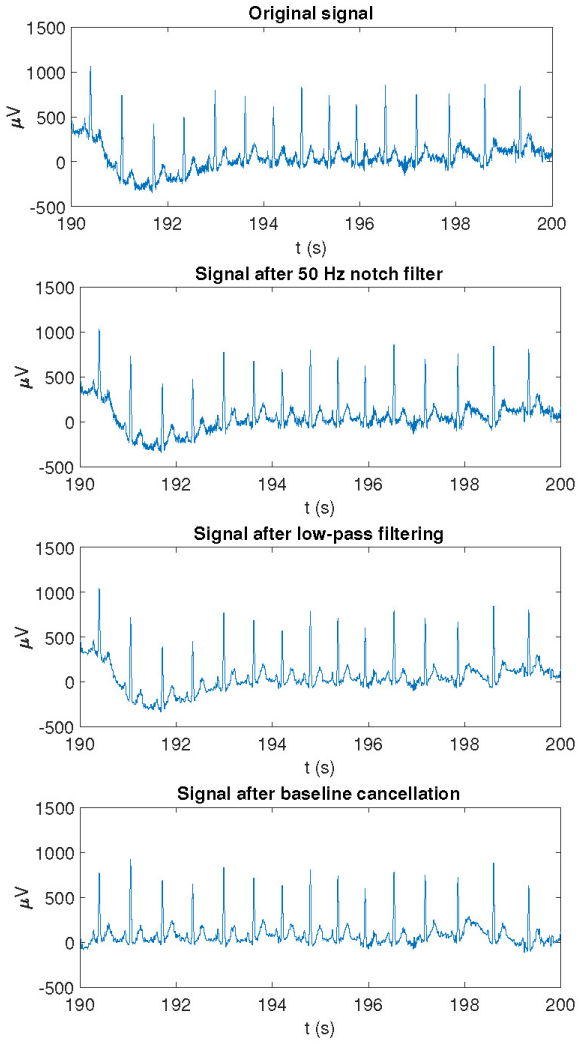

Figure 2.5 Example of an ECG recording as originally acquired and after application of different preprocessing steps

QRS positions. Specifically, T_{on} (or T_{off}) was located at a distance from the corresponding QRS fiducial point equal to the median interval between the QRS position and the T_{on} position (or T_{off} position) of 30 beats around that beat.

As T-wave boundaries change on a beat-to-beat basis and may be influenced by delineation errors, the angle between each two consecutive T

waves was computed by defining a unique temporal window for both waves being analyzed. Specifically, for each angle calculation, the window onset was set at the latest T_{on} of both analyzed beats calculated with respect to their QRS fiducial points, while the window end was set at the earliest T_{off} of both beats computed from their QRS fiducial points.

3. A constant value was subtracted from each T wave in each of the analyzed leads so that the amplitude at T_{off} was set to 0 mV. Subsequently, an average T-wave vector was calculated for each T wave. The angle dT$^\circ$ between two consecutive T waves, which is associated with the instantaneous degree of repolarization instability, was calculated using the dot product of each pair of consecutive average T-wave vectors.

4. The dT$^\circ$ time series was filtered by using a 10th-order median filter to attenuate outliers and avoid very abrupt changes in the time series.

Steps (1) to (3) are illustrated in Figure 2.6.

2.3.3 PRD Computation

After the series of angles was obtained, PRD was calculated. Two different methods, based on CWT and PRSA, respectively, were developed based on the initial methodology proposed in [343, 341]. Whereas the original method in [343] used spherical coordinates, the present method used Cartesian coordinates, which reduced errors for cases where the T-wave vectors were near the axes. These methods were tested for quantification of the low-frequency components of the beat-to-beat dT$^\circ$ series.

PRD computation using Continuous Wavelet Transform

CWT is one of the most widely used tools for time-frequency analysis [5]. Based on the dT$^\circ$ series calculated as described in 2.3.2, the next steps were followed to calculate PRD [343]:

5. The dT$^\circ$ series was linearly interpolated at 2 Hz and a 10-sample moving average filter was applied in order to remove artifacts.

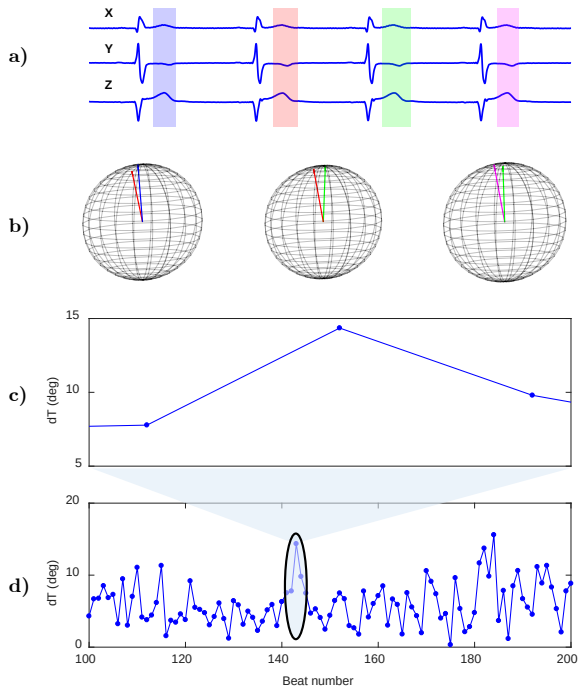

Figure 2.6 Illustration of steps for PRD calculation from ECG recording in Frank lead configuration: a) T waves for four consecutive beats. b) Three-dimensional visualization of each pair of T-wave vectors. c) and d) Angle between two consecutive T-wave vectors, dT°, along 100 beats.

6. CWT was calculated on all scales from 1 to 40 using a a 4th-order Gaussian wavelet to quantify the low-frequency oscillations of dT°. Wavelet coefficients were obtained for each scale at each time point, and an average wavelet coefficient was computed for each scale.

7. Each scale, a, was transformed into pseudo-frequencies (F_a, measured in Hz) using the following Equation 2.1 ([3]), considering the center frequency of the wavelet in Hz, F_c and the sampling period in seconds, Δ:

$$F_a = \frac{F_c}{a \cdot \Delta} \tag{2.1}$$

PRD_{CWT} was defined as the average wavelet coefficient in the frequency range between 0.025 and 0.1 Hz.

Note that the number of samples used for the moving average filter in this study is 10, but originally [343], it was 30. This change minimizes the distortion of relevant information in the frequency band of interest.

PRD computation using PRSA

An alternative method to compute oscillatory fluctuations has been proposed, with less computational requirements, based on PRSA [36]. The following steps were followed to calculate PRD from the dT° series [341]:

5. Anchor points were defined by comparing averages of M=9 values of the dT° series previous and posterior to the anchor point candidate (x_i). A beat i is considered an anchor point if:

$$\frac{1}{M}\sum_{j=0}^{M-1} x_{i+j} > \frac{1}{M}\sum_{j=1}^{M} x_{i-j} \tag{2.2}$$

6. Windows of 2L values were defined around each anchor point. If an anchor point was so close to the beginning or end of the dT° series that there were not enough samples before or after it, it was disregarded. In this study, L=20 was chosen because it was the minimum value to detect frequencies in the range of interest (0.025 - 0.1) Hz.

7. PRSA series was obtained by averaging the dT° series in all defined windows.

PRD_{PRSA} was defined as the peak-to-peak amplitude of the PRSA series. This computational technique is different from the original method, which used spectral analysis, and is therefore less computationally demanding.

A graphical summary of the steps described for both methods (PRD_{CWT} and PRD_{PRSA}) is shown in Figure 2.7.

2.3.4 Heart Rate Variability Analysis

RR interval series were computed from QRS detection marks obtained in section 2.3.1 for all 5-minute segments analyzed at baseline, as well as at the

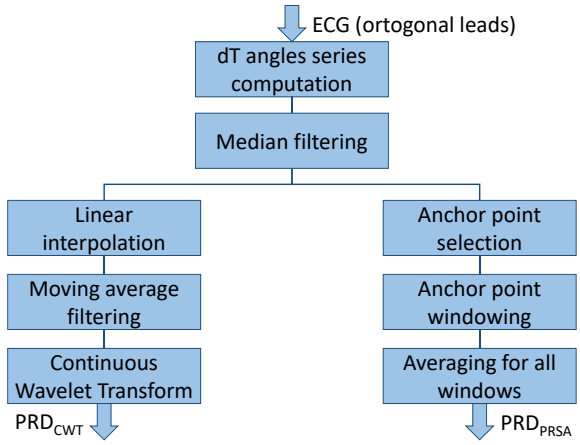

Figure 2.7 Steps applied to compute PRD from orthogonal ECG leads through Continuous Wavelet Transform (CWT) and Phase-Rectified Signal Averaging (PRSA) techniques.

beginning and end of TTT. Instantaneous heart rate (HR) variability (HRV) series were calculated following the method described in [27]. For each segment, the power spectral density (PSD) of HRV was computed using the periodogram method. A high-frequency band (HF, [0.15, 0.4] Hz) and a low-frequency band (LF, [0.04, 0.15] Hz) were defined for HRV analysis in the frequency domain and the LF and HF powers were calculated by integrating the power spectrum in each of those two bands, respectively. The normalized LF power (LFn), the normalized HF power (HFn), and the ratio between the power in the LF and HF bands (LF / HF) were calculated [233]. The median HR (HR_{median}) was also calculated.

2.3.5 Statistical Analysis

Data are presented as median ([interquartile range, IQR]), unless otherwise specified. The Mann-Whitney U test (or Wilcoxon rank-sum test) was used to compare independent samples, as when comparing each countermeasure subgroup (JUMP or NUTR) with the corresponding CTRL subgroup. The Wilcoxon signed-rank test was used for the comparison of paired samples, as when comparing changes induced by HDBR or TTT in a given group of subjects. The Spearman correlation coefficient ρ and Kendall's τ were

used to quantify the rank correlation between CWT and PRSA. All statistical analyses were performed with MATLAB R2017a (9.2).

2.4 Results

2.4.1 Comparison of PRD Computed by CWT- and PRSA-Based Methods

Figure 2.8 shows the two analyzed recordings, at PRE-HDBR and POST-HDBR, of a volunteer who presented small and large magnitudes of low-frequency oscillations in ventricular repolarization, respectively. The three plots represent the dT° series, the frequency pseudospectra (in terms of squared wavelet coefficients) and the PRSA series. The blue line corresponds to the ECG segment in PRE-HDBR and the red line corresponds to the ECG segment at POST-HDBR. Note that the case shown in blue presents low-frequency oscillations in dT° of small magnitude, which translates into low values of PRD_{CWT} and PRD_{PRSA}. The red case, in contrast, presents low-frequency oscillations in dT° of greater magnitude and is associated with considerably higher PRD values, both when measured by using CWT- and PRSA-based methods.

Figure 2.9 shows the correlation of PRD values computed using the CWT-based method (X-axis) and the PRSA-based method (Y-axis) for all segments analyzed (baseline, beginning, and end of the tilt phase) in the CTRL group of the DLR and MEDES campaigns, both PRE-HDBR and POST-HDBR. The scatterplot shows a strong correlation between both methods. The rank correlation coefficients were: Spearman's $\rho = 0.93$ ($p < 10^{-50}$), Kendall's $\tau = 0.79$ ($p < 10^{-35}$).

Taking into account the correlation results between both methods, PRD will be computed using the PRSA technique, PRD_{PRSA}.

2.4.2 Tilt-Test-Induced Effects on PRD

After finding that both PRD calculation methods are statistically equivalent, the response of the cardiovascular system to TTT is analyzed.

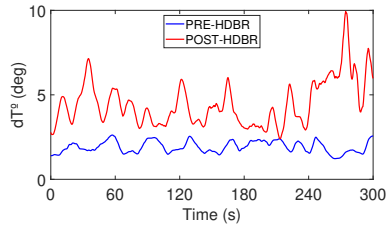

(a) dT° series computed from a ECG recording during PRE-HDBR (in blue) and POST-HDBR (in red)

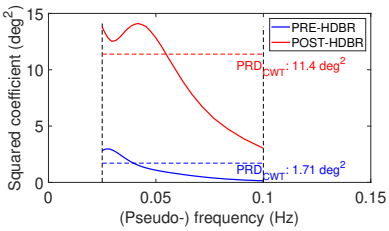

(b) Frequency pseudospectra and PRD values for signal recorded during PRE-HDBR (in blue) and POST-HDBR (in red)

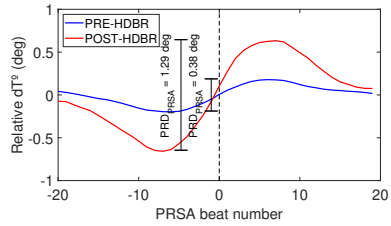

(c) PRSA series and associated PRD values for dT° during PRE-HDBR (in blue) and POST-HDBR (in red)

Figure 2.8 (a) Examples of dT° series, (b) frequency pseudospectra and (c) PRSA series for a 5-minute ECG recording from a subject days before (in blue) and after long-term HDBR (in red)

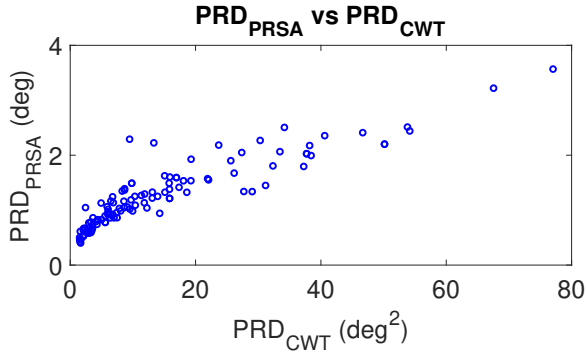

Figure 2.9 Scatterplot of PRD values measured by CWT- and PRSA-based methods

Figure 2.10, top panel, shows the results of the analysis of three 5-minute segments of the dT° series, corresponding to the baseline (before tilt) and the beginning and end of the tilt phase, for all volunteers in the CTRL group of both campaigns (DLR and MEDES). Results are presented separately for PRE-HDBR (before HDBR) and POST-HDBR (after HDBR). As can be seen in the figure, PRD increased after tilt compared to baseline, with the results being statistically significant when the segment at the beginning of the tilt phase was analyzed. This was true for both PRE-HDBR and POST-HDBR. The results on the effects of tilt on the HRV indices LFn and LF/HF are presented in the bottom panels of the figure 2.10. Both indices showed significantly higher values in response to tilt, indicating an increase in sympathetic drive during orthostatic stress, both at PRE-HDBR and POST-HDBR. The effect of tilt on other HR and HRV indices is presented in Figure 2.11, which shows a significant increase in HR_{median} and a significant decrease of HFn in response to tilt.

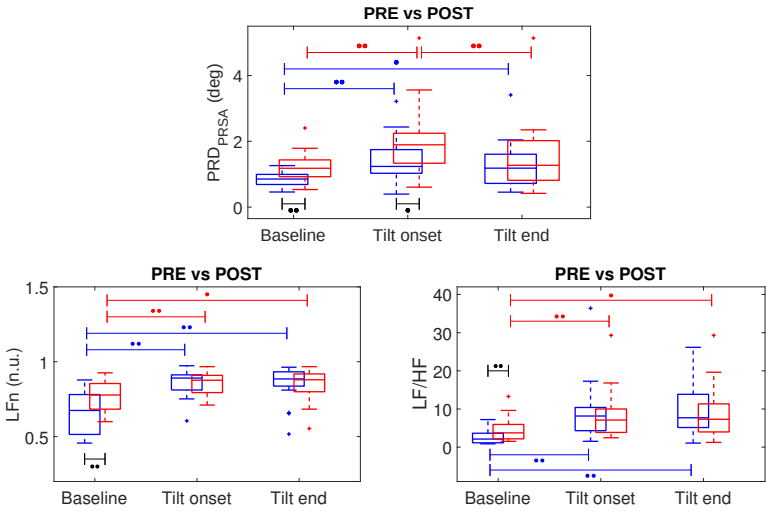

Figure 2.10 Boxplots of PRD, LFn and LF/HF at PRE-HDBR (in blue) and POST-HDBR (in red) evaluated at three TTT stages: baseline, the beginning and end of the TTT. ••p<0.01, •p<0.05 (Wilcoxon signed-rank test)

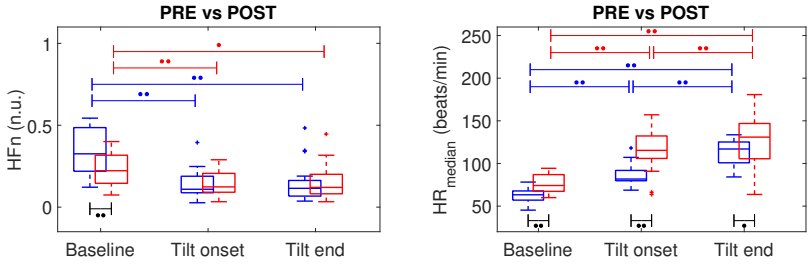

Figure 2.11 Boxplots of HFn and HR_{median} at PRE-HDBR (in blue) and POST-HDBR (in red) evaluated at three TTT stages: baseline, the beginning and end of the TTT. ••p<0.01, •p<0.05 (Wilcoxon signed-rank test)

2.4.3 Microgravity-Induced Effects on PRD

The effects of microgravity exposure on PRD obtained by comparing PRE-HDBR and POST-HDBR for the CTRL group of the DLR and MEDES campaigns can be observed from Figure 2.10. At baseline (before TTT), PRD increased significantly in POST-HDBR compared to PRE-HDBR, changing from 0.85 [0.31] deg at PRE-HDBR to 1.18 [0.51] deg at POST-HDBR ($p<0.01$), as presented in the left columns of Figure 2.10.

Taking into account the analysis at the start of the tilt phase, PRD also increased at POST-HDBR compared to PRE-HDBR, changing from 1.24 [0.72] deg at PRE-HDBR to 1.89 [0.91] deg at POST-HDBR ($p<0.05$), as shown in the middle columns of Figure 2.10.

No statistically significant differences were observed in PRD in POST-HDBR versus PRE-HDBR when analyzed at the end of the tilt phase (right columns in Figure 2.10), although there was a trend to increase PRD in POST-HDBR compared to PRE-HDBR. Specifically, PRD increased from 1.18 [0.88] deg at PRE-HDBR to 1.27 [1.21] deg at POST-HDBR (n.s.).

In the case of the HRV indices LFn and LF/HF, statistically significant microgravity-induced increases were observed when the baseline period was analyzed (see Figure 2.10). Specifically, LFn changed from 0.67 [0.27] n.u. at PRE-HDBR to 0.78 [0.17] n.u. at POST-HDBR ($p<0.01$). LF/HF changed from 2.12 [2.51] in PRE-HDBR to 3.74 [3.78] at POST-HDBR ($p<0.01$). The index HFn decreased significantly from PRE-HDBR to POST-HDBR when evaluated at baseline, whereas HR_{median} increased significantly due to

microgravity, either when evaluated at baseline or at the beginning and end of the tilt test (figure 2.11).

2.4.4 Relation between PRD and HRV

A correlation analysis between the HRV indices (LFn, LF/HF and HR_{median}) and PRD has also been carried out to verify if there is any relation between them. This analysis applied to tilt-induced changes (for onset or end of tilt with respect to baseline) in PRD and HRV indices before and after microgravity simulation, is illustrated in figure 2.12. The results show that no significant correlation was detected between the effect of the tilt test on PRD and on HR or HRV, neither in PRE-HDBR nor in POST-HDBR, since Spearman's correlation coefficient (ρ) remained below 0.15 in all evaluated cases (n.s.).

2.4.5 Effectiveness of Exercise-Based Countermeasure

The effectiveness of the applied jump-based countermeasure in counteracting the effects of simulated microgravity was assessed by comparing PRD values at PRE-HDBR and POST-HDBR in both the CTRL and JUMP subgroups of the DLR campaign. PRD values for each phase of the TTT are presented in table 2.3. Although there were increases in PRD values from PRE-HDBR to POST-HDBR in both the CTRL and JUMP subgroups, the increase was much more attenuated in the JUMP subgroup. Significant differences were found at the start of the tilt for both the CTRL and JUMP subgroups (Table 2.3). Due to the high PRD values, the relative terms (ΔPRD) are evaluated. Illustrations of the effects of the JUMP countermeasure are presented in figure 2.13 (left panel), which shows the values of Δ PRD, calculated as the difference of PRD values in POST-HDBR minus the PRD value at PRE-HDBR for each subject. From the figure it is clear that while the median values of ΔPRD were mostly positive in the CTRL subgroup, particularly during the tilt phase, the values were remarkably closer to 0 in the JUMP subgroup.

2.4.6 Effectiveness of Nutrition-Based Countermeasure

The results on the effectiveness of a nutrition-based countermeasure are presented in table 2.4. Figure 2.13 (right panel) illustrates these results in terms

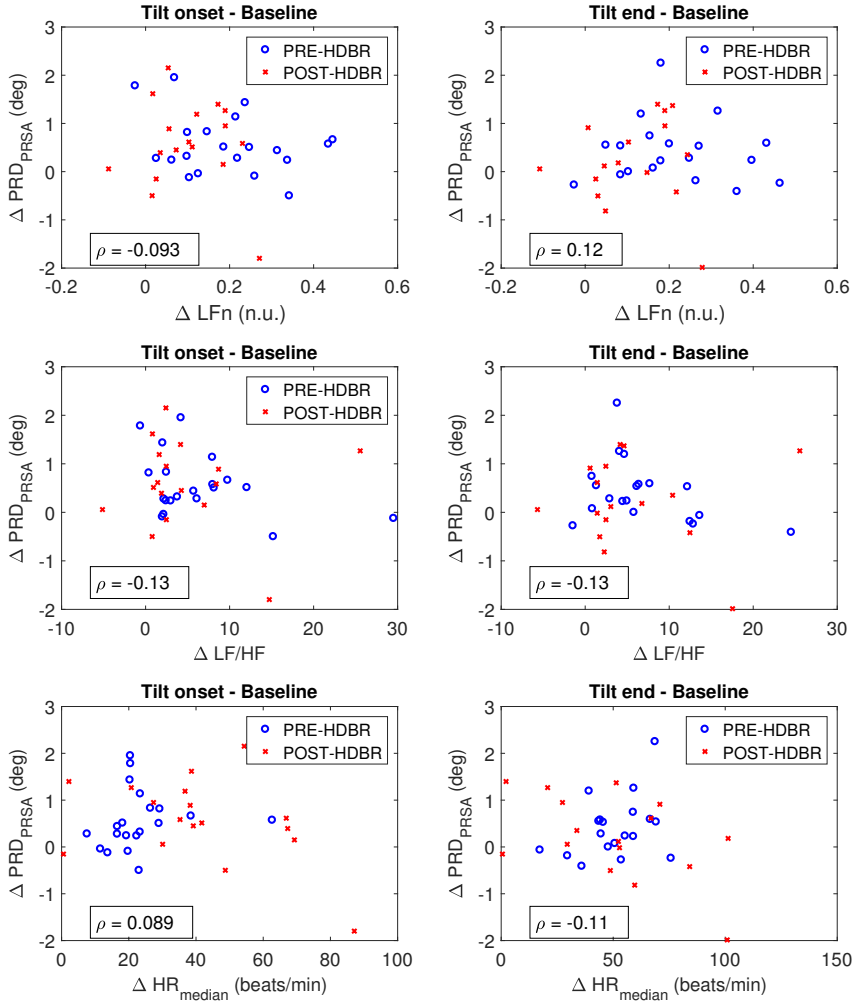

Figure 2.12 Scatterplots of ΔPRD_{PRSA} and change in HR or HRV indices measured as the difference between the values at the beginning of the tilt phase with respect to baseline values. Values corresponding to PRE-HDBR are shown in blue circles and those corresponding to POST-HDBR are shown in red crosses. Spearman's correlation coefficient ρ is shown for each tested association.

	PRD	PRE-HDBR (deg)	POST-HDBR (deg)
Baseline	CTRL	0.78 [0.40]	0.93 [0.79]
	JUMP	0.72 [0.34]	0.81 [0.47]
Tilt onset	CTRL	1.32 [1.40]	2.04 [0.99] *
	JUMP	0.77 [0.29]	1.28 [0.77] *
Tilt end	CTRL	0.95 [0.98]	1.48 [1.12]
	JUMP	0.85 [0.51]	1.02 [0.59]

Table 2.3 PRD values (median [IQR]) at all phases of TTT for PRE-HDBR and POST-HDBR in CTRL and JUMP subgroup. *p<0.05 (with respect to PRE-HDBR)

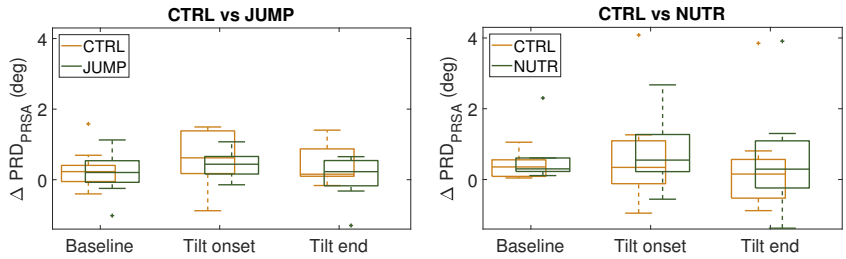

Figure 2.13 Boxplots with ΔPRD values (median ± IQR) measured respect to PRE-HDBR for the CTRL subgroups (in orange) and the countermeasure (JUMP or NUTR) subgroups (in green) at baseline, beginning and end of TTT. (n.s., Wilcoxon rank-sum test)

of ΔPRD (differences between POST-HDBR and PRE-HDBR calculated for each subject in the subgroups analyzed). As can be seen in Table 2.4, baseline PRD increased significantly from PRE-HDBR to POST-HDBR in both the CTRL and NUTR subgroups of the MEDES campaign. When comparing the values at the beginning of the tilt test, PRD increased at POST-HDBR with respect to PRE-HDBR, although the differences were not statistically significant. At the end of the tilt phase, PRD showed a trend of increase in the NUTR group but not in the CTRL group. The results shown in figure 2.13 (right panel) confirm the lack of effectiveness of the nutrition-based countermeasure evaluated in terms of repolarization dynamics.

	PRD	PRE-HDBR (deg)	POST-HDBR (deg)
Baseline	CTRL	0.92 [0.19]	1.32 [0.33] **
	NUTR	1.10 [0.51]	1.22 [1.04] *
Tilt onset	CTRL	1.22 [0.23]	1.59 [0.98]
	NUTR	1.32 [1.02]	1.93 [1.72]
Tilt end	CTRL	1.27 [0.88]	1.13 [0.96]
	NUTR	1.19 [0.74]	1.41 [1.76]

Table 2.4 PRD values (median [IQR]) at all phases of TTT for PRE-HDBR and POST-HDBR in CTRL and NUTR subgroup. **p<0.01, *p<0.05 (with respect to PRE-HDBR)

2.5 Discussion

This study aimed to investigate the alterations in ventricular repolarization associated with long-term exposure to simulated microgravity conditions induced by 60-day HDBR. Two methods have been used for the quantification of low-frequency oscillations in the T wave of the ECG, departing from the original methodology proposed in [343, 341]. These methods, one using CWT and the other using PRSA, have been shown to produce concordant results in terms of the index of PRD, a marker of low-frequency repolarization oscillations [356], whose increase has been shown to be a predictor of ventricular arrhythmias and sudden cardiac death [343, 341]. This study has shown that microgravity significantly enhances PRD, particularly when evaluated in response to sympathetic stimulation induced by tilt test. An exercise-based countermeasure has been shown to partially reverse microgravity-induced effects on PRD, whereas a nutrition-based countermeasure has been shown not to be effective at all.

The methods developed in this study for PRD quantification departed from the CWT-based and PRSA-based methods proposed in [343] and [341], respectively. The present method introduced several modifications to reduce delineation errors or uncertainties and became more robust calculations. For both modified CWT- and PRSA-based methods, correlation analysis has confirmed a strong agreement between them. In a comparative analysis using

the original PRD calculation methodologies [356], both techniques were also found to be highly correlated.

The PRD values obtained by our modified method are markedly different from those obtained in [343, 341]. However, the agreement between the CWT-based and PRSA-based methods is consistent with the findings reported in [341], where a PRSA-based approach was presented as an alternative to the approach using the CWT technique. The advantage of the PRSA approach is the relevant reduction in computational costs associated with PRD computation. This facilitates its use in applications with limited computational resources.

The analysis carried out in this study has shown that TTT-induced autonomic changes manifest themselves as an increase in PRD, both when measured at PRE-HDBR and at POST-HDBR. These changes in PRD can be attributed to increased sympathetic drive, as evidenced by increases in the HRV indices LFn and LF/HF, in line with numerous other studies on HRV, including those pioneering spectral HRV analysis during TTT [296, 297]. Sympathetic stimulation is well known to influence ventricular repolarization and modify the characteristics of the T wave in the ECG [332]. The results of the present study showing an increase in PRD in response to TTT are consistent with the changes in PRD reported in response to variations in sympathetic activity or β-adrenergic modulation [343, 341]. In the present study, these changes are shown not to be associated with HRV changes but reflect direct autonomic modulation of the ventricular myocardium, in accordance with the findings reported in [343, 341].

In vivo studies in patients have shown that the same low-frequency oscillatory behavior of ventricular repolarization occurs locally, as measured from activation recovery intervals (ARIs) obtained from unipolar epicardial electrograms during ventricular pacing [153, 318]. In these studies, elevated arousal of the sympathetic nervous system was induced and maintained by mental stress or by the Valsalva maneuver, which allowed the characterization of low-frequency oscillations in ARI, a surrogate of APD, showing that these oscillations are coupled with oscillations in systolic and diastolic blood pressure [153, 318]. Computational studies have provided information on the mechanisms underlying sympathetically-mediated low-frequency oscillations

of APD and the observed inter-individual differences [323, 352]. Specifically, phasic changes in both β-adrenergic stimulation and hemodynamic loading, a known accompaniment of enhanced sympathetic activity, have been demonstrated to contribute to low-frequency oscillations in APD, with these two actions being synergistic [323]. Ionic differences in the densities of the L-type calcium (I_{CaL}), rapid delayed rectifier potassium (I_{Kr}) and inward rectifier potassium (I_{K1}) currents have been identified as the main drivers of inter-individual differences in the magnitude of low-frequency APD oscillations [352].

The present results have provided evidence of significant effects of long-duration microgravity simulation on cardiac electrical activity. In line with previously published studies, this work has confirmed that microgravity markedly alters ventricular repolarization [98, 145, 351, 49, 50, 65, 241], with these alterations being more manifest when evaluated in response to sympathetic stimulation. This study adds one more T-wave characteristic to the list of ECG repolarization properties that have been shown to be modulated by microgravity. The quantified PRD index represents a form of temporal variability in ventricular repolarization, specifically focused on oscillations at frequencies below 0.1 Hz. Although other measures of ECG temporal variability have been investigated during or immediately after simulated microgravity exposure [351, 50], PRD can provide a more robust characterization of repolarization instability by encompassing global T-wave vector information.

In addition, the PRD index, which accounts for frequencies below 0.1 Hz, has been proven to be related to sympathetic modulation of ventricular repolarization [341]. Based on the fact that increased sympathetic activity is associated with adverse outcomes in different populations of patients [414], the evaluated PRD index is of great interest for risk prediction. The enhancement of spatial and/or temporal ventricular heterogeneities observed in this and other studies in relation to long-term exposure to microgravity conditions suggests that microgravity could accentuate repolarization instability and thus increase the risk of ventricular arrhythmias, especially immediately after gravity restoration. In particular, this study has shown that PRD quantified after 60-day HDBR is highly elevated, up to 50% at rest and up to 100% in response to TTT, with respect to the PRE-HDBR values. The degree of

change in PRD values measured immediately after 60 days of HDBR could be associated with a high arrhythmic risk, taking as reference previous studies on risk assessment in patients with post-myocardial infarction, where those extents of change were found in patients who died vs those who survived during follow-up [343, 342]. This is in line with other studies that have reported on subjects presenting long-term microgravity-induced changes in ECG repolarization to an extent similar to those associated with a more than three-fold increased hazard ratio for sudden cardiac death in general populations [351].

This study has evaluated the ability to counteract the detrimental effects of microgravity on ventricular repolarization using two types of countermeasures. On the one hand, a countermeasure based on high-intensity resistance exercise partially attenuated the effects of microgravity when measuring the PRD index. Similar findings have been reported in other studies [198, 229, 64, 329] that also analyzed the same countermeasure to mitigate the effects of microgravity on the skeletal and cardiovascular systems. In previous research, exercise-based countermeasures have been shown to be very effective in preserving bone and muscle conditions [250, 198, 229].

However, a second countermeasure tested, consisting of a nutritional supplement containing antioxidants and an anti-inflammatory dietary mix, has been shown to be far from effective in reducing microgravity-induced effects on ventricular repolarization. This finding is in agreement with other studies that point to the lack of effectiveness of this countermeasure in counteracting the effects of microgravity exposure on bone turnover [25]. Importantly, omega-3 fatty acid intake, which are components of the dietary mix, and their possible protection of cardiovascular health should also be considered in relation to the potential increased risk of ventricular arrhythmias. However, the relationship between omega-3 fatty acids and arrhythmias remains controversial, with some studies suggesting adverse arrhythmogenic effects, while others propose minimal effects or significant antiarrhythmic potential [9, 427, 83, 400]. Although one reason to include this type of acid in a dietary support was its protective effects on bones [461], the findings of the present study show that the dietary mix could not reduce the adverse cardiac effects of simulated microgravity. More studies are needed that include a larger number of subjects to confirm or refute these findings.

Furthermore, it is relevant to note that, when evaluating the effects of the countermeasures tested, the CTRL subgroups of the JUMP and NUTR studies did not share the same ventricular repolarization characteristics as those evaluated by PRD, despite the fact that the subjects of both studies had similar physical conditions. Specifically, subjects in the CTRL subgroup of the DLR campaign (exercise-based countermeasure) presented higher PRD values, both in PRE-HDBR and POST-HDBR.

Therefore, it would be advisable to explore other types of exercise [180], as high-intensity exercises may not succeed in counteracting the effects of long-term exposure to microgravity [367, 195, 199, 161]. Furthermore, testing other dietary supplements [73], artificial gravity [118], or a combination of them could serve as an alternative countermeasure to compensate for adverse microgravity-induced effects on ventricular repolarization.

A limitation of the current study is the low number of participants. Further studies that included a larger number of subjects could confirm or refute the results obtained in this study. The inclusion of a larger number of subjects would definitely allow a more robust analysis of absolute and relative microgravity-induced changes.

2.6 Conclusions

The effects of long-duration microgravity on ventricular repolarization have been assessed by evaluating the PRD index, a marker of low-frequency repolarization oscillations whose increase is associated with a high risk of ventricular arrhythmias and sudden cardiac death. Two methods have been implemented for robust PRD quantification, which have shown to be in very good agreement. Long-term microgravity exposure has been proven to markedly elevate PRD, particularly when evaluated in response to enhanced sympathetic activity induced by a tilt-table test. A countermeasure based on exercise training has been shown to partially counteract microgravity-induced changes in ventricular repolarization as assessed immediately after gravity restoration.

I don't feel like I've done anything extraordinary but
take my little light and shine it in darkness.

Leymah Gbowee

3

Sudden cardiac death prediction by Periodic Repolarization Dynamics

3.1 Motivation

Approximately 1 to 2% of the adult population in western societies is diagnosed with HF [315, 360], including more than 10% of people 70 years of age or older [179]. 64 million people will suffer from HF worldwide and the total associated cost in health programs is estimated to reach $400 billion by 2030, according to some estimates [218]. HF is a clinical syndrome accompanied by a high burden of comorbidities [51] and a poor prognosis [77].

In patients with CHF, SCD accounts for 30-50% of mortality cases [292] and constitutes more than 60% of all cardiovascular deaths that occur out of hospital [4]. SCD is defined as death from an unexpected circulatory arrest that occurs within an hour of the onset of symptoms or during sleep [7]. PFD is another common cause of mortality in CHF, resulting from progressive pump dysfunction. Therapy involving β-blockers and ICDs has

shown efficacy in preventing SCD, improving the quality of life of affected patients, and altering the mode of death from SCD to PFD [210]. Based on this evidence, there is an important need to successfully predict the risk of both modes of cardiac death in CHF, which could lead to a more cost-effective use of medications or devices.

Several noninvasive indices derived from resting ECGs or ambulatory Holter recordings have been proposed to stratify CHF patients according to their risk of PFD and SCD. These include, among others, HRV [280], QT interval variability index (QTVi) [37], QT dispersion [121], baroreflex sensitivity [42], fragmented QRS [97, 8], T-wave alternans [415, 263] and turbulence slope [127].

Autonomic imbalance, characterized by increased sympathetic activity and withdrawal of vagal tone, is a recognized hallmark of HF [124] and is associated with a worse prognosis in CHF patients [191], with an increased risk of PFD and SCD [122, 164]. On this basis, PRD, which was used in the previous chapter to assess the effect of exposure to simulated microgravity, is proposed as a stratification marker of SCD in patients with CHF. PRD is a measurement of low-frequency oscillations (below 0.1 Hz) in the T-wave vector [343]. In previous work in the literature, elevated PRD has been shown to be associated with an increased risk of arrhythmias in various cardiac conditions [343, 342, 152, 370].

This chapter aims to evaluate the predictive ability of the PRD index, calculated using the algorithm introduced in Chapter 2, to stratify the risk of SCD and PFD in CHF patients. The stratification ability of PRD is analyzed individually and in combination with other repolarization- and autonomic-related ECG indices to predict the risk of SCD and PFD.

3.2 Materials

3.2.1 Study population

For this work, the ECG data from the MUSIC study (MUerte Sbita en Insuficiencia Cardiaca) [240] have been analyzed. The original study population consisted of 992 consecutive patients with symptomatic CHF corresponding to NYHA classes II and III. This study is a prospective, multicenter, lon-

gitudinal study designed to assess risk predictors of cardiac mortality and SCD in ambulatory patients with CHF. A two- (3%) or three-lead (97%) 24-h Holter ECG sampled at 200 Hz was recorded in each patient at enrollment using ELA Medical equipment (Sorin Group, Paris, France). Patients were consecutively enrolled in the specialized CHF clinics of eight University Hospitals between April 2003 and December 2004. All had symptomatic CHF (NYHA class II–III) and were treated according to institutional guidelines. The MUSIC study included patients with reduced and preserved LVEF, ranging from 10% to 70%. Patients with preserved LVEF were included if they had CHF symptoms and prior hospitalization for HF or some objective signs of HF confirmed by chest X-ray (findings of pulmonary congestion) and/or echocardiography (abnormal LV filling pattern and LV hypertrophy). Patients were excluded if they had recent acute coronary syndrome or severe valvular disease amenable for surgical repair. Patients with other concomitant diseases expected to reduce life expectancy were also excluded. All patients gave their informed consent in writing and the study protocol was approved by all the institutional ethics and investigation committees of the following participating hospitals. Valme Hospital, Santiago de Compostela Hospital, Son Dureta Hospital, Arrixaca Hospital, Gregorio Marañón Hospital, Joan XXIII Hospital, Insular Las Palmas Hospital, Sant Pau Hospital [411].

The population analyzed in this work consisted of 569 CHF patients (409 men and 160 women), aged 20 to 80 years (mean 63 ± 12). Of the 992 patients included in the original MUSIC study, 341 patients had atrial fibrillation, flutter, or pacemaker and were excluded for the present analysis. Of the remaining 651 patients, 82 patients did not have an available high-resolution ECG recording and therefore were not included. The mean LVEF was 37.0 + 13.8% (range 12 to 70%), and most patients (55%) had LVEF$\leq$ 35%. Half of the patients (50.1%) had ischemic cardiomyopathy and 259 patients had previous myocardial infarction (45.5%). Detailed characteristics of the study population are shown in Table 3.1.

3.2.2 Study protocol

For each patient, two ECG recordings were available: an ambulatory 24-hour ECG sampled at 200 Hz in 3 orthogonal X, Y, and Z leads using SpiderView

Clinical Variables	
Age (years)	64 (16)
Gender (male)	409 (71.9%)
NYHA class III	99 (17.4%)
LVEF $\leq$ 35%	312 (54.8%)
Ischemic etiology	285 (50.1%)
Diabetes mellitus	212 (37.3%)
Amiodarone	53 (9.3%)
NT-proBNP>1000 pg/mL	186 (32.7%)
Prior MI	259 (45.5%)
ECG Variables	
Median RR (ms)	857 (179)
RR range (ms)	697 (279)
QRS > 120ms	234 (41.1%)
NSVT and VPB > 240 in 24-h	148 (26.0%)
IAA $\geq$ 3.7 μV	139 (24.4%)
TS $\leq$ 2.5 ms/RR	249 (43.8%)

Table 3.1 Clinical and ECG variables of database. Data are represented as median (interquartile range) for continuous variables and as number (percentage) for dichotomized variables. IAA, index of average alternans (obtained from [263]); LVEF, left ventricular ejection fraction; NSVT, nonsustained ventricular tachycardia; NYHA, New YorkHeart Association; TS, turbulence slope (obtained from [95]); VPB, ventricular premature beat. The values of the ECG variables in this table were measured in 24-hour Holter recordings.

recorders (ELA Medical, SorinGroup, Paris, France) and a previous 20-minute ECG sampled at 1,000 Hz while patients were resting in a supine position. In this study, PRD was measured from the 20-minute ECG recording. Patients were followed every 6 months on an outpatient basis for a median of 44 months (range 28-51). The primary endpoints were SCD and PFD. Death was defined as SCD if it was: (i) a witnessed death occurring within 60 min from the onset of new symptoms, unless a cause other than cardiac was obvious; (ii) an unwitnessed death (<24h) in the absence of pre-existing progressive circulatory failure or other causes of death; or (iii) a death during attempted resuscitation. Deaths occurring in hospital as a result of refractory progressive end-stage CHF, or CHF patients undergoing heart transplantation,

were defined as PFD. Patients lost to follow-up were censored in survival analysis. Patients who underwent cardiac transplantation were defined as PFD at the time of surgery, according to previously published CHF studies [211, 266]. The endpoints were reviewed and classified by the MUSIC Study Endpoint Committee. A description of clinical data for the overall population and more detailed information on the study protocol can be found in Vazquez et al. [411].

3.3 Methods

3.3.1 ECG preprocessing

High-resolution ECG signals were preprocessed with a 50 Hz notch filter to remove powerline interference. QRS complexes were identified using Aristotle software [265]. The heart timing method described in Mateo and Laguna [246] was used to identify premature beats. After applying a low-pass filter to the ECG signals to eliminate noise, the baseline wander was estimated using cubic splines interpolation and subsequently removed.

In contrast to the definition of the T-wave window used in the previous chapter, in this work the T-wave window for each beat i was defined from the onset of the T-wave, T_{on_i}, to the end of the T-wave, T_{off_i}, according to the following rules, expressed as a function of the corresponding QRS fiducial point (QRS_i) and the RR interval (RR_i).

- If $RR_i < 720$ ms,

$$T_{on_i} = QRS_i + 90 \text{ ms}$$
$$T_{off_i} = QRS_i + \min(360, \tfrac{2}{3} RR_i) \text{ ms}.$$

- If $RR_i \geq 720$ ms,

$$T_{on_i} = QRS_i + 90 \text{ ms}$$
$$T_{off_i} = QRS_i + 360 \text{ ms}.$$

The noise level was estimated in each lead and beat by measuring the root mean square value of the high-frequency components (above 15 Hz) in a window around the T wave, in a way similar to that used in [258]. A global measure of noise for each beat i was obtained by adding the noise levels of all leads and denoted by $V_{noise}^{RMS}(i)$. If a beat was too noisy ($V_{noise}^{RMS} > 140\ \mu V$), the associated T-wave marks (T_{on} and T_{end}) were discarded for further analysis, but the associated QRS mark was retained.

3.3.2 PRD computation

PRD was measured in the preprocessed signal using the PRSA method described in Chapter 2 (Periodic Repolarization Dynamics in simulated microgravity). The steps are described briefly as follows:

1. T waves were selected using the T-wave windows defined in the previous section (ECG preprocessing).

2. A constant value was subtracted from each T wave in each of the analyzed leads so that the amplitude at T_{end} was set to 0 mV.

3. The average electrical vector was calculated for each T-wave window and the angle dT° between two consecutive T-wave windows was calculated by the dot product of the corresponding average vectors.

4. A median filter was used to attenuate outliers and artifacts in the dT° time series.

For the obtained dT° time series, a method based on PRSA [36] was applied to evaluate the oscillations measured by the PRD index. In Chapter 2, this technique was shown to be in close agreement with the one based on CWT, while having a lower computational cost. The steps are fully described in Chapter 2 and are briefly summarized as follows:

5. Anchor points were defined from averages values of the dT° series calculated before and after each anchor point candidate, x_i.

6. A window was defined around each anchor point. Anchor points at the beginning or end of the dT° series were discarded.

7. The PRSA series was obtained by averaging the dT° values in all windows contained in each 5-minute segment.

For each 5-minute segment, a PRD value was calculated as the difference between the maximum and minimum values of the PRSA series. For the 20-minute recording of each subject, a unique PRD value was calculated as the minimum PRD for the 5-minute segments analyzed with 4-minute overlap.

Examples of dT° and PRSA time series from two selected subjects, a SCD victim and a survivor, are shown in Figure 3.1.

A cuttof point of 1.33 deg was identified to maximize the geometric mean of sensitivity and specificity for SCD as endpoint and, consequently, two groups were defined: PRD^{+}, containing those patients with PRD above the cutoff value and PRD^{-}, containing the remaining patients. Furthermore, the median PRD in the study population was considered, yielding a value of 1.31 deg. Similarly, the optimum value for CD as endpoint was 1.32 degrees.

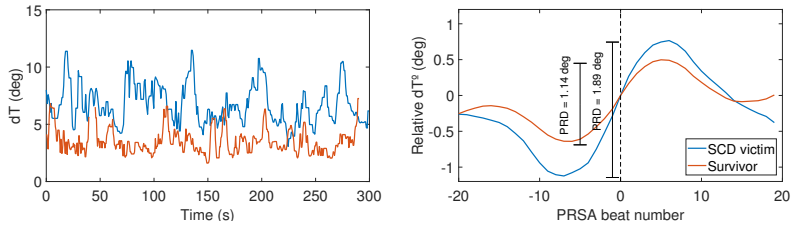

Figure 3.1 dT series along 300 seconds (left panel) and PRSA curve (right panel), where anchor beats were set to 0 deg, from a SCD victim and a survivor.

3.3.3 Heart Rate Variability Analysis

In the same manner as described in previous chapter, HRV analysis was performed. For that purpose, the methodology described by Bailón et al. ([27]) was followed. HRV indices were computed for the 5-minute segment with minimum PRD. The PSD was estimated based on the periodogram. LF and HF powers were calculated as the areas under the PSD within the 0.04–0.15 Hz and 0.15–0.5 Hz frequency bands, respectively. LFn and HFn

were obtained by dividing the LF and HF powers by the sum of the two. The ratio between LF and HF powers, LF/HF, was additionally computed [233].

3.3.4 Clinical variables and other Holter-based ECG indices

Clinical variables for patients with HF, such as LVEF $\leq 35\%$, NT-proBNP $>$1000 pg/mL, nonsustained ventricular tachycardia (NSVT) and a number of ventricular premature beats (VPB) > 240, are shown in table 3.2. These variables, whose capacity for prediction of the risk of SCD and PFD has been previously shown [411], were included in the current analysis.

In addition, other Holter-based indices calculated in previous studies of our group were considered based on their risk prediction power. The index of average alternans, IAA, which quantifies the average amplitude of T-wave alternans over a 24-hour period, was calculated by automatic ECG analysis [263]. IAA was shown to stratify the risk for SCD in the study population analyzed here when dichotomized at 3.7 μV to define IAA^+ and IAA^- groups [263]. The turbulence slope, TS, which describes the initial phase of sinus rhythm deceleration after a VPB, was determined as the maximum positive slope of a regression line assessed over any of five consecutive RR intervals within the first 20 sinus RR intervals after a VPB during the 24-hour ECG recording [95]. TS was shown to stratify the risk for both SCD and PFD when dichotomized at 2.5 ms/RR, with TS^+, denoting the group of patients with TS below the threshold, being associated with higher risk than the group TS^- containing the remaining patients [95].

Baseline characteristics HF patients (N = 992)	
Age, years	65±12
Gender, male	718 (72.4%)
Diabetes mellitus	356 (35.9%)
Ischaemic aetiology	453 (45.7%)
Prior pacemaker	135 (13.6%)
Body mass index, kg/m^2	28.5 ± 4.5
NYHA class II	778 (78.4%)
NYHA class III	214 (21.6%)
Systolic blood pressure, mmHg	127 ± 22
Haemoglobin, g/L	137.2 ± 15.9
Total cholesterol, mmol/L	4.83 ± 1.07
NT-proBNP > 1.000 ng/L	452 (45.6%)
LVEF, %	37.0 ± 14.1
LVEF < 45%	748 (75.4%)
LVEF ≤ 35%	534 (53.8%)
Sinus rhythm	703 (70.9%)
Atrial fibrillation	191 (19.3%)
QRS duration, ms	125.5 ± 35.1
Nonsustained VT	352 (35.5%)
Frequent VPBs (>240 VPBs in 24 h)	480 (48.4%)
Nonsustained VT and frequent VPBs	284 (28.6%)
Beta-blocker	675 (68.0%)

Table 3.2 Qualitative data are presented as absolute frequencies and percentages and quantitative data as mean ± standard deviation. NYHA class, New York Heart Association class; NT-proBNP, amino-terminal pro-brain natriuretic peptide; VPBs, ventricular premature beats; VT, ventricular tachycardia. Adapted from [411]

3.3.5 Statistical analysis

Continuous variables are presented as median [IQR]. Univariate comparisons of continuous variables between patient groups were performed using the

Mann-Whitney U test (or Wilcoxon rank-sum test). The survival probability was estimated by Kaplan-Meier analysis, with group differences assessed using the log-rank test. The prediction of endpoints was made using univariate and multivariate Cox proportional hazards regression models [86], and Fine & Gray analysis for competing risk [123]. Hazard ratios (HR) and 95% confidence intervals (CI), expressed as HR [95% CI], were calculated. Statistical significance was considered for the p-values < 0.05. Variables that showed significant differences between groups in the univariate analysis were included in the multivariate Cox regression model. Data analysis was performed using MATLAB R2017a (9.2), SPSS (version 24.0), and R software (version 4.1).

3.4 Results

3.4.1 Association of PRD with cardiac events

PRD was dichotomized based on the optimal cut-off points determined from ROC analysis for each of the investigated endpoints. The optimal cut-off values were 1.33 degrees for SCD, 1.31 degrees for PFD (which coincided approximately with the median PRD in the study population), and 1.32 degrees for cardiac death (CD), which comprises both SCD and PFD. For each endpoint, PRD^+ and PRD^- subgroups were established to include patients with PRD values above and below the cutoff point, respectively.

Figure 3.2 illustrates the percentages of victims of SCD, PFD and CD in the PRD^+ and PRD^- groups. In the study population, there were 106 victims of CD (18.6%), 53 deaths attributed to SCD and 53 to PFD. The mortality rate due to SCD was significantly higher (p = 0.018) in the PRD^+ group (33 victims, 11.7%) compared to the PRD^- group (20 victims, 7%). Regarding PFD, there were no significant differences in mortality rates between the PRD^+ and PRD^- groups (28 victims, 10% in PRD^+ vs 25 victims, 8.7% in PRD^-). Significant differences were observed for CD, with mortality being markedly higher in the PRD^+ group compared to the PRD^- group (22.3% vs 15%).

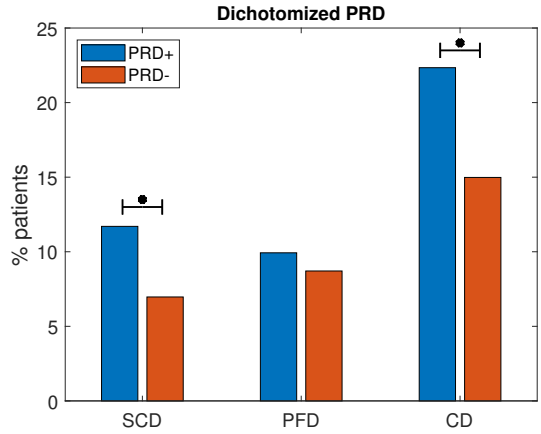

Figure 3.2 Percentages of SCD, PFD and CD victims in PRD^+ and PRD^- groups. $^*p<0.05$

3.4.2 SCD and PFD risk prediction based on PRD and other individual variables

Kaplan-Meier survival analysis showed that PRD^+ patients had significantly lower SCD survival probability than PRD^- patients (p=0.024), as illustrated in Figure 3.3. When accounting for PFD as a competing risk, Fine & Gray analysis [123] showed that the cumulative incidence curves of SCD for patients with PRD^+ and PRD^- were statistically significantly different (p=0.048). When PFD was considered an end point, no significant differences in survival rates were found between the PRD^+ and PRD^- groups (Figure 3.4).

The results of the univariate Cox analysis for the prediction of the risk of SCD by the PRD index, as well as by demographical, clinical, and other ECG variables are shown in Table 3.3. The variables significantly associated with SCD were New York Heart Association (NYHA) class III, LVEF $\leq$ 35%, NSVT and VPB $>$ 240, N-terminal prohormone of brain natriuretic peptide (NT-proBNP)$>$1000 pg/mL, IAA^+, TS^+ and PRD^+. None of the HRV variables (LFn, HFn, or LF / HF) was associated with the risk of SCD. Regarding PFD, PRD^+ was unable to predict this endpoint, while age, ischemic etiology, previous myocardial infarction, NYHA class, NT-proBNP$>$1000 pg/mL and TS^+ were significant predictors (Table 3.4).

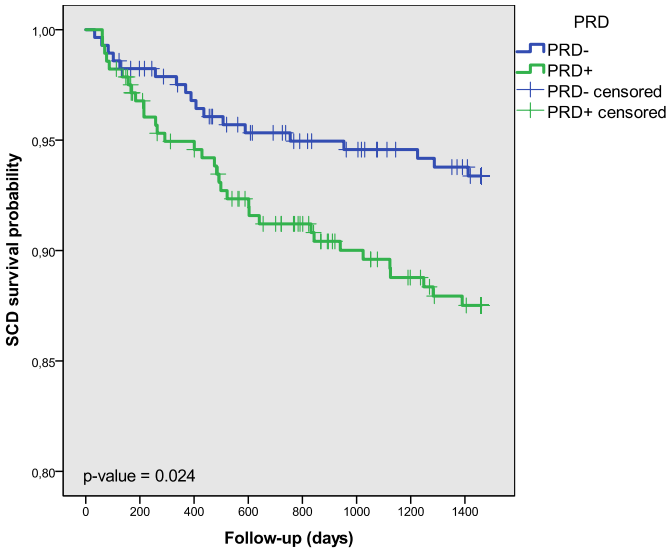

Figure 3.3 Estimated probability curve of SCD survival for PRD^+ and PRD^- groups.

The multivariate Cox proportional hazards regression model for the prediction of SCD that includes clinical variables such as the combination of NSVT and VPB > 240, LVEF $\leq 35\%$, NYHA class and NT-proBNP$>$1000 pg/mL together with PRD^+ led to the results presented in Table 3.5. PRD^+ and some of the clinical variables were independent predictors of SCD, being associated with similar HR values. When considering PFD as a competing risk event, the regression model for SCD as endpoint included clinical variables and PRD, the latter with an HR of 1.65, even if it was only marginally predictive ($p = 0.095$).

When tested in the non-ischemic etiology CHF subpopulation, PRD was able to predict SCD in the multivariate model (HR = 2.497, $p = 0.05$). In the subpopulation of patients with CHF of ischemic etiology, PRD was not predictive of SCD in the univariate model and therefore was not included in a multivariate model.

Finally, the capacity of PRD^+ for CD prediction is tested. The HRs for the univariate and multivariate Cox analyses were 1.64 ($p = 0.014$) and 1.63

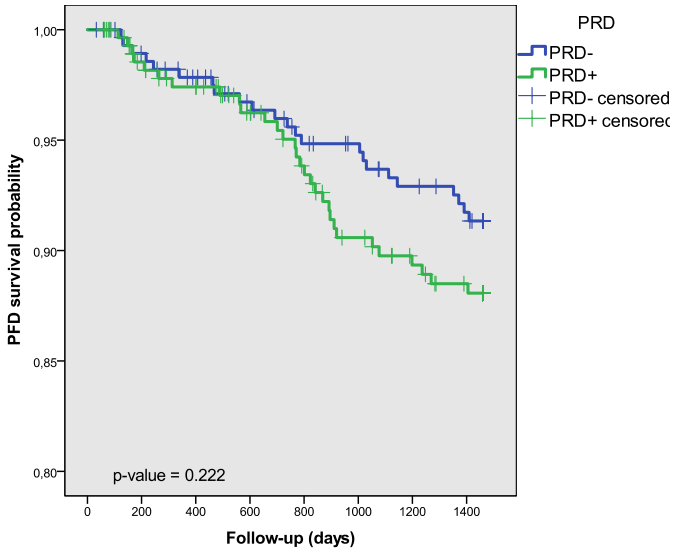

Figure 3.4 Estimated probability curve of PFD survival for PRD^+ and PRD^- groups.

($p = 0.016$), respectively. Other demographical, clinical, and ECG variables were also able to predict CD in a univariate Cox model (Table 3.6).

If, rather than dichotomizing the PRD based on optimum cut-off points, the dichotomization was performed according to the median PRD over the whole study population, the results only slightly changed. In particular, the HR for the prediction of SCD using PRD^+ decreased from 2.001 to 1.934 for the univariate Cox analysis and from 2.002 to 1.934 for multivariate Cox analysis.

3.4.3 SCD and PFD risk prediction based on the combination of PRD with other variables

To improve the predictive power for the risk of SCD, the combination of PRD with other Holter-based variables, such as IAA and TS, was assessed. As shown in Figure 3.5, patients with $PRD^+\&TS^+$ had significantly higher SCD mortality ($p < 0.05$) and PFD mortality ($p < 0.001$) than the rest of the patients. CD mortality was also significantly higher. The results for the combination of PRD and IAA are presented in Figure 3.6. Patients with $PRD^+\&IAA^+$ had

		Univariate	
		HR (95%)	p-value
Endpoint: SCD	Age	1.016 (0.992-1.040)	0.198
	Gender	1.967 (0.960-4.030)	0.064
	Ischemic etiology	1.630 (0.940-2.827)	0.082
	Prior MI	1.639 (0.952-2.823)	0.074
	NYHA class III	2.370 (1.318-4.263)	0.004**
	LVEF$\leq$ 35%	2.231 (1.227-4.056)	0.009**
	LFn	2.198 (0.556-8.687)	0.261
	HFn	0.455 (0.115-1.799)	0.261
	LF/HF	1.080 (0.998-1.168)	0.055
	NSVT and VPB>240	2.167 (1.255-3.743)	0.006**
	Diabetes mellitus	1.378 (0.800-2.372)	0.248
	NT-proBNP>1000 pg/mL	2.339 (1.349-4.056)	0.002**
	IAA^+	2.312 (1.318-4.055)	0.003**
	TS^+	2.619 (1.418-4.838)	0.002**
	PRD^+	2.001 (1.127-3.554)	0.018*

Table 3.3 Univariate Cox analysis for SCD as endpoint. Age, gender, ischemic etiology, prior myocardial infarction, NYHA class, LVEF, HRV indices (LFn, HFn, LF / HF), combined NSVT and VPB>240, diabetes, NT-proBNP>1000 pg/mL, IAA^+, TS^+ and PRD^+ were the analyzed variables. *p<0.05, **p<0.01.

increased SCD mortality (p = 0.007) and CD mortality (p = 0.023) than the rest of the population. No significant differences were found with respect to PFD mortality (p=0.816).

Figures 3.7 and 3.8 show Kaplan-Meier probability curves for the survival of SCD using the combined variables PRD^+&TS^+ and PRD^+&IAA^+, respectively. For the two variables, significantly lower survival was found in patients with positive PRD and TS or IAA. When PFD was considered an end point, the differences in survival probabilities were only statistically significant when using PRD^+&TS^+. Taking into account PFD as a competing risk event for SCD, Fine & Gray analysis showed a significantly higher cumulative SCD incidence for PRD^+&TS^+ (PRD^+&IAA^+, respectively) patients than the rest of the population (p < 0.001 in all cases). When taking into account SCD as a competing risk event for PFD, the cumulative incidence of

		Univariate	
		HR (95%)	p-value
Endpoint: PFD	Age	1.051 (1.024-1.079)	$1.9{\cdot}10^{-4***}$
	Gender	1.135 (0.616-2.090)	0.685
	Ischemic etiology	1.946 (1.110-3.411)	0.020^{*}
	Prior MI	1.941 (1.119-3.365)	0.018^{*}
	NYHA class III	2.715 (1.524-4.836)	0.001^{**}
	LVEF$\leq$ 35%	1.743 (0.987-3.077)	0.056
	LFn	0.802 (0.219-2.939)	0.739
	HFn	1.247 (0.340-4.570)	0.739
	LF/HF	0.957 (0.846-1.083)	0.488
	NSVT and VPB>240	1.738 (0.991-3.047)	0.054
	Diabetes mellitus	1.903 (1.110-3.260)	0.019^{*}
	NT-proBNP>1000 pg/mL	4.945 (2.692-9.082)	$2.6{\cdot}10^{-7***}$
	IAA^{+}	1.115 (0.594-2.093)	0.735
	TS^{+}	4.964 (2.477-9.947)	$6{\cdot}10^{-6***}$
	PRD^{+}	1.242 (0.724-2.129)	0.431

Table 3.4 Univariate Cox analysis for PFD as endpoint. Age, gender, ischemic etiology, prior myocardial infarction, NYHA class, LVEF, HRV indices (LFn, HFn, LF / HF), combined NSVT and VPB>240, diabetes, NT-proBNP>1000 pg/mL, IAA^{+}, TS^{+} and PRD^{+} were the analyzed variables. $^{*}p<0.05$, $^{**}p<0.01$, $^{***}p<0.001$.

PFD for patients with $PRD^{+}\&TS^{+}$ was significantly higher than for the rest of the patients in the population ($p < 0.001$).

In the univariate Cox analysis (Table 3.7) with SCD as endpoint, $PRD^{+}\&TS^{+}$ as well as $PRD^{+}\&IAA^{+}$ were risk predictors, with associated HRs of 3.1 and 2.8, respectively. For PFD as endpoint, $PRD^{+}\&TS^{+}$ patients presented more than two and a half times higher risk than the rest of the population. For CD as endpoint, $PRD^{+}\&TS^{+}$ was associated with an HR of 3.1, while $PRD^{+}\&IAA^{+}$ with a HR of 1.9.

The results of the multivariate Cox proportional hazard regression analysis that included the NYHA class, LVEF $\leq$ 35%, NSVT and VPB>240 and NT-proBNP>1000 pg/mL as well as one of the two combined ECG variables at a time, are presented in Table 3.8 for SCD as endpoint. Both $PRD^{+}\&IAA^{+}$ and $PRD^{+}\&TS^{+}$ independently predicted the risk of SCD

		Multivariate	
		HR (95%)	p-value
Endpoint: SCD	NYHA class III	1.606 (0.850-3.036)	0.144
	LVEF$\leq$ 35%	2.034 (1.050-3.940)	0.035*
	NSVT and VPB>240	1.516 (0.840-2.734)	0.167
	NT-proBNP>1000 pg/mL	1.632 (0.908-2.933)	0.101
	PRD$^+$	1.825 (1.019-3.268)	0.043*

Table 3.5 Multivariate SCD risk prediction including the following variables: NYHA class, LVEF$\leq$ 35%, combined NSVT and VPB>240, NT-proBNP>1000 pg/mL and PRD$^+$. *p<0.05

with HRs of 3.0 and 2.1, respectively. Multivariate regression analysis for SCD with PFD as a competing risk indicated that the combined variable PRD$^+$&IAA$^+$ (PRD$^+$&TS$^+$, respectively) predicted SCD independently of other clinical variables, with an associated HR of 2.9 (2.4, respectively, being $p < 0.01$ in all cases). Furthermore, the NYHA class and NSVT and VPB>240 are significant when they are in the PRD$^+$&TS$^+$ model.

In the subpopulation of patients with CHF of non-ischemic etiology, PRD$^+$&TS$^+$ predicted SCD with HR 3.2 ($p = 0.012$) and PFD with HR 3.43 ($p = 0.011$) independently of other clinical variables. PRD$^+$&IAA$^+$ predicted SCD risk in both ischemic and non-ischemic etiology subpopulations, with associated HR of 3.3 and 2.9, respectively.

To complete this study, the combined variables' capacity for predicting CD risk was tested. Table 3.9 shows the results for the two multivariate proportional hazard models tested. Both PRD$^+$&IAA$^+$ and PRD$^+$&TS$^+$ predicted CD risk independently of other demographic and clinical variables with HRs of 2.4 and 2.0, respectively.

3.5 Discussion

This work investigates the performance of PRD, characterizing the oscillatory behavior of the T wave, for stratification of cardiac risk in a population of patients with CHF. Although PRD has previously been used in various contexts [343, 371, 151, 256, 369, 163], in this study, PRD is calculated in a

		Univariate	
		HR (95%)	p-value
Endpoint: CD	Age	1.032 (1.014-1.050)	$3.6{\cdot}10^{-4***}$
	Gender	1.461 (0.921-2.319)	0.108
	Ischemic etiology	1.780 (1.201-2.636)	0.004^{**}
	Prior MI	1.783 (1.211-2.624)	0.003^{**}
	NYHA class	2.537 (1.681-3.830)	$9{\cdot}10^{-6***}$
	LVEF$\leq$ 35%	1.965 (1.303-2.965)	0.001^{**}
	LFn	1.304 (0.508-3.344)	0.581
	HFn	0.767 (0.299-1.968)	0.581
	LF/HF	1.030 (0.963-1.102)	0.384
	NSVT and VPB>240	1.944 (1.315-2.874)	0.001^{**}
	Diabetes mellitus	1.620 (1.106-2.372)	0.013^{*}
	NT-proBNP>1000 pg/mL	3.330 (2.227-4.979)	$4.6{\cdot}10^{-9***}$
	IAA^{+}	1.637 (1.083-2.474)	0.019^{*}
	TS^{+}	3.552 (2.251-5.604)	$5{\cdot}10^{-9***}$
	PRD^{+}	1.636 (1.104-2.425)	0.014^{*}

Table 3.6 Univariate Cox analysis for SCD and PFD victims (CD as endpoint). Age, gender, ischemic etiology, prior myocardial infarction, NYHA class, LVEF, HRV indices (LFn, HFn, LF / HF), combined NSVT and VPB>240, NT-proBNP>1000 pg/mL, IAA^{+}, TS^{+} and PRD^{+} were the variable to analyze in this model. $^{*}p<0.05$, $^{**}p<0.01$, $^{***}p<0.001$.

large CHF cohort to predict the risk of the two most common modes of death, namely SCD and PFD, both considering PRD on its own and in combination with other ECG-based indices.

The results show that CHF patients with high PRD values have nearly twice the risk of suffering SCD than CHF patients with low PRD. These findings are in agreement with previous clinical studies showing a relationship between increased PRD and increased mortality, particularly due to ventricular arrhythmias, in different patient populations [343, 341]. Specifically in post-myocardial infarction patients with impaired LVEF, elevated PRD has been associated with increased risk of SCD [342]. In addition, PRD has been suggested to be potentially useful in guiding clinical decisions on prophylactic implantation of ICD in patients with ischemic and non-ischemic cardiomyopathy [34].

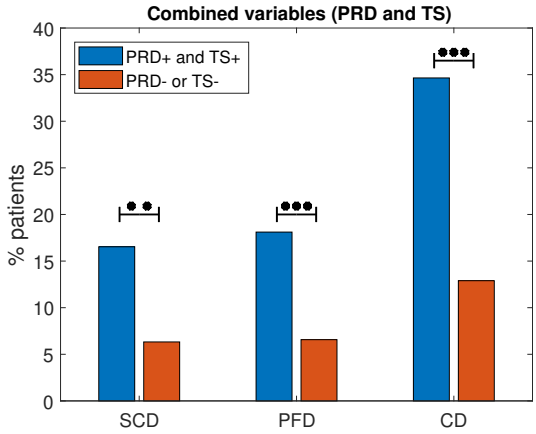

Figure 3.5 Percentages of SCD, PFD and CD victims in the PRD$^+$&TS$^+$ group and in the rest of patients. $^{**}p<0.01$, $^{***}p<0.001$

PRD measures the magnitude of LF oscillations in the T-wave vector of the ECG and has been postulated to reflect sympathetic modulation of ventricular repolarization [343]. The same range of LF oscillations in the T-wave vector accounted for by PRD has been reported for the APD in *in vivo* studies in patients with HF [318]. Through *in silico* simulations, synergistic β-adrenergic and mechanical effects induced by sympathetic activation have been shown to contribute to the generation of these LF oscillations of APD [323, 352]. Those results have been supported by subsequent experimental studies showing that increased sympathetic activity enhances these oscillations and β-adrenergic blockade attenuates them [318, 108]. In the presence of calcium overload and/or reduced repolarization reserve, both commonly associated with HF, the amplitude of LF oscillations of APD has been theoretically shown to be magnified, facilitating the occurrence of arrhythmogenic events [352, 353]. A recent *in vivo* study in a canine model of ventricular remodeling caused by chronic atrioventricular block has provided evidence that dogs inducible for ventricular arrhythmias have higher LF oscillations of repolarization than non-inducible dogs [385]. Based on all these observations, the results of the present study possibly suggest that patients with CHF with high PRD have increased repolarization variability that can lead to destabilization of repolarization and promote arrhythmogenesis.

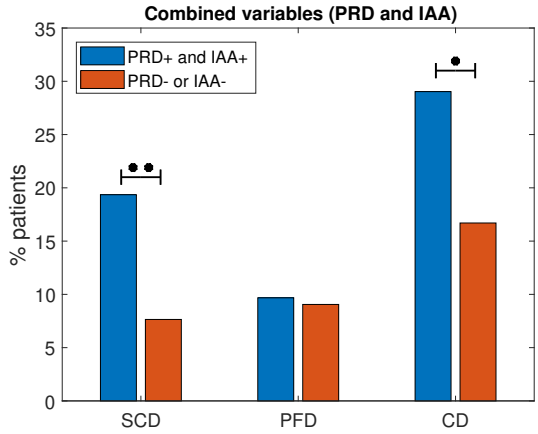

Figure 3.6 Percentages of SCD, PFD and CD victims in the PRD^{+}&IAA^{+} group and the rest of patients. $^{*}p<0.05$, $^{**}p<0.01$.

Since CHF is a complex clinical syndrome, some studies have reported the benefit of using combined ECG risk markers and/or a risk score integrating information from various clinical and ECG variables to improve clinical decision making [208, 58, 140, 204, 330]. The use of markers that provide information on different pathophysiological processes associated with CHF has been shown to be very useful [338, 224]. Here, a combination of PRD and other ECG-based indices is tested for the prediction of SCD and PFD risk. For the prediction of PFD, the combination of PRD with TS, measuring heart rate turbulence, stratifies the study population into two groups according to the risk of PFD. The risk of dying from PFD is two and half times higher in patients with high PRD (PRD^{+}) and low TS (TS^{+}) than in the rest of the patients. Nevertheless, the capacity for PFD prediction of TS on its own is already very good, as reported in previous studies [94], and PRD only slightly improves it. TS represents a vagally-mediated response of heart rate to ventricular premature beats with the involvement of baroreflex sensitivity. TS has been considered an excellent marker of neurohormonal activation in patients with CHF [95, 94]. Since autonomic dysfunction and neurohormonal activation play a relevant role in the progression of CHF, current results on the capacity to stratify the risk of PFD of combined PRD and TS support the noninvasive evaluation of such CHF landmarks from short-term ECG (for

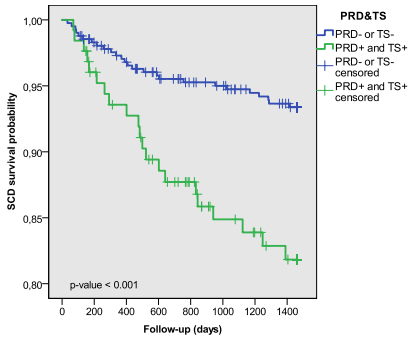

Figure 3.7 Estimated probability curve of SCD for two subgroups defined by PRD^+&TS^+

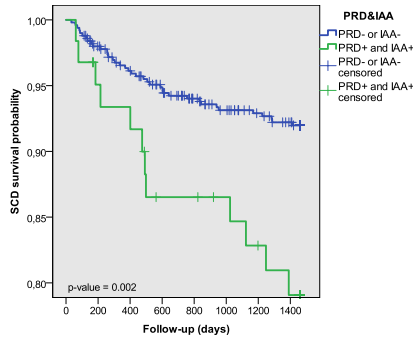

Figure 3.8 Estimated probability curve of SCD for two subgroups defined by PRD^+&IAA^+.

		Univariate	
		HR (95%)	p-value
Endpoint: SCD	PRD^+&TS^+	3.090 (1.729-5.522)	$1.4{\cdot}10^{-4}$ ***
	PRD^+&IAA^+	2.803 (1.465-5.364)	0.002**
Endpoint: PFD	PRD^+&TS^+	2.758 (1.572-4.838)	$4{\cdot}10^{-4}$ ***
	PRD^+&IAA^+	0.763 (0.275-2.117)	0.603
Endpoint: CD	PRD^+&TS^+	3.089 (2.066-4.617)	$3.8{\cdot}10^{-8}$ ***
	PRD^+&IAA^+	1.888 (1.134-3.142)	0.015*

Table 3.7 Univariate Cox analysis results for PRD^+&TS^+, PRD^+&IAA^+ separately considering SCD, PFD or both as endpoints. *p<0.05, **p<0.01, ***p<0.001.

PRD evaluation) and Holter recordings (for TS evaluation). In terms of SCD prediction, the stratifying ability of PRD is enhanced when combined with the IAA marker that evaluates the amplitude of the T-wave alternans over 24 hours. Although T-wave alternans, measured by IAA in this work, are related to abnormal cardiac function [263], PRD measures changes in sympathetic modulation of ventricular repolarization [343]. The synergistic information provided by the two variables serves to improve the prediction of SCD. In the findings described above, the PRD risk stratification capacity is maintained when accounting for competing risk events in survival analyses.

The concentration of NT-proBNP, dichotomized using the threshold (1000 pg/mL) proposed in the original MUSIC study [411], was not a significant

predictor of SCD in multivariable regression models comprising PRD or combined ECG markers. When the endpoint was CD, NT-proBNP>1000 pg/mL could significantly predict CD in a multivariable model. Other studies have proposed alternative thresholds for NT-proBNP, like NT-proBNP>5180 pg/mL [176], and found that the dichotomized variable is a predictor of both SCD and PFD. However, since the CHF population analyzed includes only patients in NYHA classes II and III, only 7% of the patients had NT-proBNP values above 5180 pg/mL.

Based on previous studies showing that PRD is not related to HRV and respiratory activity [343], the PRD and HRV markers could add complementary information. However, the results of this study show that HRV markers have no relationship with SCD or PFD, and therefore, HRV markers were not combined with PRD for risk stratification purposes. On the other hand, of the clinical variables assessed in this study, the NYHA class and LVEF $\leq 35\%$ are the two with the highest HR for both PFD and SCD. In any case, the HR of these two clinical variables is lower than that obtained for the combined ECG variables PRD & TS in the prediction of PFD and PRD & IAA in the prediction of SCD. LVEF is widely used in clinics to identify high-risk patients, but its precision is low [244]. Regarding the NYHA class, as it reflects a subjective assessment and can change frequently over short periods of time [411], its interpretation is more critical than other variables. The analysis carried out in this work suggests that the adjunct use of clinical variables and ECG-based markers can improve the prognostic value of all of them and produce a risk score with remarkably superior performance to predict the two most common modes of death in patients with CHF.

An important aspect regarding the use of PRD is the fact that it can be measured from 5-minute ECGs by using the PRSA-based method employed in this study, first described by Rizas et al.[341] and later updated in the previous chapter (2. Periodic Repolarization Dynamics in simulated microgravity). In the present work, 20-minute ECGs were used, from which the 5-minute segment associated with minimum PRD is selected. This is an advantage compared to several markers previously analyzed, such as IAA [263], QTVi [37], TS [363], $\Delta\alpha^{\mathrm{QT}}$ [335], $\Delta\alpha^{\mathrm{Tpe}}$ [258] or TMR [331], which require longer ECG recordings or specific protocols, such as stress tests or steady

heart rate, for their evaluation. Although the combination of PRD with other Holter-based markers improves risk stratification, it requires long-duration recordings. On this basis, the proposal in this work is that PRD could be used in an initial step to select patients with high CD risk. In those selected patients, the use of longer duration signals and associated variables could be useful to specifically predict each of the death modes. Several works have proposed other markers related to repolarization variability measured from short-term ECG recordings, such as the variance normalized by the mean of QT end, QT peak or T-peak-to-T-end (Te) intervals, and have evaluated them in CHF populations. In recent studies, the mean and/or standard deviation of Te have been shown to predict 30-day mortality [306, 307] and mortality in hospital [308] among patients with decompensated CHF.

In summary, this chapter shows the prognostic value of PRD in combination with other Holter-derived markers to predict PFD and SCD in a large cohort of CHF patients. Future studies in CHF cohorts that include a greater number of victims of SCD and PFD would allow for more robust statistical analysis to confirm the findings reported here. In addition, studies in larger populations would facilitate the evaluation of PRD's capacity for risk stratification in specific subpopulations of patients with CHF, such as those with reduced or preserved LVEF or in different NYHA classes, among others.

3.6 Conclusions

This study examines PRD, a noninvasive marker indicative of repolarization instability associated with low-frequency oscillations in sympathetic activity, as a prognostic indicator for the risk of SCD and PFD in CHF patients. The combination of PRD with a T-wave alternans index further enhances its predictive capacity for the stratification of the risk of SCD. Furthermore, the combination of PRD with the slope of heart rate turbulence facilitates the prediction of the risk of PFD. In general, the importance of ECG markers, derived from short-term ECG or ambulatory Holter recordings, is highlighted as a valuable tool to improve prognosis in CHF patients beyond conventional clinical variables.

Endpoint: SCD	Multivariate		Multivariate	
	HR (95%)	p-value	HR (95%)	p-value
NYHA class III	1.586 (0.813-3.092)	0.176	1.858 (0.987-3.497)	0.055
LVEF$\leq$ 35%	2.084 (1.028-4.225)	0.042*	2.228 (1.136-4.371)	0.020*
NSVT and VPB>240	1.278 (0.679-2.405)	0.447	1.552 (0.861-2.798)	0.144
NT-proBNP>1000 pg/mL	1.560 (0.831-2.930)	0.167	1.807 (0.997-3.275)	0.051
PRD^+&TS^+	1.998 (1.068-3.738)	0.030*	—	—
PRD^+&IAA^+	—	—	3.046 (1.578-5.877)	0.001**

Table 3.8 Multivariable SCD risk prediction including the following variables: NYHA class, LVEF$\leq$ 35%, combined NSVT and VPB>240, NT-proBNP>1000 pg/mL and a combined ECG variable that can be either PRD^+&TS^+ or PRD^+&IAA^+. *p<0.05, **p<0.01.

Endpoint: CD	Multivariate		Multivariate	
	HR (95%)	p-value	HR (95%)	p-value
Age	1.015 (0.995-1.035)	0.135	1.021 (1.001-1.041)	0.035*
Ischemic etiology	1.515 (0.776-2.956)	0.224	2.038 (1.058-3.923)	0.033*
Prior MI	1.009 (0.523-1.946)	0.980	0.947 (0.500-1.791)	0.866
NYHA class	1.771 (1.119-2.801)	0.015*	1.914 (1.226-2.988)	0.004*
LVEF$\leq$ 35%	1.568 (0.977-2.517)	0.062	1.727 (1.089-2.737)	0.020*
NSVT and VPB>240	1.236 (0.789-1.937)	0.354	1.489 (0.969-2.287)	0.069
NT-proBNP>1000 pg/mL	2.092 (1.326-3.302)	0.002**	2.293 (1.478-3.557)	$2{\cdot}10^{-4}$***
PRD$^+$&TS$^+$	1.893 (1.215-2.947)	0.005**	—	—
PRD$^+$&IAA$^+$	—	—	2.431 (1.446-4.085)	0.001**

Table 3.9 Multivariable CD risk prediction including the following variables: Age, ischemic etiology, prior myocardial infarction, NYHA class, LVEF$\leq$ 35%, combined NSVT and VPB>240, NT-proBNP>1000 pg/mL and a combined ECG variable that can be either PRD$^+$&TS$^+$ or PRD$^+$&IAA$^+$. *p<0.05, **p<0.01, ***p<0.001.

Neo, sooner or later you're going to realize, just as I did, that there's a difference between knowing the path and walking the path.

The Matrix (1999)

4

Short-term evaluation of ECG ventricular depolarization and repolarization response to conventional and physiological pacing

4.1 Motivation

Cardiac arrhythmias affect 1.5% to 5% of the general population and account for up to 20% of all deaths worldwide [103, 299]. Cardiac pacing is the current elective therapy for patients with symptomatic bradyarrhythmias and/or cardiac conduction dysfunction [203]. Pacemakers apply electrical stimulation to restore the electrical activity of the heart to a normal cardiac rhythm.

During the past several decades, RVP, administered through implantable pacemakers, has been the predominant technique for the treatment of bradyarrhythmias. Common locations for RVP stimulation are the right ventric-

ular apex (so-called right ventricular apex pacing, RVAP) and the septum (so-called right ventricular septal pacing, RVSP). Pacing at both locations initiates a non-physiological ventricular depolarization conduction pattern that may lead to dyssynchronous contractions of the heart.

Despite the successful results of RVP for the treatment of bradyarrhythmias, numerous studies have shown its detrimental effects in terms of electrical and mechanical dyssynchrony of the ventricles, which predispose patients to develop mitral and tricuspid regurgitation, atrial fibrillation, cardiomyopathy, HF and death [299, 30, 6, 2, 272].

As an alternative to conventional, nonphysiological RVP, physiological pacing techniques have been proposed, which stimulate the specialized cardiac conduction system to provide more physiological ventricular activation [22]. These techniques include HBP and LBBAP. HBP in patients who required pacemaker implantation was initially described by Deshmuk et al. [104] and, since then, its feasibility and safety have been shown in different investigations. Importantly, HBP has been associated with a significant reduction, compared to RVP, in the combined endpoint of all-cause mortality, hospitalization for HF and upgrade to biventricular pacing [1]. However, several issues limit its application, including the difficulty of lead implantation in the His bundle due to its small size and the fibrous nature of the surrounding tissue, the high and commonly unstable pacing capture threshold and the risk of causing damage to the bundle during the intervention [446, 452]. In contrast, LBBAP offers relative ease in lead placement, has a lower and more consistent capture threshold, and has been shown to generate narrow paced QRS complexes and highly synchronized activation of the LV when applied to patients with LBBB, as it paces the conduction system distal to the His bundle to circumvent the region of conduction block [446]. Despite these advantages of LBBAP, larger randomized studies should be conducted to confirm its feasibility, long-term safety, and effectiveness [166]. Figure 4.1 illustrates the different physiological stimulation regions currently used in clinical practice.

To improve the characterization of ventricular activation in response to physiological pacing compared to conventional pacing, several studies have been conducted in recent years based on the standard ECG and the VCG. Most

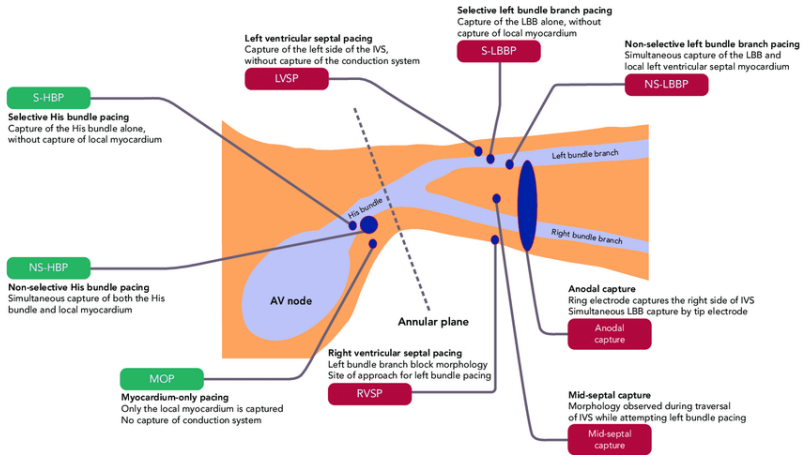

Figure 4.1 Regions and techniques applied to stimulate the heart through cardiac conduction system. Adapted from [21]

of these studies have evaluated QRS morphology, duration, and area [217, 67]. In addition, ventricular depolarization patterns have been characterized from ultra-high-frequency ECG (UHF-ECG) recordings [182, 260]. By proposing and validating novel measures of local depolarization duration and ventricular electrical dyssynchrony derived from UHF-ECG recordings, these studies have compared interventricular synchrony and time for LV wall depolarization between various conventional and physiological pacing techniques [182, 93, 431, 91, 92, 90, 442].

Research on the effects of pacing on ventricular repolarization is much more scarce than on ventricular activation. Some studies have quantified the duration of classical repolarization intervals, such as the heart rate-corrected QT interval, the JT interval, and the T-peak-to-T-end interval. These studies have shown a prolongation of the repolarization intervals after RVP but not following HBP or LBBAP [431, 442, 304, 317]. Other studies have reported changes in the T wave, even if mostly from a qualitative point of view, without providing quantitative measures of the characteristics of the T wave [290, 425, 454].

The purpose of this chapter is to extend the analysis of ECG ventricular depolarization and repolarization by processing UHF-ECG recordings from patients with physiological ventricular activation undergoing pacemaker im-

plantation for bradycardia therapy. The spatial and temporal features of the depolarization and repolarization phases are quantified during spontaneous rhythm and in response to different types of conventional and physiological pacing. The hypothesis of this chapter is that physiological pacing techniques can lead to QRS and T-wave patterns that better resemble those of spontaneous rhythm in the analyzed patients without ventricular conduction abnormalities and that LBBP techniques may be an equally effective option as HBP in reducing ventricular activation dyssynchrony, particularly in the LV, and in preserving ventricular repolarization characteristics.

4.2 Materials

4.2.1 Ultra-high-frequency ECG Recordings

In this work, we study a population of patients without bundle branch block and with an indication for pacemaker therapy due to bradycardia. Six hundred and fifty-eight 14-lead UHF-ECG recordings, sampled at 5,000 Hz, were obtained from 178 patients (76.8 [8.5] years old, 74% male) using VDI (Ventricular Dyssynchrony Imaging) UHF-ECG (VDI Technologies, Brno, Czech Republic) at the Cardiocenter of Faculty Hospital Kralovske Vinohrady and the Third Medical Faculty of Charles University, Prague, Czech Republic. More than 53% of the patients had atrioventricular block and almost 32% reported sick sinus syndrome. The UHF-ECG recordings included 12 standard leads and two left posterior chest wall leads on the axillary line and on the scapula, V7 and V8, recorded as described in [182]. UHF-ECG recordings were acquired for 1 to 10 minutes in a resting supine position.

Patients were subjected to different types of conventional and physiological pacing types. Conventional pacing types included RVAP and RVSP. Physiological pacing types included various subtypes of HBP and LBBP. For HBP subtypes, selective HBP (sHBP) was characterized by pure His capture pacing, whereas non-selective HBP (nsHBP) involved the capture of both the His and the adjacent myocardial tissue. For LBBP, the following three subtypes were considered: selective LBB pacing (sLBBP), entailing exclusive LBB capture; non-selective LBB pacing (nsLBBP), with capture of both the

LBB and the adjacent left septal myocardium; and LV septal pacing (LVSP), when the lead failed to capture LBB but reached the LV subendocardium.

The distribution of the applied pacing types in the available dataset was: 37 recordings with RVAP, 102 with RVSP, 50 with sHBP, 160 with nsHBP, 13 with sLBBP, 47 with nsLBBP and 87 with LVSP. In addition, 199 recordings were acquired during spontaneous heart rhythm. All patients signed an informed consent prior to enrollment.

Pacemaker implantation

The pacing electrode was placed in a typical His-bundle pacing region as described in previous work [1]. The His bundle region was mapped using a SelectSecure TM lead (model 3830, 69 cm, Medtronic Inc., Minneapolis, MN), delivered through a fixed-curve sheath (C315HIS, Medtronic). sHBP and nsHBP capture was defined as previously described [424, 90]. For LBBAP, the lead was moved towards the right ventricle (RV), along a line between the His bundle region and the RV apex, and screwed deep into the septum to obtain a position on the left side of the interventricular septum showing a paced QRS morphology of RBBB/pseudo-RBBB in lead V1 [91]. sLBBp, nsLBBp and LVSP capture were described as in previous studies [91, 92]. For RVAP and RVSP, the RV leads were implanted in a standard form at the apex or septum of the RV [424, 90].

4.3 Methods

4.3.1 ECG preprocessing

UHF-ECG signals (sampled at 5 kHz) were high-pass filtered using an eighth-order Butterworth filter (cut-off frequency at 0.5 Hz) to remove baseline wander. A 50 Hz digital 20th-order IIR notch filter was applied to attenuate powerline interference. A semi-automated algorithm, based on the method of Haq et al. [155], was used to remove pacing artifacts. The steps of the algorithm are as follows.

1. Orthogonal leads X, Y, and Z were obtained from the standard 12-lead ECG using the Kors transformation matrix [196]. The vector

magnitude, v(n), was computed as:

$$\mathrm{v(n)} = || \, v(\mathrm{n}) \, || = \sqrt{\mathrm{x}^2(\mathrm{n}) + \mathrm{y}^2(\mathrm{n}) + \mathrm{z}^2(\mathrm{n})} \tag{4.1}$$

where $|| \, v(\mathrm{n}) \, ||$ is the vector norm of $v(\mathrm{n})$, with x(n), y(n) and z(n) being the three orthogonal leads in $v(\mathrm{n})$.

2. The magnitude slope, dv/dt, was calculated from the difference between consecutive samples of the time series v(n). The onset and end of the pacing artifact were selected as the first sample $\mathrm{n_o}$ and the last sample $\mathrm{n_e}$ for each beat of the time series v(n), respectively, that satisfied the following conditions:

$$\frac{\mathrm{dv(n)}}{\mathrm{dt}} > \alpha_{\mathrm{on}} \qquad \frac{\mathrm{dv(n)}}{\mathrm{dt}} < \alpha_{\mathrm{end}} \tag{4.2}$$

where α_{on} and α_{end} are thresholds to determine the onset and end of the pacing spike. In this study, the threshold values were set to $\alpha_{\mathrm{on}} = 0.5$ mV/ms and $\alpha_{\mathrm{end}} = -0.5$ mV/ms.

3. The pacing spike was removed by linear interpolation between the signal amplitude at $\mathrm{n_o}$ and $\mathrm{n_e}$. Figure 4.2 shows a segment of an ECG lead before and after removing the pacing spike by applying the described algorithm.

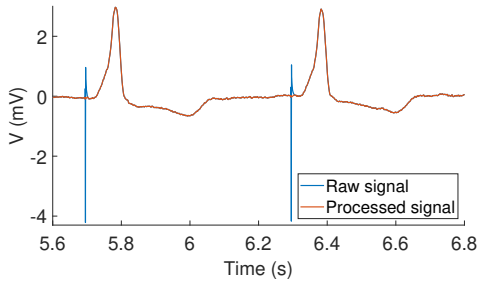

Figure 4.2 Pacing spike cancellation in a segment of an ECG lead. The signals before and after removing the pacing spike are shown in blue and red, respectively.

The QRS complexes in each signal were detected and classified according to their morphology following previously proposed methods [312]. Subsequently, the delineation of the peaks, onsets, and ends of all ECG waves was performed using a single-lead wavelet-based automatic delineation software [242].

A representative beat for each recording was defined as the median beat of all the beats presenting the dominant morphology. The applied algorithm follows these steps:

1. RR intervals were computed from the fiducial points of the QRS complex.

2. The statistical mode of the RR interval time series was calculated for each recording. An RR histogram was computed using 20-ms bins. The bin containing the RR mode was selected and the median of the beats corresponding to the RR intervals in that bin was computed.

3. All beats within the RR bin were aligned with respect to the computed median beat by maximizing the cross-correlation.

4. The rank correlation between the initially calculated median beat and each of the aligned beats was calculated. Beats with rank correlation coefficients below 0.85 were discarded.

5. The final median beat was computed from the aligned beats that were not discarded.

4.3.2 Depolarization indices

The duration of single-lead local depolarization (Vxd) and electrical dyssynchrony in the ventricles (e-DYS) were calculated from UHF-ECG by first dividing the spectrum from 150 Hz to 1,000 Hz in 16 frequency bands, following the method described in [182]. For each band and precordial lead (V1-V8), the amplitude envelopes were calculated using the Hilbert transform, with the amplitude envelopes segmented according to the QRS onset and end annotations. The median amplitude envelope in each frequency band was normalized so that its integral was one. e-DYS was calculated as the maximal

time difference between the center of mass of the QRS above the 50 percent threshold of the baseline-to-peak amplitude for the leads V1-V8. The sign of e-DYS was associated with the order of ventricular activation. Negative e-DYS values indicated that the LV was activated earlier than the RV.

Additionally, the local activation duration in a given lead, defined between the crossings at half the maximum peak magnitude of the average of the normalized median envelopes in that lead, was defined as Vxd. Low Vxd values were related to high apparent conduction velocities, presumably due to the contribution of the intrinsic conduction system, while high Vxd values were related to a non-homogeneous substrate or non-physiological origin of myocardial propagation. Vd was calculated as the mean of all the computed Vxd values and represented the average duration of the depolarization propagation.

QRS durations (QRS_d) were measured in each median beat (computed as described in Section 4.3.1) as the time between the start and end of the QRS complex using the associated marks and a post-processing selection rule for all single-lead locations [242] to obtain a unique multilead QRS_d.

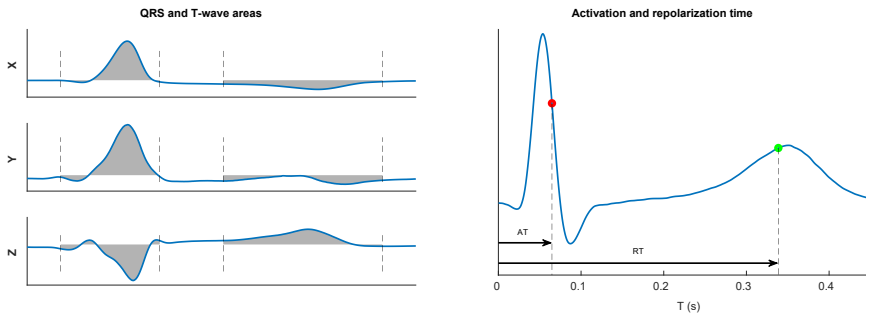

Figure 4.3 a) QRS and T-wave areas (shaded areas) in orthogonal leads. b) ECG beat for one lead with identified time points used to compute activation time, AT (red), and repolarization time, RT (green).

From the eight independent leads of the median beat, the vectorcardiogram (VCG) was synthesized using the Kors method [235]. The QRS area (QRS_a) in each orthogonal lead (X, Y, and Z) was calculated as the integral

of the absolute value of the QRS complex, from the beginning to the end of the QRS, as illustrated in Figure 4.3a). The total QRS_a was calculated as:

$$QRS_a = \sqrt{QRS_{a,X}^2 + QRS_{a,Y}^2 + QRS_{a,Z}^2} \tag{4.3}$$

where $QRS_{a,X}$, $QRS_{a,Y}$ and $QRS_{a,Z}$ denote the QRS areas in leads X, Y and Z.

In addition, the local AT was calculated for each individual precordial lead as the center of mass of the absolute QRS complex of the representative median beat, using the multilead QRS onset as a reference. An example is shown in Figure 4.3b), where the AT is marked with a red point. The difference between the last and the first AT values within the 6 precordial leads V1-V6 was defined as the dAT. This dispersion was calculated as the absolute value of the difference or by including a negative sign when the number of the first activated lead (1 to 6 for V1 to V6) was greater than that of the last activated lead (denoted as dATs).

To specifically assess activation dyssynchrony within the LV, analogous measurements of AT dispersion were calculated focusing only on leads V4-V6. These variables were denoted as dAT_{4-6} and $dATs_{4-6}$ when the absolute value and the signed value of AT dispersion in V4-V6 were measured, respectively.

4.3.3 Repolarization indices

The QT interval, which represents the time needed for ventricular activation and repolarization, was calculated as the interval between the multilead QRS complex onset and the multilead T-wave end of the median beat. Both times were determined by applying post-processing selection rules to the delineation marks of individual leads [242]. Taking into account the QT intervals of all recordings in the dataset, a correction was performed for the effects of heart rate. To derive the correction formula, different regression models were first fitted to the QT and RR measurements, with the regression models being linear, hyperbolic, parabolic, logarithmic, shifted logarithmic, exponential, arc tangent, hyperbolic tangent, arc hyperbolic sine, and arc hyperbolic cosine [324]. The regression model leading to the lowest residual of the fitting was selected, and the corresponding correction formula was derived by projecting

the QT interval to a standard RR level equal to one second. The corrected QT intervals calculated according to the derived formula were denoted by QT_c.

In each precordial lead, the RT was determined as the center of mass of the absolute T wave of the representative median beat (represented as a green point in Figure 4.3b), measured from the multilead QRS onset mark. A corrected RT, denoted RT_c, was calculated by deriving a correction formula, analogously to the QT interval correction, to remove any influence of RR on RT. The dRT was calculated as the difference between the maximum and minimum values of RT_c within the 6 precordial leads V1-V6. The signed dispersion of RT, denoted as dRTs, included a negative sign for the value of dRT when the number of the first repolarized lead (1 to 6 for V1 to V6) was higher than that of the last repolarized lead.

In parallel to dAT_{4-6}, the dispersion of RT within the LV was specifically calculated by focusing the analysis on the leads V4-V6 only. The corresponding unsigned and signed variables were denoted as dRT_{4-6} and $dRTs_{4-6}$.

The T-wave area (T_a) was calculated from the orthogonal leads X, Y, and Z according to the following equation:

$$T_a = \sqrt{T_{a,X}^2 + T_{a,Y}^2 + T_{a,Z}^2} \tag{4.4}$$

where $T_{a,X}$, $T_{a,Y}$ and $T_{a,Z}$ denote the T-wave areas in leads X, Y, and Z. An example of the calculation of the T-wave area is shown in Figure 4.3a).

Another studied repolarization marker was the PRD, which was proposed to assess sympathetic modulation of ventricular repolarization by measuring low-frequency (below 0.1 Hz) oscillations in the T-wave vector. The PRD index was computed using the method described in Section 3.3.1. This method included the following steps:

1. T waves were selected using a window related to the QRS position and the RR interval for each beat. The onset of the T-wave window, denoted by T_{on_i}, was set at 90 ms after the QRS_i mark: $T_{on_i} = QRS_i + 90\,ms$. The end of the T-wave window, denoted by T_{end_i}, was defined as $T_{end_i} = QRS_i + \min(360\,\text{ms}, \frac{2}{3}RR_i)$ for RR_i below 720 ms, or $T_{end_i} = QRS_i + 360\,\text{ms}$, in other cases.

2. A constant value was subtracted from each T wave in each of the analyzed leads so that the voltage at T_{end} was set to 0 mV.

3. The average electrical vector was calculated for each T-wave window. The angle dT° between two consecutive T-wave windows was calculated from the dot product of the normalized average vectors.

4. A 10th-order median filter was applied to attenuate outliers and artifacts in the dT° time series.

As in previous chapters, the applied method to evaluate the oscillations measured by the PRD index [341] was based on PRSA [36]. The steps applied are summarized here:

5. Anchor points were defined as points meeting the following condition:

$$\frac{1}{M}\sum_{j=0}^{M-1} x_{i+j} > \frac{1}{M}\sum_{j=1}^{M} m_{i-j} \tag{4.5}$$

   Where M=9 in order to allows detecting frequencies in the range of interest (from 0.025 to 0.1 Hz), as fully described in [36].

6. Windows were defined around each anchor point and anchor points at the beginning or end of the dT° series were discarded.

7. The PRSA series was obtained by averaging the dT° values in all selected windows contained in each recording.

Finally, PRD was defined as the difference between the maximum and minimum values of the PRSA series.

4.3.4 Statistical analysis

Continuous and discrete variables are presented as median [IQR] and counts (percentages), respectively. The Mann–Whitney U test (or Wilcoxon rank-sum test) was used for univariate comparisons of continuous variables between independent groups. All statistical analyses were performed with MATLAB R2020a (9.8). Differences were considered statistically significant if the associated p-value<0.05. NS is used to denote nonsignificant.

4.4 Results

4.4.1 Depolarization indices

QRS duration

Figure 4.4 shows the median values and interquartile ranges of QRS_d for all the pacing types analyzed in this study. The QRS complexes in spontaneous rhythm have a median duration of 103.6 [18.4] ms. The widest QRS complexes were observed after RVP, both RVSP (139.6 [30.1] ms, p<0.001 with respect to spontaneous rhythm) and RVAP (144.0 [24.9] ms, p<0.001). LBBAP led to shorter QRS complexes than RVP (123.2 [23.2] ms, 125.1 [34.7] ms, and 111.8 [20.4] ms for sLBBP, nsLBBP and LVSP, respectively), although still significantly longer than in spontaneous rhythm (p<0.001 for all tests). sHBP stimulation induced mean QRS_d values similar to those in spontaneous rhythm (104.9 [23.8] ms, NS) while nsHBP pacing was associated with the lowest QRS_d values (95.8 [22.9] ms, p-value<0.001 with respect to spontaneous rhythm).

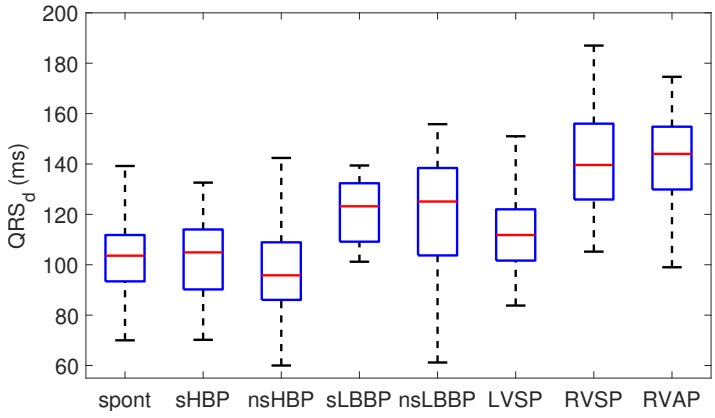

Figure 4.4 Box plots of QRS_d for spontaneous rhythm and each of the pacing types.

Electrical dyssynchrony index (e-DYS) and local activation duration (Vd)

Figure 4.5 shows the box plots for e-DYS (blue boxes) and Vd (red boxes) in spontaneous rhythm and in response to the seven pacing types analyzed. In spontaneous rhythm, there is minimal electrical dyssynchrony and a short activation duration (e-DYS = 4.70 [12.33] ms; Vd = 32.20 [8.50] ms). Similarly to the observations for QRS_d, the RVP techniques (RVSP and RVAP) showed the largest dyssynchrony and activation duration (e-DYS = 24.93 [18.57] ms; Vd = 45.80 [16.46] ms for RVSP and e-DYS = 21.93 [32.92] ms, Vd = 58.78 [15.82] ms for RVAP).

LBBAP techniques (sLBBP, nsLBBP and LVSP) induced negative e-DYS values indicative of earlier activation of the LV wall (-6.53 [11.25] ms, -11.47 [9.28] ms and -5.67 [8.13] ms, $p<0.001$ with respect to spontaneous rhythm), with activation duration similar to spontaneous rhythm. HBP techniques (sHBP and nsHBP) generated low positive e-DYS values (8.67 [11.33] and 11.00 [9.97] ms, respectively, $p=0.02$ and $p<0.001$) and low Vd values, again similar to those of spontaneous rhythm.

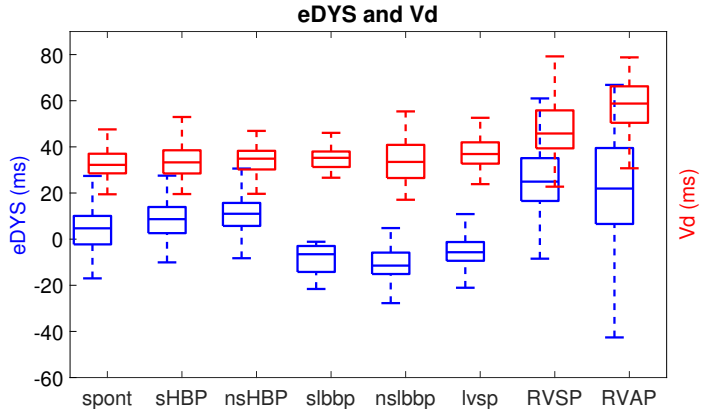

Figure 4.5 Box plots of ventricular electrical dyssynchrony (e-DYS) and average of duration of local depolarization (Vd) for each pacing type in UHF-ECG database.

Area of QRS complex

The QRS_a values during spontaneous rhythm were 50.06 [27.23] μVs (figure 4.6). The highest QRS_a values were found for RVAP and RVSP (153.94 [50.67] μVs and 84.93 [13.46] μVs, p-values < 0.001 with respect to spontaneous rhythm). sLBBP, nsLBBP and sHBP showed the lowest QRS_a values, which were close to those measured in spontaneous rhythm (42.74 [15.29] μVs, 51.24 [31.19] μVs, and 53.80 [33.29] μVs).

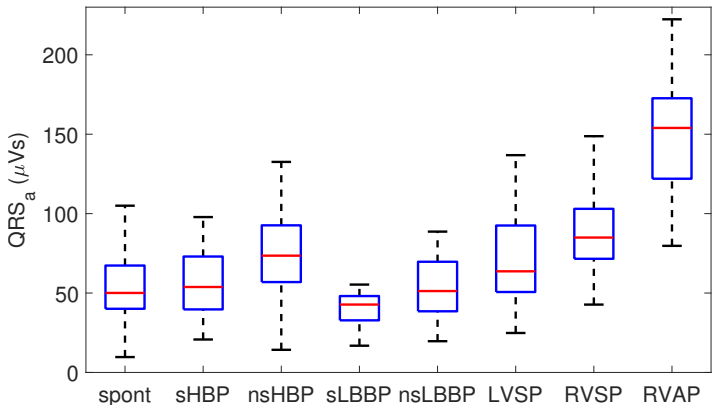

Figure 4.6 Box plots of QRS_a for spontaneous rhythm and each of the pacing types.

Activation time patterns

Figure 4.7 shows the average AT values in the precordial leads V1-V6 for spontaneous rhythm and each cardiac pacing type. As can be seen in the figure, leads V1, V5 and V6 present the earliest activation in spontaneous rhythm (54.5 ms in lead V6) while V2-V4 present the latest activation (59.5 ms in lead V3). Similarly, sHBP and nsHBP show activation patterns in which the regions corresponding to leads V1, V5, and V6 are activated earlier than the regions corresponding to leads V2-V4. LBBAP pacing types, as expected, present the earliest activations in leads V4-V6 (earliest activation at 60.0 ms for sLBBP, 66.5 ms for nsLBBP and 57.4 ms for LVSP), while the latest activations are found in leads V1-V3 (latest activation at 70.9 ms, 76.2

ms and 61.5 ms, respectively). The AT values for RVP types are the largest in practically all leads compared to other pacing types and spontaneous rhythm. For RVAP, the activation starts in V4 and ends in V1 and V6. For RSVP, the activation starts in V1 and ends in V4 and V6.

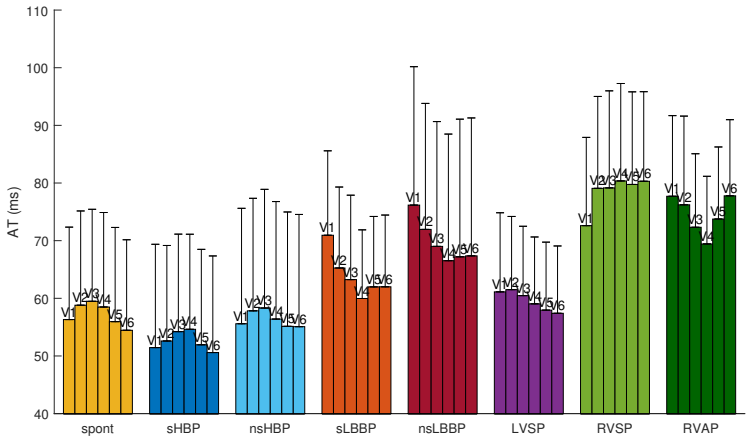

Figure 4.7 Average activation time (AT) in precordial leads V1-V6.

Dispersion of activation time

The median dAT for spontaneous rhythm was 8.80 [5.00] ms, as shown in Figure 4.8. sHBP and nsHBP rendered the closest median dAT values to those observed for the intrinsic rhythm (9.40 [7.00] ms and 9.50 [5.70] ms respectively, NS for both cases). sLBBP and nsLBBP had significantly higher dAT values (15.20 [11.20] ms and 15.60 [10.25] ms, respectively with $p<0.001$), while dAT for LVSP was higher than for spontaneous rhythm ($p<0.001$) and HBP types ($p<0.05$) but lower than for sLBBP (NS) and nsLBBP ($p<0.01$). The highest dAT values were associated with RVAP, 17.00 [7.20] ms ($p<0.001$ with respect to spontaneous rhythm).

When considering the sign of dispersion, dATs, techniques that stimulate the His bundle, sHBP and nsHBP, were found to exhibit median values of dATs (-3.10 [20.20] ms and -6.00 [18.20] ms, respectively) similar to spontaneous rhythm (-6.60 [16.20] ms, NS). sLBBP, nsLBBP and LVSP rendered slightly more negative dATs values (-15.20 [11.20] ms, -13.00 [13.35] ms and -8.00 [22.45] ms, $p<0.05$, respectively). RVAP led to comparable dATs values

(-12.60 [33.10] ms, NS), but RVSP was associated with the highest positive dATs values (12.60 [27.40] ms, p<0.05). The corresponding results for dATs are presented in 4.9.

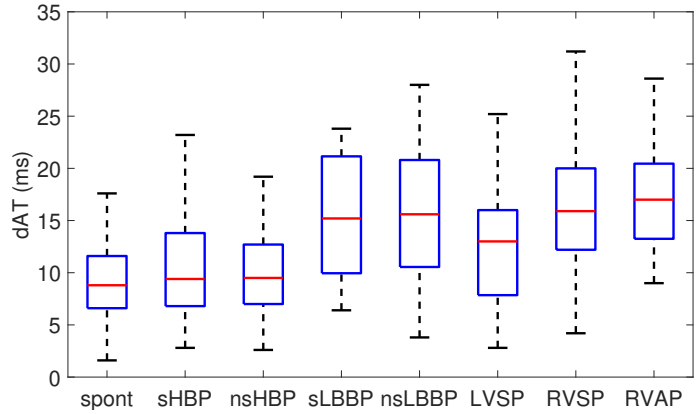

Figure 4.8 Box plots of dAT for spontaneous rhythm and each of the pacing types.

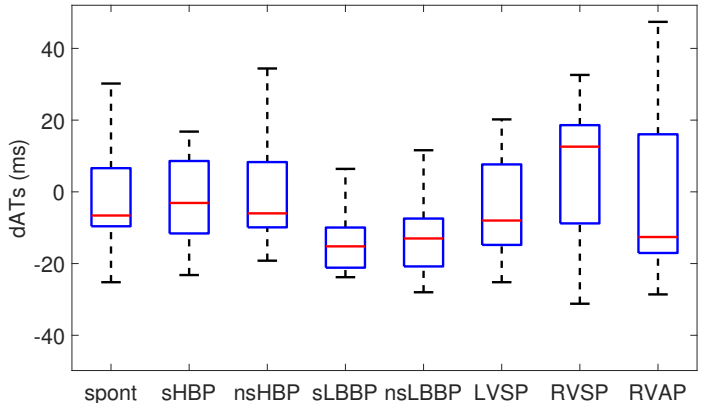

Figure 4.9 Box plots of dATs for spontaneous rhythm and each of the pacing types.

The results for AT dispersion within the LV, represented by the variable dAT_{4-6}, are shown in Figure 4.10. Spontaneous rhythm recordings presented a median value of 4.30 [5.20] ms. sLBBP and nsLBBP led to lower median

values of dAT_{4-6}, which were not significantly different from those of spontaneous rhythm (2.20 [3.80] ms and 3.80 [4.15] ms, respectively). LVSP also had lower median values (2.40 [3.95] ms, p<0.001). sHBP and nsHBP increased dAT_{4-6} (6.00 [7.40] ms and 3.00 [3.50] ms, p<0.05 with respect to spontaneous rhythm). The conventional pacing types had the highest dAT_{4-6} values (7.10 [8.60] ms for RVSP and 8.20 [6.15] ms for RVAP, p<0.001 in both cases). The corresponding results for $dATs_{4-6}$ are presented in 4.11.

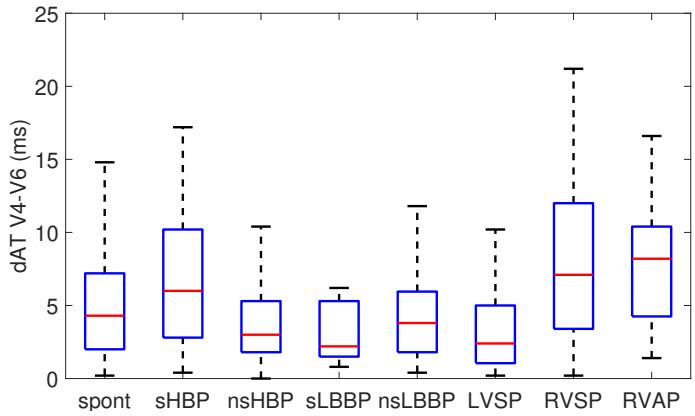

Figure 4.10 Box plots of dAT_{4-6} for spontaneous rhythm and each of the pacing types.

4.4.2 Repolarization indices

Corrected QT

The median QT_c was 429 [43] ms during spontaneous rhythm (Figure 4.12). Of the HBP types, sHBP led to significantly higher QT_c values (451 [32] ms, p=0.03), while nsHBP led to significantly lower values (421 [29] ms, p=0.008) than spontaneous rhythm. Of the LBBAP types, sLBBP and nsLBBP led to significantly higher QT_c values (462 [21] ms, p<0.001 and 444 [51] ms, p=0.03), while QT_c values after LVSP were similar to those in spontaneous rhythm (435 [30] ms, NS). The two RVP types, i.e. RVSP and RVAP, also induced larger QT_c values (455 [27] ms, p<0.001 and 451 [33] ms, p<0.001).

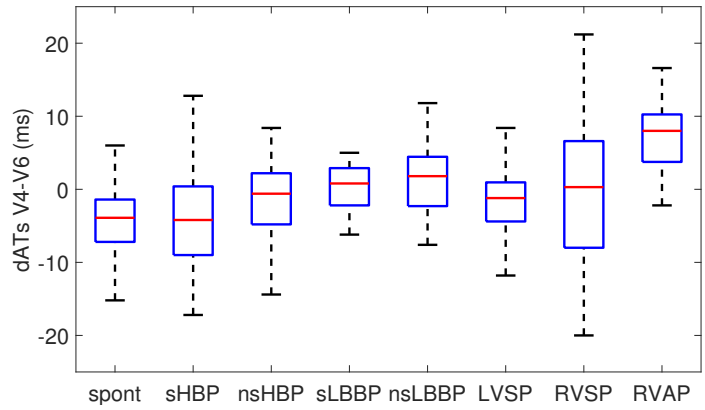

Figure 4.11 Box plots of $dATs_{4-6}$ for spontaneous rhythm and each of the pacing types.

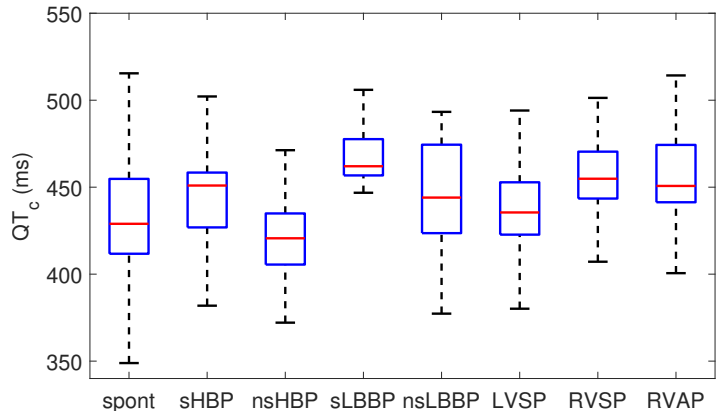

Figure 4.12 Box plots of QT_c for spontaneous rhythm and each of the pacing types.

Area of T wave

Figure 4.13 shows the values of T_a for each type of cardiac pacing. Interestingly, the observed trend is very similar to that observed for QRS_a, shown in Figure 4.6. The value of T_a for spontaneous rhythm was 30.50 [27.83] μVs. The highest T_a values were found for RVSP (63.56 [33.24] μVs, p<0.001) and RVAP (157.05 [59.97] μVs, p<0.001). Physiological pacing approaches,

particularly sHBP, nsHBP, sLBBP and nsLBBP, presented reduced T_a values, which were similar to that of spontaneous rhythm (sHBP: 30.80 [29.53] μVs, NS; nsHBP: 43.81 [30.87] μVs, p<0.001; sLBBP: 22.78 [11.12] μVs, p=0.03; nsLBBP: 32.04 [19.66] μVs, NS; LVSP: 50.05 [28.32], p<0.001).

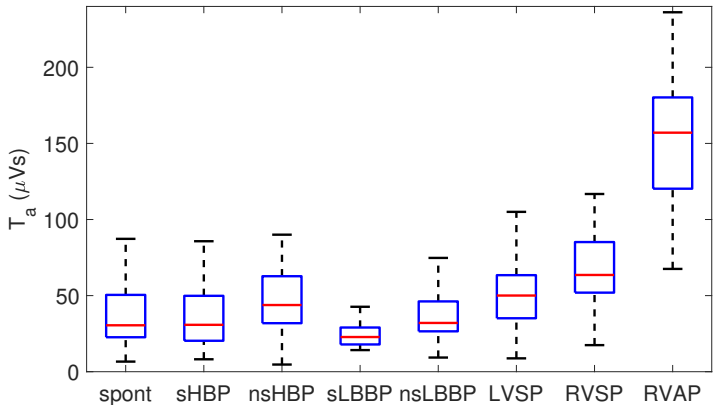

Figure 4.13 Box plots of T_a for spontaneous rhythm and each of the pacing types.

Periodic Repolarization Dynamics

As illustrated in Figure 4.14), PRD took values of 4.94 [3.93] degrees in spontaneous rhythm. This value was similar for nsLBBP (5.03 [3.35] degrees, NS), sLBBP (3.53 [1.38], NS) and RVSP (3.90 [3.03] degrees, NS). RVAP led to the lowest PRD values (2.87 [2.89] degrees, p<0.05 with respect to intrinsic rhythm). sHBP, nsHBP and LVSP also reduced the magnitude of low-frequency oscillations in ventricular repolarization (3.25 [3.57], 3.31 [2.79] and 3.14 [2.66] degrees, respectively, p<0.05 in all cases).

Repolarization time patterns

Figure 4.15 shows the average RT values corrected for the RR interval in the precordial leads V1-V6 for spontaneous rhythm and each cardiac pacing type. For spontaneous rhythm, the first lead to repolarize was V2 (321.6 ms), with lead V5 being the last lead to repolarize (336.5 ms). Similar RT

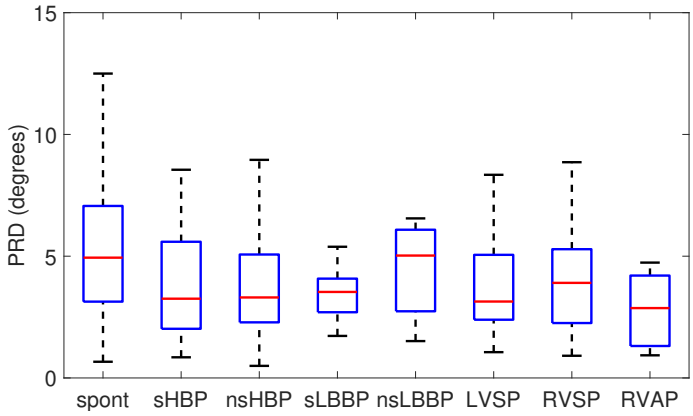

Figure 4.14 Box plots of PRD for spontaneous rhythm and each of the pacing types.

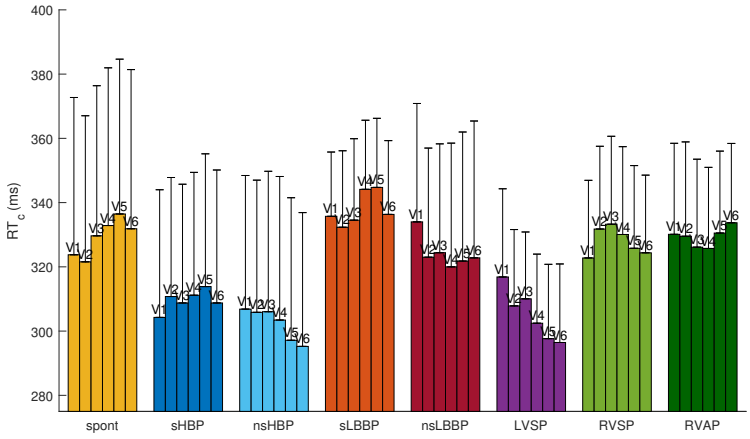

Figure 4.15 Average repolarization time (RT) corrected by RR duration in precordial leads V1-V6.

patterns were found for the two types of selective physiological pacing, i.e. sHBP and sLBBP, with the earliest repolarization in V1-V2 and the latest repolarization in V5. The RT patterns for nsHBP, nsLBBP, and LVSP were similar to the corresponding AT patterns, with V4, V5 and V6 being the first leads to repolarize in the three cases. RVAP showed RT patterns similar to those of AT, but in this case lead V6 was the latest to repolarize. For RVSP, the repolarization took longer to complete in lead V3.

Dispersion of repolarization time

As shown in Figure 4.16, the median dRT for spontaneous rhythm was 31.2 [22.2] ms. Similar dRT values were found for sHBP (27.6 [18.4] ms, NS), nsHBP (29.5 [20.4] ms, NS), sLBBP (23.8 [14.2] ms, NS), nsLBBP (36.2 [24.9] ms, NS), LVSP (30.4 [19.0] ms, NS) and RVSP (29.7 [21.2] ms, NS). RVAP, however, had significantly reduced dRT values (19.8 [13.4] ms, $p<0.001$).

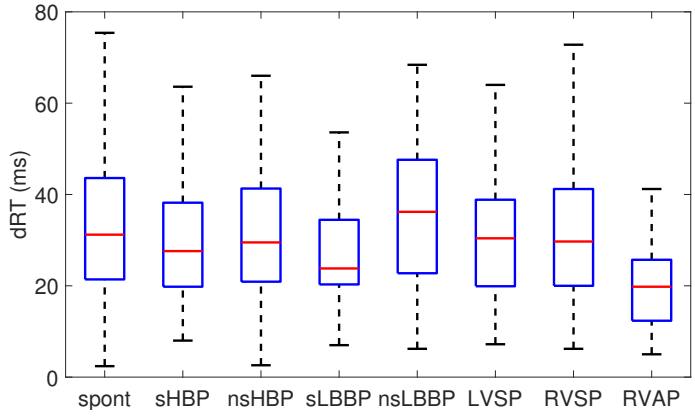

Figure 4.16 Box plots of dRT for spontaneous rhythm and each of the pacing types.

Figure 4.17 shows the results of dRT focused on leads V4-V6 only. As can be seen in the figure, the recordings stimulated with nsHBP, sLBBP, LVSP, and RVAP had the lowest median values of dRT_{4-6} (7.40 [19.90] ms, 4.60 [12.15] ms, 7.80 [11.40] and 6.00 [8.85] ms, respectively), with such values being statistically significantly different from those observed in spontaneous rhythm (12.50 [18.40] ms, p-value<0.05 in all cases).

The corresponding results for dRTs and $dRTs_{4-6}$ are presented in Figures 4.18 and 4.19.

4.5 Discussion

This chapter provides a detailed description of the response of ventricular depolarization and repolarization to seven different types of cardiac pacing

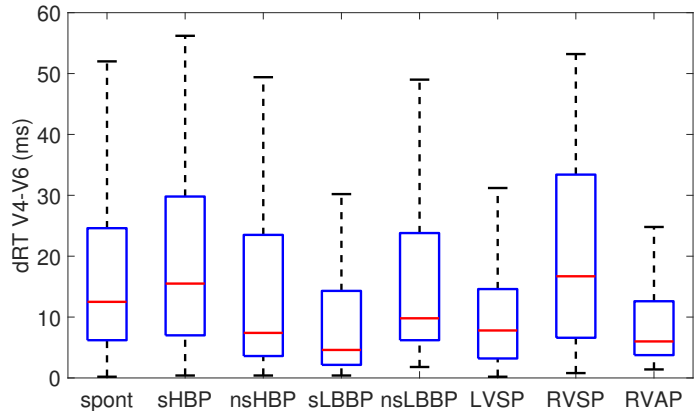

Figure 4.17 Box plots of dRT for spontaneous rhythm and each of the pacing types.

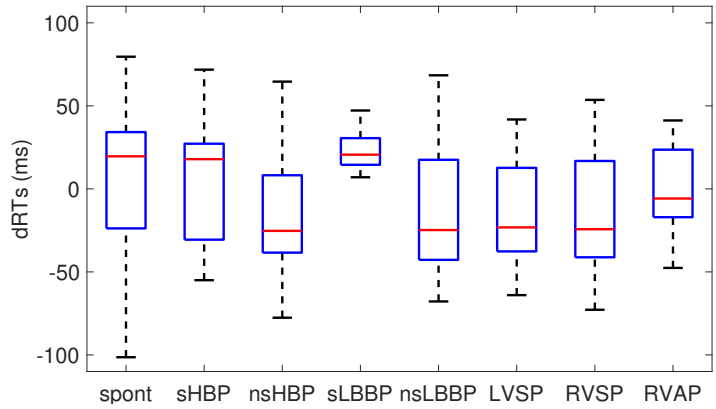

Figure 4.18 Box plots of dRTs for spontaneous rhythm and each of the pacing types

in patients without abnormalities in ventricular conduction and an indication for pacemaker implantation due to bradycardia. In addition to quantifying depolarization and repolarization indices commonly used in other studies, we propose additional markers to describe the spatial dispersion of the activation and repolarization times from UHF-ECG recordings. Properties related to the duration, area, and spatial heterogeneity of ECG activation and repolarization waves are shown to differentiate the effects of each of the tested physiolog-

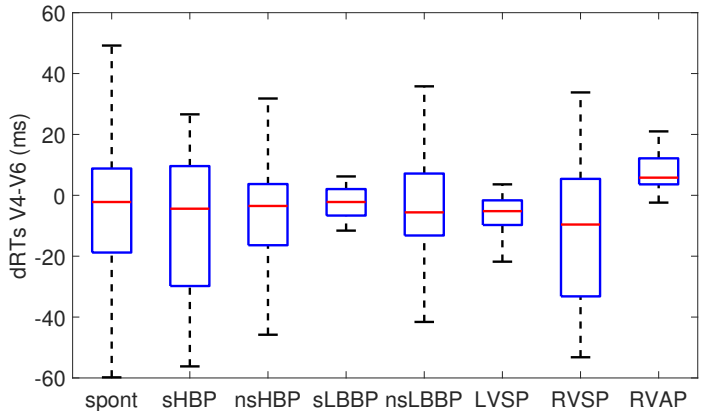

Figure 4.19 Box plots of $dRTs_{4-6}$ for spontaneous rhythm and each of the pacing types.

ical and conventional cardiac pacing techniques, with implications for the development of deleterious effects on cardiac function.

4.5.1 Pacing-induced effects on ventricular depolarization

For the characterization of cardiac pacing effects on ventricular depolarization, this study first examined classical ECG markers reported in the literature, such as duration and area of the QRS complex. Other more recently proposed markers quantified from UHF-ECG recordings were also analyzed, including Vd (measure of local activation duration) and e-DYS (measuring activation dyssynchrony). Finally, novel markers that can be quantified from standard ECGs (not necessarily sampled at very high frequency) were proposed based on ATs in different ECG leads and their spatial dispersion across the entire ventricles and across those leads facing the LV only.

From the analysis of all the described markers, we found that the physiological pacing techniques sHBP and nsHBP exhibit an electrical response comparable to that observed in spontaneous rhythm in patients without any conduction disorder. LBBAP techniques, including sLBBP, nsLBBP, and LVSP, despite presenting larger differences with respect to spontaneous rhythm than HBP-based techniques, are able to preserve the synchrony in the activation of the LV, with only a delayed activation in the RV. The conventional pacing

techniques RVSP and RVAP show markedly different responses to those found in spontaneous rhythm, with high dispersion in the ventricular ATs. This behavior was also observed in previous studies [91, 92, 90].

QRS_d has been commonly used to assess ventricular synchrony. Changes in QRS_d have been associated with the occurrence of major adverse cardiovascular events [231, 350]. Here, we find that sHBP and nsHB have a similar QRS_d to spontaneous rhythm. The longest QRS_d values were found for RVSP and RVAP. The three LBBAP techniques, that is, sLBBP, nsLBBP, and LVSP, were associated with lower QRS_d than RVSP and RVAP, but significantly higher than the intrinsic rhythm. Our results are in line with those reported in previous studies that compared the ventricular activation synchrony of sLBBP and nsLBBP techniques with that of LVSP [160] and RVAP [396]. The higher QRS_d values found for sLBBP, nsLBBP, and LVSP compared to spontaneous or His-paced activations can be attributed to the fact that the electrical pacing impulse is rapidly transmitted to the LV through the LBB or the myocardium close to it, but the RV is activated with some delay.

Activation indices derived from the VCG have been suggested to predict the response to cardiac resynchronization therapy more accurately than QRS_d [225]. Here, QRS_a was measured from the VCG. QRS_a has been reported to be less sensitive to uncertainty in the determination of the QRS boundaries, as the extremes of the QRS complex contribute scarcely to the area [115, 313], and to present less variability in its measurement than QRS_d [409]. Previous works have reported QRS_a to be an index of dyssynchrony in electrical activation, with a large QRS_a corresponding to delayed activation of the posterolateral wall of the LV, independently of QRS morphology [228]. Our results show that sHBP and sLBBP have QRS_a values similar to those in spontaneous rhythm, whereas nsHBP, nsLBBP and LVSP have somewhat higher values, which are still far from the large values associated with RVSP and, particularly, RVAP. Considering that a decrease in QRS_a has been shown to be an independent predictor of survival and reverse cardiac remodeling [138], the results of the present study indicate that physiological pacing, especially through selective HBP or LBBP techniques, entails significantly lower risk than conventional pacing techniques.

Using markers specifically derived from UHF-ECG recordings, such as e-DYS and Vd, the ventricular response to different pacing techniques has been investigated in previous studies [182, 93, 91]. These studies have shown that HBP produces physiological activation times and patterns, preserving fast activation of the LV lateral wall and avoiding any deterioration in interventricular synchrony. No significant differences between sHBP and nsHBP in terms of ventricular activation patterns were reported when tested in patients without conduction disorders. The results of this chapter are in line with those previous findings. In addition, the median values of e-DYS and Vd in response to sLBBP and nsLBBP were found to be similar to those of sHBP and nsHBP in absolute terms. However, the sign of e-DYS differed between the HBP and LBBP techniques, with negative values for LBBP indicating that repolarization began in the posterior regions of the heart (leads V5-V6). This also applied to LVSP. The positive e-DYS values for HBP were very close to those found for intrinsic rhythm, in agreement with previously reported results [72, 20, 449].

The local activation time describes the sequence of the heart wavefront and is therefore related to cardiac electrical activity [362]. Our results indicate that HBP techniques preserve the activation synchrony of spontaneous rhythm, as manifested by similar dAT values. For LBBAP techniques, the synchrony is reduced, but only because RV activates later, whereas the synchrony in LV activation, quantified by dAT_{4-6}, is higher than for spontaneous rhythm. Conventional pacing through RVSP or RVAP leads to increased dispersion in activation of the two ventricles or LV alone. Increases in the dispersion of both ventricular activation and repolarization have been shown to be important in the genesis and maintenance of ventricular arrhythmias and sudden cardiac death [410, 17].

4.5.2 Patient-induced effects on ventricular repolarization

Differences in ventricular repolarization as a function of pacing techniques were investigated by measuring the QT_c interval, the T-wave area, the PRD index reflecting the magnitude of low-frequency oscillations in the T wave and RTs across the precordial leads V1-V6 together with their dispersion.

The QT_c interval has been widely used in the literature to provide an overall measure of the duration of repolarization after compensating for the effects of heart rate. In previous work, patients with significantly prolonged QT_c intervals who underwent permanent pacemaker have been reported to face a higher risk of new-onset LV systolic dysfunction, cardiac death, ventricular arrhythmias, and sudden cardiac death [178, 102, 368]. Other studies have shown that the pacing-induced increase in QT_c, with respect to intrinsic rhythm, was less pronounced for LBBP techniques than for RVSP [431]. In our study, nsHBP and LVSP are associated with similar QT_c values than spontaneous rhythm, whereas sHBP, sLBBP, nsLBBP, RVSP and RVAP present higher values. Nevertheless, when each pacing recording was compared with its corresponding spontaneous recording, the differences between physiological pacing techniques and spontaneous rhythm ΔQT_c were not significant, as shown in figure 4.20.

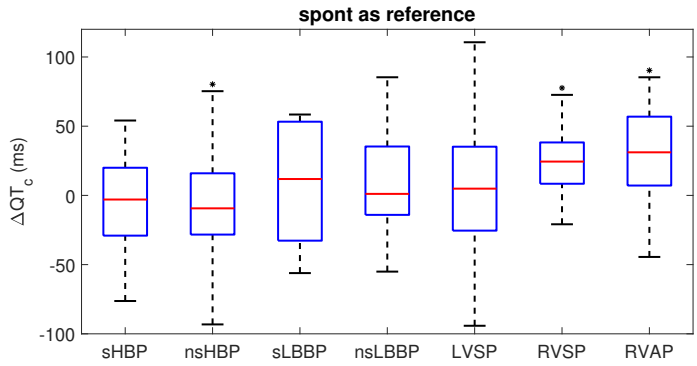

Figure 4.20 Box plots of QT_c for each pacing type relative to spontaneous rhythm.

T_a has been postulated to carry long-term prognostic information on cardiovascular mortality in apparently healthy populations [144, 15, 186]. Furthermore, T_a has been suggested to be a sensitive feature to characterize the response of ventricular repolarization to pacing, with the capacity to track minor ST-segment and T-wave abnormalities [186], and to be a marker that can predict the response to CRT [115, 428]. The results of our work indicate that conventional pacing techniques, RVSP and RVAP, lead to high values of T_a, while physiological pacing techniques lead to values of T_a close to

those found for intrinsic rhythm. These findings extend those of previous work by adding the characterization of T_a in response to a large number of conventional and physiological pacing techniques [275, 418, 110] and confirm the suitability of HBP and LBBAP techniques in terms of ventricular repolarization effects.

PRD is an arrhythmic risk marker that measures the magnitude of low-frequency oscillations in the T-wave vector modulated by sympathetic nervous system activity. Increased PRD values have been shown to be a strong predictor of all-cause mortality, cardiac mortality, and ventricular arrhythmias in various cardiac diseases and conditions [343, 342, 152, 370, 48, 214]. The present results show that all cardiac pacing techniques induce a decrease in the median PRD values found in spontaneous rhythm, except nsLBBP, which presents similar values. Nevertheless, when each pacing recording is compared with its own intrinsic recording, all pacing techniques, including nsLBBP, lead to a reduction in PRD (Figure 4.21). The basis for such results deserves further investigation. Although no significant correlation was found between PRD and heart rate, in agreement with the results presented in the second chapter (Periodic Repolarization Dynamics in simulated microgravity), additional studies are needed to fully rule out the impact of heart rate on the reduction induced by pacing in PRD.

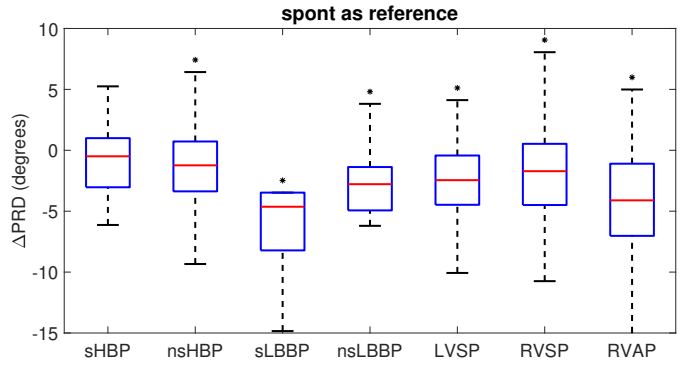

Figure 4.21 Box plots of PRD for each pacing type relative to spontaneous rhythm.

To further characterize the response of ventricular repolarization to cardiac pacing, here we evaluated the dispersion of RTs across the six precordial

leads V1-V6 as well as focusing only on V4-V6. No significant differences were found between most cardiac pacing techniques and spontaneous rhythm. In particular, the values of dRT and dRT_{4-6} for sHBP and nsHBP are similar to those of spontaneous rhythm. For nsLBBP and LVSP, although their dRT values are somewhat higher than those for spontaneous rhythm, this is only indicative of a slightly later repolarization in the RV, as the values of dRT_{4-6} for these techniques are lower than those for spontaneous rhythm. Thus, even if enhanced dispersion of ventricular repolarization has been suggested as indicative of reverse remodeling [209, 29] and a greater susceptibility to arrhythmias such as Torsades de Pointes [109], our results support the suitability of all physiological pacing techniques, including LBBAP techniques, based on their ability to reduce the dispersion of LV repolarization.

In summary, our results confirm previous evidence on the large similarities between HBP, particularly sHBP, and spontaneous rhythm in patients without ventricular conduction disorders [93]. The LBBAP techniques, despite differing from spontaneous rhythm in some global measurements of ventricular AT and RT dispersion, are confirmed to lead to high synchrony in LV activation and repolarization. However, conventional RVP techniques are associated with the highest global and LV-specific dyssynchrony characteristics, which could have long-term adverse effects on ventricular function [171]. Based on our conducted research, the effects of LBBAP and the technical advantages, such as the requirement of stimulation thresholds lower than those of HBP or the ease of capture and implementation, support their use as physiological pacing techniques alternative to HBP that overcome the shortcomings associated with conventional RVP.

4.5.3 Limitations

This work included ECGs of patients who underwent different types of cardiac pacing. However, there is a large variability in the number of patients subjected to each type of pacing. In particular, only 13 recordings were available for sLBBP, while more than 150 recordings were available for nsHBP or spontaneous rhythm. Another limitation is the lack of access to follow-up information. Long-term follow-up studies with a large representative number

of patients for each type of pacing are required to corroborate the present results.

It is also important to note that most of the recordings were obtained by applying one stimulation technique after another. Although there was some waiting time between the application of a type of cardiac stimulation and the next one, the influence of the so-called cardiac memory phenomenon [346], particularly on ventricular repolarization, cannot be ruled out. Therefore, studies with longer time intervals between the application of different types of stimulation or the use of recordings without sequential pacing would be required to confirm the present findings.

Currently, the number of hospitals and medical centers where UHF-ECG signals are recorded is limited. Future studies should confirm the clinical value of the proposed markers dAT, dRT, dAT_{4-6} and dRT_{4-6}, which can be measured from a standard ECG, as an adjunt or substitute for the marker e-DYS quantified from UHF-ECG signals.

4.6 Conclusions

This study analyzed a set of markers to characterize ventricular depolarization and repolarization in response to seven different types of cardiac stimulation. Physiological stimulation by both HBP and LBBAP types produced functional behaviors that were close to those of intrinsic rhythm in patients without cardiac disorders, whereas conventional RV stimulation was highly different from them. The differences between HBP and LBBAP were minor for most markers, particularly when they were referred to LV depolarization and repolarization. This suggests that LBBAP could be recommended for patients with narrow QRS complexes as an alternative to HBP that allows pushing back the limits of conventional pacing.

Few are those who see with their own eyes and feel with their own hearts.

Albert Einstein

5

Long-term evaluation of ECG ventricular depolarization and repolarization response to conventional and physiological pacing

5.1 Motivation

A wide range of noninvasive markers derived from ECG, electrocardiographic imaging, and vectorcardiography have been proposed to assess the efficacy of different cardiac stimulation techniques. Some of these are derived from very high-frequency ECG recordings, while others can be calculated from the ECG regardless of the sampling frequency, as shown in the previous chapter (Chapter 4). The present scientific understanding is based on the prevailing international guidelines that employ electrical dyssynchrony measurements obtained from 12-lead surface ECGs to determine the best approach to cardiac pacing [141, 114].

The ability to measure changes in ventricular synchrony, both in the depolarization and repolarization phases, is important to obtain more personalized treatment strategies for patients. As shown in the previous chapter, physiological cardiac stimulation techniques, such as HBP and LBBP, have similar cardiac responses in a short-term analysis, as confirmed by similar values of ventricular markers that characterize ECG depolarization and repolarization. In contrast, the analysis performed in Chapter 4 corroborated that conventional pacing techniques were associated with greater ventricular dyssynchrony. The effects of all these techniques in the long term have been less investigated, particularly with regard to LBBAP.

Although RVP is easily accessible, stable and well established as a standard treatment in patients with severe bradyarrhythmia [131, 100, 79], LBBP has recently emerged as an alternative to overcome ventricular dyssynchrony associated with RVP and limitations associated with previously proposed physiological techniques [167, 425, 68, 285, 333], as detailed in Chapter 4.

Several studies have shown that long-term RVP may result in left ventricular remodeling and myocardial perfusion defects. Importantly, RVP has been associated with an increased risk of atrial fibrillation, congestive heart failure, mortality, and electrical dyssynchrony [439, 390, 216, 159, 398, 171, 111, 1]. The main cause of this dyssynchrony is the inability to use the physiological pathway of the His–Purkinje system [30]. LBBP, as an alternative to HBP, is associated with a lower and more stable pacing threshold and a large R wave with a lower risk of developing a distal conduction block [446, 425]. However, these conclusions have been based on relatively short clinical follow-up. Therefore, there is still uncertainty about its long-term safety and effectiveness, which need to be further studied [166, 316, 76].

The objective of this chapter is to evaluate a set of characteristics related to heterogeneity in ventricular depolarization and repolarization of the ECG before and after pacemaker implantation in patients who receive RVP and LBBP. The ventricular response will be analyzed not only in the short term (immediately after implantation and 24 hours after it), but, importantly, also in the long term (after one year of implantation).

5.2 Materials

5.2.1 Study population and protocol

The study population consisted of 195 patients who underwent permanent pacemaker implantation from March 2020 to September 2023 at Hospital Clínico Universitario Lozano Blesa, Zaragoza, Spain. All demographic, procedural, electrocardiographic, echocardiographic, and clinical data were documented (Table 5.1). The present research was approved by the institutional committee for ethical research.

Baseline characteristics (N=195)	
Age (years)	77±10
Male	122 (62.6%)
LBBP patients	116 (59.5%)
RVOSP patients	40 (20.5%)
RVAP patients	33 (16.9%)
RVSP patients	6 (3.1%)
Diabetes mellitus	72 (36.9%)
Arterial hypertension	126 (72.4%)
Atrioventricular block II	38 (19.5%)
Complete atrioventricular block	76 (39.0%)
Recording at Y1	124 (63.6%)

Table 5.1 Demographic information of the study population. LBBP, left bundle branch pacing; RVOSP, right ventricular outflow tract septal pacing; RVAP, right ventricular apical pacing; RVSP, right ventricular septal pacing.

Of the 195 patients, 79 patients received RVP and 116 patients received LBBP. In the RVP group, 13 patients (16% of the group) had ventricular conduction disorders, including LBBB and RBBB. In the LBBP group, the corresponding number was 25 patients (22%).

The protocol for implanting the left bundle electrode in the His bundle pacing region has been previously described at [1, 75, 166]. A brief explanation of this protocol is given in the following paragraph.

A 3D electroanatomical mapping system (Carto3; Biosense Webster Inc.) was used to identify the different regions. The electrophysiologist accessed the venous system through a left axillary puncture and introduced the wire,

positioning it in the inferior vena cava. Through this access, a deflectable decapolar navigation catheter (Decanav; Biosense Webster) was introduced to generate a 3D electroanatomical map of the right atrium and ventricle. After completion of the right ventricular map, the decapolar catheter was advanced to find His potential and find a paced QRS morphology with a "W" pattern in lead V1, with a notch at the nadir of the QRS. The preformed sheath (Medtronic C315) was advanced over a guidewire and the pacing lead (SelectSecure 3830; Medtronic) was guided along the sheath to the right ventricle to reach the septum. The penetration of the electrode into the septum was continuously monitored through changes in ECG, intracavitary electrograms, and impedance values. [334]

5-minute ECG recordings were obtained at a sampling rate of 1,000 Hz during sinus rhythm prior to pacemaker implantation (called baseline or BL) and just after the end of the intervention (D0 recordings). The following day (D1) another ECG recording was acquired to evaluate changes in ventricular response after 24 hours of pacing. Furthermore, ECG signals were recorded one year after pacemaker implantation (Y1 recordings) to assess the long-term effects of pacing. D1 and Y1 recordings were 10 minutes long and were acquired at a sampling rate of 1,000 Hz using Mortara Instrument (Milwaukee, WI) H-12 Holter recorders. Within the group of patients who received LBBP, 76 patients had a QRS duration greater than 120 ms, while the remaining 40 had QRS complexes with a duration equal to or less than 120 ms. Among patients who underwent RVP, 47 had a wide QRS complex (greater than 120 ms), while 32 had a narrow QRS complex ($\leq$120 ms). Figure 5.1 illustrates a schematic timeline of ECG acquisition.

5.3 Methods

5.3.1 ECG preprocessing

12-lead ECG signals were preprocessed by high-pass filtering to remove baseline wander. To detect and remove the pacing spikes, the semi-automated algorithm described in Chapter 4 was used. In short, the algorithm was applied twice. The first time, the threshold values were set to $\alpha_{\text{on}} = 30\mu V/ms$ and $\alpha_{\text{end}} = -30\mu V/ms$. The second time, the values were $\alpha_{\text{on}} = 200\mu V/ms$ and

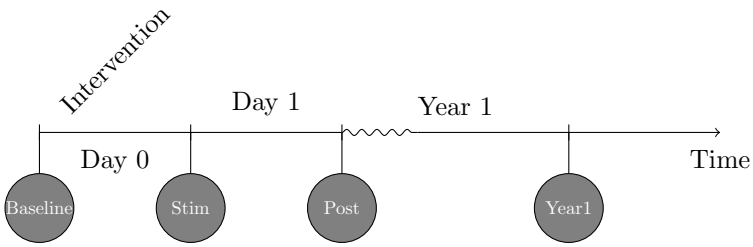

Figure 5.1 The first two ECG recordings are taken before and immediately after cardiac pacemaker implantation, BL and D0, respectively. The following day, D1, a post-implant ECG recording is obtained. After one year, an ECG recording is acquired (Y1).

$\alpha_{\text{end}} = -200\mu V/ms$. These values were selected to remove pacing spikes of different amplitudes. Figure 5.2 shows an example of a beat in which the pacing spikes were removed according to the described steps.

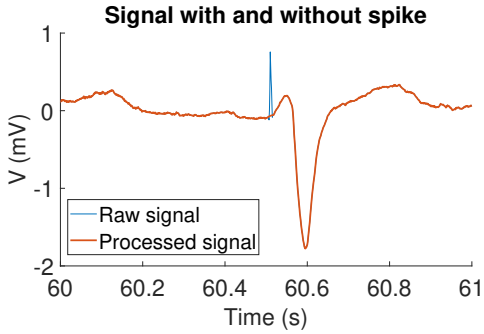

Figure 5.2 ECG beat with a spike, in blue before and in red after applying the algorithm for pacing spike removal.

After spike removal, a 50 Hz notch filter was applied to remove powerline interference, followed by a 40 Hz low-pass filter to remove high-frequency electrical and muscle noise components. QRS complexes were detected and ECG waves were delineated using a wavelet-based algorithm [242]. For each patient and stage (BL, D0, D1 and Y1), a median beat was calculated using the algorithm described in Chapter 4. All ECG markers were calculated from this median beat.

5.3.2 Depolarization markers

The duration of the QRS complex (QRS_d) was measured for each median beat as the time between the onset and the end of the QRS complex using the associated marks and a post-processing selection rule on all single-lead locations [242], as described in Chapter 4.

The area of the QRS complex was first evaluated on each of the orthogonal leads X, Y, and Z calculated from the Kors-derived vectorcardiogram (VCG) [235]. Specifically, in each orthogonal lead X, Y, and Z, the area was calculated as the integral between the absolute value of the QRS complex in that lead and the baseline in the time interval from the onset to the end of the QRS complex. QRS_d was subsequently evaluated according to the formula:

$$QRS_a = \sqrt{QRS_{a,X}^2 + QRS_{a,Y}^2 + QRS_{a,Z}^2}. \tag{5.1}$$

Furthermore, as described in the previous chapter, the local AT was calculated to later derive measurements of electrical dyssychrony. ATs of individual leads were obtained as the difference in time between the time corresponding to the center of mass of the QRS complex in the representative median beat and the time corresponding to the multilead QRS onset. An example is shown in figure 5.3, with the AT computed from 0 (time of QRS onset) to the red point (time of QRS center of mass). The median AT computed from the ATs of all precordial leads was associated with each ECG recording. The dispersion of activation times, dAT, was defined as the difference between the last and first AT values on the six precordial leads (V1–V6). In addition, the temporal dispersion of ATs restricted to the precordial leads corresponding to the left ventricle (V4-V6), called dAT_{4-6}, was calculated.

5.3.3 Repolarization markers

The QT interval was calculated as the time between the onset of the QRS complex and the end of the T wave, indicating the time comprising ventricular depolarization and repolarization. This interval was corrected for changes in heart rate, QT_c, using the optimal formula associated with the QT/RR relationship, as fully described in Chapter 4. In short, to identify the regression model that best fitted the QT/RR relationship, a set of functions, including

linear, hyperbolic, parabolic, logarithmic, shifted logarithmic, exponential, arcus tangent, hyperbolic tangent, arcus hyperbolic sine, and arcus hyperbolic cosine, were tested. The model leading to the lowest regression residuum was the one chosen to perform the QT correction following the method described in [324].

Local RT was determined, for each lead, as the time associated with the center of mass of the T wave in the representative median beat (see Chapter 4 for more information), measured from the time corresponding to the multilead QRS onset. Figure 5.3 shows an ECG beat, with RT calculated from 0 (time of QRS onset) to the green point (time of center of mass of the T wave). A single RT for each recording was calculated from each ECG recording as the median values of local RTs in all precordial leads (RT). The dispersion of RT, denoted as dRT, was calculated as the difference between the maximum and minimum RT values in the 6 precordial leads V1-V6. The dispersion of RT within the left ventricle, dRT_{4-6}, was calculated from the precordial leads V4-V6, denoted dAT_{4-6}.

Note that in this study, unlike the study in previous chapter, the signs of dAT and dRT were not taken into account but only the absolute value of the differences was considered.

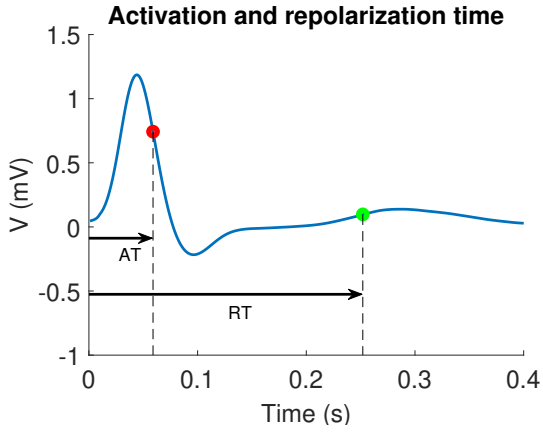

Figure 5.3 ECG beat for one lead with identified time points used to compute local AT (red) and local RT (green), using the QRS onset mark as temporal reference.

The area of the T wave (T_a) was calculated from the Kors VCG in a way analogous to that described for the QRS complex:

$$T_a = \sqrt{T_{a,X}^2 + T_{a,Y}^2 + T_{a,Z}^2} \tag{5.2}$$

where $T_{a,X}$, $T_{a,Y}$ and $T_{a,Z}$ denote the areas of the T wave in leads X, Y, and Z.

From the preprocessed signal and using the method described in Chapter 3, PRD was calculated. In short, the methodology for the calculation was based on the following steps:

1. T waves were selected using the T-wave windows defined in Chapter 3. The criteria based on the QRS fiducial point and the RR interval were as follows. For each beat i, the onset of the T-wave window, denoted T_{on_i}, was set at 90 ms after the fiducial mark QRS_i: $T_{on_i} = QRS_i + 90\,\text{ms}$. The end of the T-wave window, denoted T_{end_i}, was defined as $T_{end_i} = QRS_i + \min(360\,\text{ms}, \frac{2}{3}RR_i)$ for RR_i below 720 ms and $T_{end_i} = QRS_i + 360\,\text{ms}$, in other cases.

2. A constant value was subtracted from each T wave so that the amplitude at T_{end} was set to 0 mV.

3. The average electrical vector was calculated for each T-wave window and the angle dT° between two consecutive T-wave windows was calculated by the dot product of the corresponding average vectors.

4. A median filtering was applied to attenuate outliers and artifacts in the dT° time series.

For the obtained dT° time series, a method based on PRSA [36] was applied to evaluate the oscillations measured by the PRD index [341]:

5. Anchor points were defined by comparing averages of M values of the dT° series previous and posterior to the anchor point candidate x_i. A point x_i was considered an anchor point if:

$$\frac{1}{M}\sum_{j=0}^{M\text{-}1} x_{i+j} > \frac{1}{M}\sum_{j=1}^{M} x_{i\text{-}j} \tag{5.3}$$

The value for M=9, as already done in Chapter 4, was established because it allows the detection of frequencies in the range of interest (from 0.025 to 0.1 Hz).

6. Windows were defined around each anchor point. Anchor points in the last L samples of the dT° series were discarded.

7. The PRSA series was obtained by averaging the dT° values in all windows contained in each 5-minute recording.

The PRD index was defined as the difference between the maximum and minimum values of the PRSA series.

5.3.4 Statistical analysis

Continuous variables were expressed as median (and IQR). The Mann–Whitney U test (Wilcoxon rank-sum test) and Wilcoxon signed-rank test were used to compare continuous variables for different stimulation techniques and different time points with respect to pacemaker implantation. A p-value below 0.05 was considered statistically significant. Signal processing and subsequent analysis were performed with software written in MATLAB R2020a (9.8).

5.4 Results

5.4.1 Depolarization markers

The following results are presented separately for two subpopulations defined according to the baseline value of QRS_d: patients with a wide baseline QRS complex ($>$120 ms) and patients with a narrow baseline QRS ($\leq$120 ms).

The ECG markers of ventricular depolarization for the LBBP and RVP groups at each time point BL, D0, D1 and Y1 are shown in Tables 5.2 and 5.3 for patients with narrow and wide QRS complexes, respectively.

The baseline values of the analyzed ECG depolarization markers did not show significant differences between the two pacing techniques in BL, and this was applicable to both the group of patients with narrow QRS complexes and the group of patients with wide QRS complexes.

		LBBP (Narrow QRS)	RVP (Narrow QRS)	p-value
QRS_d (ms)	BL	106.0 (13.0)	101.0 (15.1)	NS
	D0	139.0 (30.5)*	156.0 (22.5)*	7.7×10^{-3}
	D1	114.5 (28.0)*	145.0 (24.8)*	3.7×10^{-5}
	Y1	119.0 (25.8)*	140.0 (18.0)*	1.5×10^{-3}
QRS_a (μVs)	BL	40.4 (18.6)	40.3 (14.3)	NS
	D0	51.5 (28.6)*	77.9 (44.1)*	1.7×10^{-4}
	D1	54.2 (36.1)*	97.9 (45.3)*	3.6×10^{-5}
	Y1	41.9 (22.4)	93.6 (59.8)*	1.7×10^{-3}
AT (ms)	BL	56.0 (14.0)	49.0 (16.5)	NS
	D0	67.0 (27.4)*	82.0 (14.0)*	6.4×10^{-3}
	D1	62.3 (19.3)*	74.5 (10.9)*	1.2×10^{-3}
	Y1	59.0 (12.3)*	72.5 (8.0)*	3.6×10^{-3}
dAT (ms)	BL	11.0 (5.4)	12.0 (6.4)	NS
	D0	17.0 (9.3)*	15.0 (13.0)	NS
	D1	16.5 (8.5)*	17.0 (10.0)*	NS
	Y1	18.0 (7.8)*	16.0 (4.8)	NS
dAT_{4-6} (ms)	BL	7.0 (7.5)	7.0 (7.0)	NS
	D0	10.0 (8.0)*	6.3 (8.0)	6.6×10^{-3}
	D1	8.0 (7.5)*	9.5 (9.0)	NS
	Y1	7.0 (9.8)	10.0 (7.3)	NS

Table 5.2 ECG depolarization markers measured at BL D0, D1 and Y1 in patients with narrow QRS, separated in two groups according to whether they received LBBP or RVP. Data are represented as median (interquartile range). LBBP, left bundle branch pacing; RVP, right ventricular pacing; QRS_d, QRS duration; QRS_a, QRS area; AT, median activation time over leads; dAT, AT dispersion in all precordial leads; dAT_{4-6}, AT dispersion in leads V4-V6. *p-value < 0.05 with respect to BL.

In patients without ventricular conduction disorders who had narrow QRS complexes at baseline, significant differences were observed between patients undergoing LBBP and RVP for most of the ECG depolarization markers and most time points, as shown in Table 5.2. Specifically for QRS_d and QRS_a, patients receiving LBBP showed transient increases in the values of these markers in D0 and D1, which one year after pacemaker implantation returned to values closer to those measured in BL. However, patients receiving RVP

		LBBP (Wide QRS)	RVP (Wide QRS)	p-value
QRS_d (ms)	BL	159.0 (28.3)	156.0 (25.3)	NS
	D0	149.0 (33.5)	165.0 (27.0)*	2.5×10^{-3}
	D1	134.0 (25.8)*	156.0 (28.8)	8.3×10^{-7}
	Y1	132.0 (26.0)*	150.5 (34.5)	0.036
QRS_a (μVs)	BL	58.0 (35.7)	47.1 (47.7)	NS
	D0	57.0 (23.9)	81.7 (46.0)*	4.9×10^{-5}
	D1	61.7 (28.7)	93.3 (68.9)*	4.4×10^{-6}
	Y1	55.4 (40.9)	85.9 (71.2)*	3.2×10^{-3}
AT (ms)	BL	82.0 (18.5)	79.0 (17.5)	NS
	D0	84.0 (26.8)	87.8 (19.3)*	NS
	D1	74.0 (19.4)*	79.0 (16.4)	0.015
	Y1	70.5 (17.5)*	76.8 (11.8)	NS
dAT (ms)	BL	26.0 (15.8)	24.0 (17.0)	NS
	D0	24.0 (10.0)	19.0 (12.0)*	1.3×10^{-3}
	D1	22.0 (10.0)*	20.0 (9.8)*	NS
	Y1	19.0 (12.0)*	17.0 (13.0)*	NS
dAT_{4-6} (ms)	BL	12.0 (13.0)	12.0 (13.5)	NS
	D0	12.0 (10.0)	5.0 (10.0)*	3.4×10^{-3}
	D1	9.0 (10.8)*	12.0 (8.5)	NS
	Y1	10.0 (6.0)	12.0 (8.0)	NS

Table 5.3 ECG depolarization markers measured at BL D0, D1 and Y1 in patients with wide QRS, separated in two groups according to whether they received LBBP or RVP. Data are represented as median (interquartile range). LBBP, left bundle branch pacing; RVP, right ventricular pacing; QRS_d, QRS duration; QRS_a, QRS area; AT, median activation time over leads; dAT, AT dispersion in all precordial leads; dAT_{4-6}, AT dispersion in leads V4-V6. *p-value < 0.05 with respect to BL.

presented increased values in D0, D1, and Y1 with respect to BL. The values of QRS_d and QRS_a were significantly higher in the RVP group than in the LBBP group at the three time points D0, D1 and Y1.

As expected, the median AT was significantly higher for patients receiving RVP. This was observed at D0, D1, and Y1. Similarly to QRS_d and QRS_a, the median AT transiently increased at D0 and D1 and subsequently decreased at Y1 in the LBBB group, reaching values close to those of BL. Although a

similar trend was observed for RVP, AT values were almost 50% higher in Y1 than in BL in this pacing group. When analyzing the spatial dispersion dAT across all precordial leads, since this was based on the times of left and right ventricular activation, no significant differences were observed between RVP and LBBP at any of the time points D0, D1, and Y1. When analyzing the spatial dispersion dAT_{4-6} across the precordial leads overlooking the left ventricle, LBBP led to recovery of BL values in Y1, while RVP was associated with slightly higher values in Y1, even if the differences between the two groups were not significant.

In patients with ventricular conduction disorders who had wide QRS complexes at baseline, significant differences were also observed between the LBBP and RVP groups, as shown in Table 5.3. In the LBBP group, QRS_d progressively decreased at D0, D1 and Y1, but in the RVP group, QRS_d increased transiently and subsequently decreased. The values of QRS_d were consistently higher for RVP than for LBBP at all the time points evaluated after pacemaker implantation. When analyzing the area rather than the duration of the QRS complex, significantly higher values of QRS_a were found for RVP compared to LBBP at D0, D1, and Y1. After one year of pacing, QRS_a returned to the BL values when applying physiological pacing, but not when applying conventional pacing.

The median AT calculated for the subgroup of patients with wide QRS complexes revealed a trend of increased values in the RVP group, even if significant differences between LBBP and RVP were only identified in D1. In terms of AT spatial dispersion, no statistically significant differences were found for dAT or dAT_{4-6} between the LBBP and RVP groups, except when analyzed at time D0. At time points D1 and Y1, the median values of dAT_{4-6} were slightly higher for RVP than for LBBP, but no statistical significance was reached.

To better illustrate the changes between RVP and LBBP at the different time points, ΔX, where X is the index analyzed, was calculated as the difference between the value at a time point after pacemaker implantation (D0, D1, Y1) minus the respective value at BL. Figure 5.4 shows the values of ΔQRS_a for patients with narrow (left) and wide (right) QRS complexes. As can be seen in the figure, patients undergoing RVP exhibited significant increases

in QRS_a compared to BL, and these increases were significantly higher than those observed in patients undergoing LBBP.

The behavior observed for ΔdAT_{4-6} is shown in Figure 5.5. For patients with narrow and wide QRS complexes, a significant increase in dAT_{4-6} with respect to BL was observed in the RVP group at time D0 and in the LBBP group at time Y1.

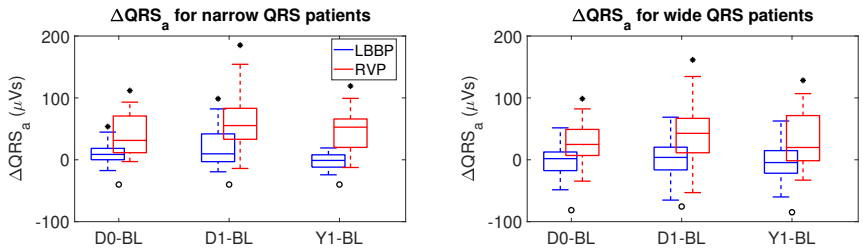

Figure 5.4 Boxplots of ΔQRS_a for patients with narrow (left panel) and wide (right panel) QRS complexes. Results for the LBBP group are shown in blue and for the RVP group in red. •p<0.05 for differences at D0, D1 or Y1 with respect to BL, °p<0.05 for differences between LBBP and RVP.

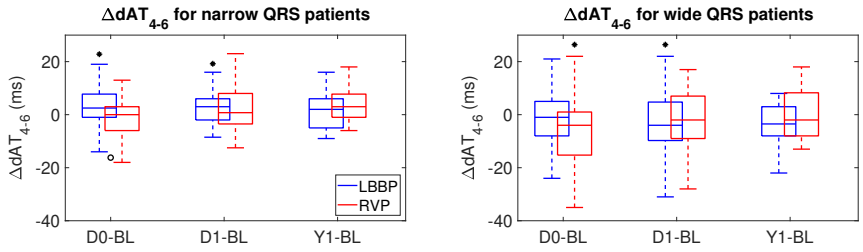

Figure 5.5 Boxplots of ΔdAT_{4-6} for patients with narrow (left panel) and wide (right panel) QRS complexes. Results for the LBBP group are shown in blue and for the RVP group in red. •p<0.05 for differences at D0, D1 or Y1 with respect to BL, °p<0.05 for differences between LBBP and RVP.

5.4.2 Repolarization markers

The ECG markers of ventricular repolarization for the LBBP and RVP groups at each time point BL, D0, D1, and Y1 are shown in Tables 5.4 and 5.5 for patients with narrow and wide QRS complexes, respectively.

		LBBP (Narrow QRS)	RVP (Narrow QRS)	p-value
QT	BL	407 (123)	442 (71.0)	NS
(ms)	D0	411 (49.0)	451 (42.5)	0.011
	D1	400 (30.8)	417 (47.0)	0.033
	Y1	425 (47.0)	421 (26.0)	NS
QT_c	BL	436 (48.7)	453 (68.9)	NS
(ms)	D0	445 (32.6)	468 (34.8)	0.022
	D1	429 (28.1)	446 (29.4)	0.043
	Y1	441 (25.3)	438 (32.5)	NS
RT	BL	313 (101.6)	331 (70.3)	NS
(ms)	D0	296 (54.6)	318 (34.5)	0.015
	D1	294 (32.8)	304 (42.3)*	NS
	Y1	310 (49.6)	307 (15.1)*	NS
dRT	BL	45.0 (21.0)	41.0 (23.8)	NS
(ms)	D0	39.0 (23.0)	38.3 (26.0)	NS
	D1	43.5 (26.0)	40.5 (22.0)	NS
	Y1	45.0 (17.0)	41.0 (20.3)	NS
dRT_{4-6}	BL	25.0 (27.0)	18.0 (28.5)	NS
(ms)	D0	20.0 (17.5)	12.0 (16.0)	NS
	D1	22.5 (23.0)	25.5 (27.0)	NS
	Y1	19.0 (25.3)	31.0 (18.5)	NS
T_a	BL	23.1 (22.8)	37.3 (29.3)	0.043
(μVs)	D0	39.6 (45.8)*	92.8 (96.8)*	4.4×10^{-6}
	D1	53.5 (44.2)*	79.5 (69.1)*	1.2×10^{-3}
	Y1	43.7 (41.3)*	64.2 (32.2)*	0.034
PRD	BL	5.00 (3.86)	4.01 (3.13)	NS
(degrees)	D0	3.95 (3.30)	2.44 (2.56)*	NS
	D1	4.06 (3.59)	2.68 (3.28)	NS
	Y1	3.94 (2.67)	3.79 (4.06)	NS

Table 5.4 ECG repolarization markers measured at BL D0, D1 and Y1 in patients with narrow QRS, separated in two groups according to whether they received LBBP or RVP. Data are represented as median (interquartile range). LBBP, left bundle branch pacing; RVP, right ventricular pacing; QT_c, corrected QT interval; RT, median repolarization time over leads; dRT, RT dispersion in all precordial leads; dRT_{4-6}, RT dispersion in leads V4-V6; T_a, T-wave area; PRD, Periodic repolarization dynamics. *p-value < 0.05 with respect to BL.

		LBBP (Wide QRS)	RVP (Wide QRS)	p-value
QT (ms)	BL	442 (82.0)	483 (100.5)	NS
	D0	444 (59.0)	453 (56.0)	NS
	D1	409 (45.5)*	428 (51.0)*	2.6×10^{-3}
	Y1	415 (61.0)*	443 (60.0)*	NS
QT_c (ms)	BL	455 (50.5)	476 (67.8)	0.029
	D0	467 (44.9)	476 (42.2)	NS
	D1	440 (40.2)*	459 (33.6)*	1.3×10^{-3}
	Y1	440 (43.2)*	458 (36.7)	0.010
RT (ms)	BL	326 (75.2)	347 (79.0)	NS
	D0	320 (47.8)	324 (32.5)*	NS
	D1	298 (42.8)*	316 (39.9)*	0.013
	Y1	311 (47.5)*	318 (49.5)*	NS
dRT (ms)	BL	47.0 (29.8)	48.5 (27.0)	NS
	D0	40.0 (24.0)	37.8 (23.5)*	NS
	D1	43.0 (23.8)	42.0 (30.0)*	NS
	Y1	40.0 (22.0)	45.0 (25.0)	NS
dRT_{4-6} (ms)	BL	21.0 (26.0)	28.0 (28.0)	NS
	D0	20.0 (16.8)	10.5 (14.0)*	5.0×10^{-3}
	D1	24.0 (18.8)	24.0 (26.8)	NS
	Y1	16.5 (16.0)	25.0 (29.0)	NS
T_a (μVs)	BL	45.2 (25.7)	46.0 (47.2)	NS
	D0	57.7 (28.2)*	91.2 (118.7)*	1.0×10^{-3}
	D1	47.5 (30.3)	81.0 (83.7)*	1.8×10^{-5}
	Y1	37.7 (23.8)	74.8 (69.1)	0.043
PRD (degrees)	BL	3.97 (3.82)	3.50 (2.36)	NS
	D0	2.66 (3.59)*	1.79 (1.79)*	8.0×10^{-4}
	D1	2.64 (2.88)*	1.79 (2.27)*	9.0×10^{-4}
	Y1	3.60 (3.72)	1.92 (2.62)	0.018

Table 5.5 ECG repolarization markers measured at BL D0, D1 and Y1 in patients with wide QRS, separated in two groups according to whether they received LBBP or RVP. Data are represented as median (interquartile range). LBBP, left bundle branch pacing; RVP, right ventricular pacing; QT_c, corrected QT interval; RT, median repolarization time over leads; dRT, RT dispersion in all precordial leads; dRT_{4-6}, RT dispersion in leads V4-V6; T_a, T-wave area; PRD, Periodic repolarization dynamics. *p-value < 0.05 with respect to BL.

The baseline values of the analyzed ECG repolarization markers did not show any significant differences between the two pacing techniques in BL, and this was applicable to both the group of patients with narrow QRS complexes and the group of patients with wide QRS complexes. The only exceptions were QT_c and T_a, which showed higher BL values for RVP than for LBBP in patients with wide and narrow QRS complexes, respectively.

In patients with narrow QRS complexes in BL, significantly higher QT and QT_c interval values were found in D0 and D1, whereas the values of these two markers returned to their BL values after one year of pacing.

The median RT was significantly higher for patients receiving RVP than for patients receiving LBBP in D0, but not in D1 and Y1. When analyzing the spatial dispersion dRT in all precordial leads and dRT_{4-6} in the precordial leads overlooking the left ventricle, no significant differences were observed between RVP and LBBP at any of the time points D0, D1, and Y1. For dRT_{4-6}, LBBP led to the recovery of BL values in Y1 whereas RVP was associated with higher values after one year of pacemaker implantation, although the differences between the two groups were not significant.

Regarding the T-wave area, T_a, it was found to be significantly different between the two techniques at all time points D0, D1, and Y1. Statistically significantly higher T_a values were found for RVP, with differences indicating areas more than double in RVP than in LBBP. PRD did not show relevant differences between the two pacing groups. RVP led to a transient decrease in D0, which was no longer maintained in D1 or Y1.

In patients with wide QRS complexes in BL, the interval values of QT and QT_c were higher in RVP than in LBBP, reaching statistical significance in D1 and/or Y1. RT, dRT and dRT_{4-6} only showed relevant differences at specific time points, with RT higher in the RVP group at time point D1 and dRT_{4-6} higher in the LBBP group at time point D0. T_a was remarkably higher after conventional pacing than after physiological pacing, with consistent differences between the two pacing groups at all time points D0, D1, and Y1. In contrast, PRD was significantly lower following RVP compared to LBBP at the same three time points.

Similarly to ventricular depolarization analysis, ΔX was calculated for each X repolarization index as the difference between the value at a time point

after pacemaker implantation (D0, D1, Y1) minus the respective value at BL. Figure 5.6 illustrates the results for ΔT_a. In patients with narrow and wide QRS complexes, ΔT_a values took statistically significantly higher values of T-wave area in the RVP group than in the LBBP group in D0 and D1. The differences in Y1 were not significant when calculated only for the patients who had acquired ECG recordings in BL, D0, D1, and Y1, who were the ones selected to be represented in the figure.

Figure 5.7 illustrates the results for ΔdRT_{4-6}. No significant differences in dRT_{4-6} were found with respect to BL, except in D0 for patients with wide QRS complexes undergoing RVP.

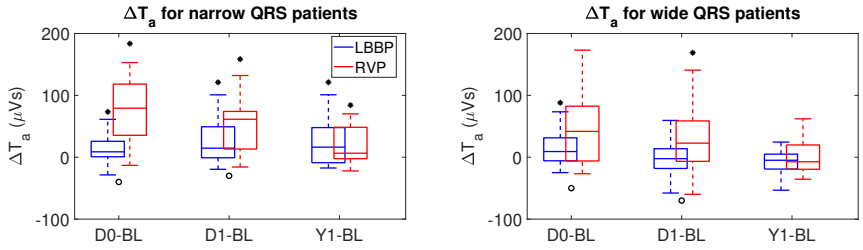

Figure 5.6 Boxplots of ΔT_a for patients with narrow (left panel) and wide (right panel) QRS complexes. Results for the LBBP group are shown in blue and for the RVP group in red. •p<0.05 for differences at D0, D1 or Y1 with respect to BL, °p<0.05 for differences between LBBP and RVP.

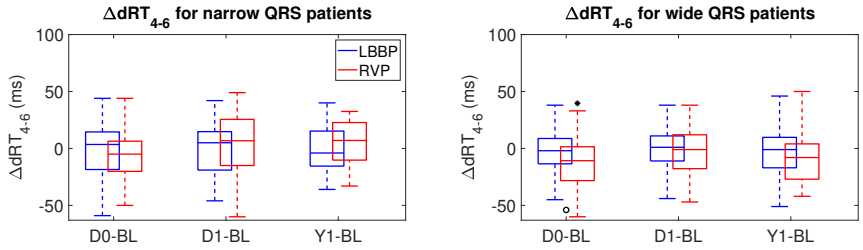

Figure 5.7 Boxplots of ΔdRT_{4-6} for patients with narrow (left panel) and wide (right panel) QRS complexes. Results for the LBBP group are shown in blue and for the RVP group in red. •p<0.05 for differences at D0, D1 or Y1 with respect to BL, °p<0.05 for differences between LBBP and RVP.

5.5 Discussion

This study assesses electrophysiological changes induced by two types of cardiac pacing techniques, LBBP and RVP, by characterization of various markers of ventricular depolarization and repolarization. The results of this study indicate that there are significant differences in ventricular electrical activity between patients who underwent RVP and LBBP.

5.6 Analysis of ventricular depolarization

In general, our results on the effects of pacing on ventricular activation are in agreement with previous studies investigating conventional and physiological pacing techniques.

The marker QRS_d reflects the duration of ventricular depolarization and is negatively related to cardiac function [238, 382]. In this study, QRS_d increases after LBBP in patients with narrow QRS complexes, which is explained by stimulation of only the LBB of the conduction system, and notably decreases in patients with wide QRS complexes, which is indicative of improved electrical synchrony. In contrast, RVP more notably prolongs the QRS complex in patients with narrow QRS complexes and leads to wider paced QRS complexes in patients with already wide QRS complexes in BL.

In studies investigating pacemaker-indicated patients with normal cardiac function, LBBP has been reported to lead to significantly shorter paced QRS complexes than those observed with right ventricular septal pacing [165]. The capture of the LBB led to the achievement of favorable electrical and mechanical synchrony of the LV. Patients with LBBP with LBB potential had a shorter left ventricular activation time compared to patients without LBB potential. This result suggests that pacing the septum without engaging the His-Purkinje system may result in a relatively delayed activation of the LV free wall. Improved electrical synchrony and mechanical LV synchrony were reported in patients with LBB potential compared to those without it.

Our results are consistent with those reported in previous work [75, 389, 443, 451]. Differences in the paced QRS complex associated with conventional and physiological pacing techniques were also found in a pediatric

population (less than 7 years) in [212]. In a follow-up study with 12 children [438], QRS_d was found to be similar at implantation and months later when the children underwent LBBP but not when they underwent RVP. The feasibility and safety of LBBP have been analyzed in other populations, including elderly patients (more than 75 years) with an indication for cardiac resynchronization therapy (CRT) [146], and the results have shown that the LBBP technique induced synchronous ventricular activation measured by QRS_d.

In a systematic review [373], the feasibility and safety of LBBP and HBP were assessed in patients with prosthetic heart valves. The results indicated that patients who underwent LBBP had paced QRS_d values similar to those undergoing HBP, and a significantly higher success rate. High success rates were also found when LBBP was applied to patients with atrioventricular conduction disease [336] or patients with third-degree atrioventricular block [443].

The improved electrical synchrony associated with LBBP compared to RVP is corroborated in our study by the analysis of AT and the spatial dispersion of AT in all precordial leads and in precordial leads overlooking the LV. Patients who underwent LBBP generally showed lower values of AT and their dispersion, particularly when focusing on the V4-V6 leads. Previous work in the literature has shown the benefits of a reduction in AT in populations different from the one investigated here [314].

This study investigated other ECG depolarization markers derived from the VCG, such as the QRS area, which have been suggested to provide greater accuracy than QRS_d in predicting responses to various pacing techniques [225]. Furthermore, they can be measured with reduced variability compared to QRS_d [409] due to the temporal uncertainty in precisely determining the beginning and end of the QRS complex, which, however, minimally contributes to the area calculation [115, 313]. The marker QRS_a serves as a representation of dyssynchronous electrical activation, where a larger QRS_a corresponds to more delayed activation of the posterolateral wall of the LV, independent of QRS morphology [228]. Our results indicate an increase in QRS_a immediately after pacemaker implantation and after 24 hours for the two pacing techniques in patients with wide and narrow QRS, but the values of QRS_a are significantly higher in the RVP group than in the LBBP

group. Importantly, there is a recovery to the original values in patients undergoing LBBP, but not in patients undergoing RVP. These results point to an improved electrical synchrony with LBBP, which could be indicative of a better prognosis based on previous literature reports. In fact, a reduction in QRS_a has been explored as an independent predictor of survival and reverse cardiac remodeling [138, 239].

5.7 Analysis of ventricular repolarization

Prolongation of the QT interval is a recognized risk factor for the development of ventricular arrhythmias [368] and its measurement allows estimation of the associated risk for different types of cardiac stimulation. Here, QT_c was found to be significantly higher after RVP than after LBBP. The results obtained the day after pacemaker implantation are comparable to those reported in previous studies [431], where significant differences in QT and QT_c intervals were described between RVP, septal area pacing, and LBBP 48 hours after implantation. Importantly, our study performed after one year of pace finding significant differences in QT_c between conventional and physiological pacing techniques in the long term.

To date, not many studies have calculated RT from the surface ECG, although it has been studied along with ventricular AT in electrograms in canine hearts [288] and human hearts [154]. Furthermore, few studies have assessed the changes in RT that occur in patients subjected to different types of cardiac stimulation. In the previous chapter, conducted in patients with narrow QRS and indication of pacemakers (Short-term evaluation of ECG ventricular depolarization and repolarization response to conventional and physiological pacing), ECG records acquired at time D0 (immediately after pacemaker implantation) showed that LBBP was associated with RT values similar to those at baseline. This behavior was not observed with RVP recordings. The results of the present study indicate that RT after one year of pacing is similar between both types of stimulation (LBBP and RVP) and preserved with respect to BL in patients with narrow QRS but reduced in patients with wide QRS. Similar observations apply to dRT and dRT_{4-6}. Previous studies in the literature have shown that dispersion of repolarization times has clinical

value. Patients at high risk of cardiomyopathy, such as those with moderate or severe left ventricular dysfunction, show an increase in the heterogeneity of ventricular RT [388].

Another ECG marker that we analyzed in the present study is T_a. Our results indicate that RVP subjects have higher T_a values immediately after and the day after pacemaker implantation, that is, D0 and D1, compared to LBBP subjects. After one year, Y1, the values of T_a are similar or lower than in BL only for LBBP but not for RVP in patients with wide QRS complexes. The value of T_a to assess the response to pacing has been tested in previous work. In [115], baseline T_a was found to predict the response to CRT, in terms of LVEF, in patients with heart failure and LBBB. In [428], a larger baseline T_a was proposed to improve the selection of patients most likely to benefit from CRT. Other studies suggested using T_a together with QRS_a to improve clinical outcome defined as a combination of all-cause mortality, heart transplantation, and left ventricular assist device implantation[110].

To complete the repolarization analysis, in the present study, we investigated changes in PRD in response to pacing. No significant differences are found between narrow QRS patients who underwent LBBP and RVP. However, patients with wide QRS show that RVP is associated with lower PRD values compared to LBBP. Future work should further evaluate PRD and identify the causes of the lower values in RVP versus LBBP. Since PRD has been shown to be a strong predictor of mortality in different patient populations, it is of great interest to understand the mechanisms underlying the pacing-induced changes, with a separate analysis of patients with different conduction disorders, such as LBBB and RBBB [343, 340, 34, 35, 48].

Based on our characterization of ventricular depolarization and repolarization on the ECG immediately after pacemaker implantation up to one year after it, the advantages of LBBBP over RVP are clear. Although some studies [452, 455] indicate that LBBP requires more procedural time or more sophisticated instruments than RVP or LVSP, it activates the LV earlier, causes less mechanical dyssynchrony of the LV [237] and leads to a lower dispersion of electrical activation and repolarization of the ventricles, as supported by our findings. This, taken together with the fact that it overcomes some of the shortcomings associated with HBP, represents an advantage over conven-

tionally used pacing methods. Our results are in line with other studies that report positive clinical outcomes after one year of LBBP [148, 252, 375, 417], including a reduction in hospitalization related to HF compared to conventional techniques [105]. The current work contributes additional supporting evidence for the long-term efficacy of this technique.

5.8 Study limitations

The analysis was performed on data collected from a large single-center prospective study and did not include information on the clinical follow-up of the patients, including the incidence of subacute and chronic complications. In addition, the complete list of medications prior to the procedure was not included in the interpretation of the results.

Our findings must be confirmed in extensive multicenter trials with clinical follow-up and randomized studies with large ECG data to generalize the findings and confirm the potential clinical benefits of LBBP.

5.9 Conclusions

Patients who undergo LBBP show improved electrical synchrony in ventricular depolarization and repolarization compared to patients who undergo RVP, particularly in the long term (after a year of pacing). This is supported by the analysis of standard ECG indices of ventricular activation, such as QRS_d and QRS_a, but also by other proposed indices quantifying AT and its spatial dispersion. Regarding ventricular repolarization, our findings are based on ECG markers such as QT and QT_c intervals and QRS_a as well as other novel ECG characteristics such as RT, its spatial dispersion and PRD, which have not been fully explored for the analysis of pacing effects.

The future will be determined in part by happenings that it is impossible to foresee; it will also be influenced by trends that are now existent and observable.

Emily Greene Balch

6 Conclusions and future work

6.1 Summary and main conclusions

The main objectives of this thesis were to identify ECG-derived markers to quantify ventricular repolarization in populations with cardiac pathologies or under conditions that affect the cardiovascular system and to investigate the effects of cardiac pacing on ventricular electrical dyssynchrony. To achieve these objectives, robust algorithms have been developed and implemented to measure variations in the oscillations of the T wave of the surface ECG. In addition, several novel markers have been proposed to describe the spatial dispersion of ventricular activation and repolarization in response to different forms of pacing.

6.1.1 Changes in PRD due to simulated microgravity

A robust method was developed for the calculation of PRD, a marker related to the magnitude of low-frequency oscillations in the angle between consecutive T waves in response to sympathetic activity. PRD was computed using two

techniques that were developed based on the original definition of PRD [343]. One of these techniques works with the CWT, and the other technique uses the PRSA method.

For the delineation of T waves from ECG recordings, algorithms developed by our research group and validated in previous studies were used. Robust delineation marks for the onset and end of each T wave were obtained by comparing the marks of each beat with those of contiguous beats to improve the delineation accuracy. In addition, to ensure that changes in the T-wave duration did not influence the angle measurements, the same time window was used to calculate the angle between consecutive beats.

In Chapter 2, the two techniques implemented for PRD calculation were applied on ECG recordings of healthy volunteers who underwent a long-term (60 days) period of simulated microgravity using a ground-based model known as HDBR. Furthermore, as part of a broader study on the effects of long-time exposure to microgravity on the human body, some subjects were subjected to specific countermeasures, either physical or nutritional, to counteract the harmful effects of microgravity, while others remained in the control group with no countermeasures applied. All volunteers underwent a tilt-table test two days before and immediately after the end of the HDBR procedure. The purpose of this test was to provoke sympathetic activation and observe the changes of the body in response to it.

When testing the similarities between the two techniques for the PRD calculation, these were found to be highly correlated, which was indicative of their ability to compute PRD and quantify the low-frequency oscillations of ventricular repolarization. Since the PRSA technique had lower computational costs and its use could be preferable in devices with limited computational resources, depending on the final application, this technique was selected for subsequent studies.

PRD values were found to increase after HDBR and also after TTT, with the latter supporting the fact that PRD is influenced by sympathetic activation. Considering the effects of microgravity on the ECG, this thesis validates that simulated microgravity induces an increase in sympathetic activation that is reflected in an increased magnitude of the repolarization oscillations, which cannot be explained by HRV changes.

The exercise-based countermeasure was found to be capable of partially counteracting the negative effects of microgravity on the T wave, whereas the dietary countermeasure was not.

6.1.2 Prediction of sudden cardiac death and pump failure death by PRD

In Chapter 3, the capacity of PRD to predict the risk of SCD and PFD in patients with CHF was tested. 20-minute ECG signals recorded in the supine position were processed and PRD was measured using the PRSA technique described in Chapter 2.

Methodologically, the noise level of each ECG recording was measured using the root mean square. Based on this information, T waves with an associated noise level higher than a threshold were excluded. In addition, as in Chapter 2, the same definition of the time window used to calculate the angle between consecutive T waves was applied. This updated method increases the robustness of the PRD calculation.

An increase in PRD values was associated with a higher risk of suffering from SCD in patients with CHF. Since access to long-duration signals (> 10 minutes) was also available, ECG markers from short and long recordings were tested. When PRD was combined with another Holter-based ECG marker, the IAA, the PRD capacity to stratify the risk of SCD was found to increase. The combination of PRD and the TS, increased the ability to identify CHF patients with a higher risk of PFD.

6.1.3 Electrical dyssynchrony related to cardiac pacing techniques

Electrical dyssynchrony is a factor that can significantly increase mortality in pacemaker patients, as it compromises the mechanical efficiency of blood pumping and can lead to the development of pacing-induced cardiomyopathy. Chapters 4 and 5 of this thesis investigated the ventricular changes observed after various cardiac pacing techniques, such as RVP, LVSP, LBBAP, and HBP. Multiple ECG markers, including the duration of the QRS complex, the areas of the QRS complex and the T wave, PRD, AT dispersion, and RT

dispersion, were evaluated to assess which pacing technique offered better performance in minimizing ventricular electrical dyssynchrony during both short- and long-term follow-up periods.

By analyzing high-frequency (1,000 Hz) and ultra-high-frequency (5,000 Hz) ECG recordings from different populations, it was confirmed that physiological pacing, which targets specific parts of the cardiac conduction system, induces better electrical responses compared to conventional techniques, which capture the right ventricular myocardium.

In terms of ventricular depolarization, HBP showed an electrical activation response comparable to that of spontaneous rhythm in patients without any conduction disorder. LBBP and LVSP, although they had greater differences with respect to spontaneous rhythm than HBP, were capable of preserving synchrony in LV activation, with only delayed activation in the RV. Conventional pacing on the RV led to high depolarization dyssynchrony, as manifested by large dAT values. The benefits of physiological pacing versus conventional pacing were maintained up to one year after pacemaker implantation.

Regarding ventricular repolarization, this thesis confirmed previous observations on the large similarities between HBP and spontaneous rhythm in patients without ventricular conduction disorders. LBBP, although different from spontaneous rhythm in some global measurements of ventricular RT dispersion, was confirmed to lead to high synchrony in LV repolarization. In contrast, RVP was associated with high dyssynchrony in ventricular repolarization, particularly in the LV. Our findings and the technical advantages of LBBP compared to HBP suggest LBBP as a physiological pacing alternative to HBP that overcomes the limitations of conventional RVP.

6.1.4 Clinical significance

ECG recordings can noninvasively provide information on electrical activation and recovery of the heart and its autonomic modulation. By measuring periodic low-frequency dynamics of the T wave through the PRD index, it is possible to quantify increases in sympathetic modulation of ventricular repolarization that can be indicative of increased arrhythmic risk when subjects are exposed to microgravity for prolonged periods of time.

In addition, PRD has been shown to be a strong risk stratification marker in patients with CHF, which can be measured from short 20-minute ECG recordings. Elevated PRD values are associated with a high risk of SCD, and when combined with other Holter-derived markers, its ability to stratify patients with CHF not only by the risk of SCD, but also by the risk of PFD, is shown to be significantly improved.

Pacemakers are the standard treatment for patients with bradycardia. By analyzing commonly used ECG markers and proposing new ones, this thesis shows the benefits and limitations of conventional and physiological pacing techniques in terms of dyssynchrony in ventricular activation and recovery. Importantly, this thesis addresses the effects of pacing not only in the short term (immediately after and one day after pacemaker implantation) but also in the long term (one year after implantation), providing novel findings to be considered when taking a clinical decision on the pacing technique to be applied.

6.2 Future work

Based on the findings presented in this thesis, future research directions are proposed in the following.

- The methodologies proposed for the PRD calculation should be validated in other study populations to assess its predictive value and the reproducibility of the results.
- PRD calculation was performed by proposing modifications to two methods previously described in the literature. Throughout most of this thesis, the method with lower computational cost, based on PRSA, was used, as it was able to track ventricular changes induced by sympathetic activation in a similar way to the CWT method. Future studies could derive an explicit formula to convert the values obtained with the two calculation methods to facilitate comparisons between studies that use either method for the PRD calculation.
- In the ECG signals of healthy volunteers exposed to artificial microgravity, additional ECG markers of ventricular repolarization and au-

tonomic activity could be evaluated to more thoroughly characterize microgravity-induced changes in cardiac function and assess the effectiveness of countermeasures.

- The prognostic value of the PRD index and other ECG-based markers has been validated for SCD and PFD risk stratification using the MUSIC database, which includes CHF patients. More studies incorporating other endpoints and a larger number of patients with SCD and PFD could be useful to confirm the findings of this thesis and validate the clinical benefit of the individual and combined markers investigated in this thesis.

- Although physiological pacing techniques, such as HBP and LBBAP, have demonstrated benefits in reducing electrical dyssynchrony after intervention compared to conventional RVP, the long-term impact of these physiological pacing techniques requires a more comprehensive analysis. The studies conducted in this thesis could be extended to investigate longer follow-up periods and perform clinical characterizations to include, among others, information on the development of pacing-induced cardiomyopathy. In addition, those long-term studies should include a larger and more representative number of ECG recordings of patients undergoing each of the stimulation modalities under analysis.

- Some of the signals analyzed in this work were recorded using ultra-high-frequency sampling (5,000 Hz), which requires specific equipment that is not easily accessible by many hospitals. Future studies could assess the feasibility of obtaining similar information using widely available ECG recorders that allow a sampling frequency of up to 1,000 Hz.

Bibliography

[1] Abdelrahman, M., Subzposh, F. A., Beer, D., Durr, B., Naperkowski, A., Sun, H., Oren, J. W., Dandamudi, G., and Vijayaraman, P. (2018). Clinical Outcomes of His Bundle Pacing Compared to Right Ventricular Pacing. *Journal of the American College of Cardiology*, 71(20):2319–2330.

[2] Abdin, A., Aktaa, S., Vukadinović, D., Arbelo, E., Burri, H., Glikson, M., Meyer, C., Munyombwe, T., Nielsen, J. C., Ukena, C., Vernooy, K., and Gale, C. P. (2021). Outcomes of conduction system pacing compared to right ventricular pacing as a primary strategy for treating bradyarrhythmia: Systematic review and meta-analysis. *Clinical Research in Cardiology*, pages 1–12.

[3] Abry, P. (1997). *Ondelettes et turbulences: Multirésolutions, algorithmes de décomposition, invariance d'échelle et signaux de pression*. Nouveaux essais. Diderot éd.

[4] Adabag, A. S., Luepker, R. V., Roger, V. L., and Gersh, B. J. (2010). Sudden cardiac death: Epidemiology and risk factors. *Nature Reviews Cardiology*, 7(4):216.

[5] Addison, P. S. (2005). Wavelet transforms and the ECG: a review. *Physiological Measurement*, 26(5):R155–R199.

[6] Akerström, F., Pachón, M., Puchol, A., Jiménez-López, J., Segovia, D., Rodríguez-Padial, L., and Arias, M. A. (2014). Chronic right ventricular apical pacing: Adverse effects and current therapeutic strategies to minimize them. *International Journal of Cardiology*, 173(3):351–360.

[7] Al-Khatib, S. M., Stevenson, W. G., Ackerman, M. J., Bryant, W. J., Callans, D. J., Curtis, A. B., Deal, B. J., Dickfeld, T., Field, M. E., Fonarow, G. C., Gillis, A. M., Granger, C. B., Hammill, S. C., Hlatky, M. A., Joglar, J. A., Kay, G. N., Matlock, D. D., Myerburg, R. J., and Page, R. L. (2018). 2017 AHA/ACC/HRS Guideline for Management of Patients With Ventricular Arrhythmias and the Prevention of Sudden Cardiac Death. *Circulation*, 138(13):e272–e391.

[8] Alattar, F., Imran, N., Shamoon, F., Alattar, F., Imran, N., and Shamoon, F. (2015). Fragmented QRS and Ejection Fraction in Heart Failure Patients Admitted to the Hospital. *IJC Heart & Vasculature*, 9:11–14.

[9] Albert, C. M. (2012). Omega-3 fatty acids, ventricular arrhythmias, and sudden cardiac death. *Circulation: Arrhythmia and Electrophysiology*, 5(3):456–459.

[10] Ambrosy, A. P., Fonarow, G. C., Butler, J., Chioncel, O., Greene, S. J., Vaduganathan, M., Nodari, S., Lam, C. S., Sato, N., Shah, A. N., and Gheorghiade, M. (2014). The global health and economic burden of hospitalizations for heart failure: Lessons learned from hospitalized heart failure registries. *Journal of the American College of Cardiology*, 63(12):1123–1133.

[11] Amin, A. S., Tan, H. L., and Wilde, A. A. (2010). Cardiac ion channels in health and disease. *Heart Rhythm*, 7(1):117–126.

[12] Amirova, L., Navasiolava, N., Rukavishvikov, I., Gauquelin-Koch, G., Gharib, C., Kozlovskaya, I., Custaud, M.-A., and Tomilovskaya, E. (2020). Cardiovascular system under simulated weightlessness: Head-down bed rest vs. dry immersion. *Frontiers in Physiology*, 11:395.

[13] Andersen, M., Xue, J., Graff, C., Hardahl, T., Toft, E., Kanters, J., Christiansen, M., Jensen, H., and Struijk, J. (2007). A robust method for quantification of IKr-related T-wave morphology abnormalities. In *2007 Computers in Cardiology*, pages 341–344.

[14] Anker, S. D. et al. (2016). Traditional and new composite endpoints in heart failure clinical trials: Facilitating comprehensive efficacy assessments and improving trial efficiency. *European Journal of Heart Failure*, 18(5):482–489.

[15] Anttila, I., Nikus, K., Kähönen, M., Jula, A., Reunanen, A., Salomaa, V., Nieminen, M. S., Lehtimäki, T., Virtanen, V., Verrier, R. L., Varis, J., Sclarovsky, S., and Nieminen, T. (2010). Prognostic implications of quantitative ST-segment characteristics and T-wave amplitude for cardiovascular mortality in a general population from the Health 2000 Survey. *Annals of Medicine*, 42(7):502–511. PMID: 20854212.

[16] Antzelevitch, C. (2001). Transmural dispersion of repolarization and the T wave. *Cardiovascular Research*, 50(3):426–431.

[17] Antzelevitch, C., Sicouri, S., Di Diego, J. M., Burashnikov, A., Viskin, S., Shimizu, W., Yan, G.-X., Kowey, P., and Zhang, L. (2007). Does Tpeak–Tend provide an index of transmural dispersion of repolarization? *Heart Rhythm*, 4(8):1114–1116.

[18] Antzelevitch, C., Yan, G. X., and Shimizu, W. (1999). Transmural dispersion of repolarization and arrhythmogenicity: The Brugada syndrome versus the long QT syndrome. *Journal of Electrocardiology*, 32(Suppl:158-65.):;.

[19] Ark, C. R. V. and Reynolds, E. W. (1970). An experimental study of propagated electrical activity in the canine heart. *Circulation Research*, 26(4):451–460.

[20] Arnold, A. D., Shun-Shin, M. J., Ali, N., Keene, D., Howard, J. P., Chow, J.-J., Qureshi, N. A., Koa-Wing, M., Tanner, M., Lefroy, D. C., Linton, N. W., Ng, F. S., Lim, P. B., Peters, N. S., Kanagaratnam, P., Francis, D. P., and Whinnett, Z. I. (2021). Left ventricular activation time and pattern are preserved with both selective and nonselective His bundle pacing. *Heart Rhythm O2*, 2(5):439–445.

[21] Arnold, A. D., Whinnett, Z. I., and Vijayaraman, P. (2020). His–purkinje conduction system pacing: State of the art in 2020. *Radcliffe Cardiology*.

[22] Arora, V. and Suri, P. (2021). Physiological pacing: A new road to future. *Indian Journal of Clinical Cardiology*, 2(1):32–43.

[23] Arteyeva, N. V. (2020). Dispersion of ventricular repolarization: Temporal and spatial. *World Journal of Cardiology*, 12(9):437–449.

[24] Auricchio, A. and Yu, C. M. (2004). Beyond the measurement of QRS complex toward mechanical dyssynchrony: Cardiac resynchronisation therapy in heart failure patients with a normal QRS duration. *Heart*, 90(5):479.

[25] Austermann, K., Baecker, N., Zwart, S. R., Fimmers, R., Frippiat, J.-P., Stehle, P., Smith, S. M., and Heer, M. (2021). Antioxidant supplementation does not affect bone turnover markers during 60 days of 6° head-down tilt bed rest: Results from an exploratory randomized controlled trial. *The Journal of Nutrition*, 151(6):1527–1538.

[26] Aydin, A. E., Soysal, P., and Isik, A. T. (2017). Which is preferable for orthostatic hypotension diagnosis in older adults: Active standing test or head-up tilt table test? *Clinical Interventions in Aging*, 12:207.

[27] Bailón, R., Laouini, G., Grao, C., Orini, M., Laguna, P., and Meste, O. (2011). The integral pulse frequency modulation model with time-varying threshold: Application to heart rate variability analysis during exercise stress testing. *IEEE Transactions on Biomedical Engineering*, 58(3):642–652.

[28] Balion, C., Santaguida, P. L., Hill, S., Worster, A., McQueen, M., Oremus, M., McKelvie, R., Booker, L., Fagbemi, J., Reichert, S., and Raina, P. (2006). Testing for BNP and NT-proBNP in the diagnosis and prognosis of heart failure. *Evid. Rep./Technol. Assess.*, 142:1–147.

[29] Banavalikar, B., Thajudeen, A., Namboodiri, N., Nair, K. K. M., Pushpangadhan, A. S., and Valaparambil, A. K. (2017). Long-term effects

of cardiac resynchronization therapy on electrical remodeling in heart failure—A prospective study. *Pacing and Clinical Electrophysiology*, 40(11):1279–1285.

[30] Bank, A. J., Gage, R. M., and Burns, K. V. (2012). Right Ventricular Pacing, Mechanical Dyssynchrony, and Heart Failure. *Journal of Cardiovascular Translational Research*, 5(2):219–231.

[31] Baran, R., Marchal, S., Garcia Campos, S., Rehnberg, E., Tabury, K., Baselet, B., Wehland, M., Grimm, D., and Baatout, S. (2022). The cardiovascular system in space: Focus on in vivo and in vitro studies. *Biomedicines*, 10(1).

[32] Bardy, G. H., Lee, K. L., Mark, D. B., Poole, J. E., Packer, D. L., Boineau, R., Domanski, M., Troutman, C., Anderson, J., Johnson, G., McNulty, S. E., Clapp-Channing, N., Davidson-Ray, L. D., Fraulo, E. S., Fishbein, D. P., Luceri, R. M., and Ip, J. H. (2005). Amiodarone or an Implantable Cardioverter–Defibrillator for Congestive Heart Failure. *New England Journal of Medicine*, 352(3):225–237. PMID: 15659722.

[33] Battipaglia, I. and Lanza, G. A. (2014). The Autonomic Nervous System of the Heart. In *Autonomic Innervation of the Heart: Role of Molecular Imaging*, pages 1–12. Springer, Berlin, Germany.

[34] Bauer, A. et al. (2019). Prediction of mortality benefit based on periodic repolarisation dynamics in patients undergoing prophylactic implantation of a defibrillator: A prospective, controlled, multicentre cohort study. *The Lancet*.

[35] Bauer, A. et al. (2022). Telemedical cardiac risk assessment by implantable cardiac monitors in patients after myocardial infarction with autonomic dysfunction (SMART-MI-DZHK9): A prospective investigator-initiated, randomised, multicentre, open-label, diagnostic trial. *The Lancet Digital Health*, 4(2):e105–e116.

[36] Bauer, A., Kantelhardt, J. W., Bunde, A., Barthel, P., Schneider, R., Malik, M., and Schmidt, G. (2006). Phase-rectified signal averaging detects quasi-periodicities in non-stationary data. *Physica A: Statistical Mechanics and its Applications*, 364:423–434.

[37] Baumert, M., Porta, A., Vos, M. A., Malik, M., Couderc, J.-P., Laguna, P., Piccirillo, G., Smith, G. L., Tereshchenko, L. G., and Volders, P. G. (2016). QT interval variability in body surface ECG: measurement, physiological basis, and clinical value: position statement and consensus guidance endorsed by the European Heart Rhythm Association jointly with the ESC Working Group on Cardiac Cellular Electrophysiology. *EP Europace*, 18(6):925–944.

[38] Baumert, M., Starc, V., and Porta, A. (2012). Conventional QT Variability Measurement vs. Template Matching Techniques: Comparison of Performance Using Simulated and Real ECG. *PLOS ONE*, 7(7):1–8.

[39] Bessière, F., Mondésert, B., Chaix, M.-A., and Khairy, P. (2021). Arrhythmias in adults with congenital heart disease and heart failure. *Heart Rhythm O2*, 2(6, Part B):744–753. Arrhythmias in Heart Failure.

[40] Bestetti, R. B., Restini, C. B. A., and Couto, L. B. (2014). Development of Anatomophysiologic Knowledge Regarding the Cardiovascular. *Arq. Bras. Cardiol.*, 103(6):538.

[41] Bhatt, A. G., Musat, D. L., Milstein, N., Pimienta, J., Flynn, L., Sichrovsky, T., Preminger, M. W., and Mittal, S. (2018). The efficacy of his bundle pacing: Lessons learned from implementation for the first time at an experienced electrophysiology center. *JACC: Clinical Electrophysiology*, 4(11):1397–1406.

[42] Billman, G. E., Schwartz, P. J., and Stone, H. L. (1982). Baroreceptor reflex control of heart rate: a predictor of sudden cardiac death. *Circulation*, 66(4):874–880.

[43] Bird, S., Doevendans, P., van Rooijen, M., Brutel de la Riviere, A., Hassink, R., Passier, R., and Mummery, C. (2003). The human adult cardiomyocyte phenotype. *Cardiovascular Research*, 58(2):423–434.

[44] Blecker, S., Paul, M., Taksler, G., Ogedegbe, G., and Katz, S. (2013). Heart Failure–Associated Hospitalizations in the United States. *Journal of the American College of Cardiology*, 61(12):1259–1267.

[45] Bleeker, G. B., Schalij, M. J., Molhoek, S. G., Verwey, H. F., Holman, E. R., Boersma, E., Steendijk, P., Van der Wall, E. E., and Bax, J. J. (2004). Relationship Between QRS Duration and Left Ventricular Dyssynchrony in Patients with End-Stage Heart Failure. *Journal of Cardiovascular Electrophysiology*, 15(5):544–549.

[46] Blomqvist, G. C. (1996). Regulation of the systemic circulation at microgravity and during readaptation to 1G. *Med. Sci. Sports Exercise*, 28(10):9.

[47] Blottner, D., Bosutti, A., Degens, H., Schiffl, G., Gutsmann, M., Buehlmeier, J., Rittweger, J., Ganse, B., Heer, M., and Salanova, M. (2014). Whey protein plus bicarbonate supplement has little effects on structural atrophy and proteolysis marker immunopatterns in skeletal muscle disuse during 21 days of bed rest. *J. Musculoskelet. Neuronal Interact.*, 14(4):432–444.

[48] Boas, R., Sappler, N., von Stülpnagel, L., Klemm, M., Dixen, U., Thune, J. J., Pehrson, S., Køber, L., Nielsen, J. C., Videbæk, L., Haarbo, J., Korup, E., Bruun, N. E., Brandes, A., Eiskjær, H., Thøgersen, A. M., Philbert, B. T., Svendsen, J. H., Tfelt-Hansen, J., Bauer, A., and Rizas, K. D. (2022). Periodic Repolarization Dynamics Identifies ICD Responders in Nonischemic Cardiomyopathy: A DANISH Substudy. *Circulation*.

[49] Bolea, J., Caiani, E. G., Pueyo, E., Laguna, P., and Almeida, R. (2012). Microgravity effects on ventricular response to heart rate changes. In *Engineering in Medicine and Biology Society (EMBC), 2012 Annual International Conference of the IEEE*, pages 3424–3427. IEEE.

[50] Bolea, J., Laguna, P., Caiani, E. G., and Almeida, R. (2013). Heart rate and ventricular repolarization variabilities interactions modification by microgravity simulation during head-down bed rest test. In *Computer-Based Medical Systems (CBMS), 2013 IEEE 26th International Symposium on*, pages 552–553. IEEE.

[51] Böhm, M. et al. (2018). Duration of Chronic Heart Failure Affects Outcomes With Preserved Effects of Heart Rate Reduction With Ivabradine: Findings From SHIFT. *Eur. J. Heart Fail.*, 20(2):373–381.

[52] Bosutti, A., Mulder, E., Zange, J., Bühlmeier, J., Ganse, B., and Degens, H. (2020). Effects of 21 days of bed rest and whey protein supplementation on plantar flexor muscle fatigue resistance during repeated shortening contractions. *European Journal of Applied Physiology*, pages 1–15.

[53] Bosutti, A., Salanova, M., Blottner, D., Buehlmeier, J., Mulder, E., Rittweger, J., Yap, M. H., Ganse, B., and Degens, H. (2016). Whey protein with potassium bicarbonate supplement attenuates the reduction in muscle oxidative capacity during 19 days of bed rest. *Journal of Applied Physiology*, 121(4):838–848. PMID: 27516541.

[54] Boukens, B. J., Hoogendijk, M. G., Verkerk, A. O., Linnenbank, A., van Dam, P., Remme, C.-A., Fiolet, J. W., Opthof, T., Christoffels, V. M., and Coronel, R. (2012). Early repolarization in mice causes overestimation of ventricular activation time by the QRS duration. *Cardiovascular Research*, 97(1):182–191.

[55] Boullin, J. and Morgan, J. M. (2005). The development of cardiac rhythm. *Heart*, 91(7):874–875.

[56] Bozkurt, B. et al. (2021). Universal definition and classification of heart failure: a report of the Heart Failure Society of America, Heart Failure Association of the European Society of Cardiology, Japanese Heart Failure Society and Writing Committee of the Universal Definition of Heart Failure. *European Journal of Heart Failure*, 23(3):352–380.

[57] Bragazzi, N. L., Zhong, W., Shu, J., Abu Much, A., Lotan, D., Grupper, A., Younis, A., and Dai, H. (2021). Burden of heart failure and underlying causes in 195 countries and territories from 1990 to 2017. *European Journal of Preventive Cardiology*, 28(15):1682–1690.

[58] Braunwald, E. (2008). Biomarkers in heart failure. *New England Journal of Medicine*, 358(20):2148–2159. PMID: 18480207.

[59] Brennan, T. and Tarassenko, L. (2012). Review of T-wave morphology-based biomarkers of ventricular repolarisation using the surface electrocardiogram. *Biomedical Signal Processing and Control*, 7(3):278–284. BioSignal Processing for Engineering and Computing: the MEDICON conference case.

[60] Brutsaert, D. L. and Andries, L. J. (1992). The endocardial endothelium. *American Journal of Physiology-Heart and Circulatory Physiology*, 263(4):H985–H1002. PMID: 1415782.

[61] Buckey, J. C., Gaffney, F. A., Lane, L. D., Levine, B. D., Watenpaugh, D. E., Wright, S. J., Yancy, C. W., Meyer, D. M., and Blomqvist, C. G. (1996a). Central venous pressure in space. *Journal of Applied Physiology*, 81(1):19–25. PMID: 8828643.

[62] Buckey, J. C., Lane, L. D., Levine, B. D., Watenpaugh, D. E., Wright, S. J., Moore, W. E., Gaffney, F. A., and Blomqvist, C. G. (1996b). Orthostatic intolerance after spaceflight. *Journal of Applied Physiology*, 81(1):7–18. PMID: 8828642.

[63] Budts, W. et al. (2020). Recommendations for participation in competitive sport in adolescent and adult athletes with Congenital Heart Disease (CHD): position statement of the Sports Cardiology & Exercise Section of the European Association of Preventive Cardiology (EAPC), the European Society of Cardiology (ESC) Working Group on Adult Congenital Heart Disease and the Sports Cardiology, Physical Activity and Prevention Working Group of the Association for European Paediatric and Congenital Cardiology (AEPC). *European Heart Journal*, 41(43):4191–4199.

[64] Caiani, E., Landreani, F., Costantini, L., Mulder, E., Gerlach, D., Vaïda, P., and Migeotte, P.-F. (2018). Effectiveness of high-intensity jump training countermeasure on mitral and aortic flow after 58-days head-down bed-rest assessed by phase-contrast MRI. In *International Astronautical Congress*, volume 2018, pages 135–41.

[65] Caiani, E. G., Pellegrini, A., Bolea, J., Sotaquira, M., Almeida, R., and Vaïda, P. (2013). Impaired T-wave amplitude adaptation to heart-rate induced by cardiac deconditioning after 5-days of head-down bed-rest. *Acta Astronautica*, 91:166 – 172.

[66] Camelliti, P., Borg, T. K., and Kohl, P. (2005). Structural and functional characterisation of cardiac fibroblasts. *Cardiovascular Research*, 65(1):40–51.

[67] Cano, Ó., Jover, P., and Vijayaraman, P. (2023). An evidence-based update on physiological pacing. *Current Treatment Options in Cardiovascular Medicine*, 25(10):415–439.

[68] Cano, Ó. and Vijayaraman, P. (2021). Left Bundle Branch Area Pacing: Implant Technique, Definitions, Outcomes, and Complications. *Curr. Cardiol. Rep.*, 23(11):155–9.

[69] Caraballo, C., Desai, N. R., Mulder, H., Alhanti, B., Wilson, F. P., Fiuzat, M., Felker, G. M., Piña, I. L., O'Connor, C. M., Lindenfeld, J., Januzzi, J. L., Cohen, L. S., and Ahmad, T. (2019). Clinical Implications of the New York Heart Association Classification. *Journal of the American Heart Association: Cardiovascular and Cerebrovascular Disease*, 8(23).

[70] Carrillo Esper, R., Díaz Ponce Medrano, J. A., Peña Pérez, C. A., Flores Rivera, O. I., Ortiz Trujillo, A., Antonio, O. C., de Jesús, J. C., and Saucedo, L. M. M. (2015). Efectos fisiológicos en un ambiente de microgravedad. *Revista de la Facultad de Medicina UNAM*, 58(3):13–24.

[71] Castro Hevia, J., Antzelevitch, C., Tornés Bárzaga, F., Dorantes Sánchez, M., Dorticós Balea, F., Zayas Molina, R., Quiñones Pérez, M. A., and Fayad Rodríguez, Y. (2006). Tpeak-Tend and Tpeak-Tend Dispersion as Risk Factors for Ventricular Tachycardia/Ventricular Fibrillation in Patients With the Brugada Syndrome. *Journal of the American College of Cardiology*, 47(9):1828–1834.

[72] Catanzariti, D., Maines, M., Cemin, C., Broso, G., Marotta, T., and Vergara, G. (2006). Permanent direct his bundle pacing does not induce ventricular dyssynchrony unlike conventional right ventricular apical pacing. *Journal of Interventional Cardiac Electrophysiology*, 16(2):81–92.

[73] Cena, H., Sculati, M., and Roggi, C. (2003). Nutritional concerns and possible countermeasures to nutritional issues related to space flight. *European Journal of Nutrition*, 42(2):99–110.

[74] Charles, J. B. and Lathers, C. M. (1994). Summary of lower body negative pressure experiments during space flight. *The Journal of Clinical Pharmacology*, 34(6):571–583.

[75] Chen, K., Li, Y., Dai, Y., Sun, Q., Luo, B., Li, C., and Zhang, S. (2018). Comparison of electrocardiogram characteristics and pacing parameters between left bundle branch pacing and right ventricular pacing in patients receiving pacemaker therapy. *EP Europace*, 21(4):673–680.

[76] Chiarazzo, E., Golia, P., Bressi, E., Grieco, D., De Ruvo, E., and Calò, L. (2025). Pacing of the specialized His Purkinje conduction system: 'HOW and FOR WHOM'. *Eur. Heart J. Suppl.*, 27(Supplement_1):i141–i148.

[77] Chioncel, O. et al. (2017). Epidemiology and one-year outcomes in patients with chronic heart failure and preserved, mid-range and reduced ejection fraction: an analysis of the ESC Heart Failure Long-Term Registry. *European Journal of Heart Failure*, 19(12):1574–1585.

[78] Christoffels, V. M., Smits, G. J., Kispert, A., and Moorman, A. F. M. (2010). Development of the Pacemaker Tissues of the Heart. *Circ. Res.*

[79] Cicchitti, V., Radico, F., Bianco, F., Gallina, S., Tonti, G., and De Caterina, R. (2016). Heart failure due to right ventricular apical pacing: the importance of flow patterns. *EP Europace*, 18(11):1679–1688.

[80] Clark, R. (2005). *Anatomy and Physiology: Understanding the Human Body*. Jones and Bartlett Publishers.

[81] Cleland, J. G., Abraham, W. T., Linde, C., Gold, M. R., Young, J. B., Claude Daubert, J., Sherfesee, L., Wells, G. A., and Tang, A. S. (2013). An individual patient meta-analysis of five randomized trials assessing the effects of cardiac resynchronization therapy on morbidity and mortality in patients with symptomatic heart failure. *European Heart Journal*, 34(46):3547–3556.

[82] Codina, P., Zamora, E., Levy, W. C., Cediel, G., Santiago-Vacas, E., Domingo, M., Ruiz-Cueto, M., Casquete, D., Sarrias, A., Borrellas, A., Santesmases, J., de la Espriella, R., Nuñez, J., Aimo, A., Lupón, J., and Bayes-Genis, A. (2023). Sudden cardiac death in heart failure: A 20-year perspective from a mediterranean cohort. *Journal of Cardiac Failure*, 29(3):236–245.

[83] Coronel, R. (2017). The pro- or antiarrhythmic actions of polyunsaturated fatty acids and of cholesterol. *Pharmacology & Therapeutics*, 176:40 – 47. Cardiac Arrhythmias.

[84] Costanzo, M. R., Mills, R. M., and Wynne, J. (2008). Characteristics of "Stage D" heart failure: Insights from the Acute Decompensated Heart Failure National Registry Longitudinal Module (ADHERE LM). *American Heart Journal*, 155(2):339–347.

[85] Couderc, J., Zareba, W., Xia, X., Andrew, M., and Moss, A. (2003). T-wave morphology and arrhythmic events in patients with dilated cardiomyopathy. In *Computers in Cardiology, 2003*, pages 149–152.

[86] Cox, D. R. (1972). Regression models and life-tables. *Journal of the Royal Statistical Society: Series B (Methodological)*, 34(2):187–202.

[87] Crespo-Leiro, M. G. et al. (2016). European Society of Cardiology Heart Failure Long-Term Registry (ESC-HF-LT): 1-year follow-up outcomes and differences across regions. *European Journal of Heart Failure*, 18(6):613–625.

[88] Crisafulli, A., Pagliaro, P., Roberto, S., Cugusi, L., Mercuro, G., Lazou, A., Beauloye, C., Bertrand, L., Hausenloy, D. J., Aragno, M., and Penna, C. (2020). Diabetic Cardiomyopathy and Ischemic Heart Disease: Prevention and Therapy by Exercise and Conditioning. *Int. J. Mol. Sci.*, 21(8):2896.

[89] Cromwell, R. L., Scott, J. M., Downs, M., Yarbough, P. O., Zanello, S. B., and Ploutz-Snyder, L. (2018). Overview of the NASA 70-day Bed Rest Study. *Medicine and science in sports and exercise*, 50(9):1909—1919.

[90] Curila, K., Jurak, P., Halamek, J., Prinzen, F., Waldauf, P., Karch, J., Stros, P., Plesinger, F., Mizner, J., Susankova, M., Prochazkova, R., Sussenbek, O., Viscor, I., Vondra, V., Smisek, R., Leinveber, P., and Osmancik, P. (2021c). Ventricular activation pattern assessment during right ventricular pacing: Ultra-high-frequency ECG study. *Journal of Cardiovascular Electrophysiology*, 32(5):1385–1394.

[91] Curila, K., Jurak, P., Jastrzebski, M., Prinzen, F., Waldauf, P., Halamek, J., Vernooy, K., Smisek, R., Karch, J., Plesinger, F., Moskal, P., Susankova, M., Znojilova, L., Heckman, L., Viscor, I., Vondra, V., Leinveber, P., and Osmancik, P. (2021a). Left bundle branch pacing compared to left ventricular septal myocardial pacing increases interventricular dyssynchrony but accelerates left ventricular lateral wall depolarization. *Heart Rhythm*, 18(8):1281–1289.

[92] Curila, K., Jurak, P., Vernooy, K., Jastrzebski, M., Waldauf, P., Prinzen, F., Halamek, J., Susankova, M., Znojilova, L., Smisek, R., Karch, J., Plesinger, F., Moskal, P., Heckman, L., Mizner, J., Viscor, I., Vondra, V., Leinveber, P., and Osmancik, P. (2021b). Left Ventricular Myocardial Septal Pacing in Close Proximity to LBB Does Not Prolong the Duration of the Left Ventricular Lateral Wall Depolarization Compared to LBB Pacing. *Frontiers in Cardiovascular Medicine*, 8.

[93] Curila, K., Prochazkova, R., Jurak, P., Jastrzebski, M., Halamek, J., Moskal, P., Stros, P., Vesela, J., Waldauf, P., Viscor, I., Plesinger, F., Sussenbek, O., Herman, D., Osmancik, P., Smisek, R., Leinveber, P., Czarnecka, D., and Widimsky, P. (2020). Both selective and nonselective His bundle, but not myocardial, pacing preserve ventricular electrical synchrony assessed by ultra-high-frequency ECG. *Heart Rhythm*, 17(4):607–614.

[94] Cygankiewicz, I. (2013). Heart rate turbulence. *Progress in Cardiovascular Diseases*, 56(2):160 – 171. Ambulatory ECG Monitoring: Clinical Practice and Research Applications.

[95] Cygankiewicz, I., Zareba, W., Vazquez, R., Vallverdu, M., Gonzalez-Juanatey, J. R., Valdes, M., Almendral, J., Cinca, J., Caminal, P., and de Luna, A. B. (2008). Heart rate turbulence predicts all-cause mortality and sudden death in congestive heart failure patients. *Heart Rhythm*, 5(8):1095 – 1102.

[96] Damasceno, A., Cotter, G., Dzudie, A., Sliwa, K., and Mayosi, B. M. (2007). Heart Failure in Sub-Saharan Africa: Time for Action. *Journal of the American College of Cardiology*, 50(17):1688–1693.

[97] Das, M. K. and Zipes, D. P. (2009). Fragmented QRS: A predictor of mortality and sudden cardiac death. *Heart Rhythm*, 6(3, Supplement):S8 – S14.

[98] D'Aunno, D. S., Dougherty, A. H., DeBlock, H. F., and Meck, J. V. (2003). Effect of short-and long-duration spaceflight on QTc intervals in healthy astronauts. *The American journal of cardiology*, 91(4A):494–494.

[99] Day, C. P., McComb, J. M., and Campbell, R. W. (1990). QT dispersion: an indication of arrhythmia risk in patients with long QT intervals. *Br. Heart J.*, 63(6):342.

[100] de Cock, C. C., Giudici, M. C., and Twisk, J. W. (2003). Comparison of the haemodynamic effects of right ventricular outflow-tract pacing with right ventricular apex pacing: A quantitative review. *EP Europace*, 5(3):275–278.

[101] De la Torre, G. G. et al. (2024). Space Analogs and Behavioral Health Performance Research review and recommendations checklist from ESA Topical Team. *npj Microgravity*, 10(98):1–16.

[102] Del-Carpio Munoz, F., Gharacholou, S. M., Scott, C. G., Nkomo, V. T., Lopez-Jimenez, F., Cha, Y.-M., Munger, T. M., Friedman, P. A., and Asirvatham, S. J. (2017). Prolonged ventricular conduction and repolarization during right ventricular stimulation predicts ventricular arrhythmias and death in patients with cardiomyopathy. *JACC: Clinical Electrophysiology*, 3(13):1580–1591.

[103] Desai, D. S. and Hajouli, S. (2023). Arrhythmias. In *StatPearls [Internet]*. StatPearls Publishing.

[104] Deshmukh, P., Casavant, D. A., Romanyshyn, M., and Anderson, K. (2000). Permanent, direct His-bundle pacing. *Circulation*, 101(8):869–877.

[105] Diaz, J. C. et al. (2024). Improved all-cause mortality with left bundle branch area pacing compared to biventricular pacing in cardiac resynchronization therapy: a meta-analysis. *Journal of Interventional Cardiac Electrophysiology*, pages 1–14.

[106] DiFrancesco, J. M. and Olson, J. M. (2015). The economics of microgravity research. *npj Microgravity*, 1(15001):1–6.

[107] Dobney, W., Mols, L., Mistry, D., Tabury, K., Baselet, B., and Baatout, S. (2023). Evaluation of deep space exploration risks and mitigations against radiation and microgravity. *Frontiers in Nuclear Medicine*, 3.

[108] Duijvenboden, S. V., Porter, B., Pueyo, E., Sampedro-Puente, D. A., Fernandez-Bes, J., Sidhu, B., Gould, J., Orini, M., Bishop, M. J., Hanson, B., Lambiase, P., Razavi, R., Rinaldi, C. A., Gill, J. S., and Taggart, P. (2020). Complex Interaction Between Low-Frequency APD Oscillations and Beat-to-Beat APD Variability in Humans Is Governed by the Sympathetic Nervous System. *Frontiers in Physiology*, 10:1582.

[109] Dunnink, A., Stams, T. R., Bossu, A., Meijborg, V. M., Beekman, J. D., Wijers, S. C., De Bakker, J. M., and Vos, M. A. (2016). Torsade de pointes arrhythmias arise at the site of maximal heterogeneity of repolarization in the chronic complete atrioventricular block dog. *EP Europace*, 19(5):858–865.

[110] Dural, M., Ghossein, M. A., Gerrits, W., Daniels, F., Meine, M., Maass, A. H., Rienstra, M., Prinzen, F. W., Vernooy, K., and van Stipdonk, A. M. W. (2023). Association of vectorcardiographic T-wave area with clinical and echocardiographic outcomes in cardiac resynchronization therapy. *EP Europace*, 26(1):euad370.

[111] Ebrille, E., DeSimone, C. V., Vaidya, V. R., Chahal, A. A., Nkomo, V. T., and Asirvatham, S. J. (2016). Ventricular pacing – electromechanical consequences and valvular function. *Indian Pacing and Electrophysiology Journal*, 16(1):19–30.

[112] Edenbrandt, L. and Pahlm, O. (1988). Vectorcardiogram synthesized from a 12-lead ECG: superiority of the inverse dower matrix. *Journal of Electrocardiology*, 21(4):361–367.

[113] Eknoyan, G. (2004). Emergence of the concept of cardiovascular disease. *Adv. Chronic Kidney Dis.*, 11(3):304–309.

[114] Ellenbogen, K., Vijayaraman, P., and Padala, S. (2022). *Advances in physiologic pacing, An Issue of Cardiac Electrophysiology Clinics, E-Book*. The Clinics: Internal Medicine. Elsevier Health Sciences.

[115] Engels, E. B., Végh, E. M., Van Deursen, C. J. M., Vernooy, K., Singh, J. P., and Prinzen, F. W. (2015). T-Wave Area Predicts Response to Cardiac Resynchronization Therapy in Patients with Left Bundle Branch Block. *Journal of Cardiovascular Electrophysiology*, 26(2):176–183.

[116] European Space Agency (2025). Microgravity and ISS. [Online; accessed 08. Apr. 2025].

[117] Eurostat (2023). Causes of death statistics.

[118] Evans, J. M., Knapp, C. F., and Goswami, N. (2018). Artificial gravity as a countermeasure to the cardiovascular deconditioning of spaceflight: Gender perspectives. *Frontiers in Physiology*, 9:716.

[119] Ewald, B., Ewald, D., Thakkinstian, A., and Attia, J. (2008). Meta-analysis of B type natriuretic peptide and N-terminal pro B natriuretic peptide in the diagnosis of clinical heart failure and population screening for left ventricular systolic dysfunction. *Internal Medicine Journal*, 38(2):101–113.

[120] Farré, J. and Wellens, H. J. (2004). Philippe Coumel: a founding father of modern arrhythmology. *EP Europace*, 6(5):464–465.

[121] Fauchier, L., Douglas, J., Babuty, D., Cosnay, P., and Fauchier, J. P. (2005). QT dispersion in nonischemic dilated cardiomyopathy. A long-term evaluation. *European Journal of Heart Failure*, 7(2):277–282.

[122] Fenton, M. and Burch, M. (2007). Understanding chronic heart failure. *Archives of disease in childhood*, 92(9):812–816.

[123] Fine, J. P. and Gray, R. J. (1999). A Proportional Hazards Model for the Subdistribution of a Competing Risk. *J. Am. Stat. Assoc.*, 94(446):496–509.

[124] Florea, V. G. and Cohn, J. N. (2014). The autonomic nervous system and heart failure. *Circulation Research*, 114(11):1815–1826.

[125] Fonarow, G. C., Stough, W. G., Abraham, W. T., Albert, N. M., Gheorghiade, M., Greenberg, B. H., O'Connor, C. M., Sun, J. L., Yancy, C. W., and Young, J. B. (2007). Characteristics, Treatments, and Outcomes of Patients With Preserved Systolic Function Hospitalized for Heart Failure: A Report From the OPTIMIZE-HF Registry. *Journal of the American College of Cardiology*, 50(8):768–777.

[126] Franciosi, S., Perry, F. K., Roston, T. M., Armstrong, K. R., Claydon, V. E., and Sanatani, S. (2017). The role of the autonomic nervous system in arrhythmias and sudden cardiac death. *Autonomic Neuroscience*, 205:1–11.

[127] Francis, J., Watanabe, M. A., and Schmidt, G. (2005). Heart Rate Turbulence: A New Predictor for Risk of Sudden Cardiac Death. *Annals of Noninvasive Electrocardiology*, 10(1):102–109.

[128] Fritsch-Yelle, J. M., Charles, J. B., Jones, M. M., and Wood, M. L. (1996). Microgravity decreases heart rate and arterial pressure in humans. *Journal of Applied Physiology*, 80(3):910–914.

[129] Fudim, M. and Borges-Neto, S. (2019). A troubled marriage: When electrical and mechanical dyssynchrony don't go along. *Journal of Nuclear Cardiology*, 26(4):1240–1242.

[130] Fukuta, H. and Little, W. C. (2008). The cardiac cycle and the physiologic basis of left ventricular contraction, ejection, relaxation, and filling. *Heart Failure Clinics*, 4(1):1–11. Diastolic Dysfunction and Heart Failure.

[131] Furman, S. and Schwedel, J. B. (1959). An Intracardiac Pacemaker for Stokes-Adams Seizures. *New England Journal of Medicine*, 261(19):943–948. PMID: 13825713.

[132] Gao, D., Madden, M., Schukat, M., Chambers, D., and Lyons, G. (2004). Arrhythmia Identification from ECG Signals with a Neural Network Classifier Based on a Bayesian Framework. *Twenty-fourth SGAI International Conference on Innovative Techniques and Applications of Artificial Intelligence*, 3(3):390–409.

[133] Gatti, P., Linde, C., Benson, L., Thorvaldsen, T., Normand, C., Savarese, G., Dahlström, U., Maggioni, A. P., Dickstein, K., and Lund, L. H. (2023). What determines who gets cardiac resynchronization therapy in Europe? A comparison between ESC-HF-LT registry, SwedeHF registry, and ESC-CRT Survey II. *Eur. Heart J. Qual. Care Clin. Outcomes*, 9(8):741–748.

[134] Gayat, E. et al. (2018). Heart failure oral therapies at discharge are associated with better outcome in acute heart failure: a propensity-score matched study. *European Journal of Heart Failure*, 20(2):345–354.

[135] Gazenko, O. G., Genin, A. M., and Egorov, A. D. (1981). Summary of medical investigations in the U.S.S.R. manned space missions. *Acta Astronautica*, 8(9-10):907–917.

[136] Gaziano, T., Reddy, K. S., Paccaud, F., Horton, S., and Chaturvedi, V. (2006). Cardiovascular Disease. In *Disease Control Priorities in Developing Countries. 2nd edition*. The International Bank for Reconstruction and Development / The World Bank.

[137] Gaziano, T. A., Bitton, A., Anand, S., Abrahams-Gessel, S., and Murphy, A. (2010). Growing Epidemic of Coronary Heart Disease in Low- and Middle-Income Countries. *Current Problems in Cardiology*, 35(2):72.

[138] Ghossein, M. A., van Stipdonk, A. M. W., Plesinger, F., Kloosterman, M., Wouters, P. C., Salden, O. A. E., Meine, M., Maass, A. H., Prinzen, F. W., and Vernooy, K. (2021). Reduction in the QRS area after cardiac resynchronization therapy is associated with survival and echocardiographic response. *Journal of Cardiovascular Electrophysiology*, 32(3):813.

[139] Giacinto, O., Lusini, M., Sammartini, E., Minati, A., Mastroianni, C., Nenna, A., Pascarella, G., Sammartini, D., Carassiti, M., Miraldi, F., Chello, M., and Pelliccia, F. (2024). Cardiovascular Effects of Cosmic Radiation and Microgravity. *Journal of Clinical Medicine*, 13(2):520.

[140] Giannessi, D. (2011). Multimarker approach for heart failure management: Perspectives and limitations. *Pharmacological Research*, 64(1):11 – 24.

[141] Glikson, M. et al. (2021). 2021 ESC Guidelines on cardiac pacing and cardiac resynchronization therapy: Developed by the Task Force on cardiac pacing and cardiac resynchronization therapy of the European Society of Cardiology (ESC) With the special contribution of the European Heart Rhythm Association (EHRA). *European Heart Journal*, 42(35):3427–3520.

[142] Grant, A. O. (2009). Cardiac ion channels. *Circulation: Arrhythmia and Electrophysiology*, 2(2):185–194.

[143] Greene, S. J., Butler, J., Albert, N. M., DeVore, A. D., Sharma, P. P., Duffy, C. I., Hill, C. L., McCague, K., Mi, X., Patterson, J. H., Spertus, J. A., Thomas, L., Williams, F. B., Hernandez, A. F., and Fonarow, G. C. (2018). Medical Therapy for Heart Failure With Reduced Ejection Fraction: The CHAMP-HF Registry. *Journal of the American College of Cardiology*, 72(4):351–366.

[144] Greenland, P., Xie, X., Liu, K., Colangelo, L., Liao, Y., Daviglus, M. L., Agulnek, A. N., and Stamler, J. (2003). Impact of minor electrocardiographic ST-segment and/or T-wave abnormalities on cardiovascular mortality during long-term follow-up. *The American Journal of Cardiology*, 91(9):1068–1074.

[145] Grenon, S. M., Xiao, X., Hurwitz, S., Ramsdell, C. D., Sheynberg, N., Kim, C., Williams, G. H., and Cohen, R. J. (2005). Simulated microgravity induces microvolt T wave alternans. *Annals of Noninvasive Electrocardiology*, 10(3):363–370.

[146] Grieco, D., Bressi, E., Sedláček, K., Čurila, K., Vernooy, K., Fedele, E., De Ruvo, E., Fagagnini, A., Kron, J., Padala, S. K., Ellenbogen, K. A., and Calò, L. (2022). Feasibility and safety of left bundle branch area pacing—cardiac resynchronization therapy in elderly patients. *Journal of Interventional Cardiac Electrophysiology*, pages 1–11.

[147] Grégoire, J.-M., Gilon, C., Vaneberg, N., Bersini, H., and Carlier, S. (2023). QT-dynamicity for atrial fibrillation detection and short-term forecast using machine learning. *Archives of Cardiovascular Diseases Supplements*, 15(1):93–94. JESFC 2023.

[148] Guo, J., Li, L., Meng, F., Su, M., Huang, X., Chen, S., Li, Q., Chang, D., and Cai, B. (2020). Short-term and intermediate-term performance and safety of left bundle branch pacing. *Journal of Cardiovascular Electrophysiology*, 31(6):1472–1481.

[149] Gupta, P., Patel, C., Patel, H., Narayanaswamy, S., Malhotra, B., Green, J. T., and Yan, G.-X. (2008). Tp-e/QT ratio as an index of arrhythmogenesis. *Journal of Electrocardiology*, 41(6):567–574.

[150] Hall, C., Gehmlich, K., Denning, C., and Pavlovic, D. (2021). Complex relationship between cardiac fibroblasts and cardiomyocytes in health and disease. *Journal of the American Heart Association*, 10(5):e019338.

[151] Hamm, W., Kassem, S., von Stülpnagel, L., Maier, F., Klemm, M., Schüttler, D., Grabher, F., Weckbach, L. T., Huber, B. C., Bauer, A., Rizas, K. D., and Brunner, S. (2020). Deceleration capacity and periodic repolarization dynamics as predictors of acute mountain sickness. *High Altitude Medicine & Biology*, 21(4):417–422. PMID: 33147080.

[152] Hamm, W., Stülpnagel, L., Vdovin, N., Schmidt, G., Rizas, K., and Bauer, A. (2017). Risk prediction in post-infarction patients with moderately reduced left ventricular ejection fraction by combined assessment of the sympathetic and vagal cardiac autonomic nervous system. *International Journal of Cardiology*, 249:1 – 5.

[153] Hanson, B., Child, N., Van Duijvenboden, S., Orini, M., Chen, Z., Coronel, R., Rinaldi, C. A., Gill, J. S., Gill, J. S., and Taggart, P. (2014). Oscillatory behavior of ventricular action potential duration in heart failure patients at respiratory rate and low frequency. *Frontiers in Physiology*, 5:414.

[154] Hanson, B., Sutton, P., Elameri, N., Gray, M., Critchley, H., Gill, J. S., and Taggart, P. (2009). Interaction of activation–repolarization coupling and restitution properties in humans. *Circulation: Arrhythmia and Electrophysiology*, 2(2):162–170.

[155] Haq, K. T., Javadekar, N., and Tereshchenko, L. G. (2021). Detection and removal of pacing artifacts prior to automated analysis of 12-lead ECG. *Computers in Biology and Medicine*, 133:104396.

[156] Hargens, A. R. and Richardson, S. (2009). Cardiovascular adaptations, fluid shifts, and countermeasures related to space flight. *Respiratory Physiology & Neurobiology*, 169:S30 – S33. Cardio-Respiratory Physiology in Space.

[157] Hatzistergos, K. E., Jiang, Z., Valasaki, K., Takeuchi, L. M., Balkan, W., Atluri, P., Saur, D., Seidler, B., Tsinoremas, N., DiFede, D. L., and

Hare, J. M. (2018). Simulated microgravity impairs cardiac autonomic neurogenesis from neural crest cells. *Stem Cells and Development*, 27(12):819–830. PMID: 29336212.

[158] Hawkins, W. R. and Zieglschmid, J. (1975). Clinical aspects of crew health. *Biomedical results of Apollo*, pages 43–81.

[159] Healey, J. S., Toff, W. D., Lamas, G. A., Andersen, H. R., Thorpe, K. E., Ellenbogen, K. A., Lee, K. L., Skene, A. M., Schron, E. B., Skehan, J. D., Goldman, L., Roberts, R. S., Camm, A. J., Yusuf, S., and Connolly, S. J. (2006). Cardiovascular outcomes with atrial-based pacing compared with ventricular pacing. *Circulation*, 114(1):11–17.

[160] Heckman, L. I., Luermans, J. G., Curila, K., Van Stipdonk, A. M., Westra, S., Smisek, R., Prinzen, F. W., and Vernooy, K. (2021). Comparing ventricular synchrony in left bundle branch and left ventricular septal pacing in pacemaker patients. *Journal of Clinical Medicine*, 10(4).

[161] Hedge, E. T., Patterson, C. A., Mastrandrea, C. J., Sonjak, V., Hajj-Boutros, G., Faust, A., Morais, J. A., and Hughson, R. L. (2022). Implementation of exercise countermeasures during spaceflight and microgravity analogue studies: Developing countermeasure protocols for bedrest in older adults (BROA). *Frontiers in Physiology*, 13:928313.

[162] Heidenreich, P. A., Albert, N. M., Allen, L. A., Bluemke, D. A., Butler, J., Fonarow, G. C., Ikonomidis, J. S., Khavjou, O., Konstam, M. A., Maddox, T. M., Nichol, G., Pham, M., Piña, I. L., and Trogdon, J. G. (2013). Forecasting the impact of heart failure in the united states. *Circulation: Heart Failure*, 6(3):606–619.

[163] Hernández-Vicente, A., Hernando, D., Vicente-Rodríguez, G., Bailón, R., Garatachea, N., and Pueyo, E. (2021). ECG Ventricular Repolarization Dynamics during Exercise: Temporal Profile, Relation to Heart Rate Variability and Effects of Age and Physical Health. *International Journal of Environmental Research and Public Health*, 18(18).

[164] Herring, N., Kalla, M., and Paterson, D. J. (2019). The autonomic nervous system and cardiac arrhythmias: current concepts and emerging therapies. *Nature Reviews Cardiology*, 16(12):707–726.

[165] Hou, X., Qian, Z., Wang, Y., Qiu, Y., Chen, X., Jiang, H., Jiang, Z., Wu, H., Zhao, Z., Zhou, W., and Zou, J. (2019). Feasibility and cardiac synchrony of permanent left bundle branch pacing through the interventricular septum. *EP Europace*, 21(11):1694–1702.

[166] Huang, W., Chen, X., Su, L., Wu, S., Xia, X., and Vijayaraman, P. (2019a). A beginner's guide to permanent left bundle branch pacing. *Heart Rhythm*, 16(12):1791–1796. Focus Issue: Devices.

[167] Huang, W., Su, L., Wu, S., Xu, L., Xiao, F., Zhou, X., and Ellenbogen, K. A. (2017). A novel pacing strategy with low and stable output: Pacing the left bundle branch immediately beyond the conduction block. *Canadian Journal of Cardiology*, 33(12):1736.e1–1736.e3.

[168] Huang, W., Su, L., Wu, S., Xu, L., Xiao, F., Zhou, X., Mao, G., Vijayaraman, P., and Ellenbogen, K. A. (2019b). Long-term outcomes of His bundle pacing in patients with heart failure with left bundle branch block. *Heart*, 105(2):137–143.

[169] Huizar, J. F., Ellenbogen, K. A., Tan, A. Y., and Kaszala, K. (2019). Arrhythmia-Induced Cardiomyopathy: JACC State-of-the-Art Review. *Journal of the American College of Cardiology*, 73(18):2328–2344.

[170] Hunt, S. A., Abraham, W. T., Chin, M. H., Feldman, A. M., Francis, G. S., Ganiats, T. G., Jessup, M., Konstam, M. A., Mancini, D. M., Michl, K., Oates, J. A., Rahko, P. S., Silver, M. A., Stevenson, L. W., and Yancy, C. W. (2009). 2009 Focused Update Incorporated Into the ACC/AHA 2005 Guidelines for the Diagnosis and Management of Heart Failure in Adults. *Circulation*, 119(14):e391–e479.

[171] Hussain, M. A., Furuya-Kanamori, L., Kaye, G., Clark, J., and Doi, S. A. R. (2015). The Effect of Right Ventricular Apical and Nonapical Pacing on the Short- and Long-Term Changes in Left Ventricular Ejection Fraction: A Systematic Review and Meta-Analysis of Randomized-Controlled Trials. *Pacing and Clinical Electrophysiology*, 38(9):1121–1136.

[172] Iacoviello, M., Forleo, C., Guida, P., Romito, R., Sorgente, A., Sorrentino, S., Catucci, S., Mastropasqua, F., and Pitzalis, M. (2007). Ventricular repolarization dynamicity provides independent prognostic information toward major arrhythmic events in patients with idiopathic dilated cardiomyopathy. *Journal of the American College of Cardiology*, 50(3):225–231.

[173] Iaizzo, P. (2015). *Handbook of Cardiac Anatomy, Physiology, and Devices*. Springer International Publishing.

[174] Ikonnikov, G. and Wong, E. (2023). Physiology of cardiac conduction and contractility – McMaster Pathophysiology Review.

[175] James, M. A. and Potter, J. F. (1999). Orthostatic blood pressure changes and arterial baroreflex sensitivity in elderly subjects. *Age and Ageing*, 28(6):522–530.

[176] Januzzi, J. L., van Kimmenade, R., Lainchbury, J., Bayes-Genis, A., Ordonez-Llanos, J., Santalo-Bel, M., Pinto, Y. M., and Richards, M. (2005). NT-proBNP testing for diagnosis and short-term prognosis in acute destabilized heart failure: an international pooled analysis of 1256 patients:

The International Collaborative of NT-proBNP Study. *European Heart Journal*, 27(3):330–337.

[177] Jastrzębski, M., Kiełbasa, G., Cano, O., Curila, K., Heckman, L., De Pooter, J., Chovanec, M., Rademakers, L., Huybrechts, W., Grieco, D., Whinnett, Z. I., Timmer, S. A. J., Elvan, A., Stros, P., Moskal, P., Burri, H., Zanon, F., and Vernooy, K. (2022). Left bundle branch area pacing outcomes: the multicentre European MELOS study. *European Heart Journal*. ehac445.

[178] jeong Cho, E., Park, S.-J., Park, K. M., On, Y. K., and Kim, J. S. (2016). Paced QT interval as a risk factor for new-onset left ventricular systolic dysfunction and cardiac death after permanent pacemaker implantation. *International Journal of Cardiology*, 203:158–163.

[179] Jones, N. R., Roalfe, A. K., Adoki, I., Hobbs, F. R., and Taylor, C. J. (2018). Survival of patients with chronic heart failure in the community: a systematic review and meta-analysis protocol. *Systematic reviews*, 7(1):151.

[180] Jones, T. W., Petersen, N., and Howatson, G. (2019). Optimization of exercise countermeasures for human space flight: Operational considerations for concurrent strength and aerobic training. *Frontiers in Physiology*, 10:584.

[181] Joseph, P., Leong, D., McKee, M., Anand, S. S., Schwalm, J.-D., Teo, K., Mente, A., and Yusuf, S. (2017). Reducing the global burden of cardiovascular disease, part 1. *Circulation Research*, 121(6):677–694.

[182] Jurak, P., Curila, K., Leinveber, P., Prinzen, F. W., Viscor, I., Plesinger, F., Smisek, R., Prochazkova, R., Osmancik, P., Halamek, J., Matejkova, M., Lipoldova, J., Novak, M., Panovsky, R., Andrla, P., Vondra, V., Stros, P., Vesela, J., and Herman, D. (2020). Novel ultra-high-frequency electrocardiogram tool for the description of the ventricular depolarization pattern before and during cardiac resynchronization. *Journal of Cardiovascular Electrophysiology*, 31(1):300–307.

[183] Kashou, A. H., Basit, H., and Chhabra, L. (2022). *Physiology, Sinoatrial Node*. StatPearls Publishing, Treasure Island (FL).

[184] Kass, D. A. (2008). An epidemic of dyssynchrony: But what does it mean? *Journal of the American College of Cardiology*, 51(1):12–17.

[185] Katz, A. M. (2011). *Physiology of the Heart Fifth Edition*. Philadelphia: Lippincott Williams & Wilkins Health.

[186] Kenttä, T. V. et al. (2018). Repolarization Heterogeneity Measured With T-Wave Area Dispersion in Standard 12-Lead ECG Predicts Sudden Cardiac Death in General Population. *Circulation: Arrhythmia and Electrophysiology*, 11(2):e005762.

[187] Khine, H. W., Steding-Ehrenborg, K., Hastings, J. L., Kowal, J., Daniels, J. D., Page, R. L., Goldberger, J. J., Ng, J., Adams-Huet, B., Bungo, M. W., and Levine, B. D. (2018). Effects of prolonged spaceflight on atrial size, atrial electrophysiology, and risk of atrial fibrillation. *Circulation: Arrhythmia and Electrophysiology*, 11(5):e005959.

[188] Khurshid, S., Choi, S. H., Weng, L.-C., Wang, E. Y., Trinquart, L., Benjamin, E. J., Ellinor, P. T., and Lubitz, S. A. (2018). Frequency of cardiac rhythm abnormalities in a half million adults. *Circulation: Arrhythmia and Electrophysiology*, 11(7):e006273.

[189] Kim, H.-N. and Januzzi, J. L. (2011). Natriuretic peptide testing in heart failure. *Circulation*, 123(18):2015–2019.

[190] King, M., Kingery, J., and Casey, B. (2012). Diagnosis and evaluation of heart failure. *Am. Fam. Physician*, 85(12):1161–1168.

[191] Kishi, T. (2012). Heart failure as an autonomic nervous system dysfunction. *Journal of Cardiology*, 59(2):117 – 122.

[192] Kobayashi, M., Watanabe, M., Coiro, S., Bercker, M., Paku, Y., Iwasaki, Y., Chikamori, T., Yamashina, A., Duarte, K., Ferreira, J. P., Rossignol, P., Zannad, F., and Girerd, N. (2019). Mid-term prognostic impact of residual pulmonary congestion assessed by radiographic scoring in patients admitted for worsening heart failure. *International Journal of Cardiology*, 289:91–98.

[193] Koh, A. S., Tay, W. T., Teng, T. H. K., Vedin, O., Benson, L., Dahlstrom, U., Savarese, G., Lam, C. S., and Lund, L. H. (2017). A comprehensive population-based characterization of heart failure with mid-range ejection fraction. *European Journal of Heart Failure*, 19(12):1624–1634.

[194] Komajda, M., Böhm, M., Borer, J. S., Ford, I., Tavazzi, L., Pannaux, M., and Swedberg, K. (2018). Incremental benefit of drug therapies for chronic heart failure with reduced ejection fraction: a network meta-analysis. *European Journal of Heart Failure*, 20(9):1315–1322.

[195] Konda, N. N., Karri, R. S., Winnard, A., Nasser, M., Evetts, S., Boudreau, E., Caplan, N., Gradwell, D., and Velho, R. M. (2019). A comparison of exercise interventions from bed rest studies for the prevention of musculoskeletal loss. *npj Microgravity*, 5(1):12.

[196] Kors, J. A., Van Herpen, G., Sittig, A. C., and Van Bemmel, J. H. (1990). Reconstruction of the Frank vectorcardiogram from standard electrocardiographic leads: diagnostic comparison of different methods. *European Heart Journal*, 11(12):1083–1092.

[197] Kors, J. A., van Herpen, G., and van Bemmel, J. H. (1999). QT Dispersion as an Attribute of T-Loop Morphology. *Circulation*, 99(11):1458–1463.

[198] Kramer, A., Kümmel, J., Mulder, E., Gollhofer, A., Frings-Meuthen, P., and Gruber, M. (2017). High-intensity jump training is tolerated during 60 days of bed rest and is very effective in preserving leg power and lean body mass: An overview of the Cologne RSL Study. *PLOS ONE*, 12(1):1–18.

[199] Kramer, A., Poppendieker, T., and Gruber, M. (2019). Suitability of jumps as a form of high-intensity interval training: effect of rest duration on oxygen uptake, heart rate and blood lactate. *European Journal of Applied Physiology*, 119(5):1149–1156.

[200] Krandycheva, V., Kharin, S., Strelkova, M., Shumikhin, K., Sobolev, A., and Shmakov, D. (2013). Ventricular repolarization in a rat model of global heart failure. *Clinical and Experimental Pharmacology and Physiology*, 40(7):431–437.

[201] Krittanawong, C., Isath, A., Kaplin, S., Virk, H. U. H., Fogg, S., Wang, Z., Shepanek, M., Scheuring, R. A., and Lavie, C. J. (2023). Cardiovascular disease in space: A systematic review. *Progress in Cardiovascular Diseases*, 81:33–41.

[202] Kunz, H., Quiriarte, H., Simpson, R. J., Ploutz-Snyder, R., McMonigal, K., Sams, C., and Crucian, B. (2017). Alterations in hematologic indices during long-duration spaceflight. *BMC Hematol.*, 17:12.

[203] Kusumoto, F. M., Schoenfeld, M. H., Barrett, C., Edgerton, J. R., Ellenbogen, K. A., Gold, M. R., Goldschlager, N. F., Hamilton, R. M., Joglar, J. A., Kim, R. J., Lee, R., Marine, J. E., McLeod, C. J., Oken, K. R., Patton, K. K., Pellegrini, C. N., Selzman, K. A., Thompson, A., and Varosy, P. D. (2019). 2018 ACC/AHA/HRS Guideline on the Evaluation and Management of Patients With Bradycardia and Cardiac Conduction Delay: Executive Summary: A Report of the American College of Cardiology/American Heart Association Task Force on Clinical Practice Guidelines, and the Heart Rhythm Society. *Circulation*, 140(8):e333–e381.

[204] Ky, B., French, B., Levy, W. C., Sweitzer, N. K., Fang, J. C., Wu, A. H., Goldberg, L. R., Jessup, M., and Cappola, T. P. (2012). Multiple biomarkers for risk prediction in chronic heart failure. *Circulation: Heart Failure*, 5(2):183–190.

[205] Laguna, P., Martínez Cortés, J. P., and Pueyo, E. (2016). Techniques for ventricular repolarization instability assessment from the ECG. *Proceedings of the IEEE*, 104(2):392–415.

[206] Lang, R. M., Badano, L. P., Mor-Avi, V., Afilalo, J., Armstrong, A., Ernande, L., Flachskampf, F. A., Foster, E., Goldstein, S. A., Kuznetsova, T., Lancellotti, P., Muraru, D., Picard, M. H., Rietzschel, E. R., Rudski, L., Spencer, K. T., Tsang, W., and Voigt, J.-U. (2015). Recommendations for cardiac chamber quantification by echocardiography in adults: An update from the american society of echocardiography and the european association of cardiovascular imaging. *Journal of the American Society of Echocardiography*, 28(1):1–39.e14.

[207] Lawson, C. A., Zaccardi, F., Squire, I., Ling, S., Davies, M. J., Lam, C. S. P., Mamas, M. A., Khunti, K., and Kadam, U. T. (2019). 20-year trends in cause-specific heart failure outcomes by sex, socioeconomic status, and place of diagnosis: a population-based study. *The Lancet Public Health*, 4(8):e406–e420.

[208] Lee, D. S. and Vasan, R. S. (2005). Novel markers for heart failure diagnosis and prognosis. *Current opinion in cardiology*, 20(3):201–210.

[209] Lellouche, N., De Diego, C., Boyle, N. G., Wiener, I., Akopyan, G., Child, J. S., and Shivkumar, K. (2011). Relationship between mechanical and electrical remodelling in patients with cardiac resynchronization implanted defibrillators. *EP Europace*, 13(8):1180–1187.

[210] Levy, W. C., Li, Y., Reed, S. D., Zile, M. R., Shadman, R., Dardas, T., Whellan, D. J., Schulman, K. A., Ellis, S. J., Neilson, M., and O'Connor, C. M. (2017). Does the implantable cardioverter-defibrillator benefit vary with the estimated proportional risk of sudden death in heart failure patients? *JACC: Clinical Electrophysiology*, 3(3):291 – 298.

[211] Levy, W. C., Mozaffarian, D., Linker, D. T., Sutradhar, S. C., Anker, S. D., Cropp, A. B., Anand, I., Maggioni, A., Burton, P., Sullivan, M. D., Pitt, B., Poole-Wilson, P. A., Mann, D. L., and Packer, M. (2006). The Seattle Heart Failure Model. *Circulation*, 113(11):1424–1433.

[212] Li, J., Jiang, H., Zhang, Y., Cui, J., Li, M., Zhou, H., and Li, X. (2022a). A Study to Analyze the Feasibility and Effectiveness of Left Bundle Branch Area Pacing Used in Young Children. *Pediatric Cardiology*. [Online; accessed 12. Jul. 2022].

[213] Li, Y., Cao, G.-y., Jing, W.-z., Liu, J., and Liu, M. (2022b). Global trends and regional differences in incidence and mortality of cardiovascular disease, 1990–2019: findings from 2019 global burden of disease study. *European Journal of Preventive Cardiology*, 30(3):276–286.

[214] Liao, D., Nedergaard, R. B., Unnisa, M., Mahapatra, S. J., Faghih, M., Phillips, A. E., Yadav, D., Singh, V. K., Olesen, S. S., Talukdar, R., Garg, P. K., Niazi, I. K., Brock, C., and Drewes, A. M. (2023). Electrocardiography Assessment of Sympatico–Vagal Balance during Resting and Pain using the Texas Instruments ADS1299. *Bioengineering*, 10(2):205.

[215] Lien, W.-P., Chen, J.-J., Wu, T.-L., and Chang, F.-Z. (1980). Automaticity of subsidiary pacemakers of patients with dysfunction of the sinus node. *Chest*, 78(5):747–752.

[216] Lin, G., Nishimura, R. A., Connolly, H. M., Dearani, J. A., Sundt, T. M., and Hayes, D. L. (2005). Severe symptomatic tricuspid valve regurgitation due to permanent pacemaker or implantable cardioverter-defibrillator leads. *Journal of the American College of Cardiology*, 45(10):1672–1675.

[217] Lin, J., Hu, Q., Chen, K., Dai, Y., Chen, R., Sun, Q., Zhou, Y., Yan, L., Lu, W., Li, Y., Jin, Y., Chen, F., Gold, M. R., and Zhang, S. (2021). Relationship of paced left bundle branch pacing morphology with anatomic location and physiological outcomes. *Heart Rhythm*, 18(6):946–953.

[218] Lippi, G. and Sanchis-Gomar, F. (2020). Global epidemiology and future trends of heart failure. *AME Medical Journal*, 5(0).

[219] Liu, X., Li, W., Wang, L., Tian, S., Zhou, X., and Wu, M. (2021). Safety and efficacy of left bundle branch pacing in comparison with conventional right ventricular pacing: A systematic review and meta-analysis. *Medicine*, 100(27):e26560.

[220] Liu, Y., Cao, X., Zhou, Q., Deng, C., Yang, Y., Huang, D., Luo, H., Zhang, S., Li, Y., Xu, J., and Chen, H. (2024). Mechanisms and Countermeasures for Muscle Atrophy in Microgravity. *Cells*, 13(24):2120.

[221] Lown, B. and Verrier, R. L. (1976). Neural activity and ventricular fibrillation. *New England Journal of Medicine*, 294(21):1165–1170. PMID: 57572.

[222] Luengo-Fernandez, R., Walli-Attaei, M., Gray, A., Torbica, A., Maggioni, A. P., Huculeci, R., Bairami, F., Aboyans, V., Timmis, A. D., Vardas, P., and Leal, J. (2023). Economic burden of cardiovascular diseases in the European Union: a population-based cost study. *European Heart Journal*, page ehad583.

[223] Luo, C. H. and Rudy, Y. (1991). A model of the ventricular cardiac action potential. depolarization, repolarization, and their interaction. *Circulation Research*, 68(6):1501–1526.

[224] Lupón, J., de Antonio, M., Galán, A., Vila, J., Zamora, E., Urrutia, A., and Bayes-Genis, A. (2013). Combined Use of the Novel Biomarkers High-Sensitivity Troponin T and ST2 for Heart Failure Risk Stratification vs Conventional Assessment. *Mayo Clinic Proceedings*, 88(3):234 – 243.

[225] Maass, A. H., Vernooy, K., Wijers, S. C., van 't Sant, J., Cramer, M. J., Meine, M., Allaart, C. P., De Lange, F. J., Prinzen, F. W., Gerritse, B., Erdtsieck, E., Scheerder, C. O. S., Hill, M. R. S., Scholten, M., Kloosterman, M., ter Horst, I. A. H., Voors, A. A., Vos, M. A., Rienstra, M., and

Van Gelder, I. C. (2018). Refining success of cardiac resynchronization therapy using a simple score predicting the amount of reverse ventricular remodelling: results from the Markers and Response to CRT (MARC) study. *Europace*, 20(2):e1–e10.

[226] Macaulay, T. R., Macias, B. R., Lee, S. M. C., Boda, W. L., Watenpaugh, D. E., and Hargens, A. R. (2016). Treadmill exercise within lower-body negative pressure attenuates simulated spaceflight-induced reductions of balance abilities in men but not women. *npj Microgravity*, 2(16022):1–8.

[227] MacDonald, M. R. et al. (2020). Regional Variation of Mortality in Heart Failure With Reduced and Preserved Ejection Fraction Across Asia: Outcomes in the ASIAN-HF Registry. *Journal of the American Heart Association*, 9(1):e012199.

[228] Mafi Rad, M., Wijntjens, G. W., Engels, E. B., Blaauw, Y., Luermans, J. G., Pison, L., Crijns, H. J., Prinzen, F. W., and Vernooy, K. (2016). Vectorcardiographic QRS area identifies delayed left ventricular lateral wall activation determined by electroanatomic mapping in candidates for cardiac resynchronization therapy. *Heart Rhythm*, 13(1):217–225.

[229] Maggioni, M. A., Castiglioni, P., Merati, G., Brauns, K., Gunga, H.-C., Mendt, S., Opatz, O. S., Rundfeldt, L. C., Steinach, M., Werner, A., and Stahn, A. C. (2018). High-intensity exercise mitigates cardiovascular deconditioning during long-duration bed rest. *Frontiers in Physiology*, 9:1553.

[230] Maisel, A. et al. (2010). Mid-Region Pro-Hormone Markers for Diagnosis and Prognosis in Acute Dyspnea: Results From the BACH (Biomarkers in Acute Heart Failure) Trial. *Journal of the American College of Cardiology*, 55(19):2062–2076.

[231] Małecka, B., Ząbek, A., and Lelakowski, J. (2010). Shortening of paced QRS complex and clinical improvement following upgrading from apical right ventricular pacing to bifocal right ventricular or biventricular pacing in patients with permanent atrial fibrillation. *Kardiologia Polska*, 68(11):1234–1241.

[232] Malik, M., Acar, B., Gang, Y., Yap, Y. G., Hnatkova, K., and Camm, A. J. (2000). QT Dispersion Does Not Represent Electrocardiographic Interlead Heterogeneity of Ventricular Repolarization. *Journal of Cardiovascular Electrophysiology*, 11(8):835–843.

[233] Malik, M., Bigger, J. T., Camm, A. J., Kleiger, R. E., Malliani, A., Moss, A. J., and Schwartz, P. J. (1996). Heart rate variability: Standards of measurement, physiological interpretation, and clinical use. *European Heart Journal*, 17(3):354–381.

[234] Malliani, A., Schwartz, P., and Zanchetti, A. (1969). A sympathetic reflex elicited by experimental coronary occlusion. *American Journal of Physiology-Legacy Content*, 217(3):703–709. PMID: 5807693.

[235] Man, S., Algra, A. M., Schreurs, C. A., Borleffs, C. J. W., Scherptong, R. W., van Erven, L., van der Wall, E. E., Cannegieter, S. C., Schalij, M. J., and Swenne, C. A. (2011). Influence of the vectorcardiogram synthesis matrix on the power of the electrocardiogram-derived spatial qrs-t angle to predict arrhythmias in patients with ischemic heart disease and systolic left ventricular dysfunction. *Journal of Electrocardiology*, 44(4):410–415.

[236] Mant, J., Doust, J., Roalfe, A., Barton, P., Cowie, M. R., Glasziou, P., Mant, D., McManus, R. J., Holder, R., Deeks, J., Fletcher, K., Qume, M., Sohanpal, S., Sanders, S., and Hobbs, F. (2009). Systematic review and individual patient data meta-analysis of diagnosis of heart failure, with modelling of implications of different diagnostic strategies in primary care. *Health Technol. Assess.*, 13(32):1–232.

[237] Mao, Y., Yang, Y., Garweg, C., Sheng, X., Zhang, J., Yang, Y., Wang, M., Yang, Y., Duchenne, J., Voros, G., Sun, Y., Ma, M., Fu, G., and Voigt, J. (2022). Left bundle branch pacing preserves ventricular mechanical synchrony better than right ventricular pacing-a two-center study. *EP Europace*, 24(Supplement_1). euac053.405.

[238] Marcassa, C., Campini, R., Verna, E., Ceriani, L., and Giannuzzi, P. (2007). Assessment of cardiac asynchrony by radionuclide phase analysis: Correlation with ventricular function in patients with narrow or prolonged QRS interval. *European Journal of Heart Failure*, 9(5):484–490.

[239] Marinko, S., Platonov, P. G., Carlson, J., and Borgquist, R. (2022). Baseline QRS Area and Reduction in QRS Area Are Associated with Lower Mortality and Risk of Heart Failure Hospitalization after Cardiac Resynchronization Therapy. *Cardiology*, 147(3):298.

[240] Martín-Yebra, A., Martínez, J. P., and Laguna, P. (2025). Music (sudden cardiac death in chronic heart failure) (version 1.0.1). *PhysioNet*.

[241] Martín-Yebra, A., Monasterio, V., Landreani, F., Laguna, P., Martínez, J. P., and Caiani, E. G. (2019). Assessment of ventricular repolarization instability in terms of T-wave alternans induced by head-down bed-rest immobilization. *Physiological Measurement*, 40(10):104001.

[242] Martinez, J. P., Almeida, R., Olmos, S., Rocha, A. P., and Laguna, P. (2004). A wavelet-based ECG delineator: evaluation on standard databases. *IEEE Transactions on Biomedical Engineering*, 51(4):570–581.

[243] Marvin, H. M. (1964). Diseases of the Heart and Blood Vessels: Nomenclature and Criteria for Diagnosis. *Archives of Internal Medicine*, 113(6):906–907.

[244] Masarone, D., Limongelli, G., Ammendola, E., Verrengia, M., Gravino, R., and Pacileo, G. (2018). Risk Stratification of Sudden Cardiac Death in Patients with Heart Failure: An update. *Journal of Clinical Medicine*, 7(11):436.

[245] Mastoi, Q.-u.-a., Wah, T. Y., Mohammed, M. A., Iqbal, U., Kadry, S., Majumdar, A., and Thinnukool, O. (2022). Novel DERMA Fusion Technique for ECG Heartbeat Classification. *Life*, 12(6).

[246] Mateo, J. and Laguna, P. (2003). Analysis of heart rate variability in the presence of ectopic beats using the heart timing signal. *IEEE Transactions on Biomedical Engineering*, 50(3):334–343.

[247] McDonagh, T. A. et al. (2021). 2021 ESC Guidelines for the diagnosis and treatment of acute and chronic heart failure: Developed by the Task Force for the diagnosis and treatment of acute and chronic heart failure of the European Society of Cardiology (ESC) With the special contribution of the Heart Failure Association (HFA) of the ESC. *European Heart Journal*, 42(36):3599–3726.

[248] McMurray, J. J. et al. (2019). Dapagliflozin in patients with heart failure and reduced ejection fraction. *New England Journal of Medicine*, 381(21):1995–2008. PMID: 31535829.

[249] McMurray, J. J., Packer, M., Desai, A. S., Gong, J., Lefkowitz, M. P., Rizkala, A. R., Rouleau, J. L., Shi, V. C., Solomon, S. D., Swedberg, K., and Zile, M. R. (2014). Angiotensin–neprilysin inhibition versus enalapril in heart failure. *New England Journal of Medicine*, 371(11):993–1004. PMID: 25176015.

[250] McRae, G., Payne, A., Zelt, J. G., Scribbans, T. D., Jung, M. E., Little, J. P., and Gurd, B. J. (2012). Extremely low volume, whole-body aerobic–resistance training improves aerobic fitness and muscular endurance in females. *Applied Physiology, Nutrition, and Metabolism*, 37(6):1124–1131.

[251] Meck, J. V., Reyes, C. J., Perez, S. A., Goldberger, A. L., and Ziegler, M. G. (2001). Marked exacerbation of orthostatic intolerance after long- vs. short-duration spaceflight in veteran astronauts. *Psychosomatic Medicine*, 63(6):865–873.

[252] Mehta, N. A., Saqi, B., Sabzwari, S. R. A., Gupta, R., Vyas, A., Gordon, J., Cossu, S., Nazir, T., Freudenberger, R., and Bozorgnia, B. (2022). Durability of left bundle branch area pacing. *Journal of Cardiovascular Electrophysiology*, 33(7):1529–1536.

[253] Meijler, F. L. and Janse, M. J. (1988). Morphology and electrophysiology of the mammalian atrioventricular node. *Physiological Reviews*, 68(2):608–647. PMID: 2451833.

[254] Melenovsky, V., Andersen, M. J., Andress, K., Reddy, Y. N., and Borlaug, B. A. (2015). Lung congestion in chronic heart failure: haemodynamic, clinical, and prognostic implications. *European Journal of Heart Failure*, 17(11):1161–1171.

[255] Migeotte, P.-F., Prisk, G. K., and Paiva, M. (2003). Microgravity alters respiratory sinus arrhythmia and short-term heart rate variability in humans. *American Journal of Physiology-Heart and Circulatory Physiology*, 284(6):H1995–H2006.

[256] Milagro, J., Hernández-Vicente, A., Hernando, D., Casajús, J. A., Garatachea, N., Bailón, R., and Pueyo, E. (2021). Estimation of the second ventilatory threshold through ventricular repolarization profile analysis. *Scandinavian Journal of Medicine & Science in Sports*, 31(2):339–349.

[257] Milne, J. R., Ward, D. E., Spurrell, R. A. J., and Camm, A. J. (1982). The Ventricular Paced QT Interval—The Effects of Rate and Exercise. *Pacing and Clinical Electrophysiology*, 5(3):352–358.

[258] Mincholé, A., Pueyo, E., Rodríguez, J. F., Zacur, E., Doblaré, M., and Laguna, P. (2011). Quantification of restitution dispersion from the dynamic changes of the T-wave peak to end, measured at the surface ECG. *IEEE Transactions on Biomedical Engineering*, 58(5):1172–1182.

[259] Miró, Ò., Aguiló, O., Trullàs, J. C., Gil, V., Espinosa, B., Jacob, J., Herrero-Puente, P., Tost, J., López-Grima, M. L., Comas, P., et al. (2023). QT interval and short-term outcome in acute heart failure. *Clinical Research in Cardiology*, 112(12):1754–1765.

[260] Mizner, J., Jurak, P., Linkova, H., Smisek, R., and Curila, K. (2022). Ventricular dyssynchrony and pacing-induced cardiomyopathy in patients with pacemakers, the utility of ultra-high-frequency ECG and other dyssynchrony assessment tools. *Arrhythmia & Electrophysiology Review*, 11.

[261] Moini, J. (2013). *Phlebotomy: Principles and Practice*. Jones & Bartlett Learning.

[262] Moliner, P., Lupón, J., de Antonio, M., Domingo, M., Santiago-Vacas, E., Zamora, E., Cediel, G., Santesmases, J., Díez-Quevedo, C., Troya, M. I., Boldó, M., Altmir, S., Alonso, N., González, B., Núñez, J., and Bayes-Genis, A. (2019). Trends in modes of death in heart failure over the last two decades: less sudden death but cancer deaths on the rise. *European Journal of Heart Failure*, 21(10):1259–1266.

[263] Monasterio, V., Laguna, P., Cygankiewicz, I., Vázquez, R., Bayés-Genís, A., Bayés de Luna, A., and Martínez, J. P. (2012). Average T-wave alternans activity in ambulatory ECG records predicts sudden cardiac death in patients with chronic heart failure. *Heart Rhythm*, 9(3):383 – 389.

[264] Monitillo, F., Leone, M., Rizzo, C., Passantino, A., and Iacoviello, M. (2016). Ventricular repolarization measures for arrhythmic risk stratification. *World Journal of Cardiology*, 8(1):57–73.

[265] Moody, G. B. and Mark, R. G. (1982). Development and evaluation of a 2-lead ECG analysis program. *Computers in cardiology*, 9:39–44.

[266] Mozaffarian, D., Anker, S. D., Anand, I., Linker, D. T., Sullivan, M. D., Cleland, J. G., Carson, P. E., Maggioni, A. P., Mann, D. L., Pitt, B., Poole-Wilson, P. A., and Levy, W. C. (2007). Prediction of mode of death in heart failure. *Circulation*, 116(4):392–398.

[267] Mulrow, C. D., Lucey, C. R., and Farnett, L. E. (1993). Discriminating causes of dyspnea through clinical examination. *J. Gen. Intern. Med.*, 8(7):383–392.

[268] Mulvagh, S. L., Charles, J. B., Riddle, J. M., Rehbein, T. L., and Bungo, M. W. (1991). Echocardiographic evaluation of the cardiovascular effects of short-duration spaceflight. *The Journal of Clinical Pharmacology*, 31(10):1024–1026.

[269] Murthy, G., Watenpaugh, D. E., Ballard, R. E., and Hargens, A. R. (1994). Supine exercise during lower body negative pressure effectively simulates upright exercise in normal gravity. *Journal of Applied Physiology*, 76(6):2742–2748. PMID: 7928909.

[270] Nadar, S. K. and Shaikh, M. M. (2019). Biomarkers in Routine Heart Failure Clinical Care. *Cardiac Failure Review*, 5(1):50.

[271] Nag, A. C. (1980). Study of non-muscle cells of the adult mammalian heart: a fine structural analysis and distribution. *Cytobios*, 28(109):41–61.

[272] Naqvi, T. Z. and Chao, C.-J. (2023). Adverse effects of right ventricular pacing on cardiac function: prevalence, prevention and treatment with physiologic pacing. *Trends in Cardiovascular Medicine*, 33(2):109–122.

[273] Navasiolava, N., Yuan, M., Murphy, R., Robin, A., Coupé, M., Wang, L., Alameddine, A., Gauquelin-Koch, G., Gharib, C., Li, Y., and Custaud, M.-A. (2020). Vascular and microvascular dysfunction induced by microgravity and its analogs in humans: Mechanisms and countermeasures. *Frontiers in Physiology*, 11:952.

[274] Nerbonne, J. M. and Kass, R. S. (2005). Molecular physiology of cardiac repolarization. *Physiological Reviews*, 85(4):1205–1253. PMID: 16183911.

[275] Nguyên, U. C., Claridge, S., Vernooy, K., Engels, E. B., Razavi, R., Rinaldi, C. A., Chen, Z., and Prinzen, F. W. (2018a). Relationship between vectorcardiographic qrsarea, myocardial scar quantification, and

response to cardiac resynchronization therapy. *Journal of Electrocardiology*, 51(3):457–463.

[276] Nguyên, U. C., Verzaal, N. J., van Nieuwenhoven, F. A., Vernooy, K., and Prinzen, F. W. (2018b). Pathobiology of cardiac dyssynchrony and resynchronization therapy. *EP Europace*, 20(12):1898–1909.

[277] Nichols, G. A., Reynolds, K., Kimes, T. M., Rosales, A. G., and Chan, W. W. (2015). Comparison of risk of re-hospitalization, all-cause mortality, and medical care resource utilization in patients with heart failure and preserved versus reduced ejection fraction. *The American Journal of Cardiology*, 116(7):1088–1092.

[278] Nicogossian, A., Williams, R., Huntoon, C., Doarn, C., Polk, J., and Schneider, V. (2016). *Space Physiology and Medicine: From Evidence to Practice*. Springer New York.

[279] Nieminen, M. S., Brutsaert, D., Dickstein, K., Drexler, H., Follath, F., Harjola, V.-P., Hochadel, M., Komajda, M., Lassus, J., Lopez-Sendon, J. L., Ponikowski, P., and Tavazzi, Luigi, o. b. o. t. E. S. I. (2006). EuroHeart Failure Survey II (EHFS II): a survey on hospitalized acute heart failure patients: description of population. *European Heart Journal*, 27(22):2725–2736.

[280] Nolan, J., Batin, P. D., Andrews, R., Lindsay, S. J., Brooksby, P., Mullen, M., Baig, W., Flapan, A. D., Cowley, A., Prescott, R. J., Neilson, J. M., and Fox, K. A. (1998). Prospective study of heart rate variability and mortality in chronic heart failure. *Circulation*, 98(15):1510–1516.

[281] Norsk, P. (2014). Blood pressure regulation IV: adaptive responses to weightlessness. *European Journal of Applied Physiology*, 114(3):481–497.

[282] Norsk, P. (2020). Adaptation of the cardiovascular system to weightlessness: Surprises, paradoxes and implications for deep space missions. *Acta Physiologica*, 228(3):e13434.

[283] Norsk, P., Asmar, A., Damgaard, M., and Christensen, N. J. (2015). Fluid shifts, vasodilatation and ambulatory blood pressure reduction during long duration spaceflight. *The Journal of Physiology*, 593(3):573–584.

[284] Norsk, P., Damgaard, M., Petersen, L., Gybel, M., Pump, B., Gabrielsen, A., and Christensen, N. J. (2006). Vasorelaxation in space. *Hypertension*, 47(1):69–73.

[285] O'Connor, M., Shi, R., Kramer, D. B., Riad, O., Hunnybun, D., Jarman, J. W., Foran, J., Cantor, E., Markides, V., and Wong, T. (2023). Conduction system pacing learning curve: Left bundle pacing compared to his bundle pacing. *IJC Heart & Vasculature*, 44:101171.

[286] Ono, N., Yamaguchi, T., Ishikawa, H., Arakawa, M., Takahashi, N., Saikawa, T., and Shimada, T. (2009). Morphological varieties of the Purkinje fiber network in mammalian hearts, as revealed by light and electron microscopy. *Archives of Histology and Cytology*, 72(3):139–149.

[287] Opie, L. H. and Gersh, B. J. (2013). *Drugs for the Heart*. Saunders.

[288] Opthof, T., Coronel, R., and Janse, M. J. (2009). Is there a significant transmural gradient in repolarization time in the intact heart? *Circulation: Arrhythmia and Electrophysiology*, 2(1):89–96.

[289] Orini, M., Pueyo, E., Laguna, P., and Bailón, R. (2018). A time-varying nonparametric methodology for assessing changes in qt variability unrelated to heart rate variability. *IEEE Transactions on Biomedical Engineering*, 65(7):1443–1451.

[290] Ortega, D. F., Barja, L. D., Logarzo, E., Mangani, N., Paolucci, A., and Bonomini, M. P. (2017). Non-selective His bundle pacing with a biphasic waveform: enhancing septal resynchronization. *EP Europace*, 20(5):816–822.

[291] Osipov, A. V., Averin, A. S., Shaykhutdinova, E. R., Dyachenko, I. A., Tsetlin, V. I., and Utkin, Y. N. (2023). Muscarinic and Nicotinic Acetylcholine Receptors in the Regulation of the Cardiovascular System. *Russ. J. Bioorg. Chem.*, 49(1):1–18.

[292] Packer, M. (2019). What causes sudden death in patients with chronic heart failure and a reduced ejection fraction? *European Heart Journal*, 41(18):1757–1763.

[293] Packer, M. et al. (2020). Cardiovascular and renal outcomes with empagliflozin in heart failure. *New England Journal of Medicine*, 383(15):1413–1424. PMID: 32865377.

[294] Padala, S. K. and Ellenbogen, K. A. (2020). Left bundle branch pacing is the best approach to physiological pacing. *Heart Rhythm O2*, 1(1):59–67.

[295] Padala, S. K., Master, V. M., Terricabras, M., Chiocchini, A., Garg, A., Kron, J., Shepard, R., Kalahasty, G., Azizi, Z., Tsang, B., Khaykin, Y., Pantano, A., Koneru, J. N., Ellenbogen, K. A., and Verma, A. (2020). Initial experience, safety, and feasibility of left bundle branch area pacing: A multicenter prospective study. *JACC: Clinical Electrophysiology*, 6(14):1773–1782.

[296] Pagani, M., Lombardi, F., Guzzetti, S., Rimoldi, O., Furlan, R., Pizzinelli, P., Sandrone, G., Malfatto, G., Dell'Orto, S., and Piccaluga, E.

(1986). Power spectral analysis of heart rate and arterial pressure variabilities as a marker of sympatho-vagal interaction in man and conscious dog. *Circulation Research*, 59(2):178–193.

[297] Pagani, M., Malfatto, G., Pierini, S., Casati, R., Masu, A. M., Poli, M., Guzzetti, S., Lombardi, F., Cerutti, S., and Malliani, A. (1988). Spectral analysis of heart rate variability in the assessment of autonomic diabetic neuropathy. *Journal of the Autonomic Nervous System*, 23(2):143 – 153.

[298] Pastore, J. M., Girouard, S. D., Laurita, K. R., Akar, F. G., and Rosenbaum, D. S. (1999). Mechanism Linking T-Wave Alternans to the Genesis of Cardiac Fibrillation. *Circulation*, 99(10):1385–1394.

[299] Patel, M. H., Sampath, S., Kapoor, A., Damani, D. N., Chellapuram, N., Challa, A. B., Kaur, M. P., Walton, R. D., Stavrakis, S., Arunachalam, S. P., and Kulkarni, K. (2021). Advances in cardiac pacing: Arrhythmia prediction, prevention and control strategies. *Frontiers in Physiology*, 12.

[300] Pathak, A., Curnier, D., Fourcade, J., Roncalli, J., Stein, P. K., Hermant, P., Bousquet, M., Massabuau, P., Sénard, J.-M., Montastruc, J.-L., and Galinier, M. (2005). QT dynamicity: a prognostic factor for sudden cardiac death in chronic heart failure. *European Journal of Heart Failure*, 7(2):269–275.

[301] Pavy-Le Traon, A., Heer, M., Narici, M. V., Rittweger, J., and Vernikos, J. (2007). From space to earth: advances in human physiology from 20 years of bed rest studies (1986–2006). *European Journal of Applied Physiology*, 101(2):143–194.

[302] Pellicori, P., Platz, E., Dauw, J., ter Maaten, J. M., Martens, P., Pivetta, E., Cleland, J. G., McMurray, J. J., Mullens, W., Solomon, S. D., Zannad, F., Gargani, L., and Girerd, N. (2021). Ultrasound imaging of congestion in heart failure: examinations beyond the heart. *European Journal of Heart Failure*, 23(5):703–712.

[303] Perhonen, M. A., Franco, F., Lane, L. D., Buckey, J. C., Blomqvist, C. G., Zerwekh, J. E., Peshock, R. M., Weatherall, P. T., and Levine, B. D. (2001). Cardiac atrophy after bed rest and spaceflight. *Journal of Applied Physiology*, 91(2):645–653. PMID: 11457776.

[304] Pestrea, C., Cicala, E., Ivascu, M., Gherghina, A., Ortan, F., and Pop, D. (2023). Comparison of Depolarization and Repolarization Parameters in Left vs. Right Ventricular Septal Pacing—An Intraprocedural Electrocardiographic Study. *Journal of Cardiovascular Development and Disease*, 10(3):108.

[305] Pestrea, C., Rusu, M., Enache, R., Cicala, E., Gavrilescu, R., Vaduva, A., Ortan, F., Iorgulescu, C., and Vatasescu, R. (2024). Feasibility of Conduction System Pacing in Patients with Baseline Bundle Branch Block—A

Single-Center Mid-Term Follow-Up Study. *Journal of Clinical Medicine*, 13(2):454.

[306] Piccirillo, G., Moscucci, F., Bertani, G., Lospinuso, I., Mastropietri, F., Fabietti, M., Sabatino, T., Zaccagnini, G., Crapanzano, D., Di Diego, I., Corrao, A., Rossi, P., and Magrì, D. (2020a). Short-period temporal dispersion repolarization markers predict 30-days mortality in decompensated heart failure. *Journal of Clinical Medicine*, 9(6).

[307] Piccirillo, G., Moscucci, F., Bertani, G., Lospinuso, I., Sabatino, T., Zaccagnini, G., Crapanzano, D., Diego, I. D., Corrao, A., Rossi, P., and Magrì, D. (2021). Short-period temporal repolarization dispersion in subjects with atrial fibrillation and decompensated heart failure. *Pacing and Clinical Electrophysiology*, 44(2):327–333.

[308] Piccirillo, G., Moscucci, F., Mariani, M. V., Di Iorio, C., Fabietti, M., Mastropietri, F., Crapanzano, D., Bertani, G., Sabatino, T., Zaccagnini, G., Lospinuso, I., Rossi, P., and Magrì, D. (2020b). Hospital mortality in decompensated heart failure. a pilot study. *Journal of Electrocardiology*, 61:147–152.

[309] Platt, S. B., Vijgen, J. M., Albrecht, P., Van Hare, G. F., Carlson, M. D., and Rosenbaum, D. S. (1996). Occult T Wave Alternans in Long QT Syndrome. *Journal of Cardiovascular Electrophysiology*, 7(2):144–148.

[310] Platts, S. H., Martin, D. S., Stenger, M. B., Perez, S. A., Ribeiro, L. C., Summers, R., and Meck, J. V. (2009a). Cardiovascular adaptations to long-duration head-down bed rest. *Aviation, Space, and Environmental Medicine*, 80(5):Suppl.

[311] Platts, S. H., Tuxhorn, J. A., Ribeiro, L. C., Stenger, M. B., Lee, S. M. C., and Meck, J. V. (2009b). Compression garments as countermeasures to orthostatic intolerance. *Aviation, Space, and Environmental Medicine*, 80(5):437–442.

[312] Plesinger, F., Jurco, J., Jurak, P., and Halamek, J. (2014). Robust multichannel QRS detection. In *Computing in Cardiology 2014*, pages 557–560.

[313] Plesinger, F., van Stipdonk, A. M., Smisek, R., Halamek, J., Jurak, P., Maass, A. H., Meine, M., Vernooy, K., and Prinzen, F. W. (2020). Fully automated QRS area measurement for predicting response to cardiac resynchronization therapy. *Journal of Electrocardiology*, 63:159–163.

[314] Ploux, S., Eschalier, R., Whinnett, Z. I., Lumens, J., Derval, N., Sacher, F., Hocini, M., Jaïs, P., Dubois, R., Ritter, P., Haïssaguerre, M., Wilkoff, B. L., Francis, D. P., and Bordachar, P. (2015). Electrical dyssynchrony induced by biventricular pacing: Implications for patient selection and therapy improvement. *Heart Rhythm*, 12(4):782–791.

[315] Ponikowski, P. et al. (2016). 2016 ESC Guidelines for the diagnosis and treatment of acute and chronic heart failure: The Task Force for the diagnosis and treatment of acute and chronic heart failure of the European Society of Cardiology (ESC)Developed with the special contribution of the Heart Failure Association (HFA) of the ESC. *European Heart Journal*, 37(27):2129–2200.

[316] Ponnusamy, S. S., Arora, V., Namboodiri, N., Kumar, V., Kapoor, A., and Vijayaraman, P. (2020). Left bundle branch pacing: A comprehensive review. *Journal of Cardiovascular Electrophysiology*, 31(9):2462–2473.

[317] Ponnusamy, S. S. and Vijayaraman, P. (2023). Pacing for atrioventricular block with preserved left ventricular function: On-treatment comparison between his bundle, left bundle branch, and right ventricular pacing. *Indian Pacing and Electrophysiology Journal*, 23(6):196–202.

[318] Porter, B., van Duijvenboden, S., Bishop, M. J., Orini, M., Claridge, S., Gould, J., Sieniewicz, B. J., Sidhu, B., Razavi, R., Rinaldi, C. A., Gill, J. S., and Taggart, P. (2018). Beat-to-beat variability of ventricular action potential duration oscillates at low frequency during sympathetic provocation in humans. *Frontiers in Physiology*, 9:147.

[319] Prenner, S. B., Shah, S. J., Goldberger, J. J., and Sauer, A. J. (2016). Repolarization Heterogeneity: Beyond the QT Interval. *Journal of the American Heart Association*, 5(5):e003607.

[320] Priest, B. T. and McDermott, J. S. (2015). Cardiac ion channels. *Channels*, 9(6):352–359. PMID: 26556552.

[321] Prisk, G. K., Guy, H. J., Elliott, A. R., Deutschman, R. A., and West, J. B. (1993). Pulmonary diffusing capacity, capillary blood volume, and cardiac output during sustained microgravity. *Journal of Applied Physiology*, 75(1):15–26. PMID: 8376261.

[322] Pueyo, E., Malik, M., and Laguna, P. (2008). A dynamic model to characterize beat-to-beat adaptation of repolarization to heart rate changes. *Biomedical Signal Processing and Control*, 3(1):29 – 43.

[323] Pueyo, E., Orini, M., Rodríguez, J. F., and Taggart, P. (2016). Interactive effect of beta-adrenergic stimulation and mechanical stretch on low-frequency oscillations of ventricular action potential duration in humans. *Journal of Molecular and Cellular Cardiology*, 97:93 – 105.

[324] Pueyo, E., Smetana, P., Caminal, P., de Luna, A. B., Malik, M., and Laguna, P. (2004). Characterization of QT interval adaptation to RR interval changes and its use as a risk-stratifier of arrhythmic mortality in amiodarone-treated survivors of acute myocardial infarction. *IEEE Transactions on Biomedical Engineering*, 51(9):1511–1520.

[325] Punske, B. B., Ni, Q., Lux, R. L., MacLeod, R. S., Ershler, P. R., Dustman, T. J., Allison, M. J., and Taccardi, B. (2003). Spatial methods of epicardial activation time determination in normal hearts. *Annals of Biomedical Engineering*, 31(7):781–792.

[326] Pérez, C., Cebollada, R., Mountris, K. A., Martínez, J. P., Laguna, P., and Pueyo, E. (2023a). The role of β-adrenergic stimulation in QT interval adaptation to heart rate during stress test. *PLOS ONE*, 18(1):1–22.

[327] Pérez, C., Pueyo, E., Martínez, J. P., Viik, J., and Laguna, P. (2023b). QT interval time lag in response to heart rate changes during stress test for Coronary Artery Disease diagnosis. *Biomedical Signal Processing and Control*, 86:105056.

[328] Raatikainen, M. P., Arnar, D. O., Zeppenfeld, K., Merino, J. L., Levya, F., Hindriks, G., and Kuck, K.-H. (2015). Statistics on the use of cardiac electronic devices and electrophysiological procedures in the European Society of Cardiology countries: 2014 report from the European Heart Rhythm Association. *EP Europace*, 17(suppl_1):i1–i75.

[329] Rabineau, J., Hossein, A., Landreani, F., Haut, B., Mulder, E., Luchitskaya, E., Tank, J., Caiani, E. G., van de Borne, P., and Migeotte, P.-F. (2020). Cardiovascular adaptation to simulated microgravity and countermeasure efficacy assessed by ballistocardiography and seismocardiography. *Scientific Reports*, 10(17694):1–13.

[330] Ramírez, J., Orini, M., Mincholé, A., Monasterio, V., Cygankiewicz, I., Bayés de Luna, A., Martínez, J. P., Laguna, P., and Pueyo, E. (2017). Sudden cardiac death and pump failure death prediction in chronic heart failure by combining ECG and clinical markers in an integrated risk model. *PLOS ONE*, 12(10):1–15.

[331] Ramírez, J., Orini, M., Mincholé, A., Monasterio, V., Cygankiewicz, I., Bayés de Luna, A., Martínez, J. P., Pueyo, E., and Laguna, P. (2017). T-Wave Morphology Restitution Predicts Sudden Cardiac Death in Patients With Chronic Heart Failure. *Journal of the American Heart Association*, 6(5):e005310.

[332] Ramirez, R. J., Ajijola, O. A., Zhou, W., Holmström, B., Lüning, H., Laks, M. M., Shivkumar, K., and Mahajan, A. (2011). A new electrocardiographic marker for sympathetic nerve stimulation: modulation of repolarization by stimulation of stellate ganglia. *Journal of Electrocardiology*, 44(6):694–699.

[333] Ramos-Maqueda, J., Cabrera-Ramos, M., Melero-Polo, J., Montilla-Padilla, I., Riaño-Ondiviela, A., and Ruiz-Arroyo, J. R. (2024). Left Bundle Branch Area Pacing Compared to Right Ventricular Outflow Tract Septal Pacing: Mid-term Results and Learning Curve. *Journal of Innovations in Cardiac Rhythm Management*, 15(12):6113.

[334] Ramos-Maqueda, J., Melero-Polo, J., Montilla-Padilla, I., Ruiz-Arroyo, J. R., and Cabrera-Ramos, M. (2023). Feasibility and safety of zero-fluoroscopy left bundle branch pacing: An initial experience. *Journal of Cardiovascular Electrophysiology*, 34(2):429–436.

[335] Ramírez, J., Laguna, P., Bayés de Luna, A., Malik, M., and Pueyo, E. (2014). QT/RR and T-peak-to-end/RR curvatures and slopes in chronic heart failure: Relation to sudden cardiac death. *Journal of Electrocardiology*, 47(6):842 – 848.

[336] Raymond-Paquin, A. et al. (2022). Left bundle branch area pacing in patients with atrioventricular conduction disease: A prospective multicenter study. *Heart Rhythm*.

[337] Renwick, J., Kerr, C., McTaggart, R., and Yeung, J. (1993). Cardiac electrophysiology and conduction pathway ablation. *Canadian Journal of Anesthesia*, 40(11):1053–1064.

[338] Richards, A. M. (2010). New biomarkers in heart failure: applications in diagnosis, prognosis and guidance of therapy. *Revista Española de Cardiología*, 63(6):635–639.

[339] Rinaldi, C. A., Burri, H., Thibault, B., Curnis, A., Rao, A., Gras, D., Sperzel, J., Singh, J. P., Biffi, M., Bordachar, P., and Leclercq, C. (2014). A review of multisite pacing to achieve cardiac resynchronization therapy. *EP Europace*, 17(1):7–17.

[340] Rizas, K. D., Doller, A. J., Hamm, W., Vdovin, N., von Stuelpnagel, L., Zuern, C. S., and Bauer, A. (2019). Periodic repolarization dynamics as a risk predictor after myocardial infarction: Prospective validation study. *Heart Rhythm*.

[341] Rizas, K. D., Hamm, W., Kääb, S., Schmidt, G., and Bauer, A. (2016). Periodic repolarisation dynamics: a natural probe of the ventricular response to sympathetic activation. *Arrhythmia & Electrophysiology Review*, 5(1):31–36.

[342] Rizas, K. D., McNitt, S., Hamm, W., Massberg, S., Kääb, S., Zareba, W., Couderc, J.-P., and Bauer, A. (2017). Prediction of sudden and non-sudden cardiac death in post-infarction patients with reduced left ventricular ejection fraction by periodic repolarization dynamics: MADIT-II substudy. *European Heart Journal*, 38(27):2110–2118.

[343] Rizas, K. D., Nieminen, T., Barthel, P., Zürn, C. S., Kähönen, M., Viik, J., Lehtimäki, T., Nikus, K., Eick, C., Greiner, T. O., Wendel, H. P., Seizer, P., Schreieck, J., Gawaz, M., Schmidt, G., and Bauer, A. (2014). Sympathetic activity–associated periodic repolarization dynamics predict mortality following myocardial infarction. *The Journal of Clinical Investigation*, 124(4):1770–1780.

[344] Roberts, W., Salandy, S., Mandal, G., Holda, M., Tomaszewksi, K., Gielecki, J., Tubbs, R. S., and Loukas, M. (2019). Across the centuries: Piecing together the anatomy of the heart. *Translational Research in Anatomy*, 17:100051.

[345] Roberts-Thomson, K. C., Lau, D. H., and Sanders, P. (2011). The diagnosis and management of ventricular arrhythmias. *Nature Reviews Cardiology*, 8(6):311–321.

[346] Rosenbaum, M. B., Blanco, H. H., Elizari, M. V., Lázzari, J. O., and Davidenko, J. M. (1982). Electrotonic modulation of the T wave and cardiac memory. *The American Journal of Cardiology*, 50(2):213–222.

[347] Rothenbühler, M., O'Sullivan, C. J., Stortecky, S., Stefanini, G. G., Spitzer, E., Estill, J., Shrestha, N. R., Keiser, O., Jüni, P., and Pilgrim, T. (2014). Active surveillance for rheumatic heart disease in endemic regions: a systematic review and meta-analysis of prevalence among children and adolescents. *The Lancet Global Health*, 2(12):e717–e726.

[348] Rubart, M. and Zipes, D. P. (2005). Mechanisms of sudden cardiac death. *The Journal of Clinical Investigation*, 115(9):2305–2315.

[349] Russomano, T. and Rehnberg, L. (2018). *Into Space: A Journey of How Humans Adapt and Live in Microgravity*. IntechOpen.

[350] Sakatani, T., Sakamoto, A., Kawamura, K., Tanigaki, T., Tsubakimoto, Y., Isodono, K., Kimura, S., Matsuo, A., Inoue, K., Kitamura, M., and Fujita, H. (2015). Clinical outcome after permanent pacemaker implantation in patients with a high percentage of ventricular pacing. *International Heart Journal*, 56(6):622–625.

[351] Sakowski, C., Starc, V., Smith, S. M., and Schlegel, T. T. (2011). Sedentary long-duration head-down bed rest and ECG repolarization heterogeneity. *Aviation, Space, and Environmental Medicine*, 82(4):416–423.

[352] Sampedro-Puente, D. A., Fernandez-Bes, J., Porter, B., van Duijvenboden, S., Taggart, P., and Pueyo, E. (2019). Mechanisms underlying interactions between low-frequency oscillations and beat-to-beat variability of celullar ventricular repolarization in response to sympathetic stimulation: Implications for arrhythmogenesis. *Frontiers in Physiology*, 10:916.

[353] Sampedro-Puente, D. A., Fernandez-Bes, J., Szentandrássy, N., Nánási, P., Taggart, P., and Pueyo, E. (2020a). Time course of low-frequency oscillatory behavior in human ventricular repolarization following enhanced sympathetic activity and relation to arrhythmogenesis. *Frontiers in Physiology*, 10:1547.

[354] Sampedro-Puente, D. A., Fernandez-Bes, J., Virág, L., Varró, A., and Pueyo, E. (2020b). Data-driven identification of stochastic model parameters and state variables: Application to the study of cardiac beat-to-beat variability. *IEEE Journal of Biomedical and Health Informatics*, 24(3):693–704.

[355] Sampedro-Puente, D. A., Raphel, F., Fernandez-Bes, J., Laguna, P., Lombardi, D., and Pueyo, E. (2021). Characterization of spatio-temporal cardiac action potential variability at baseline and under β-adrenergic stimulation by combined unscented kalman filter and double greedy dimension reduction. *IEEE Journal of Biomedical and Health Informatics*, 25(1):276–288.

[356] Sams, L. E., Wörndl, M., Bachinger, L., Villegas Sierra, L. E., Mourouzis, K., Naumann, D., Freyer, L., and Rizas, K. D. (2024). Periodic repolarization dynamics: Different methods for quantifying low-frequency oscillations of repolarization. *Journal of Electrocardiology*, 82:11–18.

[357] Sanders, G. D., Hlatky, M. A., and Owens, D. K. (2005). Cost-effectiveness of implantable cardioverter–defibrillators. *New England Journal of Medicine*, 353(14):1471–1480. PMID: 16207849.

[358] Savarese, G., Becher, P. M., Lund, L. H., Seferovic, P., Rosano, G. M. C., and Coats, A. J. S. (2022). Global burden of heart failure: a comprehensive and updated review of epidemiology. *Cardiovascular Research*, 118(17):3272–3287.

[359] Savarese, G., Costanzo, P., Cleland, J. G. F., Vassallo, E., Ruggiero, D., Rosano, G., and Perrone-Filardi, P. (2013). A meta-analysis reporting effects of angiotensin-converting enzyme inhibitors and angiotensin receptor blockers in patients without heart failure. *Journal of the American College of Cardiology*, 61(2):131–142.

[360] Savarese, G. and Lund, L. H. (2017). Global public health burden of heart failure. *Cardiac failure review*, 3(1):7–11.

[361] Scacchi, S., Franzone, P. C., Pavarino, L., and Taccardi, B. (2009). A reliability analysis of cardiac repolarization time markers. *Mathematical Biosciences*, 219(2):113–128.

[362] Schaufelberger, M., Schuler, S., Bear, L., Cluitmans, M., Coll-Font, J., Onak, Ö. N., Dössel, O., and Brooks, D. (2019). Comparison of Activation Times Estimation for Potential-Based ECG Imaging. *Computing in cardiology*, 46.

[363] Schmidt, G., Malik, M., Barthel, P., Schneider, R., Ulm, K., Rolnitzky, L., Camm, A. J., Bigger, J. T., and Schömig, A. (1999). Heart-rate turbulence after ventricular premature beats as a predictor of mortality after acute myocardial infarction. *The Lancet*, 353(9162):1390 – 1396.

[364] Schmidt, M., Baumert, M., Penzel, T., Malberg, H., and Zaunseder, S. (2019). Nocturnal ventricular repolarization lability predicts cardiovascular mortality in the Sleep Heart Health Study. *American Journal of Physiology-Heart and Circulatory Physiology*, 316(3):H495–H505. PMID: 30550351.

[365] Schmidt, M., Baumert, M., Porta, A., Malberg, H., and Zaunseder, S. (2014). Two-Dimensional Warping for One-Dimensional Signals—Conceptual Framework and Application to ECG Processing. *IEEE Transactions on Signal Processing*, 62(21):5577–5588.

[366] Schneider, S. M., Lee, S. M. C., Feiveson, A. H., Watenpaugh, D. E., Macias, B. R., and Hargens, A. R. (2016). Treadmill exercise within lower body negative pressure protects leg lean tissue mass and extensor strength and endurance during bed rest. *Physiological Reports*, 4(15):e12892.

[367] Schneider, S. M., Lee, S. M. C., Macias, B. R., Watenpaugh, D. E., and Hargens, A. R. (2009). WISE-2005: exercise and nutrition countermeasures for upright VO2pk during bed rest. *Medicine and Science in Sports and Exercise*, 41(12):2165—2176.

[368] Schurr, J. W., Grewal, P. K., Fan, R., and Rashba, E. (2022). QT interval measurement in ventricular pacing: Implications for assessment of drug effects and pro-arrhythmia risk. *Journal of Electrocardiology*, 70:13–18.

[369] Schüttler, D., Schönermarck, U., Wenner, F., Toepfer, M., Rizas, K. D., Bauer, A., Brunner, S., and Hamm, W. (2021). Large potassium shifts during dialysis enhance cardiac repolarization instability. *J. Nephrol.*, 34(4):1301–1305.

[370] Schüttler, D., Hamm, W., Bauer, A., and Brunner, S. (2020a). Routine heart rate-based and novel ECG-based biomarkers of autonomic nervous system in sports medicine. *Deutsche Zeitschrift Sportmedizin*, 71(6):141 – 150.

[371] Schüttler, D., von Stülpnagel, L., Rizas, K. D., Bauer, A., Brunner, S., and Hamm, W. (2020b). Effect of hyperventilation on periodic repolarization dynamics. *Frontiers in Physiology*, 11:1197.

[372] Seferović, P. M. et al. (2021). The Heart Failure Association Atlas: Heart Failure Epidemiology and Management Statistics 2019. *European Journal of Heart Failure*, 23(6):906–914.

[373] Shah, K., Williamson, B. D., Kutinsky, I., Bhardwaj, R., Contractor, T., Turagam, M. K., Mandapati, R., Lakkireddy, D., and Garg, J. (2022). Conduction system pacing in prosthetic heart valves. *Journal of Interventional Cardiac Electrophysiology*, pages 1–6.

[374] Sharma, P. S., Naperkowski, A., Bauch, T. D., Chan, J. Y., Arnold, A. D., Whinnett, Z. I., Ellenbogen, K. A., and Vijayaraman, P. (2018). Permanent his bundle pacing for cardiac resynchronization therapy in patients with heart failure and right bundle branch block. *Circulation: Arrhythmia and Electrophysiology*, 11(9):e006613.

[375] Sharma, P. S., Patel, N. R., Ravi, V., Zalavadia, D. V., Dommaraju, S., Garg, V., Larsen, T. R., Naperkowski, A. M., Wasserlauf, J., Krishnan, K., Young, W., Pokharel, P., Oren, J. W., Storm, R. H., Trohman, R. G., Huang, H. D., Subzposh, F. A., and Vijayaraman, P. (2022). Clinical outcomes of left bundle branch area pacing compared to right ventricular pacing: Results from the Geisinger-Rush Conduction System Pacing Registry. *Heart Rhythm*, 19(1):3–11.

[376] Shen, L., Jhund, P. S., Petrie, M. C., Claggett, B. L., Barlera, S., Cleland, J. G., Dargie, H. J., Granger, C. B., Kjekshus, J., Køber, L., Latini, R., Maggioni, A. P., Packer, M., Pitt, B., Solomon, S. D., Swedberg, K., Tavazzi, L., Wikstrand, J., Zannad, F., Zile, M. R., and McMurray, J. J. (2017). Declining risk of sudden death in heart failure. *New England Journal of Medicine*, 377(1):41–51. PMID: 28679089.

[377] Shen, M. and Frishman, W. H. (2019). Effects of spaceflight on cardiovascular physiology and health. *Cardiology in review*, 27(3):122–126.

[378] Sheta, A., Turabieh, H., Thaher, T., Too, J., Mafarja, M., Hossain, M. S., and Surani, S. R. (2021). Diagnosis of Obstructive Sleep Apnea from ECG Signals Using Machine Learning and Deep Learning Classifiers. *Applied Sciences*, 11(14):6622.

[379] Shin, S.-H., Hung, C.-L., Uno, H., Hassanein, A. H., Verma, A., Bourgoun, M., Køber, L., Ghali, J. K., Velazquez, E. J., Califf, R. M., Pfeffer, M. A., and Solomon, S. D. (2010). Mechanical dyssynchrony after myocardial infarction in patients with left ventricular dysfunction, heart failure, or both. *Circulation*, 121(9):1096–1103.

[380] Shykoff, B. E., Farhi, L. E., Olszowka, A. J., Pendergast, D. R., Rokitka, M. A., Eisenhardt, C. G., and Morin, R. A. (1996). Cardiovascular response to submaximal exercise in sustained microgravity. *Journal of Applied Physiology*, 81(1):26–32. PMID: 8828644.

[381] Silbernagel, N., Körner, A., Balitzki, J., Jaggy, M., Bertels, S., Richter, B., Hippler, M., Hellwig, A., Hecker, M., Bastmeyer, M., and Ullrich, N. D. (2020). Shaping the heart: Structural and functional maturation of ipsc-cardiomyocytes in 3d-micro-scaffolds. *Biomaterials*, 227:119551.

[382] Sipahi, I., Chou, J. C., Hyden, M., Rowland, D. Y., Simon, D. I., and Fang, J. C. (2012). Effect of QRS morphology on clinical event reduction

with cardiac resynchronization therapy: Meta-analysis of randomized controlled trials. *American Heart Journal*, 163(2):260–267.e3.

[383] Soliman, E. Z., Howard, G., Cushman, M., Kissela, B., Kleindorfer, D., Le, A., Judd, S., McClure, L. A., and Howard, V. J. (2012). Prolongation of QTc and Risk of Stroke: The REGARDS (REasons for Geographic and Racial Differences in Stroke) Study. *Journal of the American College of Cardiology*, 59(16):1460–1467.

[384] Spach, M. S. and Dolber, P. C. (1986). Relating extracellular potentials and their derivatives to anisotropic propagation at a microscopic level in human cardiac muscle. evidence for electrical uncoupling of side-to-side fiber connections with increasing age. *Circulation Research*, 58(3):356–371.

[385] Sprenkeler, D. J., Beekman, J. D. M., Bossu, A., Dunnink, A., and Vos, M. A. (2019). Pro-Arrhythmic Ventricular Remodeling Is Associated With Increased Respiratory and Low-Frequency Oscillations of Monophasic Action Potential Duration in the Chronic Atrioventricular Block Dog Model. *Frontiers in Physiology*, 10:1095.

[386] Straus, S. M., Kors, J. A., De Bruin, M. L., van der Hooft, C. S., Hofman, A., Heeringa, J., Deckers, J. W., Kingma, J. H., Sturkenboom, M. C., Stricker, B. H. C., and Witteman, J. C. (2006). Prolonged QTc Interval and Risk of Sudden Cardiac Death in a Population of Older Adults. *Journal of the American College of Cardiology*, 47(2):362–367.

[387] Struijk, J. J., Kanters, J. K., Andersen, M. P., Hardahl, T., Graff, C., Christiansen, M., and Toft, E. (2006). Classification of the long-QT syndrome based on discriminant analysis of T-wave morphology. *Medical & Biological Engineering & Computing*, 44(7):543–549.

[388] Subramanian, A., Suszko, A., Selvaraj, R. J., Nanthakumar, K., Ivanov, J., and Chauhan, V. S. (2011). Modulated dispersion of activation and repolarization by premature beats in patients with cardiomyopathy at risk of sudden death. *American Journal of Physiology-Heart and Circulatory Physiology*, 300(6):H2221–H2229. PMID: 21441312.

[389] Sun, Z., Di, B., Gao, H., Lan, D., and Peng, H. (2020). Assessment of ventricular mechanical synchronization after left bundle branch pacing using 2-D speckle tracking echocardiography. *Clin. Cardiol.*, 43(12):1562–1572.

[390] Sweeney, M. O., Hellkamp, A. S., Ellenbogen, K. A., Greenspon, A. J., Freedman, R. A., Lee, K. L., and Lamas, G. A. (2003). Adverse effect of ventricular pacing on heart failure and atrial fibrillation among patients with normal baseline QRS duration in a clinical trial of pacemaker therapy for sinus node dysfunction. *Circulation*, 107(23):2932–2937.

[391] Sy, M. R., Keefe, J. A., Sutton, J. P., and Wehrens, X. H. T. (2023). Cardiac function, structural, and electrical remodeling by microgravity exposure. *American Journal of Physiology-Heart and Circulatory Physiology*, 324(1):H1–H13. PMID: 36399385.

[392] Szydlo, K., Trusz-Gluza, M., Wita, K., Filipecki, A., Orszulak, W., Urbanczyk, D., Krauze, J., Kolasa, J., and Tabor, Z. (2008). QT/RR Relationship in Patients after Remote Anterior Myocardial Infarction with Left Ventricular Dysfunction and Different Types of Ventricular Arrhythmias. *Annals of Noninvasive Electrocardiology*, 13(1):61–66.

[393] Tanaka, K., Abe, C., Awazu, C., and Morita, H. (2009). Vestibular system plays a significant role in arterial pressure control during head-up tilt in young subjects. *Autonomic Neuroscience*, 148(1):90–96.

[394] Taylor, C. and Hobbs, R. (2010). Diagnosing Heart Failure: Experience and 'Best Pathways'. *Radcliffe Cardiology*.

[395] Taylor, G. R. (1993). Overview of spaceflight immunology studies. *Journal of Leukocyte Biology*, 54(3):179–188.

[396] Tokavanich, N., Prasitlumkum, N., Mongkonsritragoon, W., Cheungpasitporn, W., Thongprayoon, C., Vallabhajosyula, S., and Chokesuwattanaskul, R. (2021). A network meta-analysis and systematic review of change in QRS duration after left bundle branch pacing, His bundle pacing, biventricular pacing, or right ventricular pacing in patients requiring permanent pacemaker. *Scientific Reports*, 11(12200):1–8.

[397] Tomek, J., Herring, N., and Paterson, D. J. (2023). Chapter 32 - sympathetic control of the heart. In Biaggioni, I., Browning, K., Fink, G., Jordan, J., Low, P. A., and Paton, J. F., editors, *Primer on the Autonomic Nervous System (Fourth Edition)*, pages 185–191. Academic Press, fourth edition edition.

[398] Tops, L. F., Schalij, M. J., and Bax, J. J. (2009). The effects of right ventricular apical pacing on ventricular function and dyssynchrony: Implications for therapy. *Journal of the American College of Cardiology*, 54(9):764–776.

[399] Tournoux, F., Donal, E., Leclercq, C., De Place, C., Crocq, C., Solnon, A., Cohen-Solal, A., Mabo, P., and Daubert, J.-C. (2007). Concordance Between Mechanical and Electrical Dyssynchrony in Heart Failure Patients: A Function of the Underlying Cardiomyopathy? *Journal of Cardiovascular Electrophysiology*, 18(10):1022–1027.

[400] Tribulova, N., Szeiffova Bacova, B., Egan Benova, T., Knezl, V., Barancik, M., and Slezak, J. (2017). Omega-3 index and anti-arrhythmic potential of omega-3 PUFAs. *Nutrients*, 9(11):1191.

[401] Tsao, C. W. et al. (2023). Heart Disease and Stroke Statistics—2023 Update: A Report From the American Heart Association. *Circulation*, 147(8):e93–e621.

[402] Tse, G., Wong, C. W., Gong, M.-Q., Meng, L., Letsas, K. P., Li, G.-P., Whittaker, P., Bhardwaj, A., Sawant, A. C., Wu, W. K., et al. (2017). Meta-analysis of T-wave indices for risk stratification in myocardial infarction. *Journal of geriatric cardiology: JGC*, 14(12):776.

[403] Tse, G. and Yan, B. P. (2016). Traditional and novel electrocardiographic conduction and repolarization markers of sudden cardiac death. *EP Europace*, 19(5):712–721.

[404] Turitto, G. and El-Sherif, N. (2019). *ECG-Derived Evaluation of Cardiac Repolarization*, pages 131–138. Springer International Publishing, Cham, Switzerland.

[405] (UK), N. C. G. C. (2010). *Chronic Heart Failure*. Royal College of Physicians (UK), London, England, UK.

[406] Upadhyay, G. A., Cherian, T., Shatz, D. Y., Beaser, A. D., Aziz, Z., Ozcan, C., Broman, M. T., Nayak, H. M., and Tung, R. (2019). Intracardiac Delineation of Septal Conduction in Left Bundle-Branch Block Patterns. *Circulation*.

[407] Urden, L., Stacy, K., and Lough, M. (2021). *Critical Care Nursing - E-Book: Critical Care Nursing - E-Book*. Elsevier.

[408] Valenzuela, P. L., Ruilope, L. M., Santos-Lozano, A., Wilhelm, M., Kränkel, N., Fiuza-Luces, C., and Lucia, A. (2023). Exercise benefits in cardiovascular diseases: from mechanisms to clinical implementation. *European Heart Journal*, 44(21):1874–1889.

[409] van Stipdonk, A. M., ter Horst, I., Kloosterman, M., Engels, E. B., Rienstra, M., Crijns, H. J., Vos, M. A., van Gelder, I. C., Prinzen, F. W., Meine, M., Maass, A. H., and Vernooy, K. (2018). QRS Area Is a Strong Determinant of Outcome in Cardiac Resynchronization Therapy. *Circulation: Arrhythmia and Electrophysiology*, 11(12):e006497.

[410] Vassallo, J. A., Cassidy, D. M., Kindwall, K. E., Marchlinski, F. E., and Josephson, M. E. (1988). Nonuniform recovery of excitability in the left ventricle. *Circulation*, 78(6):1365–1372.

[411] Vazquez, R., Bayes-Genis, A., Cygankiewicz, I., Pascual-Figal, D., Grigorian-Shamagian, L., Pavon, R., Gonzalez-Juanatey, J. R., Cubero, J. M., Pastor, L., Ordonez-Llanos, J., Cinca, J., de Luna, A. B., and on behalf of the MUSIC Investigators (2009). The MUSIC Risk score: a simple method for predicting mortality in ambulatory patients with chronic heart failure. *European Heart Journal*, 30(9):1088–1096.

[412] Vedin, O., Lam, C. S., Koh, A. S., Benson, L., Teng, T. H. K., Tay, W. T., Braun, O. Ö., Savarese, G., Dahlström, U., and Lund, L. H. (2017). Significance of ischemic heart disease in patients with heart failure and preserved, midrange, and reduced ejection fraction. *Circulation: Heart Failure*, 10(6):e003875.

[413] Vernice, N. A., Meydan, C., Afshinnekoo, E., and Mason, C. E. (2020). Long-term spaceflight and the cardiovascular system. *Precis. Clin. Med.*, 3(4):284.

[414] Verrier, R. L. and Antzelevitch, C. (2004). Autonomic aspects of arrhythmogenesis: the enduring and the new. *Current Opinion in Cardiology*, 19(1):2.

[415] Verrier, R. L., Klingenheben, T., Malik, M., El-Sherif, N., Exner, D. V., Hohnloser, S. H., Ikeda, T., Martínez, J. P., Narayan, S. M., Nieminen, T., and Rosenbaum, D. S. (2011). Microvolt T-wave alternans: Physiological basis, methods of measurement, and clinical utility—consensus guideline by international society for holter and noninvasive electrocardiology. *Journal of the American College of Cardiology*, 58(13):1309 – 1324.

[416] Verrier, R. L. and Malik, M. (2015). Quantitative t-wave alternans analysis for guiding medical therapy: An underexploited opportunity. *Trends in Cardiovascular Medicine*, 25(3):201–213.

[417] Verstappen, A. A., Hautvast, R., Jurak, P., Bracke, F. A., and Rademakers, L. M. (2024). Ventricular dyssynchrony imaging, echocardiographic and clinical outcomes of left bundle branch pacing and biventricular pacing. *Indian Pacing and Electrophysiology Journal*.

[418] Verzaal, N. J., van Deursen, C. J. M., Pezzuto, S., Wecke, L., van Everdingen, W. M., Vernooy, K., Delhaas, T., Auricchio, A., and Prinzen, F. W. (2022). Synchronization of repolarization after cardiac resynchronization therapy: A combined clinical and modeling study. *Journal of Cardiovascular Electrophysiology*, 33(8):1837–1846.

[419] Videbaek, R. and Norsk, P. (1997). Atrial distension in humans during microgravity induced by parabolic flights. *Journal of Applied Physiology*, 83(6):1862–1866. PMID: 9390956.

[420] Vigmond, E. J. and Stuyvers, B. D. (2016). Modeling our understanding of the His-Purkinje system. *Progress in Biophysics and Molecular Biology*, 120(1):179–188. Recent Developments in Biophysics & Molecular Biology of Heart Rhythm.

[421] Viitasalo, M., Oikarinen, L., Swan, H., Väänänen, H., Glatter, K., Laitinen, P. J., Kontula, K., Barron, H. V., Toivonen, L., and Scheinman, M. M. (2002). Ambulatory Electrocardiographic Evidence of Transmural

Dispersion of Repolarization in Patients With Long-QT Syndrome Type 1 and 2. *Circulation*, 106(19):2473–2478.

[422] Vijayaraman, P., Bordachar, P., and Ellenbogen, K. A. (2017). The continued search for physiological pacing: Where are we now? *Journal of the American College of Cardiology*, 69(25):3099–3114.

[423] Vijayaraman, P., Herweg, B., Verma, A., Sharma, P. S., Batul, S. A., Ponnusamy, S. S., Schaller, R. D., Cano, O., Molina-Lerma, M., Curila, K., Huybrechts, W., Wilson, D. R., Rademakers, L. M., Sreekumar, P., Upadhyay, G., Vernooy, K., Subzposh, F. A., Huang, W., Jastrzebski, M., and Ellenbogen, K. A. (2022). Rescue left bundle branch area pacing in coronary venous lead failure or nonresponse to biventricular pacing: Results from International LBBAP Collaborative Study Group. *Heart Rhythm*, 19(8):1272–1280.

[424] Vijayaraman, P., Naperkowski, A., Subzposh, F. A., Abdelrahman, M., Sharma, P. S., Oren, J. W., Dandamudi, G., and Ellenbogen, K. A. (2018). Permanent his-bundle pacing: Long-term lead performance and clinical outcomes. *Heart Rhythm*, 15(5):696–702.

[425] Vijayaraman, P., Subzposh, F. A., Naperkowski, A., Panikkath, R., John, K., Mascarenhas, V., Bauch, T. D., and Huang, W. (2019). Prospective evaluation of feasibility and electrophysiologic and echocardiographic characteristics of left bundle branch area pacing. *Heart Rhythm*, 16(12):1774–1782. Focus Issue: Devices.

[426] Vliegen, H. W., Van Der Laarse, A., Cornelisse, C. J., and Eulderink, F. (1991). Myocardial changes in pressure overload-induced left ventricular hypertrophy: A study on tissue composition, polyploidization and multinucleation. *Eur. Heart J.*, 12(4):488–494.

[427] von Schacky, C. (2012). Omega-3 fatty acids: Anti-arrhythmic, pro-arrhythmic, or both? *Frontiers in Physiology*, 3:88.

[428] Végh, E. M., Engels, E. B., van Deursen, C. J., Merkely, B., Vernooy, K., Singh, J. P., and Prinzen, F. W. (2015). T-wave area as biomarker of clinical response to cardiac resynchronization therapy. *EP Europace*, 18(7):1077–1085.

[429] Wan, X., Li, Y., Xia, C., Wu, M., Liang, J., and Wang, N. (2016). A T-wave alternans assessment method based on least squares curve fitting technique. *Measurement*, 86:93–100.

[430] Wan, X., Yan, K., Zhang, L., and Zeng, Y. (2014). A Time-Domain Hybrid Analysis Method for Detecting and Quantifying T-Wave Alternans. *Comput. Math. Methods Med.*, 2014.

[431] Wang, J., Liang, Y., Wang, W., Chen, X., Bai, J., Chen, H., Su, Y., Chen, R., and Ge, J. (2020). Left bundle branch area pacing is superior to right ventricular septum pacing concerning depolarization-repolarization reserve. *Journal of Cardiovascular Electrophysiology*, 31(1):313–322.

[432] Watenpaugh, D. E. (2016). Analogs of microgravity: head-down tilt and water immersion. *Journal of Applied Physiology*, 120(8):904–914. PMID: 26869710.

[433] Watenpaugh, D. E., Ballard, R. E., Schneider, S. M., Lee, S. M. C., Ertl, A. C., William, J. M., Boda, W. L., Hutchinson, K. J., and Hargens, A. R. (2000). Supine lower body negative pressure exercise during bed rest maintains upright exercise capacity. *Journal of Applied Physiology*, 89(1):218–227. PMID: 10904055.

[434] Watenpaugh, D. E., Buckey, J. C., Lane, L. D., Gaffney, F. A., Levine, B. D., Moore, W. E., Wright, S. J., and Blomqvist, C. G. (2001). Effects of spaceflight on human calf hemodynamics. *Journal of Applied Physiology*, 90(4):1552–1558. PMID: 11247959.

[435] Wecke, L., van Deursen, C. J., Bergfeldt, L., and Prinzen, F. W. (2011). Repolarization changes in patients with heart failure receiving cardiac resynchronization therapy—signs of cardiac memory. *Journal of Electrocardiology*, 44(5):590 – 598.

[436] Weimer, L. H. (2010). Autonomic Testing: Common Techniques and Clinical Applications. *Neurologist*, 16(4):215.

[437] Welten, S. J., Elders, P. J., Remmelzwaal, S., Doekhie, R., Kee, K. W., Nijpels, G., and van der Heijden, A. A. (2023). Prolongation of the heart rate-corrected qt interval is associated with cardiovascular diseases: Systematic review and meta-analysis. *Archives of Cardiovascular Diseases*, 116(2):69–78.

[438] Wenlong, D., Baojing, G., Chencheng, D., and Jianzeng, D. (2022). Preliminary study on left bundle branch area pacing in children: Clinical observation of 12 cases. *Journal of Cardiovascular Electrophysiology*, 33(7):1558–1566.

[439] Wilkoff, B. et al. (2002). Dual-chamber pacing-or ventricular backup pacing in patients with an implantable defibrillator: The Dual Chamber and VVI Implantable Defibrillator (DAVID) Trial. *Journal of the American Medical Association*, 288(24):3115–3123.

[440] Woods, B., Hawkins, N., Mealing, S., Sutton, A., Abraham, W. T., Beshai, J. F., Klein, H., Sculpher, M., Plummer, C. J., and Cowie, M. R. (2015). Individual patient data network meta-analysis of mortality effects of implantable cardiac devices. *Heart*, 101(22):1800–1806.

[441] World Health Organization (2014). *Global status report on noncommunicable diseases 2014*. World Health Organization: Geneva, Switzerland.

[442] Yanagisawa, S., Inden, Y., Watanabe, R., Tsurumi, N., Suzuki, N., Nakagomi, T., Shimojo, M., Okajima, T., Riku, S., Furui, K., Suga, K., Shibata, R., and Murohara, T. (2022). Depolarization and repolarization dynamics after his-bundle pacing: Comparison with right ventricular pacing and native ventricular conduction. *Annals of Noninvasive Electrocardiology*, 27(5):e12991. e12991 ANEC-22-4499.R1.

[443] Yao, L., Qi, Y., Xiao, S., Liu, R., and Wo, J. (2022). Effect of left bundle branch pacing on left ventricular systolic function and synchronization in patients with third-degree atrioventricular block, assessment by 3-dimensional speckle tracking echocardiography. *Journal of Electrocardiology*, 72:61–65.

[444] Yılmaz, Ö. Ç., Ozkan, S., and Yavuz, B. (2021). Masked hypertension is related to alteration of myocardial arrhythmia Parameters. *Clin. Exp. Hypertens.*

[445] Zannad, F. et al. (2013). Clinical outcome endpoints in heart failure trials: a european society of cardiology heart failure association consensus document. *European Journal of Heart Failure*, 15(10):1082–1094.

[446] Zanon, F., Ellenbogen, K. A., Dandamudi, G., Sharma, P. S., Huang, W., Lustgarten, D. L., Tung, R., Tada, H., Koneru, J. N., Bergemann, T., Fagan, D. H., Hudnall, J. H., and Vijayaraman, P. (2018). Permanent His-bundle pacing: a systematic literature review and meta-analysis. *EP Europace*, 20(11):1819–1826.

[447] Zeppenfeld, K. et al. (2022). 2022 ESC Guidelines for the management of patients with ventricular arrhythmias and the prevention of sudden cardiac death: Developed by the task force for the management of patients with ventricular arrhythmias and the prevention of sudden cardiac death of the European Society of Cardiology (ESC) Endorsed by the Association for European Paediatric and Congenital Cardiology (AEPC). *European Heart Journal*, 43(40):3997–4126.

[448] Zhang, H. et al. (2010). Increasing Cardiac Contractility After Myocardial Infarction Exacerbates Cardiac Injury and Pump Dysfunction. *Circulation Research*.

[449] Zhang, J., Guo, J., Hou, X., Wang, Y., Qian, Z., Li, K., Ge, P., and Zou, J. (2017). Comparison of the effects of selective and non-selective His bundle pacing on cardiac electrical and mechanical synchrony. *EP Europace*, 20(6):1010–1017.

[450] Zhang, Q. and Yu, C.-M. (2012). Clinical Implication of Mechanical Dyssynchrony in Heart Failure. *Journal of Cardiovascular Ultrasound*, 20(3):117–123.

[451] Zhang, S. and Shan, Q. (2022). Discussion of LBBP synchronization effects in HF patients with LBBB and comparison with BiV-CRT. *Heart Failure Reviews*, pages 1–6.

[452] Zhang, S., Zhou, X., and Gold, M. R. (2019a). Left Bundle Branch Pacing: JACC Review Topic of the Week. *Journal of the American College of Cardiology*, 74(24):3039–3049.

[453] Zhang, W., Huang, J., Qi, Y., Wang, F., Guo, L., Shi, X., Wu, W., Zhou, X., and Li, R. (2019b). Cardiac resynchronization therapy by left bundle branch area pacing in patients with heart failure and left bundle branch block. *Heart Rhythm*, 16(12):1783–1790. Focus Issue: Devices.

[454] Zhong, C., Jiang, Z., Zhou, X., and Shan, Q. (2020). Reversion of cardiac memory during left bundle branch pacing. *Journal of Electrocardiology*, 59:81–83.

[455] Zhou, Y., Wang, J., Wei, Y., Zhang, W., Yang, Y., Rui, S., and Ju, C. (2022). Left ventricular septal pacing versus left bundle branch pacing in the treatment of atrioventricular block. *Annals of Noninvasive Electrocardiology*, 27(3):e12944.

[456] Ziemssen, T. and Reichmann, H. (2010). Treatment of dysautonomia in extrapyramidal disorders. *Therapeutic Advances in Neurological Disorders*, 3(1):53.

[457] Ziemssen, T. and Siepmann, T. (2019). The Investigation of the Cardiovascular and Sudomotor Autonomic Nervous System—A Review. *Frontiers in Neurology*, 10.

[458] Zipes, D. P. (2015). Contemporary approaches to treating arrhythmias. *Nature Reviews Cardiology*, 12(2):68–69.

[459] Zwart, S. R., Davis-Street, J. E., Paddon-Jones, D., Ferrando, A. A., Wolfe, R. R., and Smith, S. M. (2005). Amino acid supplementation alters bone metabolism during simulated weightlessness. *Journal of Applied Physiology*, 99(1):134–140. PMID: 15691900.

[460] Zwart, S. R., Hargens, A. R., Lee, S. M., Macias, B. R., Watenpaugh, D. E., Tse, K., and Smith, S. M. (2007). Lower body negative pressure treadmill exercise as a countermeasure for bed rest-induced bone loss in female identical twins. *Bone*, 40(2):529–537.

[461] Zwart, S. R., Pierson, D., Mehta, S., Gonda, S., and Smith, S. M. (2010). Capacity of omega-3 fatty acids or eicosapentaenoic acid to counteract weightlessness-induced bone loss by inhibiting NF-κB activation: From cells to bed rest to astronauts. *Journal of Bone and Mineral Research*, 25(5):1049–1057.

[462] Zwart, S. R., Rice, B. L., Dlouhy, H., Shackelford, L. C., Heer, M., Koslovsky, M. D., and Smith, S. M. (2018). Dietary acid load and bone turnover during long-duration spaceflight and bed rest. *The American Journal of Clinical Nutrition*, 107(5):834–844.